# NOVEL RARE-EARTH ALUMINOSILICATE GLASSES AND GLASS-CERAMICS

**Csaba Ferenc Rappensberger**

**Thesis submitted for the degree of Doctor of Philosophy (Ph.D.)**

**University of Warwick**

**Department of Physics**

**November 1996**

To Marianna:

"Jó érezni azt, hogy szeretlek
nagyon és egyre jobban.
Ott bujkálni a két szemedben,
rejtözködni a mosolyodban.
Érezni azt, hogy a szemeid már
szemeimben élnek és néznek,
S érezni azt, hogy szép, Veled szép,
és csak Veled teljes az élet."

## CONTENTS

**Figures**

**Tables**

**Acknowledgements**

I would like to thank Prof. Mike Lewis for his academic and professional guidance. Many thanks to Dr. John Lumby and Dr. Stuart Sutherland for the fruitful discussions and their eagerness to help whenever I approached them. Thanks should go to the staff, research fellows and my postgraduate colleagues in the Materials group who helped me during my three years at Warwick. I also want to thank to the Warwick University organized "Scholarship for East-Europe" scheme for financially supporting my studies, and for allowing me to get this unique and challenging opportunity.

Last but not least I would like to thank my beloved wife, Marianna, who let me chase my dreams and understood my obsession with my work, and I would like to apologize for the numerous days & nights she had to spend alone.

**Declaration**

I declare that, with the exception of the assistance acknowledged, this thesis is a result of my own studies.

This thesis has not been accepted for any other award or degree and is not currently being submitted for any other award or degree.

Signed: Clara Rappensberger

Date: 30/04/97

**Abstract**

Novel, rare-earth containing, quaternary calcium- and magnesium aluminosilicate glasses and glass-ceramics were studied using various techniques including dilatometry, hardness and flexural testing, X-ray Diffraction (XRD), Scanning Electron Microscopy (SEM) and Transmission Electron Microscopy (TEM). Three rare-earth oxides were selected for investigation: yttria, lanthana, and neodymia, which gave six compositional systems to study. The parent glass compositions were selected along the anorthite - $Ca_2Ln_8Si_6O_{21}$ and cordierite - $Ln_2Si_2O_7$ tie-lines in the Ca-Ln-aluminosilicate and Mg-Ln-aluminosilicate systems, respectively. The major aim of the study was to prepare diphasic glass-ceramics from these pseudobinary systems, which would contain the lower thermal expansion aluminosilicate phase and the higher thermal expansion rare-earth silicate phase in different ratios (depending on the parent glass composition and the heat treatment schedule applied), and would provide series of glass-ceramics with thermal expansion which is adjustable to certain specific applications.

A review is given on the structure and crystallization of aluminosilicate glasses and their glass-ceramic derivatives, as well as on the applications of rare-earths in glasses and ceramics with major emphasis on ternary rare-earth aluminosilicate glasses and their glass-ceramic derivatives. The materials preparation procedures and the property and structure investigation methods applied are described.

The glass forming ability is limited to approximately 12mol% and 21mol% of rare-earth oxide in the studied quaternary calcium- and magnesium-aluminosilicate systems, respectively. The density, refractive index, glass transition, softening and crystallization temperatures, as well as the thermal expansion of the glasses studied are increased due to the rare-earth incorporation in their structures.

Heat treatments of the parent glasses generally resulted in fully crystalline diphasic structured glass-ceramic materials. The crystallization sequence generally followed the route of pseudo-binary systems. The sintered glass-ceramic pellets resulted in fine-grained glass-ceramic materials, whereas the Ca-Ln-aluminosilicate bulk glass-ceramics were transformed into fine-grained structure after high temperature heat treatment due to the recrystallization of the previously formed coarse spherulitic microstructure. The Mg-Ln-aluminosilicate bulk glass-ceramics resulted in slightly coarser microstructure, since the previously formed, dominating dendritic structure was less susceptible towards recrystallization. Most of the glasses showed surface crystallization, although the rare-earth rich compositions also showed the signs of bulk nucleation. The addition of $TiO_2$ to Ca-Nd-aluminosilicate glass compositions has not provided bulk nucleation, although enhanced crystallization. Some previously unknown or not fully characterized crystalline phases were detected in the Ca-La-aluminosilicate, Ca-Nd-Ti-aluminosilicate and Mg-Nd-aluminosilicate glass-ceramic systems. The XRD data of these phases are tabulated.

Hot pressed glass-ceramics were prepared from most of the parent glass compositions, and the effect of rare-earth containing phases on density, thermal expansion, hardness and fracture toughness was investigated.

The glass-ceramics developed during this study provide potential candidates for high temperature structural applications or for ceramic-to-metal, ceramic-to-ceramic seals by having fully or partially crystalline fine-grained structure and thermal expansion which can be adjusted to the requirements of the applications by providing suitable ratios of the low- and high thermal expansion crystalline phases.

**Abbreviations**

- CAS: calcium aluminosilicate.
- MAS: magnesium aluminosilicate.
- Ln: abbreviation for rare-earth elements and yttrium.
- o-Ca-Al-Si: orthorhombic $CaAl_2Si_2O_8$ (JCPDS 5-528).
- Ca-La-Si *or* La-oxyapatite: apatite structured $Ca_2La_8Si_6O_{26}$ (JCPDS 29-337).
- Ca-La-Al-Si: crystalline Ca-La-aluminosilicate (oxide ratios and X-ray Powder Diffraction data are shown in Section 5.2, whereas a representative XRD trace is shown in Appendix II).
- t-La•2Si: low temperature, tetragonal $La_2Si_2O_7$ (XRD data source: [307]).
- Ca-Y-Si *or* Y-oxyapatite: apatite structured $Ca_4Y_6Si_6O_{25}$ (JCPDS 27-93).
- y-Y•2Si: monoclinic impurity stabilized yttrium disilicate, $R(Y,Ln)_5Si_6O_{21}$ (R: $Mg^{2+}$, $Al^{3+}$ etc.) (XRD data source: [296]).
- α-Y•2Si: triclinic α-$Y_2Si_2O_7$ (JCPDS 38-223).
- β-Y•2Si: monoclinic β-$Y_2Si_2O_7$ (JCPDS 38-440).
- Ca-Nd-Si *or* Nd-oxyapatite: apatite structured $Ca_2Nd_8Si_6O_{26}$ (JCPDS 28-228).
- mo-Nd•2Si: high temperature, monoclinic $Nd_2Si_2O_7$ (JCPDS 38-1456).
- t-Nd•2Si: low temperature, tetragonal $Nd_2Si_2O_7$ (JCPDS 22-1177).
- α-Ti: α-$(Ca,Nd)(Ti,Al)SiO_5$ (the oxide ratios are shown in Section 5.5, the XRD pattern is similar to JCPDS 15-158, with missing reflections).
- β-Ti: β-$(Ca,Nd)(Ti,Al)SiO_5$ (the oxide ratios and the X-ray Powder Diffraction data are shown in Section 5.5, whereas a representative XRD trace is shown in Appendix II).
- mo-La•2Si: high temperature, monoclinic $La_2Si_2O_7$ (XRD data source: [301]).
- Mg-Nd-Si: Mg-Nd-silicate (the oxide ratios and the X-ray Powder Diffraction data are shown in Section 6.4.1, whereas a representative XRD trace is shown in Appendix II).

# CHAPTER 1.

# INTRODUCTION

## 1.1. Advanced ceramics

In the last few decades the increasing level of global industrial and economic competition increased the efforts of major companies and national economies to achieve better market positions by gaining competitive advantages. One of the key factors in gaining and retaining competitive advantages is the development of new materials and technologies and their industrial implementations. The USA and Japan were among those countries, which considered the development of new materials and processes as essential to national economic prosperity [1]. Materials synthesis and processing, ceramics and composites are three among the five priority target areas identified by the Americans for materials development [1].

The advanced ceramics which were developed in the last decades (including high-technology glasses, ceramics and glass-ceramics), are capable of fulfilling a high proportion of the industrial needs, and outperforming the traditionally used metals, alloys or conventional ceramics, due to their outstanding combination of useful properties. Nevertheless, improvements have to be achieved in process and quality control of advanced ceramics [2], in order to increase reliability and reproducibility of these materials, as well as to reduce their cost [3].

Some important characteristics of advanced ceramics are: strong ionic-covalent chemical bonds, high melting point, low density (compared to that of metals), and good chemical stability. There is a long list of advanced ceramic materials developed in the last decades, including high temperature ceramic superconductors; carbon and nitrogen containing ceramics, glasses, and glass-ceramics; fibre/whisker/platelet reinforced or transformation toughened composites; and biocompatible materials.

Their development also resulted in new processing routes, including the sol-gel method, chemical vapour deposition and composite materials fabrication.

The task of materials scientists and engineers, during the development of advanced ceramic materials, is to understand the relation between the atomic, micro- and macroscopic structure of materials and their properties, as well as to achieve control over these properties by controlling the materials' structure, and also to be able to tailor the properties to the requirements of specific applications.

An important group of advanced ceramics is glass ceramics, which are "polycrystalline solids prepared by controlled crystallization of glasses" [4]. Since their development in the early sixties, glass ceramics became widespread in almost every aspect of human activity. Their applications range from cooking ware, through substrates and packaging materials for microelectronics, ceramic coatings on metals, encapsulating materials for nuclear waste, telescope mirrors and laser hosts, to bone replacement and dental application [5-7].

### 1.2. Rare-earth containing advanced ceramics

Rare-earth oxides are important constituents of a wide range of existing advanced ceramics. Rare-earth oxides are used in high temperature ceramic superconductors; they are constituents of soft ferrites (e.g. Y-Fe-garnet [8]), positive temperature coefficient thermistors (e.g. Y or La doped $BaTiO_3$ [8]), and multilayer ceramic capacitors (e.g. La modified lead titanate-lead zirconate [8]). In addition, rare-earth containing ceramics are used as fast ion conductors, similar to β-alumina (polycrystalline $Na_5YSi_4O_{12}$ [9]); as electrical heating elements ($LaCrO_3$ [8]), and as host lattices for luminescent material (oxyapatite structured $Ba_2La_8(SiO_4)_6O_2$, with $Eu^{2+}$ and $Pr^{3+}$ dopants [10]) and can provide prospective materials for high level

nuclear waste incorporation (oxyapatite structured $Ca_2Ln_8(SiO_4)_6O_2$ - the Ln position can be substituted by actinides, and the crystalline structure is resistant to $\alpha$, $\beta$, and $\gamma$ radiation [11]). Moreover, rare-earth oxides are used in aluminosilicate refractories to enhance corrosion resistance against molten aluminium [12,13]; and can be applied to stabilize the structure of zirconia, which in turn can be used as synthetic gemstones, as well as in partially stabilized form as oxygen sensors, or as reinforcement of structural ceramics [8]. Furthermore, rare-earth oxide containing ceramic-glass composites are used as core materials for dental crowns (*In-Ceram*, composite of alumina - La-aluminoborosilicate glass [14]), and few percentages of rare-earth oxides and trace elements can be used as key components of glass fertilizers, which were effectively applied in soils depleted in microelements (Ca-phosphosilicate glass doped with La, Nd & Ce, as well as Fe, Mn, Zn, B, Mo & Cu [15]).

### 1.3. Theme of the current programme

In addition to the above listed applications, rare-earth oxides can be used in high-technology glasses as well. Rare-earth aluminosilicate glasses came into the focus of scientific research in the last decade, due to their outstanding properties. These glasses are hard and highly refractory, have high elastic moduli and high refractive indices, show high chemical durability, as well as having moderate or high thermal expansion. In addition, they have valuable magneto-optical properties, such as high paramagnetic susceptibility and Verdet constant. Due to the combination of these properties, rare-earth aluminosilicate glasses are prospective materials for optoelectronic and optomagnetical applications, which can be used in high temperature corrosive environment, as well as providing refractory glass-to-metal or ceramic-to-metal seals. Scientific research prior to this work was mainly concentrated

on the investigation of glass forming in ternary rare-earth aluminosilicate glass systems, as well as the properties of the glasses produced, and only limited work has been reported on the crystallization of these glasses.

The aim of this project was to investigate quaternary, rare-earth containing Ca-aluminosilicate (CAS) and Mg-aluminosilicate (MAS) compositions, in order to reveal their glass forming abilities, as well as to study the nucleation and crystallization characteristics of these systems. The compositions studied were selected on pseudo-binary tie-lines in order to achieve glasses with good glass-forming characteristics. In addition, these glasses, after a suitable heat treatment, were expected to result in diphasic, crystalline glass-ceramic materials, which would combine the properties of the alkaline-earth aluminosilicate phase with that of the rare-earth silicate crystals.

Chapter 2 contains a review on aluminosilicate glass-ceramics as well as on the applications of rare-earth oxides in glasses and ceramics, with major emphasis on rare-earth aluminosilicate glasses and their glass-ceramic derivatives. In addition, it also gives the specific objectives of the research. Chapter 3 describes the material preparation procedures and lists the experimental techniques applied. Chapter 4 characterizes the rare-earth containing quaternary aluminosilicate glasses developed. Chapter 5&6 describes the crystallization sequence and microstructure of the rare-earth containing glass-ceramics derived from the developed parent glasses. Chapter 7 investigates the properties of hot-pressed quaternary rare-earth containing glass-ceramics. Finally, Chapter 8 summarizes the results of the current research and gives an indication of prospective future work.

## CHAPTER 2.

## GLASS-CERAMICS - A REVIEW

### 2.1. Basic Principles

In addition to the text books whose main topic is glass-ceramics [4,5,16,17], other texts [18-24] and articles [25-30] discuss the crystallization of glass. Crystallization is a conversion from the liquid state to the ordered solid state, which occurs at a temperature, which is fixed for a given pressure and known as the freezing point. Two parts of the crystallization process can be distinguished: nucleation and crystal growth. The crystallization of glass (as supercooled liquid) is controlled by the rate of these processes: the nucleation rate (the number of nuclei formed in a unit volume per unit time), and the rate of crystal growth (the velocity of the crystalline interface in the liquid).

One can differentiate surface and bulk crystallization according to their mechanisms. In the case of surface crystallization, the crystal nucleates at the glass-atmosphere interface, sometimes initiated by surface heterogeneities (e.g. dust particles, minute flaws or scratches). Due to the low density of nuclei formed on the surface, this mechanism generally results in large crystals and coarse-grained microstructure, which often degrades the mechanical strength of the glass-ceramic. Nevertheless, there are important applications, where surface crystallization mechanism plays a key role in the crystallization of the product. Multilayer packaging materials [31-33], and glass-ceramic matrix composites [34-44] are produced by the sintering of high specific surface area, fine glass powder, and are being crystallized predominantly by a surface crystallization mechanism. In addition, glasses can be

strengthened by surface crystallization, where the surface crystals encapsulate surface flaws and provide a surface compression layer [45,46].

In the case of bulk (volume) crystallization, the crystal growth originates from nucleation sites inside the material. When the crystallization is initiated by a substance, which is foreign to the bulk of the material, the nucleation is heterogeneous, whereas when the composition of the nucleus is the same as that of the bulk material, the nucleation is homogeneous. Ensuring bulk nucleation is an important condition for the preparation of bulk glass-ceramic materials.

### 2.1.1. Nucleation

a) Homogeneous nucleation

Homogeneous nucleation occurs arbitrarily in glass, without preferential nucleation sites. The necessary conditions for homogeneous nucleation are the chemical, structural and energetical homogeneity of the parent glass, as well as its lack of defects. Nevertheless, all real glasses contain some kind of defects (e.g. foreign surfaces, impurities), therefore the conditions of ideal homogeneous nucleation hardly ever can be fulfilled.

In homogeneous nucleation the first tiny seeds (embryos) arise due to local fluctuations in the structure of the liquid phase. Their radius is smaller than the critical one, therefore they are thermodynamically unstable, their reduction in size decreases the free energy of the system. If their size reaches the critical radius, they will become thermodynamically stable, and their growth will decrease the free energy of the system. From this point the tiny seeds are called nuclei. This type of nucleation can occur at high degrees of supersaturation or supercooling.

The rate of nucleation depends on two major factors: one thermodynamic and one kinetic. The thermodynamic factor is zero at the liquidus temperature and increases with supercooling. Nevertheless, at large supercooling, the second factor becomes dominant and the nucleation rate decreases with further cooling after reaching a maximum. The resulting curve is shown in Fig.2.1.

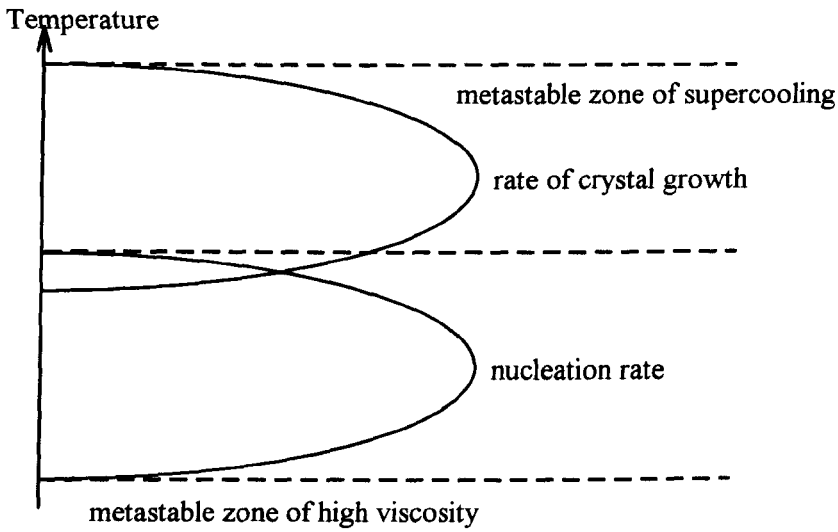


Fig.2.1. The rate of nucleation and crystal growth as a function of temperature [23].

b) Heterogeneous nucleation

In the case of heterogeneous nucleation, the nuclei of the crystallizing phase are formed on the surface of an already existing phase (substrate). The presence of the substrate decreases the thermodynamic barrier for nucleation. In glass compositions where homogeneous nucleation of the required phase is inhibited, or the nucleation rate is small, bulk crystallization with a high nucleation rate can be achieved by the addition of small amount of nucleating agents. The crystallization enhancing mechanism of nucleating agents is discussed in Section 2.1.4.

A special type of heterogeneous nucleation is called photonucleation. During photonucleation, photosensitive glass is irradiated by UV radiation (300-350nm) and

the subsequent heat treatment results in the separation of colloidal metal particles distributed throughout the bulk of the glass. The metal particles will act as heterogeneous nucleation sites for the main crystalline phase during the second heat treatment, which converts the glass into glass-ceramic.

### 2.1.2. Crystal growth

The growth rate of a crystal nucleus depends on the rate at which atoms get attached to the surface of the nucleus. The rate of crystal growth as a function of temperature yields a curve (Fig.2.1), bearing close similarities to that of the nucleation rate, since the two major factors (i.e. a thermodynamic and kinetic factor), which determine the rate of crystal growth, are rather similar to the ones determining the nucleation rate. There are three theories for crystal growth mechanism, which are based on different descriptions of the crystal-liquid interface: normal growth, surface nucleation growth, and screw dislocation growth [5,23].

### 2.1.3. Phase separation

Glass-in-glass phase separation is often encountered during the preparation of glass-ceramics. Most of the previously quoted textbooks provide detailed discussions on amorphous phase separation. Moreover, some books and papers deal particularly with this important topic [47-50]. Liquid phase separation is the separation and growth of non-crystalline phases having different composition from the original glass. The driving force for phase separation is the achievable decrease in the overall free energy of the system.

Fig.2.2/a shows the free energy curve of a system susceptible to phase separation. The Gibbs type free energy ($\Delta G$) of the system is:

$$\Delta G = \Delta H - T\Delta S \qquad 2.1.$$

where T is the temperature, $\Delta H$ is the enthalpy, and $\Delta S$ is the entropy.

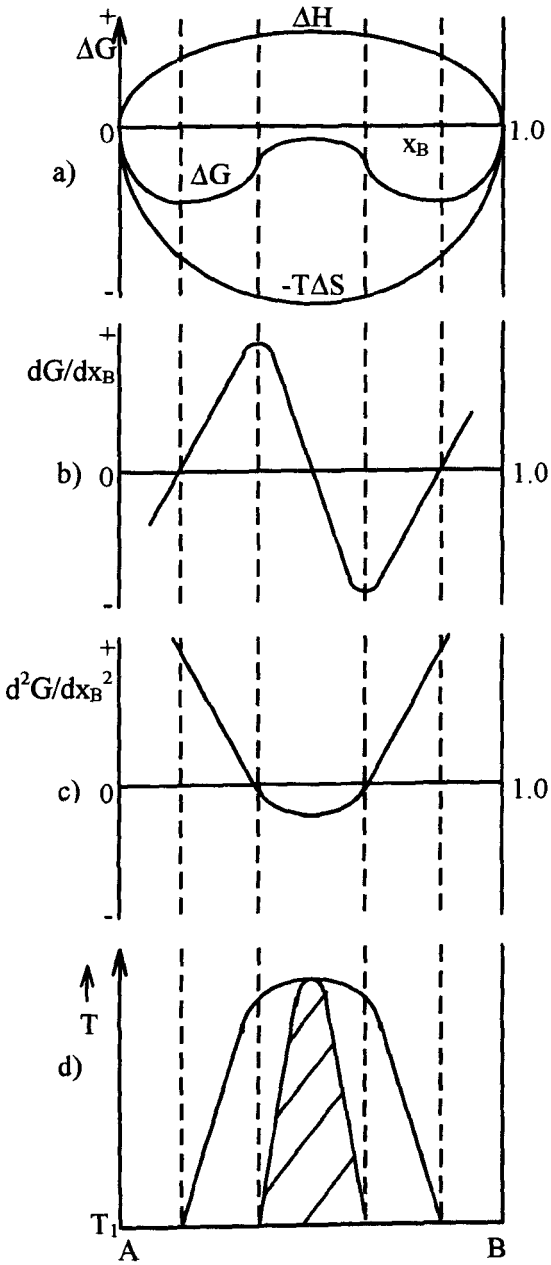


Fig.2.2. (a-c): Free energy and its derivatives as a function of concentration ($x_B$); (d): Temperature of immiscibility as a function of concentration

The compositional fluctuation has high probability at negative or small positive values of the free energy's second derivative ($d^2G/dx_B^2$, in Fig.2.2/b). When the derivative is negative, the separation of the glass into two phases is accompanied by a simultaneous decrease of free energy, and the process is called spinodal decomposition. When the derivative has a small positive value, the early stage of the phase separation causes the increase of free energy, therefore the separation will take place by nucleation and growth. The above described phenomena are easily visualized by the "immiscibility dome" (Fig.2.2/d), which is the limiting phase composition of immiscibility as the function of temperature. The inner dome is called

"spinodal", referring to spinodal decomposition. Within this dome the glass melt will spontaneously separate, and the separation process is only limited by the diffusion of the components. In the outer dome, which is called "binodal", the phase separation has an energy barrier, therefore it requires a formation of nuclei.

Introducing glass-in-glass phase separation in a controlled way prior to crystallization, can be utilized to achieve bulk nucleation and fine-grained glass-ceramics. Phase separation can initiate subsequent crystallization by providing abundant nucleation sites at the newly formed glass-glass interfaces. In addition, phase separation can increase the driving force for nucleation by inducing enrichment of some components, as well as resulting in higher atomic mobility [25].

### 2.1.4. Nucleating agents

Two major groups of nucleating agents can be distinguished according to their types and relative amounts.

a) Metal ions of Ag, Au, Pt, Rh, Pd, Cu, Ni, Cr, Fe, Mn, V, W.

These ions are added in very small amounts to the parent glass (0.01-1wt%), usually in the form of chlorides or nitrates. In ionic form they are soluble in the glass melt, but they can be easily reduced to the metallic state, which would lead to their precipitation, since the solubility of their metallic forms in glasses is very low. Suitable nucleation heat treatment of the parent glass, either by controlled cooling from the molten state, or by reheating the room-temperature glass, results in the precipitation of tiny aggregates (colloidal dispersion) of metal atoms. These aggregates will act as heterogeneous nucleation sites for the main crystalline phases during the crystallization heat treatment.

b) Various oxides (e.g. $TiO_2$, $ZrO_2$, $P_2O_5$, $SnO_2$, $Cr_2O_3$, NiO, $V_2O_5$, $WO_3$), fluorides (NaF, $Na_3AlF_6$), sulphides and selenides (CdS, CdSe).

These nucleating agents are soluble in silicate glasses, and they are usually added in larger amounts (1-20wt%). The nucleating mechanism of sulphides, selenides and fluorides is similar to that of the metal ions: they precipitate as colloidal dispersion of fine crystals during the nucleation heat treatment, and serve as heterogeneous nucleation sites for the main phase at higher temperatures [19-24]. In contrast, the nucleating mechanism initiated by oxides is more complicated and depends on the nucleating agent employed, the parent glass composition, the applied heat treatment, as well as the thermal history of the parent glass. Some oxide nucleating agents can produce liquid phase separation prior to the occurrence of crystal nucleation, since most of them form an extensive immiscibility region with silica. The phase separation can be followed by the crystallization of the separated phases as fine crystals, which in turn catalyses the further growth. Other oxide nucleating agents can crystallize in the form of simple compounds formed with some components of the glass (e.g. $MgTiO_3$), and then heterogeneously nucleate the major crystalline phase. Finally, some oxide nucleating agents did not show the characteristics of the previous two groups, they presumably increase the crystal nucleation rates by lowering the interfacial tension between the crystal and the glass, or enhance the diffusion rate of the constituents [19,22,51].

## 2.2. Aluminosilicate glass-ceramics

### 2.2.1. Ca-aluminosilicate (CAS) glass-ceramics

From a technological viewpoint, the most important crystalline phase in the $CaO$-$Al_2O_3$-$SiO_2$ system is anorthite ($CaAl_2Si_2O_8$). Achieving anorthite as the major crystalline phase in a glass-ceramic is a desirable target, because it bears a combination of valuable properties: high hardness, high temperature stability, high chemical durability, low dielectric constant and medium thermal expansion.

#### 2.2.1.1. Glass forming in the CAS system

The range of glass forming is extremely broad in the Ca-aluminosilicate system [52-64]. A range of metastable liquid phase immiscibility exists in the Ca-aluminosilicate system, though its extent is smaller than in the Mg-aluminosilicate system [5,65]. The Ca-aluminosilicate glasses are highly refractory ($T_g$=818°C), show excellent chemical durability, and their thermal expansion is in the medium/upper-medium range (5 $MK^{-1}$) [52].

Ca-aluminosilicate glasses containing 50mol% $SiO_2$, with the molar ratio of $CaO$:$Al_2O_3$=1 (i.e. the positive charge of $Ca^{2+}$ balances the charge deficiency of $2Al^{3+}$), possess a fully polymerised framework structure, consisting of corner shared tetrahedra of $AlO_4$ and $SiO_4$ structural units, as determined by Raman Spectroscopy [61,62], Fourier-Transform Infrared Spectroscopy (FTIR)[60], and $^{27}Al$ and $^{29}Si$ Magic-Angle Spinning Nuclear Magnetic Resonance Spectroscopy (MAS-NMR) [53,58,62,63,66]. The presence of extra $CaO$ in the glass (i.e. $CaO$>$Al_2O_3$) results in the increase of non-bridging oxygen and therefore leads to depolymerization of the

network, while all Al is tetrahedrally co-ordinated (FTIR [60], $^{27}Al$ & $^{29}Si$ MAS-NMR [53]). The structure of high alumina containing glasses (i.e. $Al_2O_3$>CaO) is under scientific debate. Some researchers stated, that Al is in tetrahedral co-ordination ($^{27}Al$ & $^{29}Si$ MAS-NMR [58]), others reported extreme co-ordination disorder: the presence of 4-, 5-, and 6-co-ordinated $Al^{3+}$ (Raman Spectr., $^{27}Al$ & $^{29}Si$ MAS-NMR [62]), and others proposed that the extra $Al_2O_3$ is present in the form of neutral extra-network species, called triclusters (i.e. $[Al^{3+}(AlO_2^-)_3]$) [53].

### 2.2.1.2. The structure of anorthite

Anorthite is a tectosilicate, one of the end members of the alkali feldspar series [67]. The crystal structure of anorthite at room temperature & pressure is triclinic primitive [68-71]. In the anorthite structure, the Si and Al positions are fully ordered, the Si and Al tetrahedra are alternating [70]. Anorthite is chemically most related to celsian ($BaAl_2Si_2O_8$), whereas crystallographically, its triclinic symmetry and the radius of $Ca^{2+}$ cation make it similar to albite ($Na_2Al_2Si_6O_{16}$) [69]. This similarity results in the continuous solid solution series between the Ca and Na feldspars.

In addition to the natural, triclinic anorthite, orthorhombic and hexagonal modifications of $CaAl_2Si_2O_8$ can be synthesized [72-74]. Both synthetic modifications were identified during the crystallization of Ca-aluminosilicate glasses.

### 2.2.1.3. Crystallization of calcium-aluminosilicate glasses

Ca-aluminosilicate glasses generally crystallize by a surface crystallization mechanism, which results in bulk glass ceramics with large crystalline grains and relatively high amount of residual glassy phase [33,55,56]. The crystallization of the

anorthite composition parent glass resulted in triclinic anorthite as a major phase, which was grown from the surface, whereas orthorhombic and hexagonal $CaAl_2Si_2O_8$ were detected in the bulk [33]. The orthorhombic and hexagonal phases are considered to be unstable [33,75]. In addition, the crystallization of CaO-rich glass compositions resulted in major phases of anorthite and gehlenite ($Ca_2Al_2SiO_7$) [56].

Crystallization of fly ash derived glasses resulted in fine grained glass-ceramics containing major crystalline phases of anorthite and mullite ($Al_6Si_2O_{13}$) [76]. Moreover, glass-ceramics consisting of anorthite and wollastonite ($CaSiO_3$), were produced from blast furnace slag (*Slagsitall*) [5].

Although surprisingly little research was done on the crystallization of pure Ca-aluminosilicate glasses, their glass powders are frequently used as matrices for SiC fibre reinforced glass-ceramic matrix composites [34,35,40-43]. The major crystalline phase in the matrix was anorthite, which was nucleated by the ceramic fibres. In addition, a well-developed, cryptocrystalline graphitic reaction layer was formed at the fibre-matrix interface [40,42,43], which provided high fracture toughness and high strength for these materials.

#### 2.2.1.4. The effect of nucleating agents on the crystallization of Ca-aluminosilicate glasses

Nucleating agents were applied in Ca-aluminosilicate glasses in order to provide bulk crystallization. The most frequently applied nucleating agents were $TiO_2$ and $ZrO_2$ [33,56,77]. Small amounts of $TiO_2$ (3-5wt%) provided good sintering, as well as promoted the crystallization of the triclinic anorthite and suppressed the crystallization of hexagonal and orthorhombic $CaAl_2Si_2O_8$ in an anorthite composition

CAS glass [33]. Higher amounts of titania (15-18wt%) resulted in fine-grained glass-ceramic material [56,77], containing a main phase of anorthite and minor phases of β-wollastonite, which were sometimes accompanied by sphene ($CaTiSiO_5$) [77].

In addition, small percentages of $CaF_2$ were effectively used as a nucleating agents. It lowered the viscosity of the glass melt and the crystallization temperature, as well as extended the range of immiscibility [78]. Higher amounts of $CaF_2$ containing Ca-aluminosilicate glass was crystallized through liquid phase separation, followed by crystallization of $CaF_2$, which eventually induced the crystallization of the remaining glassy phase as anorthite [79].

#### 2.2.1.5. Properties and application of anorthite glass-ceramics

Glass-ceramics containing anorthite as a major crystalline phase have a useful combination of properties, such as relatively high hardness (5.8-7.8GPa [5]), high temperature stability (anorthite $T_{melting}$=1550°C [22]), high resistance to chemical attack [5], relatively low dielectric constant (ε=7-7.7 [5]), and medium thermal expansion ($\alpha$=4.5 $MK^{-1}$ [4,22]). The low dielectric constant and the thermal expansion, which closely matches that of silicon ($\alpha_{Si}$=3.7 $MK^{-1}$), makes it a suitable candidate for dielectric circuit support [75]. The medium thermal expansion, which can be adjusted by preparing diphasic glass-ceramic, containing wollastonite as second phase ($\alpha$=9.4 $MK^{-1}$ [22]), can be utilized in glass-to-metal seals. In addition, their high temperature stability and high chemical durability suggest high temperature applications in corrosive media. Moreover, *Slagsitall*, the anorthite containing, slag derived glass-ceramic is commonly used in the construction industry as wall and floor

tiles, as well as in the chemical and petrochemical industry for various applications such as pipelines, hydrocyclone cones, Raschig-rings and corrosion resistant coatings [5].

### 2.2.2. Mg-aluminosilicate (MAS) glass-ceramics

Among the crystalline phases in the magnesium-aluminosilicate system, cordierite ($Mg_2Al_4Si_5O_{18}$) is the most important for preparation of glass ceramic materials, because of its high mechanical strength, high temperature stability, low thermal expansion, good chemical durability, high electric resistivity and good dielectric properties.

#### 2.2.2.1. Glass forming in the MAS system

The glass forming region in the $MgO$-$Al_2O_3$-$SiO_2$ system is limited to the composition range between 40 to 75mol% $SiO_2$ [5,80,81]. The MAS system showed a broad range of metastable immiscibility in the $SiO_2$-MgO rich region [5,65]. The MAS glasses are refractory ($T_g$=810°C, $M_g$=860°C), having high elastic modulus (E=96GPa), good chemical durability, and relatively low thermal expansion ($\alpha$=3.7 $MK^{-1}$) (all data quoted belong to a cordierite composition glass [82]). The charge balanced Mg-aluminosilicate glasses (i.e. $MgO:Al_2O_3$=1), similar to the CAS ones, have a fully polymerized framework structure of corner sharing $AlO_4$ and $SiO_4$ tetrahedra ($^{27}Al$ & $^{29}Si$ MAS-NMR [58,63]). In addition, according to some researchers, Al was found tetrahedrally co-ordinated over the range of glasses studied, even in the MgO-rich glasses ($^{27}Al$ MAS-NMR [58]), whereas others found

5- and 6-co-ordinated Al, in slightly MgO rich compositions, close to the $SiO_2$-$MgAl_2O_3$ join ($^{27}Al$ MAS-NMR [83]).

### 2.2.2.2. The structure of cordierite polytypes

Cordierite has two crystalline modifications: a low temperature, orthorhombic one and a high temperature, hexagonal polymorph (also called α-cordierite or indialite). Natural cordierite crystals are generally orthorhombic, and often show partial substitution of Mg by Fe and Mn [84]. The temperature range of stability of the orthorhombic polymorph is below 1450°C, whereas the hexagonal one is stable between 1450°C and the melting point of 1465°C [80], therefore it is considered to be metastable at room temperature. Despite that, hexagonal cordierite crystals were also found in nature [85], as well as crystals, which are structurally intermediate between the two polytypes [86]. In the following, the hexagonal modification will be referred to as indialite.

The orthorhombic cordierite is a tectosilicate, structurally similar to beryl [84,87,88]. Its structure consists of six-member rings of corner-sharing tetrahedra (i.e. four ($SiO_4$) & two ($AlO_4$) tetrahedra), which are stacked along the "c"-axis, and connected together by ($AlO_4$) tetrahedra into a three dimensional network [84,87,88]. The stacked rings, similarly to the structure of zeolites, form channels parallel to the "c"-axis, which can contain $H_2O$, $CO_2$, $Fe^{2+}$, $Na^+$, or even He and Ar [88-93]. In the structure of orthorhombic cordierite, the Si- and Al-tetrahedra are alternating in all directions, except for the six-member ring, where the four Si-tetrahedra are forming two pairs [84].

The structure of indialite is rather similar to that of the orthorhombic cordierite. They differs only in the degree of ordering in the tetrahedral positions of $SiO_4$ and $AlO_4$, where the structure of orthorhombic cordierite is considered as "fully ordered", whereas indialite represents a "disordered" structure, and a range of crystals exists between the two end members, having structures with a different degrees of ordering [85,86,94]. Miyashiro *et al.* [85,86], as well as Schreyer & Schairer [80,81,95] contributed detailed works on the degree of ordering in various natural and synthetic cordierite crystals. Nevertheless, the structure of cordierite polymorphs and the ordering of the Si- and Al-tetrahedra is still under research [96-102].

### 2.2.2.3. Crystallization of Mg-aluminosilicate glasses

The magnesium-aluminosilicate system is one of the most comprehensively studied glass-ceramic systems, the crystallization of Mg-aluminosilicate glass, both in the absence and in the presence of nucleating agents was investigated by several researchers. Schreyer *et al.* published valuable data in their papers [80,81,95,103], and Gregory & Veasey wrote a detailed review on the topic [104-107].

In addition to the previously described natural modifications, several metastable crystalline phases were detected during the crystallization of MAS glasses. The metastable phases can be divided into three groups. The crystals in the first group have a "stuffed" β-quartz type structure [80,81,108-110]. The structure can be derived from that of the β-quartz by isomorphic substitution of $Si^{4+}$ by $Al^{3+}$, where the charge deficiency is compensated by $Mg^{2+}$ cations located in interstitial positions [80,81,110]. The β-quartz structured phases form a solid solution series between $SiO_2$ and $MgAl_2Si_2O_8$ [81,109,110].

Metastable β-quartz structured crystals are the first phase to precipitate during the crystallization of cordierite composition glass. Its temperature range of formation is between 800°C and 1050°C. Due to its pseudohexagonal morphology, it was falsely identified as a cordierite modification, and was named as μ-cordierite [111,112]. When its real structural identity was revealed, the "silica-O" name was proposed [108], but researchers tend to use the β-quartz solid solution and the μ-cordierite names with roughly equal abundance. In order to differentiate the phase having cordierite composition, from the other β-quartz structured metastable modifications, the μ-cordierite notation will be used further on in this study.

The second group of metastable crystals are structurally similar to the natural mineral osumilite ($Na_2Mg_5Si_{12}O_{30}$ [113]), and their composition is close to $MgAl_2Si_4O_{12}$ [103]. Mg-osumilite is crystallized from $SiO_2$-rich glass compositions located on the $SiO_2$-$MgAl_2O_4$ join, and it was always accompanied by other crystalline phases such as β-quartz solid solution, indialite, and cristobalite ($SiO_2$) [103]. The temperature range of formation of Mg-osumilite is between 1050°C and 1250°C [103]. Recently, glass-ceramics containing major crystalline phase of Mg-osumilite (with composition of $Mg_2Al_4Si_{12}O_{30}$) were developed. The parent glass contained small amount of BaO, and the crystallization of small Ba-osumilite ($BaMg_2Al_6Si_9O_{30}$) crystals was followed by epitactic growth of Mg-osumilite on their surface [114,115].

The third group of metastable phases are structurally similar to the natural mineral petalite ($LiAlSi_4O_{10}$), and their composition lies between the formulae of $MgAl_2Si_8O_{20}$ and $MgAl_2Si_3O_{10}$ [103,116]. The Mg-petalite phase crystallized from glasses on the cordierite-$MgSi_2O_5$ composition line, and it was found in association

with other phases, such as β-quartz solid solution, enstatite ($MgSiO_3$), and indialite [103]. The temperature range of Mg-petalite formation lies between 900°C and 1000°C [103].

Considering the experiments of Schreyer *et al.* [80,81], Shultz *et al.* [109] and Gregory & Veasey [104-107] the crystallization of pure Mg-aluminosilicate glasses can be summarized as follows. The crystals of the β-quartz solid solution series are the first phase to crystallize (μ-cordierite in the stoichiometric cordierite glass). At certain parent glass compositions their crystallization is followed by crystallization of other metastable phases (i.e. Mg-petalite or Mg-osumilite). The reconstructive transformation of β-quartz solid solution crystals into indialite starts around 850°C, and finishes around 1000°C. In addition, at higher temperatures it is accompanied and/or followed by the recrystallization of the other metastable phases and crystallization of the residual glassy phase into indialite.

The first cordierite polymorph to crystallize from glasses is indialite [80,81], since it is a high temperature, lower symmetry modification and therefore its crystallization requires a lower activation energy. Although, indialite is considered to be a metastable phase below 1450°C, its recrystallization into orthorhombic cordierite requires long heat treatments above 1180°C, and the reaction is very slow [80,81]. The above described crystallization sequence was observed during the crystallization of bulk glasses [117-125], and sintered glass powders of pure MAS composition [126-129].

The MAS glasses crystallized by surface crystallization mechanism in the absence of nucleating agents. Lower temperature crystallizations resulted in a thin crystalline layer on the surface of bulk samples, and higher temperature heat treatments were

required for complete crystallization of bulk glasses. The crystalline grains of indialite were large and oriented, which degraded the mechanical properties of the glass-ceramic. However, fine grained glass-ceramics can be prepared from glass powders susceptible to surface nucleation by sintering. Although sintered bodies can be achieved using pure MAS glass powders [126-129], addition of certain additives, such as $P_2O_5$ and $B_2O_3$ improved their sinterability, by enhancing densification and delaying the crystallization until the densification almost reached completion [31,32,130-137].

The detailed investigations on the crystallization of Mg-aluminosilicate glass-ceramics initiated further studies on application of these glass-ceramics as matrices for ceramic fibre/whisker/platelet reinforced composites [34-40,44,138]. After sintering, the SiC fibre reinforced Mg-aluminosilicate glass-ceramic matrix composites showed the existence of the preferred, cryptocrystalline graphite reaction layer at the fibre-matrix interface [40,138].

#### 2.2.2.4. The effect of nucleating agents on the crystallization of Mg-aluminosilicate glasses

Since MAS glasses crystallized by a surface crystallization mechanism, application of nucleating agents was necessary to achieve bulk glass-ceramics with fine grained microstructure. The most frequently applied nucleating agents for MAS glasses are $TiO_2$ [139-148], $ZrO_2$ [140,141,149-153], and their combination [153,154], although $P_2O_5$ [130,131,145,155-158], $V_2O_5$ [106,107], $WO_3$ [106,107], and NiO [147] were also used. $TiO_2$ was proved to be the most effective one among them, for enhancing bulk crystallization [140,141,153].

According to Zdaniewski [139-141], the crystallization sequence of $TiO_2$ or $ZrO_2$ containing MAS glasses starts with liquid phase separation, which was followed by the nucleation of β-quartz solid solution phase and its spherulitic crystallization. At higher temperature the β-quartz solid solution recrystallized into indialite, and long heat treatment above 1100°C resulted in the gradual transformation of indialite into orthorhombic cordierite.

### 2.2.2.5. Properties and application of cordierite glass-ceramics

Glass-ceramics with the major crystalline phase of cordierite have a valuable combination of properties, such as high strength (flexural strength=137-220MPa [16]), high hardness ($H_V$=8.4GPa [159]), good abrasion resistance [5], high temperature stability (cordierite $T_{melting}$=1465°C [80]), low thermal expansion ($\alpha$=2.6 $MK^{-1}$ [4]), good thermal shock resistance [160], high chemical durability [5], high electrical resistivity ($3x10^{15}\Omega cm$ [31], and low dielectric constant ($\varepsilon$=5.35 [31]). The low dielectric constant of cordierite glass-ceramics can be utilized in microelectronic packaging applications [31,32], their high resistivity suggest their use as large electrical insulators [5], their high temperature stability, low thermal expansion and good thermal shock resistance makes them suitable as industrial heat exchanger materials [23], or as support material for catalytic converters in automobiles [161]. In addition, their high temperature stability, good thermal shock resistance, and high chemical durability can be utilized by high temperature applications in a corrosive media. Moreover, due to their high hardness, high abrasion resistance, high chemical durability, and transparency towards radar waves, they are used as missile radomes (*Pyroceram 9606* [5]).

## 2.3. Rare-earth (Ln) containing glasses, ceramics and glass-ceramics

### 2.3.1. Rare-earth oxides in glass

The term rare-earth elements refers to the group of lanthanides. In addition, yttrium is generally included, due to its similar chemical behaviour. A short description on their characteristics is given in Section 2.3.4.2.

Rare-earth oxides have been used as minor components in various glass compositions for a long time [162,163]. Rare-earth oxides are favoured glass colorants, due to their well-defined, narrow absorption bands in the visible spectrum [162]. Their incompletely occupied electron shells, which are necessary for the electron transitions, and which in turn provides the absorption bands, are protected by the outer shells from the effect of the neighbouring cations [162]. The result is reproducible colour (e.g. lilac: Nd; faint green: Pr, etc.), which depends on the rare-earth oxide employed, but independent of melting conditions (e.g. reducing or oxidizing atmosphere), and only slightly affected by the chemical composition of the matrix glass [162].

In addition, rare-earth oxides are commonly used for glass decolorising. The addition of $CeO_2$ (usually applied with other oxidizing agents such as $NaNO_3$ or $KNO_3$) helps to convert the $Fe^{2+}$ content of the glass into $Fe^{3+}$ [162,163]. The divalent iron has strong absorption band in the visible range of the optical spectrum and its presence, even in small amount, results in blue colour. The visible light transmittance of the glass can be improved by converting $Fe^{2+}$ into trivalent form, which has a less strong absorption band, and only causes a light yellow colour in the glass. The previous process is called chemical decolorising. In addition, $Nd_2O_3$, which has a narrow absorption band in the yellow range of the spectrum, can be used to

neutralize the residual colour of $Fe^{3+}$ (physical decolorising) [162,163]. In industrial practice both methods of decolorising are applied simultaneously by using the mixture of $CeO_2$ & $Nd_2O_3$ [162].

Moreover, $CeO_2$ is used in photosensitive glasses, to promote the photochemical reaction by absorbing the UV radiation more intensely than the photosensitive ions (e.g. $Cu^+$, $Ag^+$, $Au^+$), and help their precipitation in metallic forms [162,163]. The same phenomenon is used during the photonucleation process of glass-ceramics (Section 2.1.1). Furthermore, $CeO_2$ is a favoured additive for UV protective glasses used in the lighting industry [164], due to its strong absorption in the UV spectrum, especially in the harmful UV-B and UV-C regions (280-315nm and 100-280nm, respectively [331]). In addition, Ce-containing glasses can be used for nuclear radiation protection [162].

Rare-earth oxides are used for production of optical glasses having high refractive index and low dispersion (e.g., $BaO-La_2O_3-B_2O_3$ system [163]), and their properties are close to that of the fluorine crown glasses. In addition, rare-earth oxides, when added in slightly larger quantities, strongly promote the meltability of the glasses by lowering the viscosity of the glass melt, due to the high deformability of their ions and their not too strong bonds [162].

Some rare-earth ions ($Nd^{3+}$, $Er^{3+}$, $Pr^{3+}$, $Yb^{3+}$, $Eu^{3+}$, $Tm^{3+}$) are used in small concentrations in fluoride [165-170], silica [171-176], phosphate [175,177], borate [175], and aluminosilicate [178] glass hosts for various optical applications, including optical switches and amplifiers, light upconvertors, non-linear devices, intrinsic fibre sensors, and glass lasers [163,179]. The advantages of using glass as a laser host are: the easier fabrication compared to single crystals, the variety of shapes and

configurations, which can be produced with high optical quality, as well as the availability of size flexibility in the selection of the active ion employed, although the lower thermal conductivity of the glass can be a disadvantage in high power applications [163,179].

### 2.3.2. Application of rare-earth oxides in $Si_3N_4$ and SiAlON ceramics

The pressureless sintering of $Si_3N_4$ and SiAlON ceramics requires the formation of liquid phase in order to achieve dense and high strength ceramics [180-183]. Since the atomic diffusion kinetics are insufficient to provide the necessary conditions for the anisotropic growth of the required β or β` phase below the decomposition temperature of the nitride phase, application of a minor amount of liquid phase is necessary. The molten phase is formed by metallic oxide additives and $SiO_2$ (which is always present as a thin layer on the surface of $Si_3N_4$ grains), and it has an eutectic silicate composition. After the sintering process, the siliceous melt solidifies in the form of a residual glassy intergranular phase, whose presence is detrimental to some important high temperature properties, such as creep, stress-rupture and oxidation resistance.

The rare-earth oxides have shown promising results for solving these problems [180-184]. The rare-earth oxides aided the sintering process by producing a low viscosity molten phase with silica, and after the solution-reprecipitation reaction of $Si_3N_4$ or SiAlON, they can be either incorporated in α′-SiAlON crystals, occupying interstitial positions and stabilizing the crystal structure [185,186], or they can form a residual glassy phase [181,187-194], which is markedly more refractory than the ones produced by other sintering additives. In addition, the residual glassy phase, due to its

rare-earth content, can be crystallized by a post-sintering heat-treatment, which would lead to a stable, almost fully crystalline structure. The post-sintering heat treatments resulted in various crystalline phases, depending on the heat treatment schedule, on the rare-earth oxide employed, as well as on the presence of other sintering additives.

Almost all lanthanide oxides were used as sintering additives [195-199], although most researchers preferred $Y_2O_3$, $CeO_2$, $La_2O_3$, $Nd_2O_3$ because of their easier availability [180-183,185,187-193,200-225]. The post sintering heat treatment of the yttria containing $Si_3N_4$ and SiAlON ceramics resulted in various Y-Si-O-N phases (including the apatite structured $Y_5(SiO_4)_3N$), $Y_3Al_5O_{12}$ (yttrium aluminium garnet, YAG), polymorphic modifications of $Y_2Si_2O_7$, and occasionally, minor amount of $Y_2SiO_5$ [180,195,200,207,209-212,217-219,221,223,225]. The heat treatments of the $Si_3N_4$ and SiAlON ceramics, containing other rare-earth oxides, resulted in similar crystalline phases: various Ln-Si-O-N crystals (including the apatite type phase of $Ln_5(SiO_4)_3N$), and $Ln_2Si_2O_7$ [195,197-199,204,207,221]. In addition, using MgO & $Nd_2O_3$ mixed sintering additives, pseudohexagonal, apatite structured crystals were identified after the post sintering heat treatment, forming solid-solutions between $MgNd_4(SiO_4)_3O$ - $Nd_{4.67}(SiO_4)_3O$ - $Nd_5(SiO_4)_3N$ [183].

The hot pressed yttria containing $Si_3N_4$ and SiAlON ceramics resulted in the same crystalline phases as the sintered & heat treated Y-Si-O-N and Y-Si-Al-O-N ceramics [208,212,213,216,222]. In addition, $Nd_{4.67}(SiO_4)_3O$ (apatite structure) was found in hot isostatic pressed Nd-SiAlON, and it was converted into $Nd_2Si_2O_7$ upon subsequent annealing [208]. Furthermore, $Ln_2Si_2O_7$ phases (and occasionally minor amount of $Ln_2SiO_5$) were identified as high temperature oxidation products of the

rare-earth containing glassy phases [202,205,214-216], as well as arising from high temperature oxidation of apatite type crystals of $Ln_5(SiO_4)_3N$ [206] and $Y_{4.67}(SiO_4)_3O$ [220].

Among the rare-earth containing crystalline phases detected in the variously processed, heat treated or oxidised $Si_3N_4$ and SiAlON ceramics, the $Ln_2Si_2O_7$ polymorphs, $Ln_2SiO_5$, and the apatite structured phases (e.g. $Ln_5(SiO_4)_3(O,N)$, $Ln_{4.67}(SiO_4)_3O$, and $MgNd_4Si_3O_{13}$) are related to the current study, their structural aspects are discussed in Section 2.3.6.

### 2.3.3. Rare-earth containing oxynitride glasses and glass-ceramics

The research on optimising the sintering conditions of $Si_3N_4$ and SiAlON ceramics led to the discovery of oxynitride glasses. Oxynitride glasses possess improved thermal and mechanical properties, which are due to partial substitution of $O^{2-}$ by multivalent $N^{3-}$. The nitrogen anions increased the cross-linking between the network forming cations and therefore strengthened the glass structure by occupying three-coordinated anion sites [226,227]. The density, refractive index, hardness, elastic modulus, fracture toughness, dielectric constant, viscosity, and the transition and softening temperatures of these glasses are increased, as the amount of incorporated nitrogen increased, which besides resulted in the decrease of thermal expansion [228-241].

A comprehensive review was prepared by Lewis & Leng-Ward on oxynitride glasses and their glass-ceramic derivatives [241]. Among the various oxynitride glass compositions, the rare-earth containing ones are interesting from the viewpoint of the current study. Most of the research was focused on the Y-Si-Al-O-N glasses

[180,181,227,228,230-232,235-237,239,241,244-246], although considerable work was done on La- & Nd-Si-Al-O-N glasses [229,233,238,240,241,243,247,248] and oxynitride glasses containing other rare-earth oxides were also investigated [234].

Most of the research reported in this Section not only focused on the properties of the rare-earth containing oxynitride glasses, but investigated their crystallization behaviour as well. The crystallization of Y-Si-Al-O-N glasses among other phases resulted in apatite structured solid solutions (with composition between $Y_5(SiO_4)_3N$ and $Y_{4.67}(SiO_4)_3O$), $Y_2Si_2O_7$ polymorphs, and minor amount of $Y_2SiO_5$ and YAG crystals [180,181,227,231,234,235,237-239,241,242,244-246].

The crystallization of La- & Nd-Si-Al-O-N glasses among other phases resulted in N-apatite ($Ln_5(SiO_4)_3N$), $Ln_2Si_2O_7$ and $Ln_2SiO_5$ crystals [241], similarly to the Y-Si-Al-O-N glasses.

### 2.3.4. Ln-aluminosilicate glasses

During the studies of rare-earth oxynitride glasses comparative experiments were made with their oxide derivatives i.e. rare-earth silicate [218,249], and rare-earth aluminosilicate [235,237,239-242,245] glasses. The rare-earth aluminosilicate glasses quickly became the subject of expanding research, because these glasses possess a combination of valuable physical properties. Most of the published research results on rare-earth aluminosilicate glasses originated from three major groups of scientists: Makishima *et al.* [250-258], Shelby *et al.* [259-266], and Day *et al.* [267-270].

#### 2.3.4.1. Glass forming abilities

The glass forming region in binary rare-earth silicate systems is restricted, due to

the existence of liquid phase immiscibility in a broad composition range, which dominates the $SiO_2$ rich end of these systems [65,78,174]. Although glasses were prepared in the $Y_2O_3$-$SiO_2$ system at extra high melting temperature (1900-2100°C) with 20-40mol% yttria content, partial crystallization of $Y_2Si_2O_7$ polymorphs was observed, despite the applied rapid cooling [249]. The incorporation of alumina markedly improved the glass forming abilities, and clear ternary rare-earth aluminosilicate glasses were prepared using nearly all types of rare-earth oxide, with the rare-earth content ranging from few percent up to 30mol% [264,266,267], by applying melting temperature up to 1700°C. The highest amount of rare-earth oxide which can be successfully incorporated in the glass varies with rare-earth oxide, e.g. $Y_2O_3$: 28.5mol% [268], $Nd_2O_3$, $La_2O_3$: ~25mol% [252]. Generally, the size of the glass forming region decreased as the field strength ($F=Z/r^2$, where "Z" is the valence of the ion, "r" is the ionic radius) of the rare-earth ion increased (i.e. with decreasing ion radius) [250,264,266]. In addition, phase separation was frequently encountered in rare-earth aluminosilicate glass systems outside the primary glass forming region [260,264-266,268,270,271].

#### 2.3.4.2. The role of rare-earth ions in the glass structure

The structural role of cations in glass is determined by their valence and by their size. The valence of rare-earth cations is generally 3+, although some of them have two possible valences: Ce, Pr, Tb (4+ & 3+) and Sm, Eu, Yb (3+ & 2+) [162]. The ionic radii of rare-earth cations are quite small, and decrease with increasing atomic number (lanthanide contraction) [162]. Presuming predominantly ionic rare-earth-oxygen bonds, Pauling's rules can be applied for the calculation of their co-

ordination. According to the rare-earth - oxygen radius ratios, the rare-earth cations can have six- to ninefold co-ordination to oxygen [272]. Considering the calculated co-ordination numbers, the rare-earth ions occupy network modifier positions in the glass structure [273]. However, due to their small ionic radii, rare-earth cations have relatively large field strength, which is smaller than that of $Si^{4+}$ or $Al^{3+}$, but considerably larger than that of the ordinary modifier ions (e.g. $Na^{+}$, $K^{+}$, $Ca^{2+}$, $Mg^{2+}$, etc.) [266], which has considerable effect on their local structure as well as on the properties of the glass.

The indirect experiments showed that rare-earth ions (e.g. $Y^{3+}$, $La^{3+}$), when added to Na-silicate glass, resulted in linear increase of $T_g$, just like $Ca^{2+}$, therefore they were considered to be network modifiers [274,275]. The structural studies of rare-earth containing glasses by IR and Raman spectroscopy [263,266,276], and by Electron Spin Resonance Spectroscopy (EPR) [277] suggest that the rare-earth cations behave like network modifiers. In addition, the Raman studies showed highly disordered structure, with broad distribution in the types of $SiO_4$ tetrahedra (e.g. with 1, 2, 3, or even 4 non-bridging oxygen per tetrahedron) [263,266], unlike alkali- and alkali-earth aluminosilicate glasses. Moreover, the $^{27}Al$ & $^{29}Si$ MAS-NMR studies of rare-earth aluminosilicate glasses also suggested highly disordered structure, by indicating simultaneous presence of different structural units [262,266]. The direct co-ordination number measurements support the theoretical calculations: $Sm^{3+}$ had $7.1\pm0.7$ co-ordination in a Sm-aluminogermanate glass (Neutron Scattering, [278]); $Eu^{3+}$ occupied 12-fold co-ordination sites in an Eu-aluminosilicate glass ($^{151}Eu$ Mössbauer Spectroscopy, [279]); whereas slightly contrary, the measured co-

ordination of $Nd^{3+}$ was 4.5±1 in a Nd-aluminosilicate glass (Extended X-ray Absorption Fine Structure, [178]).

According to the modified random network (MRN) glass structure model, which was proposed by Greaves [280], the long range randomness in the glass structure co-exists with the short-range order of well defined local environments around network formers, and the medium-range order of well defined environments around modifying cations. This new model can be used to describe the local structure of rare-earth ions in glass [272]. Rare-earth cations, due to their relatively large field strength, tend to strongly co-ordinate the surrounding non-bridging oxygen anions. Nevertheless, the aluminosilicate network is too rigid to allow the creation of such co-ordination spheres, therefore rare-earth cations tend to form rare-earth rich regions in the glass, in order to reduce enthalpy by sharing non-bridging oxygen with other rare-earth cations [176,272]. The existence of molecular scale microclustering, initiated by the above described driving force, was indirectly detected in rare-earth doped glasses used for laser application [176,272]. The addition of extra modifier cation species, even in small amounts, helped to dissolve microclustering and arranging oxygen co-ordination around $Nd^{3+}$ favourable for laser application [176], by getting evenly distributed within the modifier rich regions, and enlarging spacing among the rare-earth cations [272].

### 2.3.4.3. Properties and application of Ln-aluminosilicate glasses

The beneficial effects of rare-earths on the properties of glasses are very similar, due to the close similarity of their essential characteristics. Rare-earth aluminosilicate glasses have high density ($\rho$=2.8-4.5g/cm$^3$) [253,256,257,260,264,266,268-270,273],

high refraction index ($n_D^{20}$=1.55-1.7) [250,253,259,260,266,268-270], high hardness ($H_V$=6.5-9.3GPa) [253,256,257,266,268-270], high elastic modulus (E=95-135GPa) [250,251,253,273], high temperature stability ($T_g$=860-900°C; $M_g$=900-950°C) [257,259,260,264,266,268,270,273], moderate thermal expansion ($\alpha$=3.1-7.0 $MK^{-1}$) [256,259,260,264,266,268-270], high alkaline durability [250,251,257,266-270], high DC electrical resistivity [259,260,268,270], extremely low He permeability [259,266], and low viscosity at melting temperature [266], as well as valuable magneto-optical properties, such as large paramagnetic susceptibility and Verdet constant [261,266]. The observed values of density, refractive index, hardness, elastic modulus, glass transition and softening temperatures, and thermal expansion are due to the incorporation of rare-earth oxides in the glass structure, and their values increased with increasing rare-earth content. Nevertheless, some researchers reported a slight decrease in glass transition and softening temperatures above certain rare-earth concentrations [260,264,266]. In addition, all the other reported properties are improved due to the rare-earth oxide incorporation. Moreover, the glass transition and softening temperatures of rare-earth aluminosilicate glasses containing different rare-earth oxides, increased with the increasing field strength (i.e. decreasing cation radius) of the rare-earth cation, whereas their thermal expansion decreased [259,264].

Similar property improvements were observed in rare-earth alkali-silicate [281-284], gallosilicate [266,284], gallogermanate [266,285], aluminogermanate [286], and borate glasses [266,287-290], due to their rare-earth content. One of the reasons behind the property improvements in rare-earth containing glasses is the considerable field strength and small size of rare-earth cations, which results in high packing

density of atoms and therefore positively affects most of the above listed properties. In addition, they create relatively strong bonds with the surrounding oxygen, and although these bonds are weaker than the silicon-oxygen ones, and being the weakest link in the glassy network structure, they are considerably stronger than the bonds created by other alkaline-, or alkaline-earth modifier ions, which provides high temperature stability.

The rare-earth aluminosilicate glasses would provide refractory glass-to-metal, glass-to-ceramic seals due to their high glass transition temperature, medium ranged thermal expansion, which is easily adjustable by changing the concentration of the rare-earth oxide, and their very high electric resistivity. These glasses can provide a fine replacement for the borosilicate glasses currently used for sealing glass to tungsten or molybdenum [260]. In addition, they can be utilized as hermetic seals due to their extremely low He permeability [259,266].

The high temperature stability and high chemical durability of rare-earth aluminosilicate glasses offer applications in extreme environment. In addition, they can be used as electrical insulators at high temperatures, due to their high temperature stability and high resistivity. Moreover, their high chemical durability and high hardness suggest their application as dental materials.

Their large paramagnetic susceptibility and Verdet constant can be utilized in various magneto-optical applications as Faraday rotators, isolators, modulators, and fast optical switches [261,266]. In addition, their optical properties and their high temperature stability can be utilized in high temperature laser applications.

There is a recently discovered, medical application of rare-earth aluminosilicate glasses. Y/Sm/Ho/Dy-aluminosilicate glass microspheres, activated by neutron

bombardment, can be used as radiation delivery vehicles, which allows an in-vivo (i.e. inside the human body) radiotherapy of cancerous organs [267,269,270]. The glass spheres, which are insoluble in the body, are able to deliver large doses of β-radiation safely to the diseased organ, therefore provide a targeted radiation treatment for tumors without damaging the surrounding healthy tissue [267,269,270].

### 2.3.5. Crystallization of Ln-aluminosilicate glasses

There were limited studies of the crystallization of rare-earth aluminosilicate glasses prior to this research described in this thesis. Some data, which can be related to the crystallization of rare-earth aluminosilicate glasses, as well as to the potential crystalline phases, originated from the post sintering heat treatment studies on $Si_3N_4$ and SiAlON ceramics (Section 2.3.2). The crystallization experiments on rare-earth containing oxynitride glasses also provided useful information (Section 2.3.3).

Direct crystallization studies were performed on Y-silicate glasses prepared initially to model the glassy phase involved in the sintering of $Si_3N_4$ and SiAlON ceramics [218,249]. Heat treatments of partially crystallized yttrium silicate glasses resulted in various polymorphs of Y-disilicate [218,249], leading to $Y_2SiO_5$ and δ-$Y_2Si_2O_7$ above 1600°C [249]. The addition of $ZrO_2$ to Y-silicate glass compositions resulted in $Y_2SiO_5$, $Y_2Si_2O_7$, and an extra phase of cubic $ZrO_2$ after crystallization [249].

Leng-Ward & Lewis [241,242] while studying oxynitride glasses and glass-ceramics, performed a comparative crystallization study on Y-aluminosilicate glasses, and detected $Y_2Si_2O_7$ polymorphs and mullite crystals after heat treatment. In addition, similar crystalline phases, including y-Y-disilicate, were found by Arita *et al.*

[271]. Moreover, crystals of $Sm_2SiO_5$ and $Sm_2Si_2O_7$ were detected by Erbe and Day in heat treated Sm-aluminosilicate glasses [269].

Ping *et al.* [291] studied the crystallization of Y-La-aluminosilicate glasses containing $CaO+CaF_2/MgO+MgF_2$, as well as $SnO_2$, $TiO_2$, $ZrO_2$ or $P_2O_5$ as nucleating agents. As a result, they found $TiO_2$ to be the most effective nucleant. They detected anorthite and gehlenite crystalline phases in the CaO containing compositions, and cordierite in the MgO containing compositions, but they have not identified the rare-earth containing phases.

The most valuable studies were done by Makishima *et al.* [254,255,258]. They investigated the glass forming abilities of Ca-Y-aluminosilicate glasses, and found hexagonal, tubular crystals of Ca-Y-oxyapatite ($Ca_4Y_6(SiO_4)_6O$) in one of the quenched glass compositions [255]. The crystallization of the glass resulted in further Ca-Y-oxyapatite crystals, as well as anorthite and $Y_2Si_2O_7$ at higher temperatures (1100°C & 1200°C, respectively). The glass ceramic material produced was machinable, due to its major phase of Ca-Y-oxyapatite, and had higher hardness, elastic modulus, and fracture toughness, as well as smaller thermal expansion, than the commercially available machinable glass-ceramic (*Macor*) [254,255,258]. In addition, these results were reproduced by Saraswati *et al.* [292].

### 2.3.6. Rare-earth silicate phases and their structure

Since $Y_2O_3$, $La_2O_3$ and $Nd_2O_3$ were used in the current study (Section 2.4), the emphasis in this Section will be on the various Y-, La-, and Nd-silicate crystals and their structure. Due to the rare-earth elements' chemical similarity, pure rare-earth compounds are unknown in nature [293], their minerals normally contain groups of

rare-earths [294]. Nevertheless, there are two minerals which are nearly pure, and predominantly containing yttrium in the rare-earth cation position. One of them is thalenite ($Y_3Si_3O_{10}(OH)$), which has monoclinic structure, and transformed into β-$Y_2Si_2O_7$ upon 1050°C heat treatment [295]. The other one is yttrialite ($(Y,Th)_2Si_2O_7$), which often contains some thorium. Yttrialite also has a monoclinic structure, and transforms into y-$Y_2Si_2O_7$ upon 1000°C heat treatment [295]. The y-$Y_2Si_2O_7$ is an impurity stabilized monoclinic structured crystal, its general formula is $R(Y,Ln)_5Si_6O_{21}$, where R can be $Mg^{2+}$, $Al^{3+}$, etc. [296], and it transforms into α-$Y_2Si_2O_7$ above 1200°C [295].

The structure and polymorphism of various rare-earth silicates are discussed by Bondar & Toropov [297,298], Ito & Johnson [296,299], Liddell & Thompson [295, 300], as well as by Felsche & Hirsinger [293,301-303]. Among them, detailed study on Y-silicates was prepared by Liddell and Thompson [295], whereas Felsche [293] as well as Leskelä & Niinistö [304] presented detailed review on rare-earth silicates.

The synthetic rare-earth silicates, which are of interest to the current study, can be divided into four major groups, such as rare-earth monosilicates, rare-earth disilicates, oxyapatite structured binary and ternary rare-earth silicates, and garnet structured rare-earth Mg-silicates.

Rare-earth monosilicates are often called oxyorthosilicates and have a general formula of $Ln_2SiO_5$ [293,304]. $La_2SiO_5$, and $Nd_2SiO_5$ have monoclinic structure [293], whereas $Y_2SiO_5$ has two modifications, a low and a high temperature one ($X_1$ and $X_2$), both having monoclinic structure [295].

The rare-earth disilicates, $Ln_2Si_2O_7$, show extensive polymorphism [293,304]. The $Y_2Si_2O_7$ has four polymorphs α (triclinic), β (monoclinic), γ (monoclinic), and δ

(orthorhombic) [295,296]. The polymorphs are transformed into each other according to the following schedule: $\alpha \rightarrow \beta$ at 1225°C, $\beta \rightarrow \gamma$ at 1445°C, and $\gamma \rightarrow \delta$ at 1535°C (N/B All arrows are representing reversible reactions) [295,296]. The $La_2Si_2O_7$ and $Nd_2Si_2O_7$ have only two polymorphs, a low temperature tetragonal, and a high temperature polymorph, which was originally identified as pseudo-orthorhombic [302], but according to a recent study, it is proved to be monoclinic [305]. The transformation temperatures of the two polymorphs are ~1214°C for the La-disilicate, and ~1471°C for the Nd-disilicate [302].

The third group of rare-earth silicates have hexagonal, apatite type structure. The apatite structure is particularly susceptible to charge coupled cation (e.g. $Ca^{2+}+P^{5+} \rightarrow Ln^{3+}+Si^{4+}$; $2Ca^{2+} \rightarrow Ln^{3+}+Na^{+}$) [306,307] and anion substitution (Section 2.3.2 & 2.3.3), as well as both cation and anion deficiency [293,303]. Rare-earth elements readily substitute $Ca^{2+}$ in natural apatites [294,306-308], and the detected $Ln_2O_3$ content was even as high as 16wt% [307]. The simple, apatite structured binary rare-earth silicates has a general formula of $Ln_{9.33}[]_{0.67}(SiO_4)_6O_2$, where [] represents cation deficiency [293,295,303]. This type of crystal was reported for Y [295], La [298], and Nd [298]. Apatite structured ternary rare-earth silicates were also identified, having the general formula of $M_2Ln_8(SiO_4)_6O_2$, where M can be $Ca^{2+}$, $Mg^{2+}$, etc. [293,299]. These types of crystals were reported for all rare-earths used in this study (i.e. Y, La & Nd [299]), although XRD data only existed for the Ca bearing crystalline modifications (the reported apatite structured Ca-Y-silicate has slightly different composition: $Ca_4Y_6(SiO_4)_6O$ - JCPDS 27-93). In addition,

Hampshire *et al.* [183] reported the existence of apatite structured $MgNd_4Si_3O_{13}$ crystals (Section 2.3.2), but they may only exist with minor amount of N substitution.

The fourth group of rare-earth silicates has the garnet structure, with the general formula $Mg_3Ln_2(SiO_4)_3$ [293]. Among the rare-earth oxides used in this study, only yttria has this type of silicate: $Mg_3Y_2(SiO_4)_3$ [293].

### 2.4. Specific objectives of the research described in this thesis

1. To examine the glass forming abilities of rare-earth oxide (i.e. $Y_2O_3$, $La_2O_3$, & $Nd_2O_3$) containing alkali-earth aluminosilicate systems (CAS & MAS), by selecting compositions on the tie-lines between the aluminosilicate (i.e. anorthite in the CAS system, and cordierite in the MAS system) and the rare-earth disilicate phases (i.e. $Y_2Si_2O_7$, $La_2Si_2O_7$, and $Nd_2Si_2O_7$).
2. To study the effects of rare-earth oxide incorporation on the physical properties of the glasses, as well as investigate the crystallization behaviour of the quaternary glasses produced.
3. Considering the result of the preliminary crystallization experiments, to select one or two prospective glass systems for detailed investigation, explore the glass forming region in the selected system(s) by working on the previously used or modified tie-line, and perform a study of the physical properties of glasses as well as their crystallization behaviour.
4. To study the effects of heat treatments on the crystalline phase development, as well as on the glass-ceramic microstructure.
5. To prepare rare-earth aluminosilicate glass-ceramics, having diphasic, fine-grained microstructure and investigate their properties.

## CHAPTER 3.

## MATERIALS PREPARATION AND EXPERIMENTAL TECHNIQUES

### 3.1. Glass preparation

Commercially available high purity powders of quartz (Wacomsil, from Japan), $Al_2O_3$ (AnalaR grade, from BDH Ltd.), $CaCO_3$ (AnalaR grade, from Hopkin & Williams), MgO (General Purpose Reagent grade, from BDH Ltd.), $TiO_2$ (Laboratory Reagent grade, from BDH Ltd.), $La_2O_3$ (99.9% REO, from Alfa Products), $Y_2O_3$ (99.99% REO, from Alfa Products) and $Nd_2O_3$ (99.9%, from Aldrich Chemicals Comp.) were used as raw materials. Powders of $La_2O_3$ and $Nd_2O_3$ were hygroscopic and readily formed hydroxides with the moisture content of the air. The decomposition temperatures of these rare-earth hydroxides have been determined by DSC experiments (Netzsch DSC 404, 10°C/min heating rate, and $Al_2O_3$ powder used as the reference material). Two endothermic peaks were observed on the DSC traces of both powders: at 295°C and 495°C for $Nd_2O_3$, and at 345°C and 530°C for $La_2O_3$, which belong to $Nd(OH)_3$, NdOOH, $La(OH)_3$, and LaOOH, respectively. In order to decompose all hydroxyl groups and therefore provide the necessary accuracy for the weighing, the $La_2O_3$ and $Nd_2O_3$ powders have been calcined in an uncovered Pt/Rh crucible at 650°C for 12 hours (heating rate 10°C/min) prior to each mixing. The conversion into $Nd_2O_3$ was clearly indicated by a colour change, since $Nd(OH)_3$ has pink colour, whereas the fully calcined $Nd_2O_3$ has a greyish-blue appearance.

The weighed raw materials (150g batch) were mixed overnight in a sealed glass jar on a rolling mixer. The glasses were prepared from the mixed batches by conventional melting in an uncovered Pt/Rh crucible (90wt% Pt+10wt% Rh) using a resistance heated, high temperature melting furnace (max. temp. 1600°C). The

melting schedule is shown in Fig.3.1. The batches were heated up from room temperature to 1500°C in 2 hours, melted there for 2 hours, then heated up to 1550°C and kept there for a further hour. The glass melts were quenched in distilled water, removed from the crucible, and after drying at 105°C, were put back into the hot furnace for remelting (1500°C/2hr+1550°C/1hr), in order to provide better mixing of the components. After the second melting, part of the molten glass was cast into a graphite coated steel-mould and the rest was water-quenched.

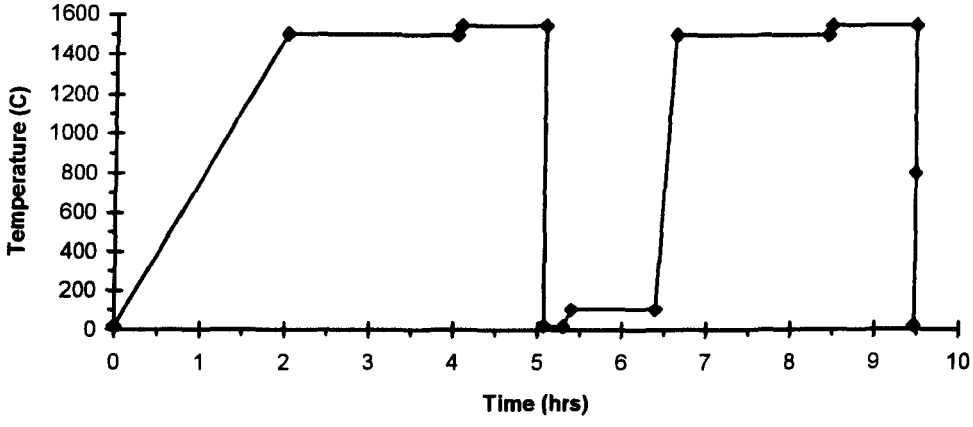


Fig.3.1. The experimental glass melting schedule

The typical size of the glass billets was 60mm x 15mm x 25mm. A representative Mg-Nd-aluminosilicate glass billet is shown in Fig.3.2. The glass billet was taken into a pre-heated, annealing furnace, immediately after a slight solidification of the glass, in order to reduce the build up of thermal stresses, which can cause cracks and can eventually lead to the fracture of the glass billet. There was no exact information on the annealing point of these glasses prior to this work, therefore for the first few glass compositions, a relatively low temperature (600°C) was selected for annealing, in order to avoid any unwanted phase separation or nucleation, but at the same time, provide sufficient time for relaxation of residual stresses by extended duration

(24hrs). After cutting, some of these glass billets resulted in only fragmented slices which proved that this annealing was not sufficient enough, some stresses still remained in the glass (Fig.3.3).

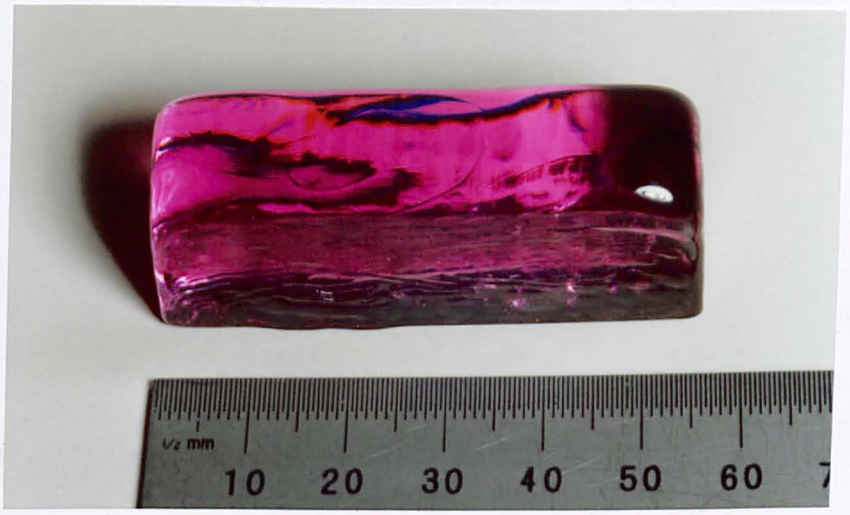


Fig.3.2. A Mg-Nd-aluminosilicate glass billet

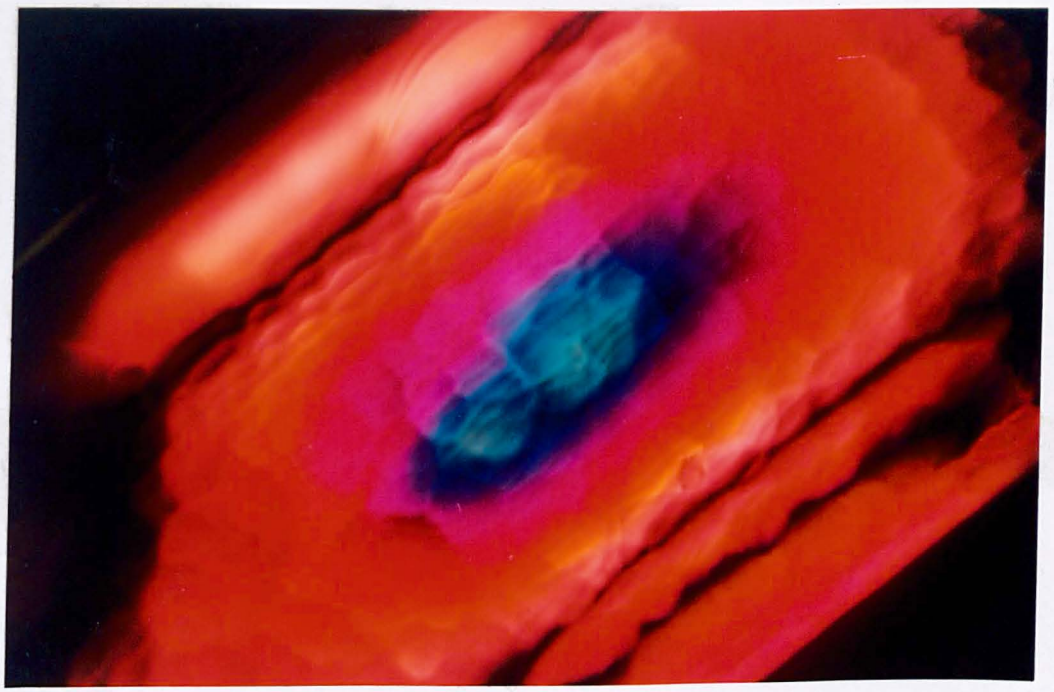

Fig.3.3. Residual stresses in a Mg-Nd-aluminosilicate glass billet (polarised light image)

The annealing was repeated at 800°C for 4 hours, using a temperature slightly below the glass transition of these compositions (as determined by DTA, see Section

4.3.4), which finally removed all residual stresses. This annealing schedule has been used for all further glass compositions.

The glass billets were cut into 3mm thick slices by a 'Capco' diamond cutting machine. After density measurement, some of the glass slices were progressively polished by SiC abrasive papers (220, 320, 400, 600, 800 and 1200 mesh size) and diamond suspensions (9, 6 and 1 μm) to 1μm finish. The polished glass slices have been used for refractive index and hardness measurements, as well as for crystallization experiments.

The water-quenched glass frit was dried, then it was crushed in a steel mortar to size under 90μm. The small fragments of steel impurities were removed by a magnet and the glass powder was ball-milled for 24 hours in an $Al_2O_3$ mill with $Al_2O_3$ balls and methanol was used as grinding medium. The slurry was sieved through a 38 μm sieve, then it was dried at room temperature under an extraction hood. As the SEM study of the crystalline pellets made of powders prepared by this method revealed, they contained fragmented pieces of $Al_2O_3$ originating from the mill and the grinding balls, which can cause defects in the structure of the final glass-ceramic product. In order to avoid this contamination the milling process was modified after the first six glass compositions. The glass frit was crushed as before, but hot isostatically pressed $Si_3N_4$ grinding bodies, having higher fracture toughness were used in a plastic mill. In addition, the grinding time was increased to 48 hours and isopropyl alcohol was used as grinding medium. The slurry was sieved and dried as before. Nevertheless, this grinding method left plastic contamination in the powder, originating from the mill. This contamination was removed by a gradual burn-out process using the following heat treatment schedule: the powders were heated from 100°C to 500°C with 50°C steps and were held at each temperature for an hour (Fig.3.4). The necessary burn

out temperature was determined by a DTA experiment. Both milling processes provided fine (≤1-2 μm in size) glass powder. The ball-milled powders were used for DTA and crystallization experiments.

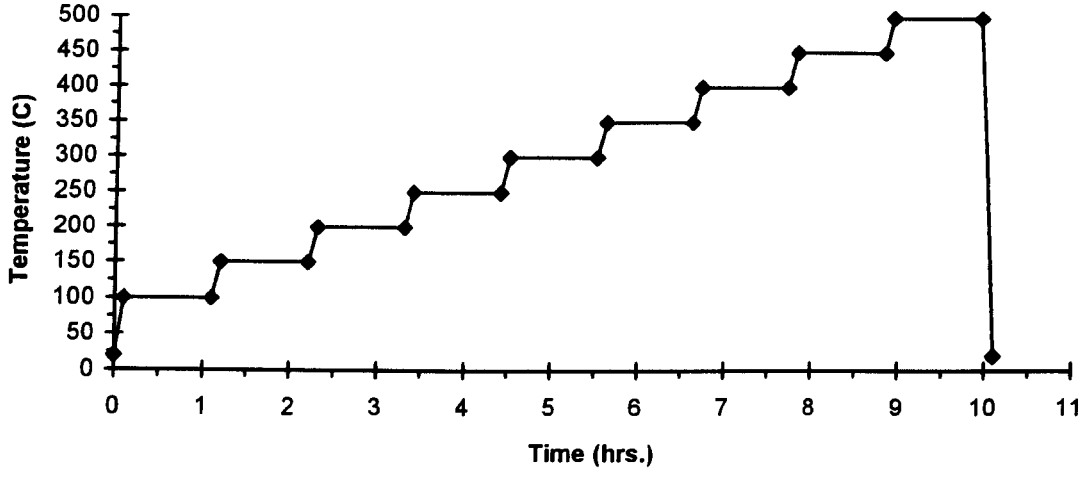


Fig.3.4. Heat treatment schedule of the plastic contamination burn out.

In addition, part of the water-quenched glass frit was hand-ground by agate pestle and mortar. These powders were used for DTA experiments as well as for some comparative crystallization studies.

### 3.2. Crystallization and Hot Pressing

Single step heat treatments were used for crystallization. The samples were heated to the crystallization temperature using 5°C/min heating rate (the kilns used for the crystallization experiments can only maintain this or a slightly higher heating rate above 1000°C), were kept there from 10 minutes up to 10 hours and were cooled down to room temperature with 5°/min cooling rate. The heat treatment schedule is shown in Fig.3.5. Resistance heated pottery kilns (max. temp.=1200°C)

as well as a high temperature furnace (max. temp.=1600°C) were used for the crystallization experiments.

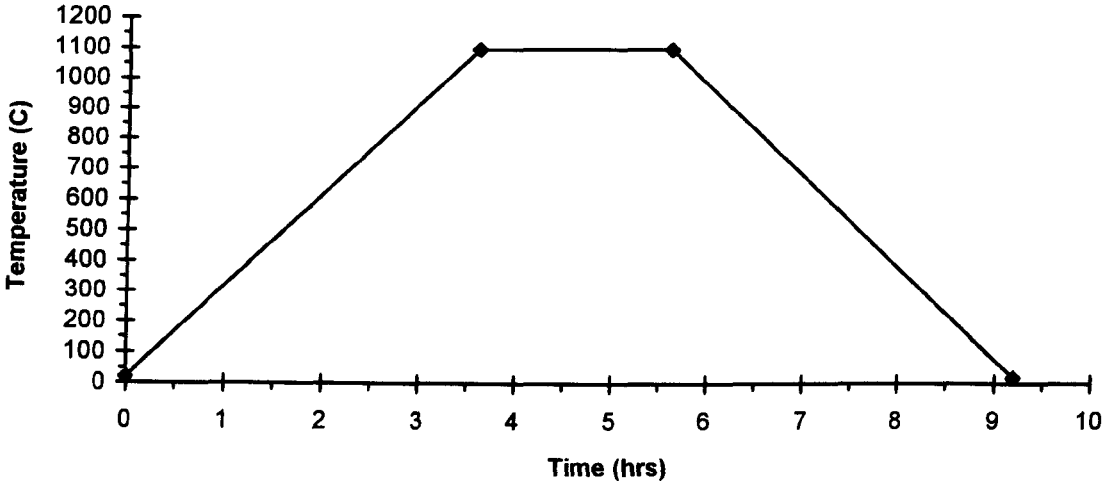


Fig.3.5. A typical crystallization heat treatment schedule.

Four types of samples were crystallized simultaneously, representing 3 different crystallization mechanisms (Section 2.4): polished-surface bulk glass slices (1μm surface finish); rough surfaced bulk glass slices (as cut); ball-milled, loose powders; and isostatically pressed pellets (from ball-milled powder). The latter two, which did not differ in crystallization mechanism, were used for different purposes: the sintered pellets were needed for SEM and TEM study, whereas the sintered powder, which was easier to crush and hand grind, was used for XRD measurements. The rough surfaced bulk glass samples only differ marginally from the polished bulk glasses, therefore after the first few crystallization experiments only polished bulk glasses were crystallized. In addition, occasionally, hand-ground powders (by agate pestle and mortar) were crystallized along with the other samples in order to find out whether their crystallization behaviour differed from the ball-milled powders. The crystallized bulk glasses were cut into three pieces by a 'Capco' diamond cutting machine: the first one was used for XRD measurements, the second one was used for

surface SEM study (and later on for TEM), and the third one was used for cross-sectional SEM investigation. In addition, some crystallized glass specimens, which showed interesting crystalline features, were studied by optical microscopy using a WILD Photomakroskop (type: M400) equipped with a WILD Photoautomat (type: MPS55).

Hot pressing was used to prepare sizeable glass-ceramic test specimens for mechanical testing. A home made, computer interfaced, radiofrequency (RF) heated, high temperature, uniaxial hot press equipment was used for the experiments. The schematic drawing of the equipment is shown in Fig.3.6.

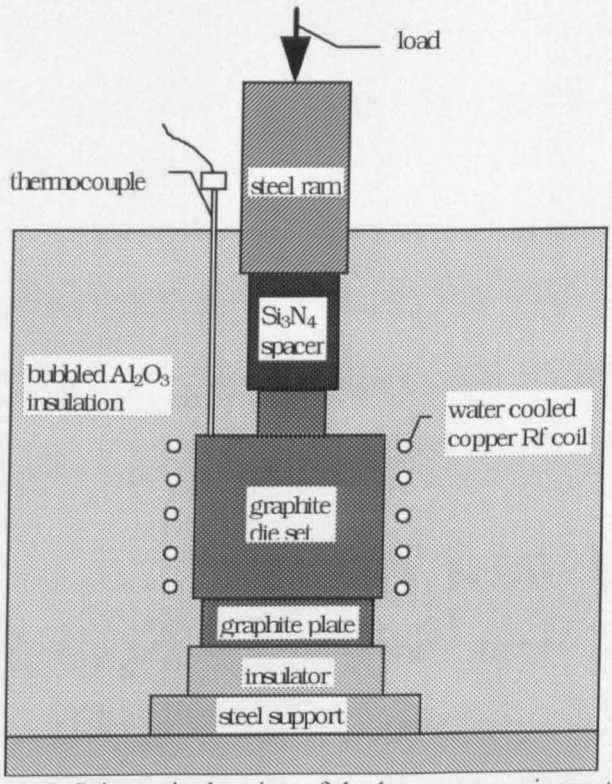


Fig.3.6. Schematic drawing of the hot press equipment.

The glass powder was loaded into a graphite die, which acted as a susceptor. The graphite die was coated inside with a thin BN layer before each experiment, in order to avoid direct contact and possible reaction of the samples with the die. In addition, thin molybdenum foils were placed under and above the glass powder. At the

beginning of the experiment the steel ram of the hot press was lowered to the die and a small, base pressure was applied on the glass powder. This pressure was held until the glass powder was heated, at 10°C/min, to the glass transition temperature. Then the pressure was increased to 5MPa in order to utilize the glass' viscous flow to enhance the densification and to provide, preferably, poreless specimens. After 5 minutes holding time the temperature was increased with the same heating rate to the actual crystallization temperature. After 2 hours of crystallization the furnace was switched off and it was allowed to cool down naturally. The pressure was decreased to zero at around 600°C. The temperature and pressure schedule are shown in Fig.3.7. The heat treatment and pressure schedules were similar to the ones which had been used for the preparation of SiC fibre reinforced magnesium aluminosilicate glass-ceramic matrix composites [138].

The 30mm x 30mm ceramic plates prepared were surface ground (Jones & Shipman surface grinder) to get two parallel faces, and then were sliced into 3mm wide test bars by a 'Capco' diamond cutting machine. The test bars were progressively polished on three faces by an automatic polishing machine (Buehler Metaserv Monopol 12) using diamond abrasive wheels and diamond suspensions (30, 6 and 1 μm) to 1 μm finish. Prior to polishing, the edges of the test bars were chamfered in order to avoid edge chipping, which could introduce flaws, and therefore could substantially reduce the strength of the test bars. The test bars were used for density, thermal expansion, hardness and flexural strength measurements.

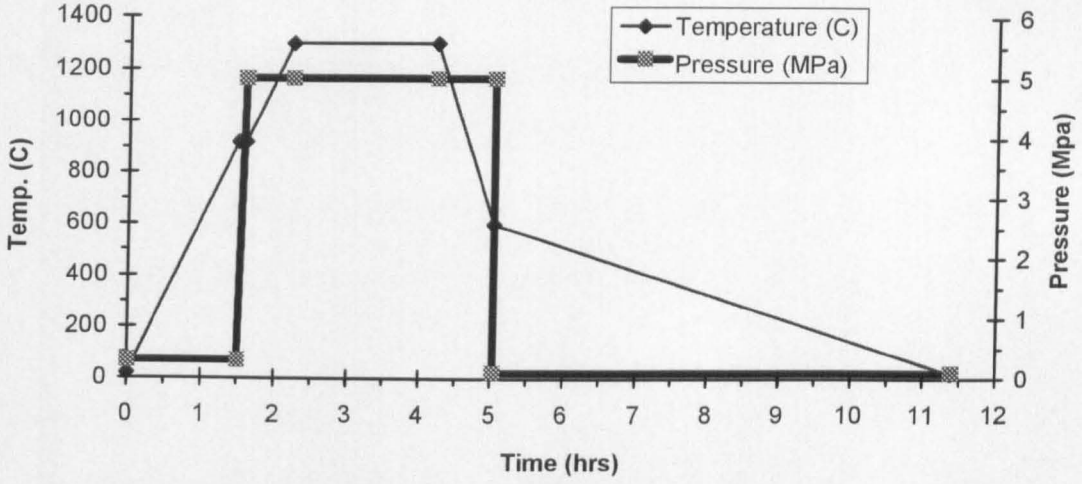


Fig.3.7. Hot pressing heat treatment and pressure schedule.

### 3.3. Density Measurement

The classical Archimedes' method was used for measuring the density of glass slices and hot-pressed test bars, using a digital balance (Precisa 125A). At first, the dry weight of specimens ($m_1$) was measured and then the wet weight ($m_2$), while samples were submerged in distilled water. By measuring the temperature of the distilled water, and knowing the density of water as a function of temperature [309], the density of specimens ($d_s$) can be calculated as follows:

$$d_s = \frac{m_1}{\frac{(m_1 - m_2)}{d_w}} \qquad (3.1.)$$

where $d_w$ is the density of water at the actual temperature.

7-13 parallel density measurements have been done with each glass and glass-ceramic composition, depending on the number of the available glass slices and test bars having similar shape and similar dry weight.

### 3.4. Measurement of Refractive Index ($n_D^{20}$)

The refractive index of the glasses was measured by a Rayner Dialdex refractometer. The refractometer was illuminated by a LED emitting light at the wavelength of the Na yellow line ($\lambda$=589.6nm), and Rayner refractometer fluid ($n_D^{20}$=1.810) was applied as contact liquid. Glass slices, progressively polished to 1$\mu$m surface finish on the contact side, were used for the measurement.

### 3.5. Hardness Measurement

Vickers indentation method was used to measure the hardness of the glasses and glass-ceramics prepared, and to get some information on their fracture toughness. A standard pyramidal Vickers diamond indenter (apex angles=136°) was applied with loads high enough to initiate radial cracks, 39.2N for the Mg-Nd-aluminosilicate and 19.6N for the Ca-Nd-aluminosilicate glass ceramics. In order to provide comparability between the parent glasses and their glass ceramic derivatives the same load values were used for the Mg-Ln-aluminosilicate and Ca-Ln-aluminosilicate glasses, respectively. An Instron 1122 universal testing equipment (loadcell: 0-50kg) was used for the experiment. The schematic drawing of the indentation arrangement is shown in Fig.3.8. During an indentation cycle the indenter was lowered towards the sample with the speed of 0.05mm/min, and after the indenter touched the sample surface, a load was applied until it reached the pre-set value. The load was maintained for 15 second, then the indenter was lifted up with the same speed as before. The load was measured by the loadcell, and the load versus time graph was recorded on a chart recorder. The tests were carried out on polished surfaced glass slices and glass-ceramic test bars (Section 3.1 & 3.2).

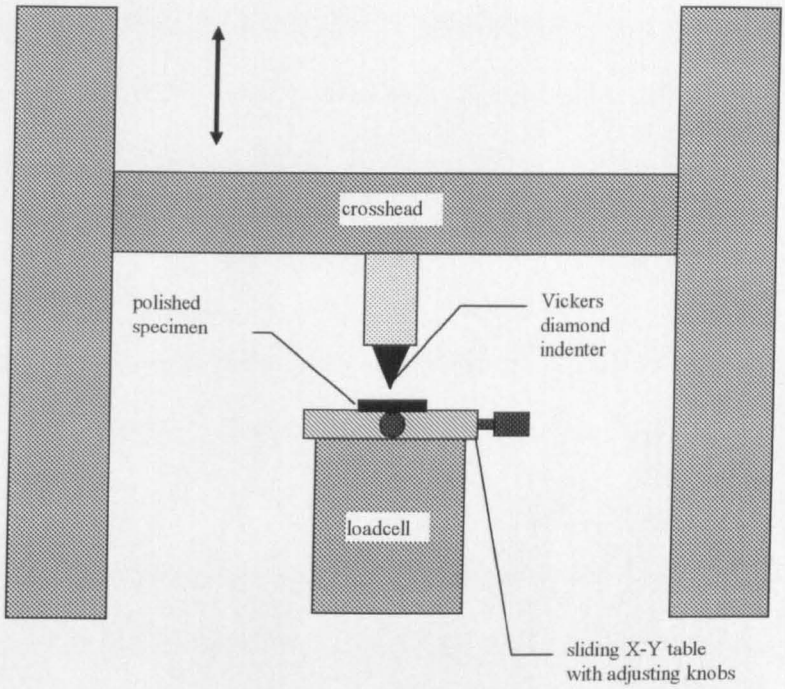


Fig.3.8. Schematic drawing of the indentation arrangement.

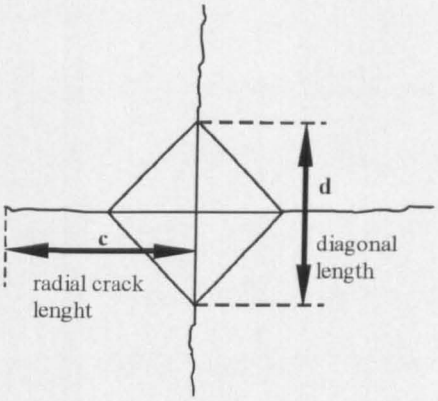


Fig.3.9. Surface view of a Vickers indent.

The surface view of a typical Vickers indent is shown in Fig.3.9. The size of the indent diagonals and the length of radial cracks were measured by optical microscopy using an Olympus BH-2 microscope with a calibrated eyepiece graticule. The following equation was used for the calculation of Vickers hardness [159]:

$$H_V = 1854.4\frac{P}{d^2} \qquad (3.2.)$$

where: $H_V$= Vickers hardness (in GPa); P= applied load (in N); d= diagonal length of the indentation (in μm).

According to McColm ([159] after [310]) the following equation can be used to calculate the indentation fracture toughness of ceramics with 20-30% confidence level where no data for Young's modulus is available:

$$K_{Ic} = 0.16 H_v a^{1/2} \left(\frac{c}{a}\right)^{-3/2} \qquad (3.3.)$$

where: $K_{ic}$= the indentation fracture toughness (in $MPam^{1/2}$); a= the half diagonal length of the indentation (in μm); c= the surface radial crack length (in μm).

### 3.6. Fracture Toughness Measurement via Indent Initiated Bend Test

Indent initiated 4-point bend test was applied to get some information on the fracture toughness of these newly developed glass-ceramic materials. The indentation introduces a major flaw, which in turn will act as the crack origin, and therefore reduces the scattering of the results. The test bar preparation was described in Section 3.2. A Vickers indent was placed on the tensile surface of the polished surfaced test bars using 19.6N load. The previously mentioned Instron 1122 universal testing machine with a 0-50 kg loadcell was used for the 4-point bend test. The experimental arrangement is shown in Fig.3.10. The moving crosshead was lowered onto the inner rods (via the brass support) with the speed of 0.05mm/min and the load was measured by the loadcell and recorded by a chart recorder. The stress at fracture ($\sigma_f$ - in MPa) can be calculated by the standard equation for the 4-point bend test [311]:

$$\sigma_f = \frac{3P(L-l)}{2bd^2} \qquad (3.4.)$$

where P= load at fracture (in N); L= the outer span (in mm); l= the inner span (in mm); b= the specimen width (in mm); d= the specimen thickness (in mm).

The following equation can be used for the calculation of fracture toughness in case of an indent initiated fracture [159]:

$$K_{Ic} = 0.59\left[\sigma_f P^{1/3}\right]^{3/4}\left(\frac{E}{H_V}\right)^{1/8} \qquad (3.5.)$$

where: $K_{Ic}$= the fracture toughness (in $MPam^{1/2}$); P= the indent load (in N); E= Youngs modulus (in GPa); $H_V$= the Vickers hardness (in GPa).

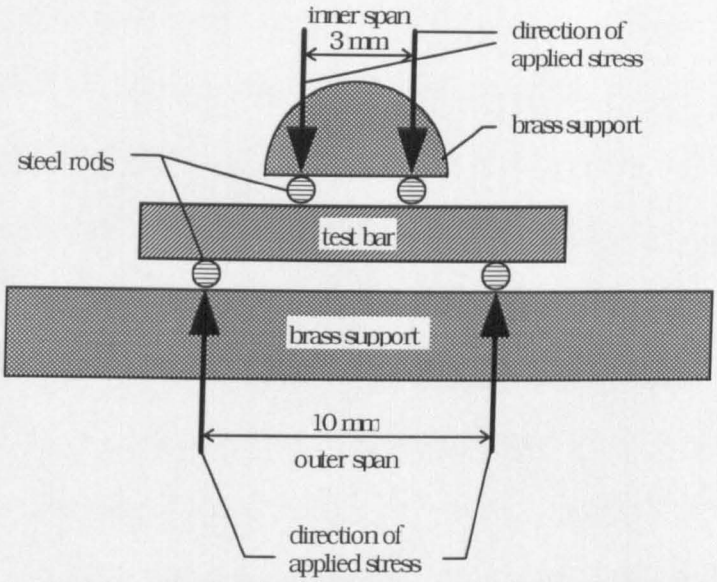


Fig.3.10. Schematic drawing of the four-point bend test apparatus.

However, the elastic modulus of these glass-ceramics is not known, therefore an alternative way had to be found. According to McColm [159], by removing the $E/H_V$ term and replacing the 0.59 factor with 0.88, will add only 10% to the error of estimation. Therefore the equation used for the calculation of the indent initiated fracture toughness was:

$$K_{Ic} = 0.88\left[\sigma_f P^{1/3}\right]^{3/4} \qquad (3.6.)$$

### 3.7. Differential Thermal Analysis (DTA)

Differential Thermal Analysis (DTA) was used for determination of crystallization temperatures of the glasses produced ($T_{cr}$), and also for estimation of their important viscosity points (i.e. glass transition temperature, $T_g$; and softening point, $M_g$) as well as the temperature of the first melting ($T_m$) of a given composition.

Computer interfaced high temperature DTA equipment (Stanton-Redcroft DTA 673-4, max. temp. 1500°C) was used for the measurements, with fine quartz powder (Wacomsil, from Japan) as the reference material. The advantage of using quartz as a reference material relies on the polymorphic transformation of α-quartz into β-quartz (573°C), which can be used as an in-situ calibration standard for the temperature scale of the DTA trace.

DTA measurements were carried out with both hand-ground and ball-milled powders (Section 3.1), using identical experimental conditions. Approximately 0.20-0.23g glass powder were weighed into standard Pt DTA crucibles. Most of the DTA experiments quoted in the literature used 5 or 10°C/min heating rate. In this particular case 5°C/min has been selected, in order to apply the same heating rate for both DTA and crystallization experiments (Section 3.2).

### 3.8. Measurement of Linear Thermal Expansion Coefficient (α)

A computer interfaced high temperature dilatometer (Netzsch 402-E; max. temp. 1500°C) was used for the measurements of linear thermal expansion coefficient (α) of the glasses and their glass-ceramic derivatives. The dilatometer had a horizontal arrangement and an alumina push rod transferred the thermal expansion of the specimens to the linear variable differential transformer (LVDT), which converted it

into an electrical output. Glass bars of approx. 20-30mm (cut from the previously prepared glass slices) and glass-ceramic test bars approx. 28-30mm (prepared for hardness measurement, without fine polishing) were used for the experiments. The ends of both types of sample were ground flat and parallel, in order to get proper contact with the push rod and the support end. The specimens were heated up with a constant, 5°C/min heating rate, until the specimens showed the first sign of softening.

### 3.9. X-Ray Powder Diffraction (XRD)

X-Ray Powder Diffraction (XRD) was used for identification of crystalline phases in the heat treated samples, as well as for checking any crystalline contamination in the ground powders. A computer interfaced Philips X-ray Diffractometer (X-ray generator type: PW 1130/00; goniometer type: PW 1380/00) was used for the measurements, with Cu $K\alpha_1$ & $K\alpha_2$ radiation. The scanning speed was 1°/min in $2\theta$, and each sample was scanned from 10° to 70° ($2\theta$). The well-known Bragg equation was used for calculating the "d" values of reflections:

$$\lambda = 2d\sin\theta \qquad (3.7.)$$

where $\lambda$ = the wavelength of the X-ray radiation (for Cu K$\alpha$ $\lambda=1.54178*10^{-10}$ m); d = the interplanar spacing (in $10^{-10}$ m); $\theta$ = the angle between the X-ray beam and Bragg plane.

Crystalline phases were identified with the help of JCPDS powder diffraction files. In addition, other results from the literature [295,296,300-302] were used for the identification of the rare-earth silicate phases. The specimens were wrapped in plastic bags (in order to avoid contamination) and crushed by a hammer and then hand-

ground with agate pestle and mortar. The fine powders were lightly pressed to the window of a standard Al XRD sample holder.

### 3.10. Scanning Electron Microscopy (SEM)

Scanning Electron Microscopy (SEM) was used for microstructural analysis, and identification of crystalline phases based on their morphology and their chemical composition (determined by Energy Dispersive X-ray Microanalysis - EDS), as well as using additional analytical information provided by the complementary technique of XRD. At the beginning, Cambridge Stereoscan 250MK3 SEM equipped with LINK AN 10/855 EDS system was used. Later on JEOL JSM 6100 SEM with LINK eXLII system was used, because it provided slightly better image resolution, which is important in the case of extra fine grained microstructures. In addition, it was equipped with a high take-off angle X-ray detector, which did not require the tilt of the specimen for analysis. This detector arrangement made it possible to analyse small crystallites ($\leq 1 \mu m$) with reasonable accuracy, using 10kV accelerating voltage.

The surface of the crystallized bulk glasses (after cutting) was studied in the as-received state. The cross section of the bulk glass samples and the isostatically pressed and sintered pellets were progressively polished by SiC abrasive papers and diamond suspensions to 1 μm finish. The specimens were glued on standard Al SEM stubs with conductive carbon cement, the edges of the specimens were coated with graphite paint, and after drying, the surface of the specimens were carbon coated in order to avoid charging under the electron beam.

### 3.11. Transmission Electron Microscopy (TEM)

Transmission Electron Microscopy (TEM) was used for refined microstructural analysis and identification of crystalline phases by means of Energy Dispersive X-ray Microanalysis (EDS) and both Selected Area- and Microbeam Electron Diffraction. JEOL JEM 2000FX system was used, at 200kV accelerating voltage, equipped with LINK eXLII EDS system. TEM samples were prepared from 300 μm thick slices, which were cut from the crystalline samples by 'Capco' diamond cutting machine. The slices were mechanically thinned down to <50μm in thickness, and were progressively polished on both sides by SiC abrasive papers and diamond suspensions to 1μm finish. The thin slices were glued on standard brass TEM rings (~2mm in diameter) with Araldite resin, and ion-beam thinned by accelerated Ar ions in a standard ion-beam thinner (the angle of bombardment was 25°). The thinned specimens were given a light C-coating on both sides in order to avoid charging under the electron beam.

## CHAPTER 4.

# GLASS CHARACTERIZATION IN THE Ln CONTAINING Ca- AND Mg-ALUMINOSILICATE SYSTEMS

### 4.1. Compositions selected for investigation

Two major systems were selected for investigation: magnesium-aluminosilicate (MAS) and calcium-aluminosilicate (CAS) systems for incorporating rare-earth oxides ($La_2O_3$, $Nd_2O_3$, $Y_2O_3$). The crystallization of glasses from both pure aluminosilicate systems was the focus of interest of several research studies (especially the crystallization of MAS), because of the favourable physical and mechanical properties of their glass-ceramic derivatives (Section 2.2). The rare-earth oxide addition could further improve their properties, and the rare-earth oxides selected for this study are the most easily available, and therefore most frequently used for glass and ceramic applications.

The first six glass compositions were selected on the tie lines between the alkali-earth aluminosilicate (anorthite in the CAS and cordierite in the MAS system) and rare-earth disilicate compositions in order to use them as parent glasses, and create diphasic glass-ceramic materials which would contain the aluminosilicate phase with low thermal expansion coefficient and rare-earth disilicate phase with higher thermal expansion. It would be possible to tailor the thermal expansion and other physical properties of these glass-ceramics to the requirement of certain applications by the ratio and morphology of these crystalline phases via the modification of the parent glass composition and the heat treatment. In addition, the simultaneous crystallization of two crystalline phases presumably results in a fine grained microstructure and the glassy residue can be preferably reduced to a minimal amount. Another reason for this

selection was to simplify these originally quaternary systems and handle them as pseudo-binary systems, which makes for easier interpretation of their crystallization.

The initial glasses had the composition of ~30mol% rare-earth disilicate and ~70mol% alkali-earth aluminosilicate (except for the $Y_2O_3$ -MAS composition, which had a composition of 36mol% Y-disilicate and 64mol% cordierite). Considering the glass forming and crystallization characteristics of these glasses and the microstructure of their glass-ceramic derivatives, two systems were selected for detailed investigation: the Nd containing MAS and CAS systems. As described below (Section 4.2 & Chapter 5), it was found that in the Ca-Ln-aluminosilicate systems the crystallizing rare-earth containing phases were not rare-earth disilicates as originally thought, but Ca-Ln-silicate phases, indicating the real equilibrium phases and real tie-lines in these systems, therefore the Nd-CAS compositions were calculated along this modified tie-line (anorthite - Ca-Nd-silicate). In addition, some titania containing glass compositions were made both in the Nd containing MAS and CAS systems, in order to evaluate the suitability or unsuitability of titania as nucleating agent enhancing bulk nucleation in these glass systems.

## 4.2. Glass forming abilities

a) Glass forming in the Ca-Ln-aluminosilicate systems

The compositions of the studied Ca-Ln-aluminosilicate glasses are shown in Table 4.1. It contains the planned glass compositions, according to the amount of expected major crystalline components (after crystallization); the calculated oxide composition both in mol% and wt%; as well as the SEM/EDS analysed composition of the melted glasses. The EDS analyses were done on fragmented glass pieces, using 10 kV accelerating voltage, area analysis mode at magnifications of x5000-7000, and

the presented results are the average of 20 measurements, done on different, relatively flat glass areas. The difference between the calculated and analysed amount of Nd and La can be a result of their X-ray intensity was measured on their characteristic L-lines, whereas the other components as Al and Si were analysed on their K-lines. The analysis of the $Y_2O_3$ containing glass composition resulted in a major overestimation of yttria which originated from the spectrum processing side, because the yttrium L-lines overlap the Si K-line, and after peak deconvolution the intensity of the yttrium peaks are overestimated, especially in the case of silica rich compositions. Generally, the calculated and analysed glass compositions were in good correlation (Table 4.1).

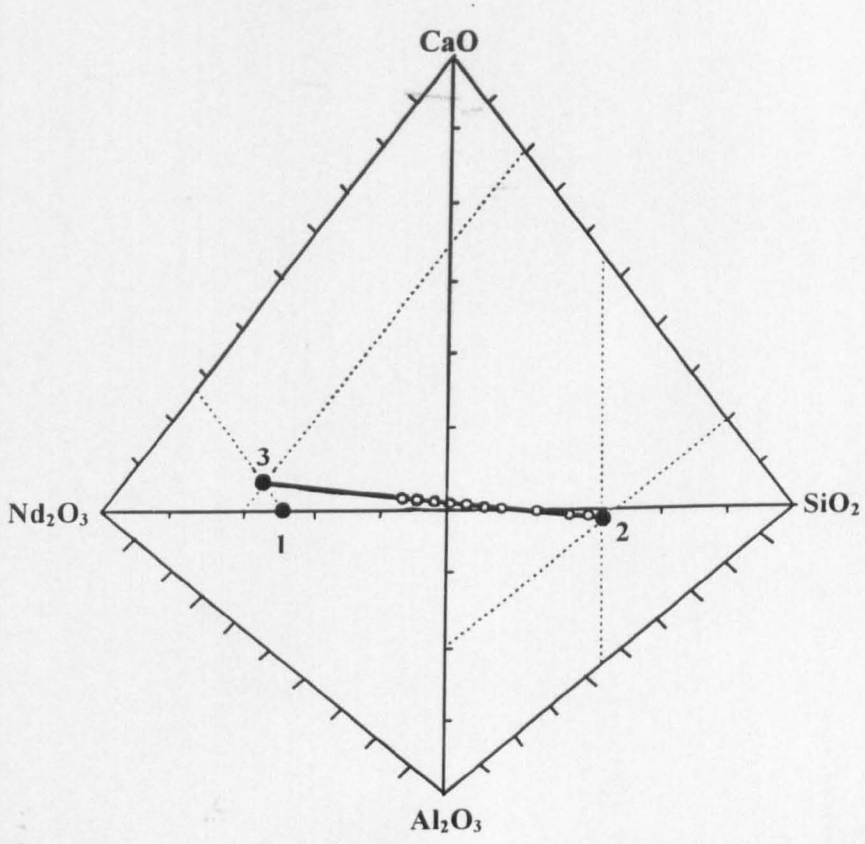


Fig.4.1: Glass compositions in the Ca-Nd-aluminosilicate system. **1)** the composition of $Nd_2Si_2O_7$, **2)** the composition of anorthite **3)** the composition of $Ca_2Nd_8(SiO_4)_6O_2$, and the empty circles represent the melted glass compositions. The scales of the diagram represent weight percentages. The diagram serves as a visual aid, and not designed to provide exact quantitative information (please use Table 4.1 instead).

Table 4.1. Compositions of Ca-Ln-aluminosilicate glasses

| | major components (wt%) | | | oxide components (mol%) | | | | | oxide components (wt%), calc. | | | | | oxide components (wt%) meas. | | | | |
|---|---|---|---|---|---|---|---|---|---|---|---|---|---|---|---|---|---|---|
| Code | Ca-Nd-silicate | anorthite | TiO2 | Nd2O3 | CaO | Al2O3 | SiO2 | TiO2 | Nd2O3 | CaO | Al2O3 | SiO2 | TiO2 | Nd2O3 | CaO | Al2O3 | SiO2 | TiO2 |
| CAS | 0 | 100 | 0 | 0.0 | 25.0 | 25.0 | 50.0 | 0.0 | 0.0 | 20.2 | 36.6 | 43.2 | 0.0 | 0.0 | 21.0 | 35.6 | 43.4 | 0.0 |
| CASN-13 | 5 | 95 | 0 | 0.8 | 24.8 | 24.4 | 50.0 | 0.0 | 3.7 | 19.5 | 34.8 | 42.0 | 0.0 | 3.8 | 19.6 | 34.9 | 41.7 | 0.0 |
| CASN-11 | 10 | 90 | 0 | 1.6 | 24.6 | 23.8 | 50.0 | 0.0 | 7.4 | 18.8 | 33.0 | 40.9 | 0.0 | 8.7 | 19.0 | 32.5 | 39.8 | 0.0 |
| CASN-10 | 20 | 80 | 0 | 3.4 | 24.1 | 22.4 | 50.0 | 0.0 | 14.8 | 17.4 | 29.3 | 38.5 | 0.0 | 16.2 | 17.0 | 29.1 | 37.7 | 0.0 |
| CASN-8 | 30 | 70 | 0 | 5.5 | 23.6 | 20.9 | 50.0 | 0.0 | 22.2 | 16.0 | 25.7 | 36.2 | 0.0 | 23.1 | 15.8 | 25.6 | 35.5 | 0.0 |
| CASN-7 | 35 | 65 | 0 | 6.6 | 23.3 | 20.0 | 50.0 | 0.0 | 25.9 | 15.3 | 23.8 | 35.0 | 0.0 | 26.2 | 15.0 | 24.4 | 34.4 | 0.0 |
| CASN-6 | 40 | 60 | 0 | 7.8 | 23.0 | 19.1 | 50.0 | 0.0 | 29.6 | 14.6 | 22.0 | 33.8 | 0.0 | 30.6 | 14.0 | 22.0 | 33.4 | 0.0 |
| CASN-5 | 45 | 55 | 0 | 9.1 | 22.7 | 18.2 | 50.0 | 0.0 | 33.3 | 13.9 | 20.2 | 32.7 | 0.0 | 35.6 | 13.5 | 19.3 | 31.6 | 0.0 |
| CASN-9 | 50 | 50 | 0 | 10.5 | 22.4 | 17.1 | 50.0 | 0.0 | 37.0 | 13.2 | 18.3 | 31.5 | 0.0 | 39.0 | 12.7 | 17.8 | 30.5 | 0.0 |
| CASN-12 | 55 | 45 | 0 | 12.0 | 22.0 | 16.0 | 50.0 | 0.0 | 40.7 | 12.5 | 16.5 | 30.3 | 0.0 | 41.7 | 12.5 | 17.0 | 28.8 | 0.0 |
| CASN9-T1 | 45 | 45 | 10 | 9.3 | 19.8 | 15.1 | 44.1 | 11.7 | 33.3 | 11.8 | 16.5 | 28.4 | 10.0 | 35.9 | 11.6 | 15.5 | 27.3 | 9.7 |
| CASN12-T1# | 49.5 | 40.5 | 10 | 10.5 | 19.3 | 14.1 | 43.9 | 12.1 | 36.6 | 11.2 | 14.8 | 27.3 | 10.0 | 30.2 | 12.7 | 16.7 | 26.8 | 13.6 |
| Code | Nd-disilicate | anorthite | TiO2 | Nd2O3 | CaO | Al2O3 | SiO2 | TiO2 | Nd2O3 | CaO | Al2O3 | SiO2 | TiO2 | Nd2O3 | CaO | Al2O3 | SiO2 | TiO2 |
| CASN-1* | 41.3 | 58.7 | 0 | 8.1 | 18.9 | 18.9 | 54.1 | 0.0 | 30.4 | 11.8 | 21.5 | 36.2 | 0.0 | 33.1 | 11.2 | 21.5 | 34.2 | 0.0 |
| Code | La-disilicate | anorthite | TiO2 | La2O3 | CaO | Al2O3 | SiO2 | TiO2 | La2O3 | CaO | Al2O3 | SiO2 | TiO2 | La2O3 | CaO | Al2O3 | SiO2 | TiO2 |
| CASL-1* | 40.7 | 59.3 | 0 | 8.1 | 18.9 | 18.9 | 54.1 | 0.0 | 29.7 | 12.0 | 21.7 | 36.6 | 0.0 | 33.0 | 12.1 | 19.9 | 35.0 | 0.0 |
| CASL-2 | 34.8 | 65.2 | 0 | 6.7 | 20.0 | 20.0 | 53.3 | 0.0 | 25.4 | 13.1 | 23.9 | 37.5 | 0.0 | 28.5 | 13.5 | 22.7 | 35.3 | 0.0 |
| Code | Y-disilicate | anorthite | TiO2 | Y2O3 | CaO | Al2O3 | SiO2 | TiO2 | Y2O3 | CaO | Al2O3 | SiO2 | TiO2 | Y2O3 | CaO | Al2O3 | SiO2 | TiO2 |
| CASY-1 | 34.8 | 65.2 | 0 | 8.1 | 18.9 | 18.9 | 54.1 | 0.0 | 22.7 | 13.1 | 23.9 | 40.3 | 0.0 | 34.4 | 12.3 | 33.1 | 20.2 | 0.0 |

*The CASN-1 and CASL-1 compositions did not melt properly, therefore the glass compositions differ from the planned ones.
The real glass compositions are: ~44.8 wt% Ca-Nd-silicate and ~55.2 wt% anorthite; ~ 45.0 wt% La-Nd-silicate and ~ 55.0wt% anorthite, respectively (calculated from the analysed glass composition).
#Small amount of crystalline residue remained after melting of CASN12-T1, therefore the glass composition was shifted away from the planned one.

The Y containing CAS composition melted properly and no bubbles or inclusions were found in the cast glass billet. However, the initial La and Nd containing CAS compositions did not melt properly and some crystalline residue remained in the crucible after melting, but the cast glass billets seemed homogeneous and were free of bubbles and inclusions. The XRD and SEM/EDS analysis of the crystalline residues showed that they contain crystals of $Ca_2La_8(SiO_4)_6O_2$ and $Ca_2Nd_8(SiO_4)_6O_2$, respectively. In addition, the SEM/EDS analysis of the glasses showed, that their compositions are nearly on the tie-line of anorthite and the actual Ca-Ln-silicate phase. In the light of these new results the further compositions in the Ca-Nd-aluminosilicate system were calculated on the tie-line of Ca-Nd-silicate and anorthite (Fig.4.1).

The Nd containing CAS glass compositions showed good glass forming characteristics, melted properly and resulted in glass rods free from bubbles or inclusions, except for CASN-12, the highest Ca-Nd-silicate content composition (55wt%), which melted properly, but the glass billet partly crystallized during casting. In addition, poor melting happened in the case of one of the titania containing compositions, CASN12-T1 (Ca-Nd silicate content was 49.5wt%), though the melt had unusually low viscosity, a small amount of crystalline residue remained in the crucible after melting, which resulted in a shift of the glass composition. Moreover, the glass of the pure anorthite composition, which was used for comparison, melted properly without any residue, but the cast glass billet contained microscopic sized air bubbles, which suggests that the glass melt was too viscous at the temperature applied, and in order to provide good refining of this composition, slightly higher melting temperature or application of viscosity lowering additives would be required. The yttrium and lanthanum calcium aluminosilicate glasses were transparent colourless, whereas the neodymium containing ones were purple in colour.

The highest amount of $Nd_2O_3$ which was successfully incorporated in the structure of calcium-aluminosilicate glasses was 12mol%, which is about half of the reported maximum achievable amount of ~25mol% $Nd_2O_3$ in aluminosilicate glasses [M-7]. However, by summarizing the amount of $Nd_2O_3$ and that of CaO (normalized to the 3+ cation charge), the estimated maximum amount of $Nd_2O_3$, which can be incorporated in the absence of CaO, would be 25.4mol%, which is equal to the previously quoted 25mol%.

b) Glass forming abilities in the Mg-Ln-aluminosilicate systems

The calculated and analysed (SEM/EDS) compositions of the studied Mg-Ln aluminosilicate glasses are shown in Table 4.2. The measurement conditions were identical with those applied for the Ca-Ln-aluminosilicate glasses, and therefore any difference between the calculated and analysed composition can be described as in the case of the Ca-Ln-aluminosilicate glasses. There was generally good correlation between the calculated and analysed compositions of Mg-Ln-aluminosilicate glasses. The rare-earth containing magnesium aluminosilicate glass compositions showed good glass forming characteristics, melted properly, and no bubbles or inclusions were found in the cast glass rods, except for the composition of highest Nd content (MASN-12), in which a few large crystals ($Nd_2SiO_5$ and $Nd_2Si_2O_7$, as determined by SEM/EDS) were grown in the upper part of the glass rod during cooling and annealing. The Mg-Nd-aluminosilicate glass compositions are shown in Fig.4.2.

Table 4.2. Compositions of Mg-Ln-aluminosilicate glasses

| | major components (wt%) | | | oxide components (mol%) | | | | | oxide components (wt%), calc. | | | | | oxide components (wt%) meas. | | | | |
|---|---|---|---|---|---|---|---|---|---|---|---|---|---|---|---|---|---|---|
| Code | Nd-disilicate | cordierite | TiO2 | Nd2O3 | MgO | Al2O3 | SiO2 | TiO2 | Nd2O3 | MgO | Al2O3 | SiO2 | TiO2 | Nd2O3 | MgO | Al2O3 | SiO2 | TiO2 |
| MAS | 0 | 100 | 0 | 0.0 | 22.2 | 22.2 | 55.6 | 0.0 | 0.0 | 13.8 | 34.9 | 51.4 | 0.0 | 0.0 | 14.6 | 34.0 | 51.4 | 0.0 |
| MASN-1 | 25 | 75 | 0 | 4.2 | 19.5 | 19.5 | 56.9 | 0.0 | 18.4 | 10.3 | 26.1 | 45.1 | 0.0 | 19.0 | 10.0 | 26.7 | 44.3 | 0.0 |
| MASN-2 | 30 | 70 | 0 | 5.2 | 18.8 | 18.8 | 57.3 | 0.0 | 22.1 | 9.6 | 24.4 | 43.8 | 0.0 | 24.8 | 9.7 | 23.9 | 41.6 | 0.0 |
| MASN-3 | 35 | 65 | 0 | 6.2 | 18.1 | 18.1 | 57.6 | 0.0 | 25.8 | 9.0 | 22.7 | 42.6 | 0.0 | 26.8 | 9.2 | 21.3 | 42.7 | 0.0 |
| MASN-4 | 40 | 60 | 0 | 7.4 | 17.3 | 17.3 | 58.0 | 0.0 | 29.5 | 8.3 | 20.9 | 41.3 | 0.0 | 28.5 | 8.7 | 21.0 | 41.8 | 0.0 |
| MASN-5 | 45 | 55 | 0 | 8.6 | 16.5 | 16.5 | 58.4 | 0.0 | 33.2 | 7.6 | 19.2 | 40.1 | 0.0 | 33.2 | 7.6 | 22.3 | 36.9 | 0.0 |
| MASN-6 | 50 | 50 | 0 | 10.0 | 15.6 | 15.6 | 58.9 | 0.0 | 36.8 | 6.9 | 17.4 | 38.8 | 0.0 | 36.1 | 7.5 | 17.0 | 39.4 | 0.0 |
| MASN-7 | 55 | 45 | 0 | 11.4 | 14.6 | 14.6 | 59.4 | 0.0 | 40.5 | 6.2 | 15.7 | 37.6 | 0.0 | 40.5 | 6.4 | 15.3 | 37.8 | 0.0 |
| MASN-8 | 60 | 40 | 0 | 13.0 | 13.5 | 13.5 | 59.9 | 0.0 | 44.2 | 5.5 | 13.9 | 36.3 | 0.0 | 43.9 | 5.3 | 13.3 | 37.5 | 0.0 |
| MASN-9 | 65 | 35 | 0 | 14.7 | 12.4 | 12.4 | 60.5 | 0.0 | 47.9 | 4.8 | 12.2 | 35.1 | 0.0 | 50.3 | 5.6 | 11.7 | 32.4 | 0.0 |
| MASN-10 | 70 | 30 | 0 | 16.6 | 11.1 | 11.1 | 61.1 | 0.0 | 51.6 | 4.1 | 10.5 | 33.8 | 0.0 | 54.1 | 4.3 | 9.4 | 32.2 | 0.0 |
| MASN-11 | 75 | 25 | 0 | 18.7 | 9.7 | 9.7 | 61.8 | 0.0 | 55.3 | 3.4 | 8.7 | 32.6 | 0.0 | 56.7 | 3.8 | 8.3 | 31.2 | 0.0 |
| MASN-12 | 80 | 20 | 0 | 21.0 | 8.2 | 8.2 | 62.6 | 0.0 | 58.9 | 2.8 | 7.0 | 31.3 | 0.0 | 61.2 | 3.6 | 6.2 | 29.0 | 0.0 |
| MASN10-T1 | 63 | 27 | 10 | 14.5 | 9.7 | 9.7 | 53.1 | 13.1 | 46.4 | 3.7 | 9.4 | 30.4 | 10.0 | not analysed | | | | |
| MASN12-T1 | 72 | 18 | 10 | 18.0 | 7.0 | 7.0 | 53.6 | 14.3 | 53.1 | 2.5 | 6.3 | 28.2 | 10.0 | not analysed | | | | |
| Code | La-disilicate | cordierite | TiO2 | La2O3 | MgO | Al2O3 | SiO2 | TiO2 | La2O3 | MgO | Al2O3 | SiO2 | TiO2 | La2O3 | MgO | Al2O3 | SiO2 | TiO2 |
| MASL-1 | 25 | 75 | 0 | 4.2 | 19.4 | 19.4 | 57.0 | 0.0 | 18.3 | 10.3 | 26.1 | 45.3 | 0.0 | 20.5 | 10.5 | 25.8 | 43.2 | 0.0 |
| Code | Y-disilicate | cordierite | TiO2 | Y2O3 | MgO | Al2O3 | SiO2 | TiO2 | Y2O3 | MgO | Al2O3 | SiO2 | TiO2 | Y2O3 | MgO | Al2O3 | SiO2 | TiO2 |
| MASY-1 | 25 | 75 | 0 | 5.3 | 18.7 | 18.7 | 57.3 | 0.0 | 16.3 | 10.3 | 26.1 | 47.2 | 0.0 | 23.6 | 8.4 | 24.5 | 43.5 | 0.0 |

In addition, the $TiO_2$ containing Mg-Nd-aluminosilicate glass compositions (MASN10-T1; MASN12-T1) showed uncontrolled phase separation forming silica rich droplet phase during pouring and solidification due to the titania addition. The texture of the phase separated glass is shown in Fig.4.3. Unfortunately, the uncontrolled nature of the phase separation made these glasses unsuitable for further crystallization studies.

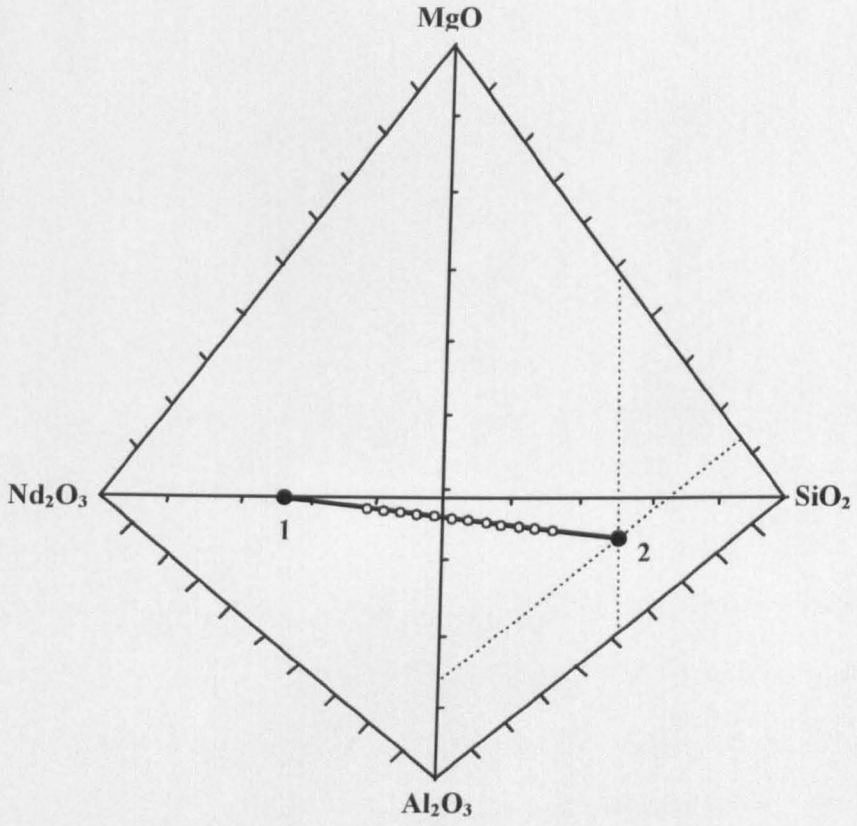


Fig.4.2. Glass compositions in the Mg-Nd-aluminosilicate system. **1)** the composition of $Nd_2Si_2O_7$, **2)** the composition of cordierite, and the empty circles represent the melted glass compositions. The scales of the diagram represent weight percentages. The diagram serves as a visual aid, and not designed to provide exact quantitative information (please use Table 4.2 instead).

Moreover, the glass of the pure cordierite composition, which was used for comparison, melted properly and resulted in a glass rod without bubbles or inclusions. The colours of the rare-earth containing magnesium aluminosilicate glasses were

similar to the calcium aluminosilicate ones, the yttrium and lanthanum containing glasses were transparent colourless and the neodymium containing glasses were purple.

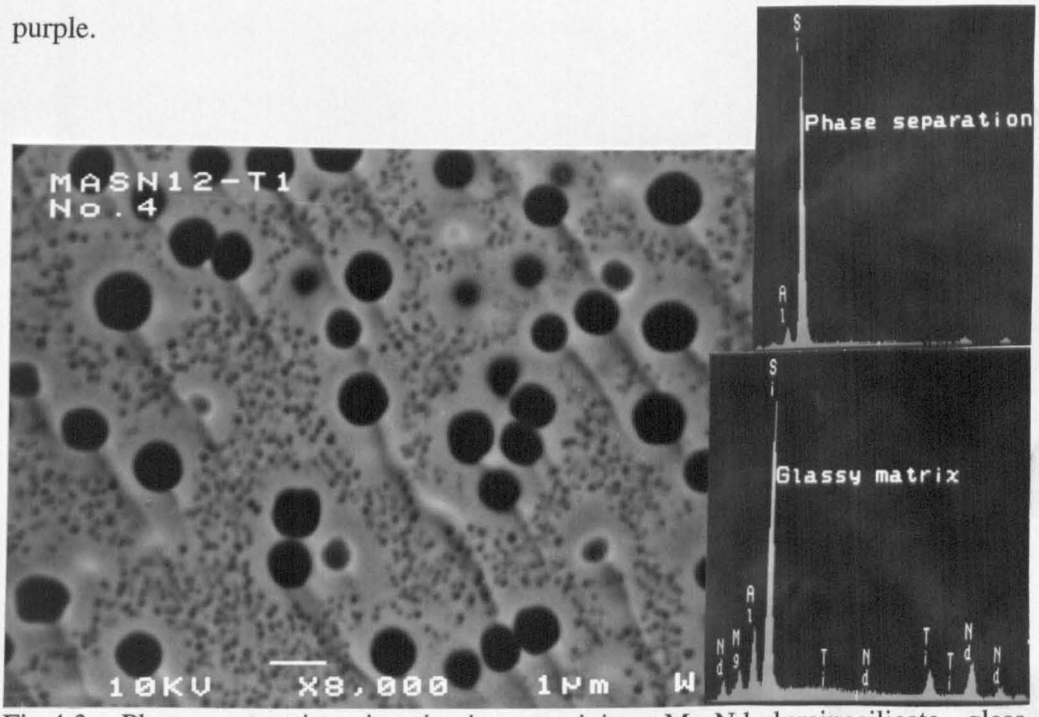


Fig.4.3. Phase separation in titania containing Mg-Nd-aluminosilicate glass immediately after quenching. The large and tiny dark circular spots are of siliceous droplet phase.

The highest amount of $Nd_2O_3$ in magnesium-aluminosilicate glasses was 21mol%, which is close to the reported maximum achievable amount of ~25mol% $Nd_2O_3$ in aluminosilicate glasses [252]. When summarizing the amount of $Nd_2O_3$ and that of MgO (normalized to the 3+ cation charge), in similar fashion as in the case of the Ca-Nd-aluminosilicate glasses, the estimated maximum amount of $Nd_2O_3$ which can be incorporated in the absence of MgO, would be 26.5mol%, which is practically equal to the previously quoted 25mol% reported by Makishima et al. [252]. This fairly constant value of cations both in the rare-earth containing calcium- and magnesium-aluminosilicate systems suggests, that the $Nd^{3+}$ cations, regardless of

their higher field strength, occupy similar modifier positions in the glass structure as $Ca^{2+}$ and $Mg^{2+}$.

A final comment concerns phase separation of rare-earth containing glasses. Regions of metastable liquid phase immiscibility exist in binary rare-earth silicate systems [65], and phase separations were reported in various rare-earth aluminosilicate glass systems [260,264-266,268,271]. The tendency of rare-earth containing glasses towards phase separation is due to the strong disturbing effect of the high field strength rare-earth cations on the Si-O-Si bond angles. Considering that, spontaneous liquid phase separation was somehow expected to arise in the studied rare-earth containing Ca- and Mg-aluminosilicate glass systems, but it was only observed in the titania containing Mg-Nd-aluminosilicate compositions, which confirms the structural stability of the developed glass compositions.

### 4.3. The properties of Ln-containing Ca- and Mg-aluminosilicate glasses

#### 4.3.1. Density

The density of glass depends on the molar weight of the components as well as on the ratio of cations in network former and modifier positions. As generally observed, the density of a glass increases with increasing amount of modifier ions, since modifier ions increase the number of atoms present in a given volume, and although at the same time they loosen the glass network, the first effect is dominant [18,24]. The density of glass is also affected by its thermal history (i.e. the rate of cooling and subsequent heat treatments).

The density of Ca-Nd-aluminosilicate glasses is also showed a linear increase with increasing Ca-Nd-silicate content (Fig.4.4).

Fig.4.4. Density of Ca-Nd-aluminosilicate glasses

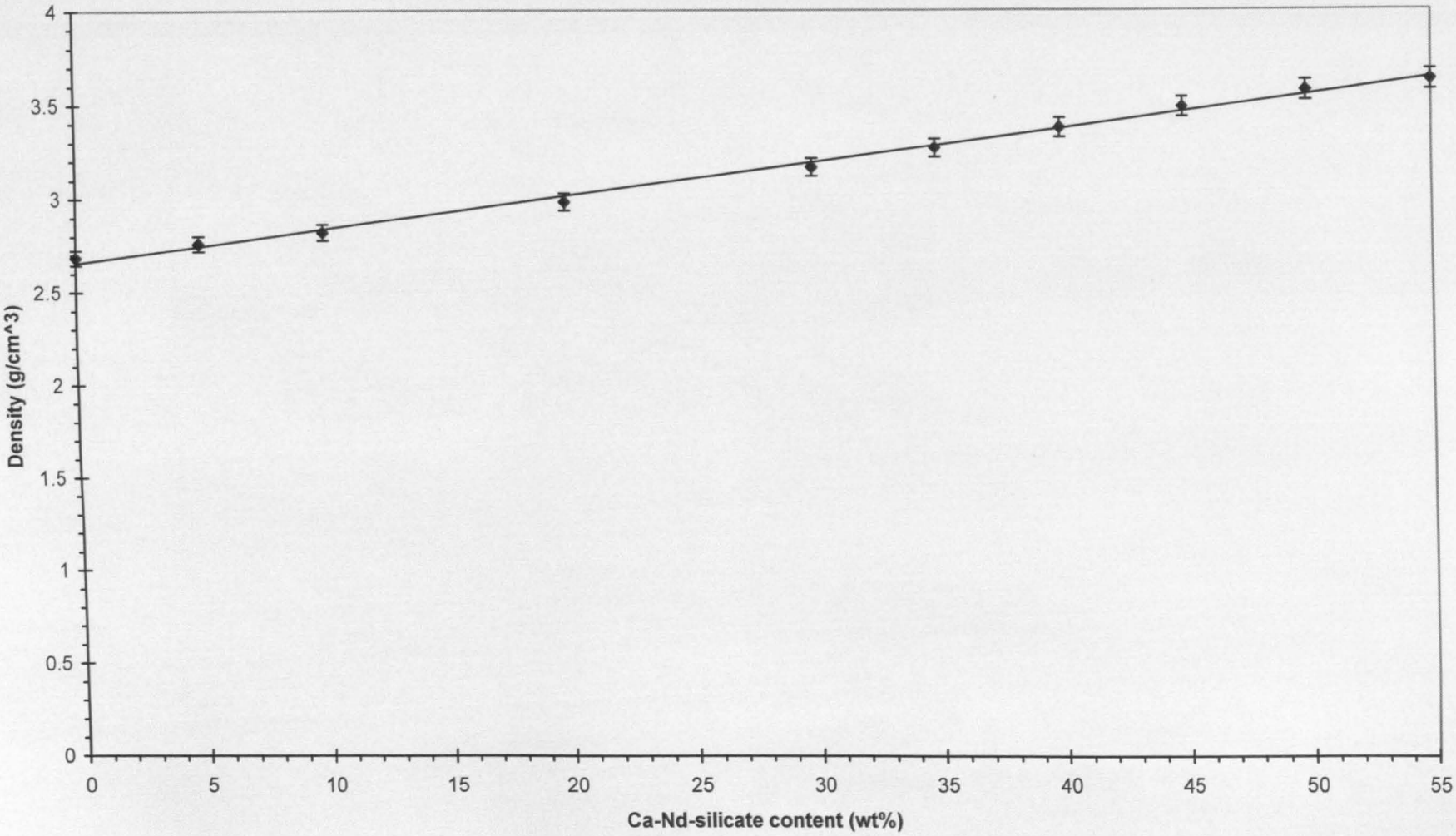

Fig.4.5. Density of Mg-Nd-aluminosilicate glasses

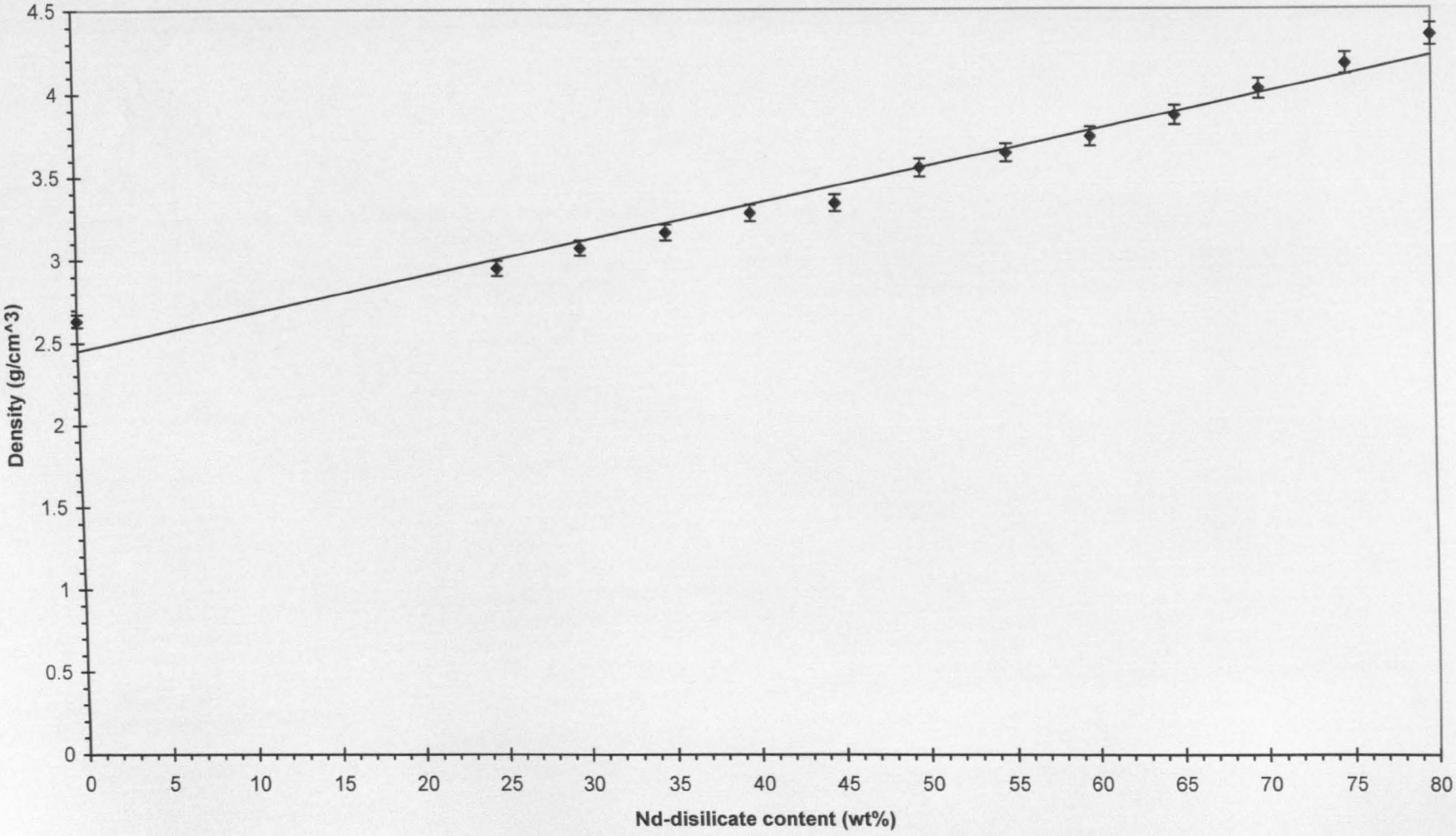

Table 4.3. Properties of Ln-Ca/Mg-aluminosilicate glasses

| Code | content of (wt%) | density | refractive index | Alpha (50C-800C) | Alpha (100C-800C) | Vickers hardness | fracture toughness | stan. dev. of Kic |
|---|---|---|---|---|---|---|---|---|
| | Ca-Nd-silicate | (g/cm^3) | nD20 | (MK^-1) | (MK^-1) | Hv (GPa) | Kic (MPam^(1/2)) | (MPam^(1/2)) |
| CASN9-T1 | 45.0 | 3.6474 | 1.709 | 9.09 | 9.36 | 6.85 | 0.74 | 0.06 |
| CASN12-T1 | 49.5 | 3.6508 | 1.738 | 8.78 | 9.15 | 7.34 | 0.99 | 0.16 |
| CASN-1* | 44.8 | 3.3015 | 1.638 | 7.65 | 7.66 | 6.47 | 1.33 | 0.21 |
| | La-disilicate | | | | | | | |
| CASL-2 | 34.8 | 3.1648 | 1.625 | 7.69 | 8.18 | 6.76 | 0.94 | 0.09 |
| | Y-disilicate | | | | | | | |
| CASY-1 | 34.8 | 3.0534 | 1.622 | 7.49 | 7.87 | 7.17 | 0.97 | 0.10 |
| | Nd-disilicate | | | | | | | |
| MASN10-T1 | 63 | N/A | N/A | N/A | N/A | N/A | N/A | N/A |
| MASN12-T1 | 72 | N/A | N/A | N/A | N/A | N/A | N/A | N/A |
| | La-disilicate | | | | | | | |
| MASL-1 | 25 | 2.9444 | 1.593 | 6.14 | 6.57 | 6.71 | 0.95 | 0.06 |
| | Y-disilicate | | | | | | | |
| MASY-1 | 25 | 2.8382 | 1.590 | 6.00 | 6.33 | 7.28 | 1.40 | 0.16 |

| | | hand-ground by agate mortar & pestle | | | | ball milled by Si3N4 grinding bodies | | | |
|---|---|---|---|---|---|---|---|---|---|
| Code | content of (wt%) | glass transition | softening point | crystallization temp. | temp. of first | glass transition | softening point | crystallization temp. | temp. of first |
| | Ca-Nd-silicate | temp., Tg (C) | Mg (C) | Tcr (C) | melting, Tm (C) | temp., Tg (C) | Mg (C) | Tcr (C) | melting, Tm (C) |
| CASN9-T1 | 45.0 | 808 | 834 | 940 | 1302 | 812 | 837 | 979, 990 | 1329 |
| CASN12-T1 | 49.5 | 798 | 843 | 957 | 1282 | 814 | 835 | 946 | 1333 |
| | Ca-Nd-silicate | | | | | ball milled by Al2O3 grinding bodies | | | |
| CASN-1* | 44.8 | 852 | 867 | 1026 | 1300 | 812 | 840 | 973 | 1280 |
| | La-disilicate | | | | | | | | |
| CASL-2 | 34.8 | 840 | 866 | 1038 | 1300 | 824 | 842 | 978 | 1326 |
| | Y-disilicate | | | | | | | | |
| CASY-1 | 34.8 | 856 | 885 | 1057 | 1300 | 847 | 868 | 1008, 1033, 1170 | 1243 |
| | Nd-disilicate | | | | | | | | |
| MASN10-T1 | 63 | 804 | 831 | 994 | 1230 | not measured | | | |
| MASN12-T1 | 72 | 827 | 846 | 1006 | 1338 | not measured | | | |
| | La-disilicate | | | | | | | | |
| MASL-1 | 25 | 815 | 842 | 1025 | 1244 | 803 | 844 | 1068, 1160, 1180 | 1231 |
| | Y-disilicate | | | | | | | | |
| MASY-1 | 25 | 829 | 859 | 1063 | 1300 | 816 | 844 | 1076, 1100, 1160 | 1308 |

The density of Mg-Nd-aluminosilicate glasses showed similar, linearly increasing trend with increasing Nd-disilicate content (Fig.4.5). The observed tendency correlates well with the results published on Nd-aluminosilicate glasses [264], Y-aluminosilicate glasses [260,268], Pr-aluminosilicate glasses [266], Sm-aluminosilicate glasses [269] and Ca-Y-aluminosilicate glasses [255]. The increasing density is the result of incorporation of increasing amount of high atomic weight rare-earth cations in the glasses' structure. In addition, the tendency also supports the theory that the rare-earth cations occupy modifier positions in the glassy network.

The density and other physical properties of Y and La containing calcium- and magnesium-aluminosilicate glasses, as well as those of the $TiO_2$ containing Ca-Nd-aluminosilicate glasses are shown in Table 4.3. These glasses, similarly to the previously described other rare-earth containing glasses, also showed high density values, due to the incorporation of rare-earth cations in their structure.

### 4.3.2. Refractive index ($n_D^{20}$)

The refractive index of glass is determined by its molar refraction. The molar refraction is a function of the electron density of the ions present and their polarizability, in which the polarizability of anions is dominant. In oxide glasses, the polarizability of the oxygen anions depends on their structural position (i.e. the non-bridging oxygen having higher polarizability), as well as on the polarizing influence of cations, which in turn is determined by their field strength [312]. Therefore the amount and type of modifying cations have major effect on the refractive index of glass. In addition, molar refraction depends on the molar volume of the glass: the refractive index increases with decreasing molar volume, i.e. as the glass gets denser [24,312].

Moreover, the thermal history of the glass (e.g. rate of cooling) also affects the refractive index by changing the density of the glass [312].

The refractive index of Ca-Nd-aluminosilicate glasses, similar to their density values, showed a linear increase with increasing Ca-Nd-silicate content (Fig.4.6). The refractive index of Mg-Nd-aluminosilicate glasses also showed linearly increasing tendency with increasing Nd-disilicate content (Fig.4.7). Similar tendency was reported on Y-aluminosilicate glasses [260,268], Pr-aluminosilicate glasses [266] and Sm-aluminosilicate glasses [269]. The increase of refractive index with increasing amount of rare-earth cations incorporated in the glasses is due to the strong polarizing effect of these high field strength cations. Also, the increasing ratio of rare-earth cations in these glasses, if they act as modifiers, would mean an increase of non-bridging oxygen, which provides more anions having higher polarizability, and hence results in glasses having even higher refractive index.

The Y and La containing calcium- and magnesium-aluminosilicate glasses in Table 4.3 also showed high refractive indexes, supporting the previous statements. In addition, the $TiO_2$ containing Ca-Nd-aluminosilicate glasses showed exceptionally high refraction index values due to the additional strong polarizing effect of titanium cations.

### 4.3.3. Hardness and indentation fracture toughness

The hardness of glass depends on the bond strength of its components and the packing density of the ions in its structure [286]. In addition, it has strong correlation with molar refractivity of the glass, the polarizing influence of modifier cations and the softening temperature [159]. Moreover, residual stresses also can modify the observed hardness value [23].

Fig.4.6. Refractive index of Ca-Nd-aluminosilicate glasses

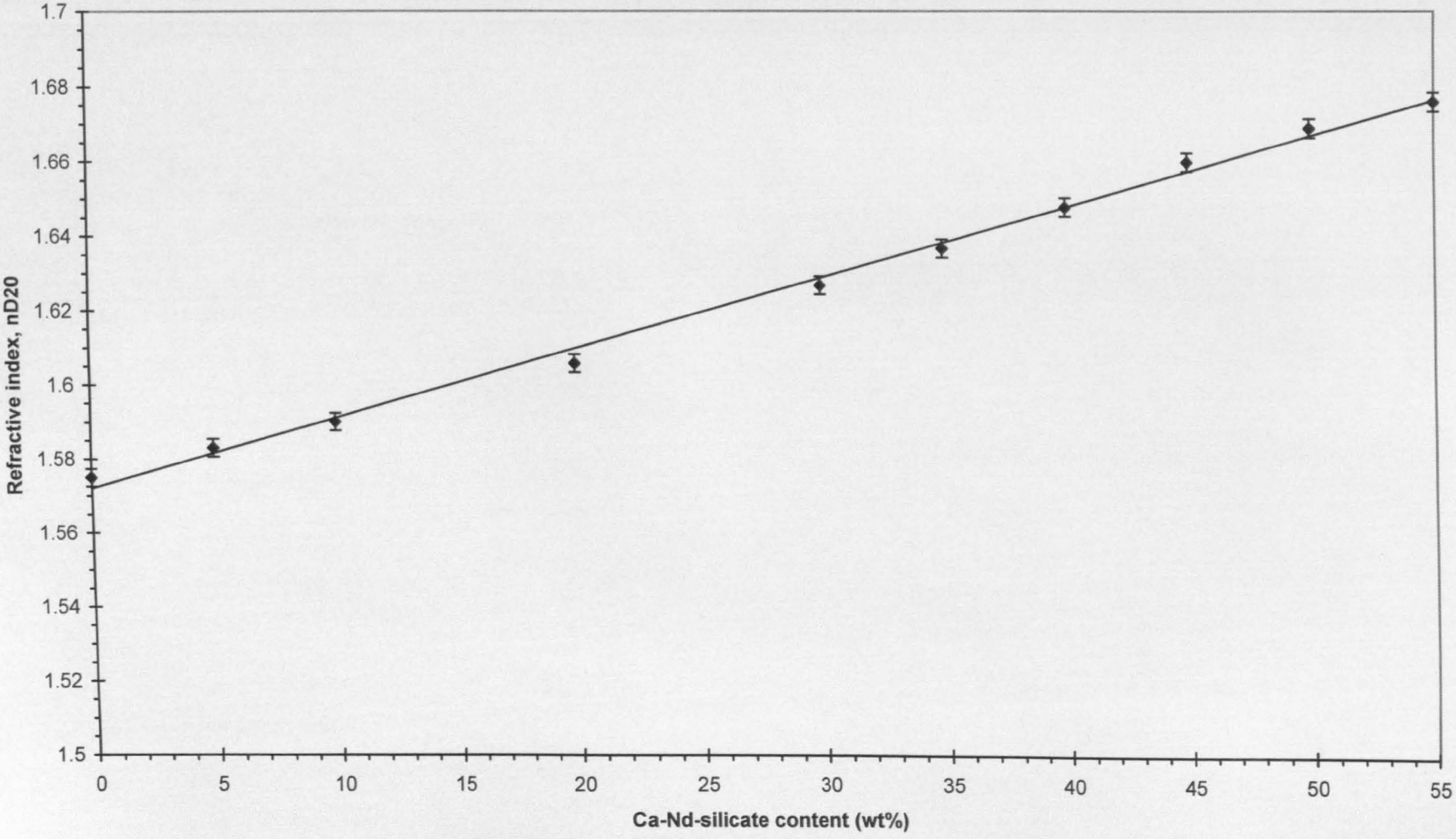

Fig.4.7. Refractive index of Mg-Nd-aluminosilicate glasses

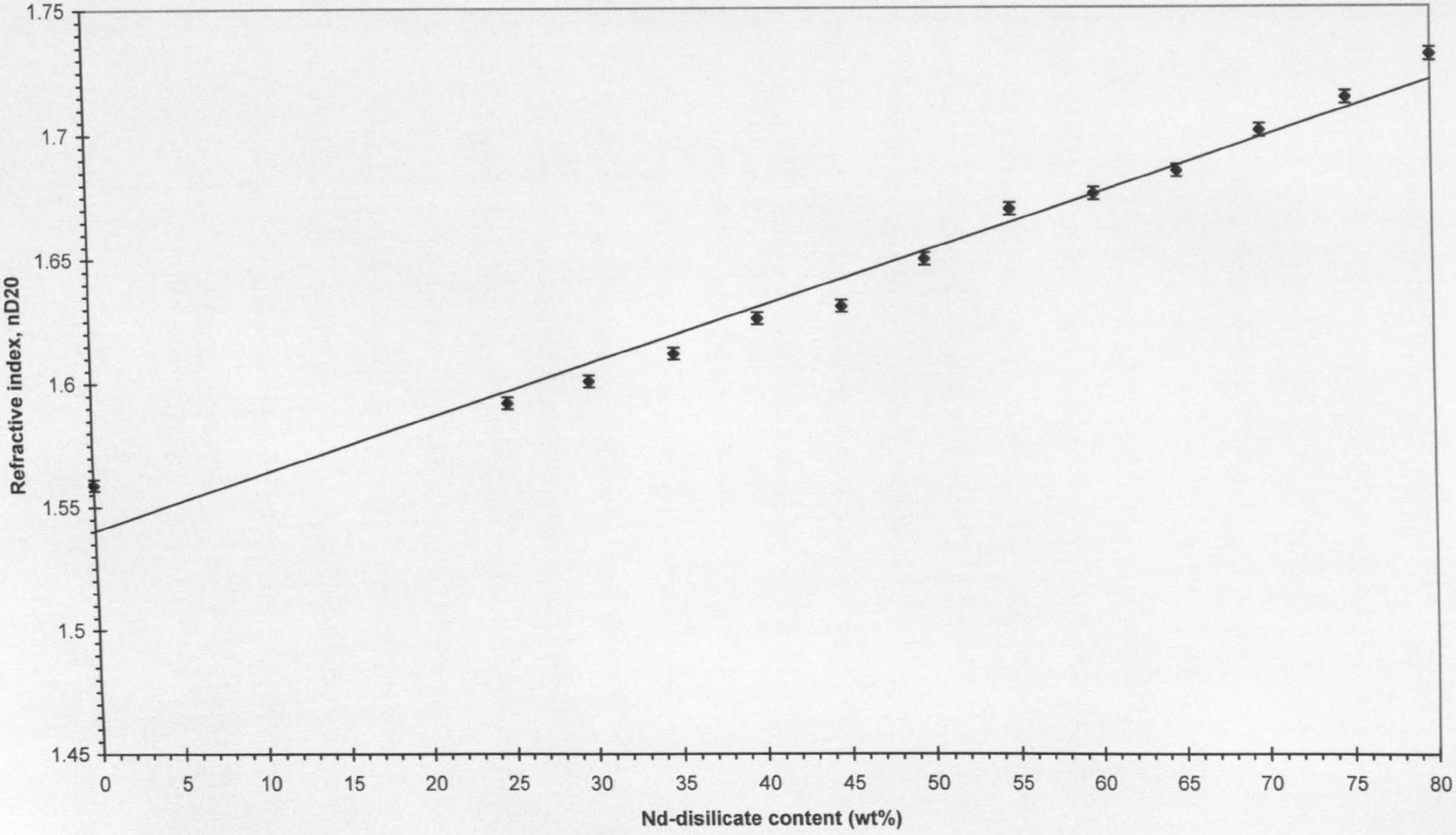

The Vickers hardness of the Ca-Nd-aluminosilicate glasses remained almost constant in the studied composition range (Fig.4.8), and their indentation fracture toughness, after an initial increase at the 5wt% Ca-Nd-silicate composition, were almost constant and have a slight declining trend, starting at the higher Ca-Nd-silicate concentrations. The Vickers hardness values of the Mg-Nd-aluminosilicate glasses showed small changes over the studied composition range (Fig.4.9), and their indentation fracture toughness, after a higher value at the 25wt% Nd-disilicate containing composition, showed a slight decreasing trend towards the Nd-disilicate rich compositions. Though in the literature hardness values increased with increasing rare-earth content, as reported for pure aluminosilicate glasses [266,268,269], the increase of rare-earth oxides in those cases was at the expense of $SiO_2$, whereas in the studied Ca-Nd-aluminosilicate compositions the amount of $SiO_2$ (in mol%) were constant and in the Mg-Nd-aluminosilicate compositions were only slightly changed (Table.4.1 & 4.2), and the increases of rare-earth oxides were at the expense of $Al_2O_3$ and/or Ca/Mg. In the studied glasses the relatively constant amount of the major network former $SiO_2$ can have substantial influence on the observed hardness.

Although, both Vickers hardness and the indentation fracture toughness values showed little changes over the studied composition range, their values were relatively high, which is due to the incorporation of rare-earth cations. The rare-earth ions have high ionic charge and small ionic radii, can fill the interstitial positions in the glassy network, therefore increase the packing density, as well as create stronger bonds with oxygen than the ordinary modifier cations, and as a result of all, creating higher resistance towards compression.

Fig.4.8. Vickers hardness and indentation fracture toughness of Ca-Nd-aluminosilicate glasses

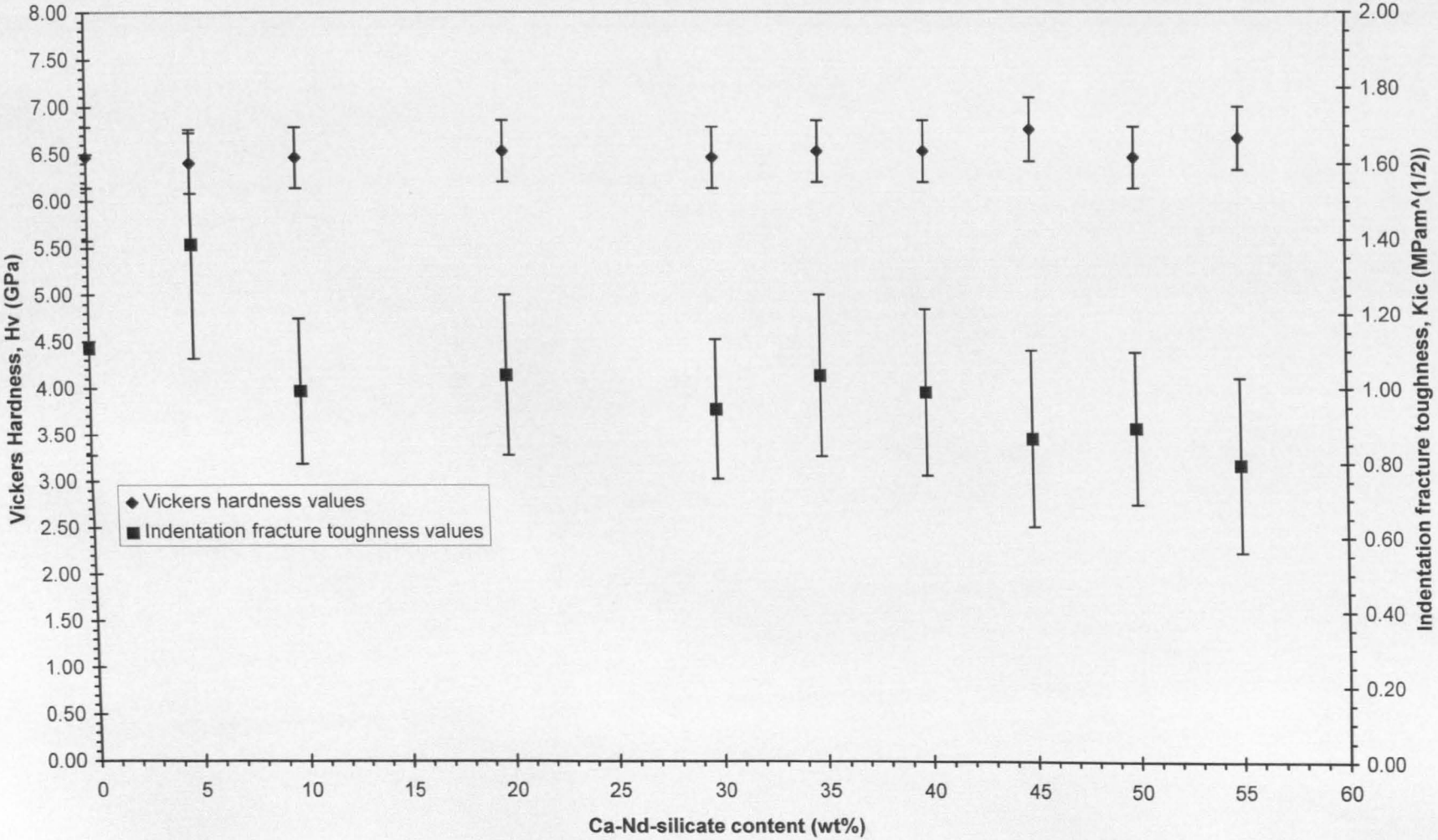

Fig.4.9. Vickers hardness and indentation fracture toughness of Mg-Nd-aluminosilicate glasses

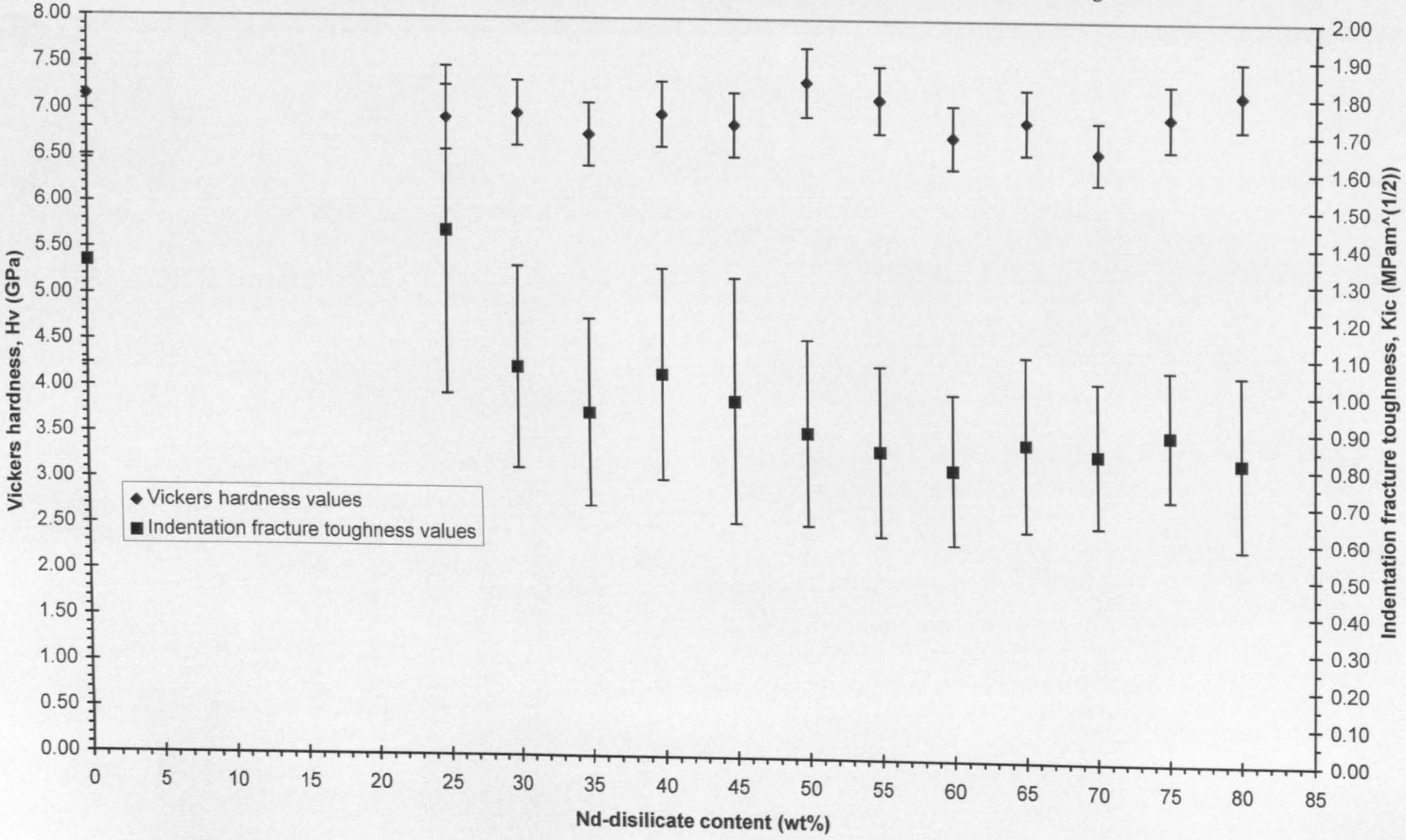

Similar, relatively high Vickers hardness and fracture toughness values were measured for the Y and La containing calcium- and magnesium-aluminosilicate glasses, and for the $TiO_2$ containing Ca-Nd-aluminosilicate glasses (Table 4.3).

### 4.3.4. Thermal properties determined by DTA

The Differential Thermal Analysis is a useful tool to estimate glass transition ($T_g$), softening ($M_g$) and crystallization temperatures ($T_{cr}$) and to give indication of the start of the melting reactions ($T_m$). It should be noted however, that the maximum temperature, shape, and number of crystallization exotherms depend on two major experimental factors: the applied heating rate and the particle size of the glass powder. The smaller the particle size, the larger the specific surface and the number of nucleation sites, which results in decrease of the crystallization temperature. If the measurement is repeated with different particle size samples, this effect can give indication on the nucleation mechanism [5]. When the glass composition studied is susceptible to surface nucleation, the degree of shift of the crystallization exotherm is significant, whereas when the glass composition susceptible to bulk nucleation, the shift is negligible. Nevertheless, in the case of finely ground glass powders, having high specific surface and numerous nucleation sites, surface nucleation is the dominating mechanism. The shift of the crystallization temperature due to the different heating rate applied can be used for calculation of the activation energy of crystallization. There are several equations for the calculation and the most frequently used one is the Kissinger-equation [313,314] or its modified version [315]. The effect of particle size and heating rate on the crystallization exotherm can be minimized by using identical grinding parameters and measurement conditions for all glass compositions. When all of the applied processing and experimental conditions are the

same, the measured properties are characteristic of the structure of the given glass, therefore mainly dependent on the chemical composition of the glass and its thermal history. A representative DTA trace is shown in Fig.I.1 (Appendix I). The glass transition temperature ($T_g$) was assigned to the slope change of the DTA curve and it was determined by the intercept method. The softening temperature ($M_g$) was assigned to the first endothermic dip after the glass transition. The crystallization temperatures ($T_{cr}$) were assigned to the maxima of the exothermic crystallization peaks, whereas the melting temperature ($T_m$) was assigned to the deep endothermic peak after crystallization. The figure also shows a seemingly exothermic peak at 573°C, which is due to the endothermic reaction in the quartz reference material (transformation from $\alpha$ to $\beta$ quartz), and served as a in-situ calibration standard.

In order to compare the effect of different powder processing conditions on the glass crystallization, both agate-ground and ball-milled (with $Si_3N_4$ grinding bodies and isopropyl alcohol grinding medium) glass powders were studied by DTA. The glass transition ($T_g$) and softening temperatures ($M_g$) of agate-ground Ca-Nd-aluminosilicate glasses are shown in Fig.4.10. Both $T_g$ and $M_g$ show a slight decrease at lower Ca-Nd-silicate contents (<20wt%), and then stabilized around almost constant values. The $Si_3N_4$-ground Ca-Nd-aluminosilicate glasses showed a similar tendency (Fig.4.11), and the measured $T_g$ and $M_g$ values were almost the same as the agate ground glasses. In the glasses studied, the amount of $Si^{4+}$ was constant and the amount of $Ca^{2+}$ only slightly decreased, therefore the increase of $Nd^{3+}$ was mainly at the expense of $Al^{3+}$ (mol% columns in Table 4.1), which meant introduction of slightly weaker bonds, which in turn makes the levelling $T_g$ & $M_g$ values understandable.

Fig.4.10.Glass transition and softening temperatures of agate ground Ca-Nd-aluminosilicate glasses

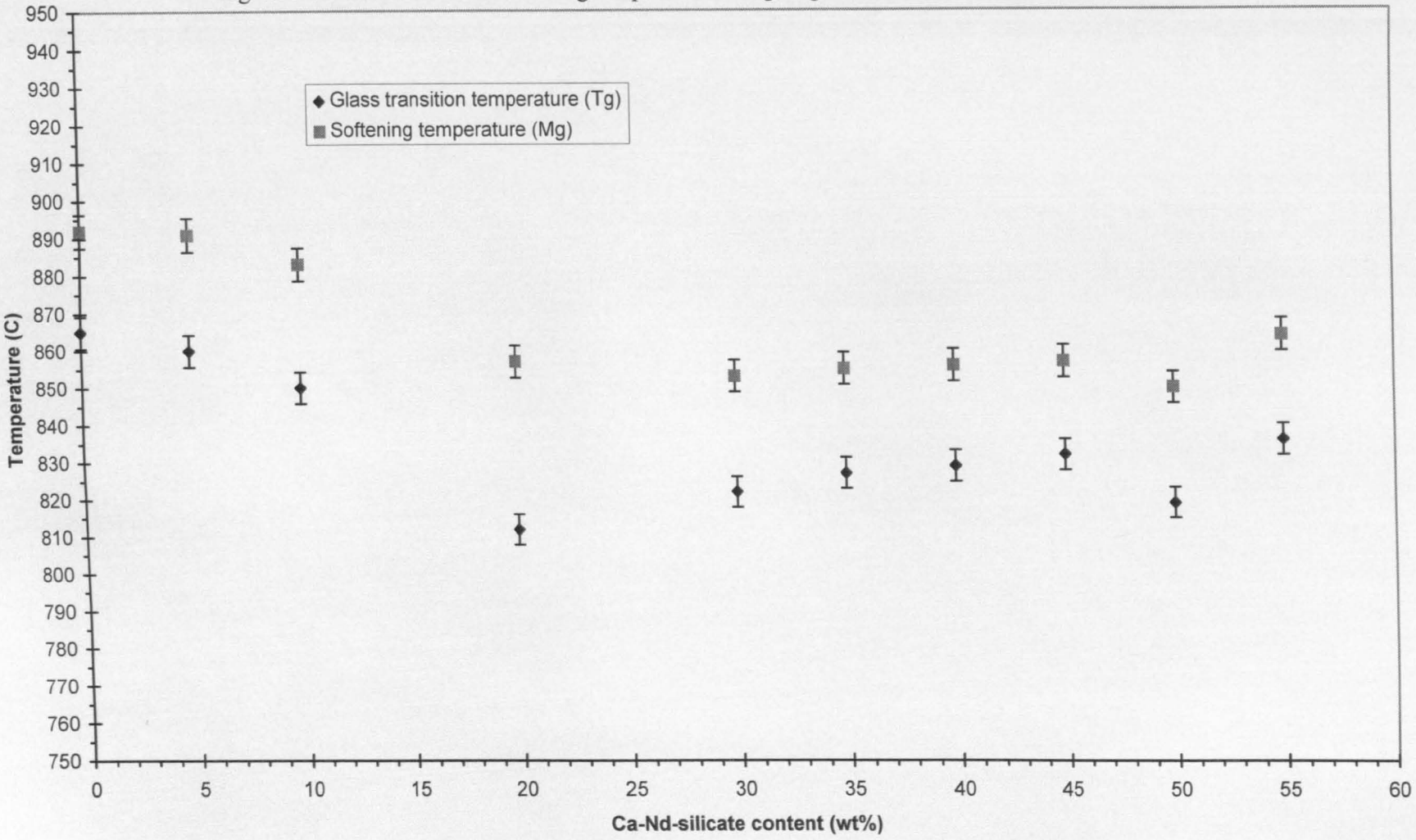

Fig.4.11. Glass transition and softening temperatures of Si3N4-ground Ca-Nd-aluminosilicate glasses

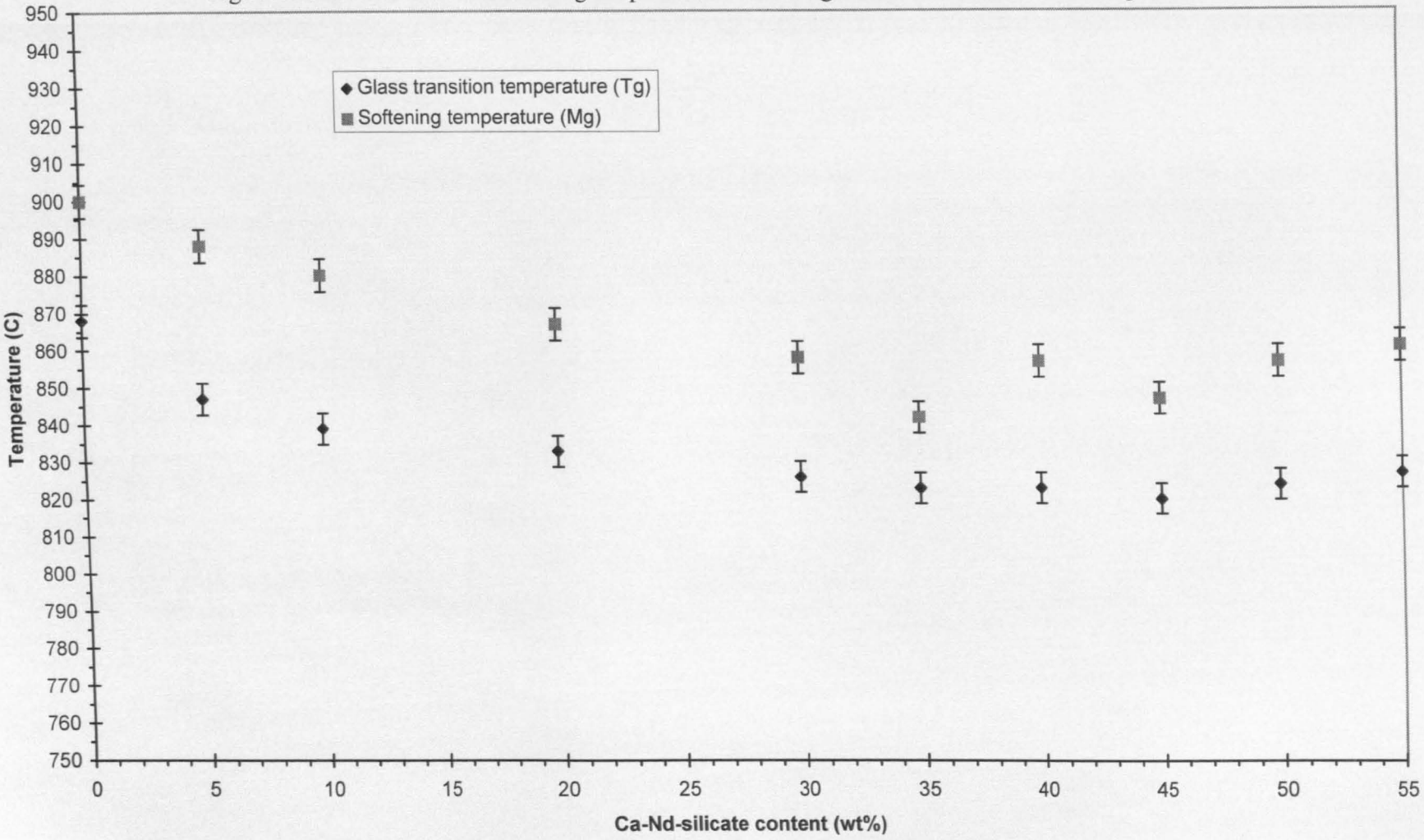

Table 4.4. Some DTA data of agate- and Si3N4-ground Ca- and Mg-Nd-aluminosilicate glasses

| | | agate-gound glasses | | Si3N4-ground glasses | | | | | agate-gound | Si3N4-ground |
|---|---|---|---|---|---|---|---|---|---|---|
| Code | Ca-Nd-Si content (wt%) | crystallization temp. Tcr (C) | temp. of first melting Tm (C) | crystallization temp. Tcr-1 (C) | crystallization temp. Tcr-2 (C) | temp. of first melting Tm (C) | Code | Nd disilicate content (wt%) | temp. of first melting Tm (C) | temp. of first melting Tm (C) |
| CAS | 0 | 1018 | 1380 | 1039 | | 1400 | MAS | 0 | 1410 | not measured |
| CN13 | 5 | 1008 | 1324 | 1014 | | >1341 | MN1 | 25 | 1243 | 1255 |
| CN11 | 10 | 1002 | 1376 | 1018 | | >1339 | MN2 | 30 | 1270 | 1267 |
| CN10 | 20 | 994 | 1436 | 1024 | | >1355 | MN3 | 35 | 1247 | 1274 |
| CN8 | 30 | 1010 | 1442 | 1025 | | >1300 | MN4 | 40 | 1251 | 1274 |
| CN7 | 35 | 1012 | 1442 | 1025 | | >1300 | MN5 | 45 | 1264 | 1268 |
| CN6 | 40 | 1010 | 1446 | 1013 | | >1300 | MN6 | 50 | 1270 | 1270 |
| CN5 | 45 | 1008 | 1450 | 1006 | | 1442 | MN7 | 55 | 1271 | 1274 |
| CN9 | 50 | 1015 | 1440 | 1020 | | >1333 | MN8 | 60 | 1272 | 1274 |
| CN12 | 55 | 1000 | 1324 | 1002 | 1029 | >1351 | MN9 | 65 | 1270 | 1278 |
| | | | | | | | MN10 | 70 | 1272 | 1274 |
| | | | | | | | MN11 | 75 | 1265 | 1274 |
| | | | | | | | MN12 | 80 | 1268 | 1269 |

Fig.4.12. Glass transition and softening temperatures of agate-ground Mg-Nd-aluminosilicate glasses

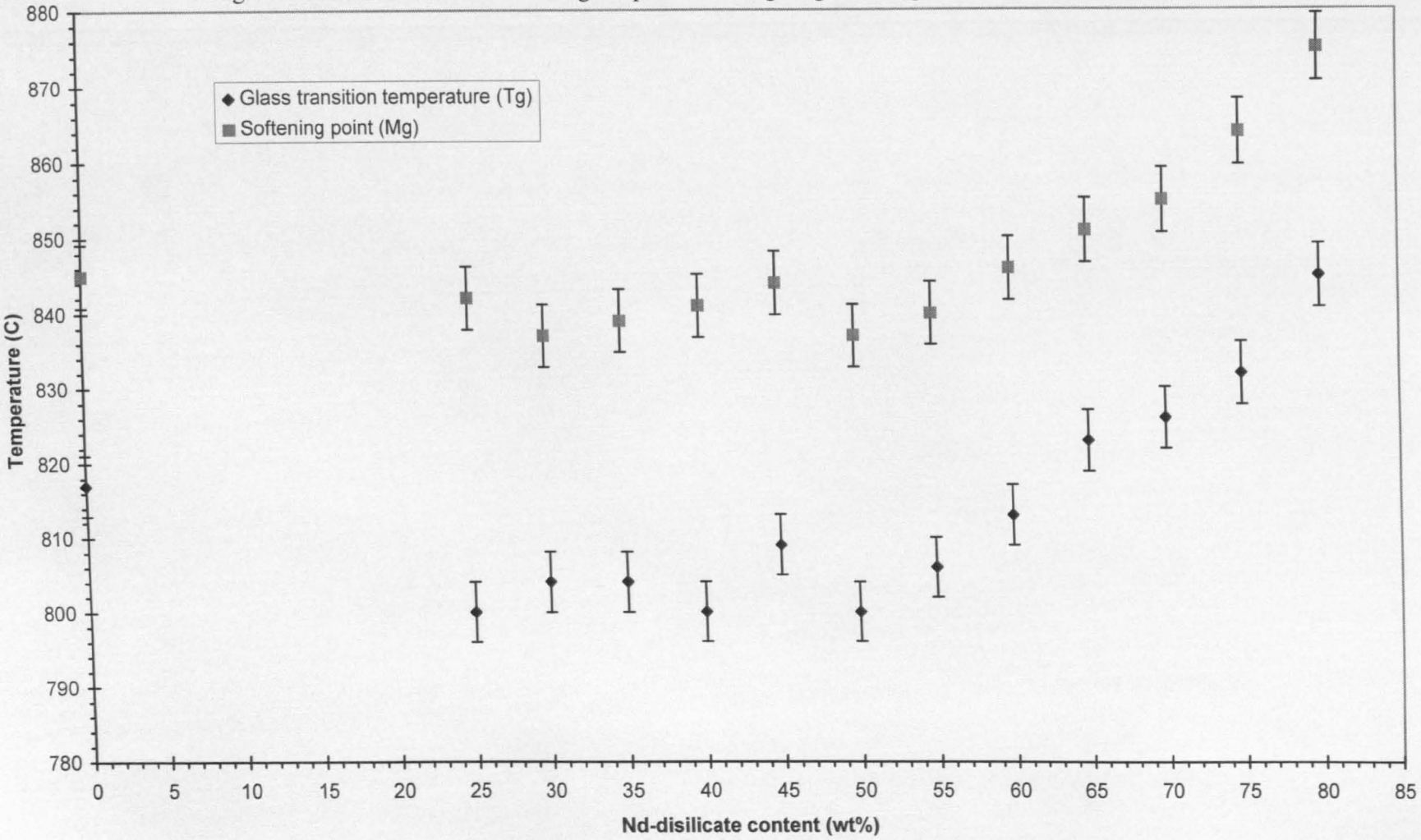

Fig.4.13. Glass transition and softening temperatures of Si3N4-ground Mg-Nd-aluminosilicate glasses

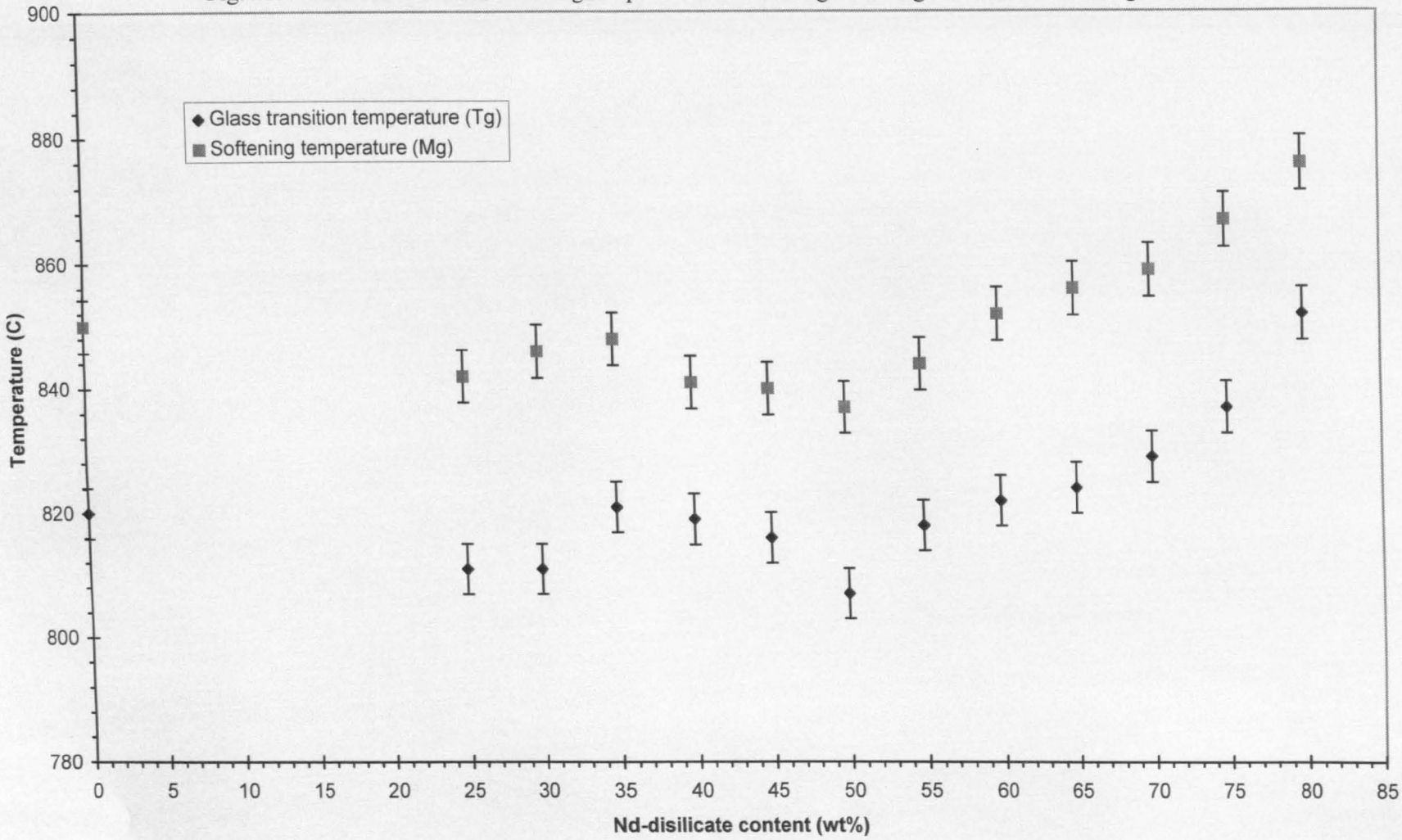

Fig.4.14. Crystallization temperatures of agate-ground Mg-Nd-aluminosilicate glasses

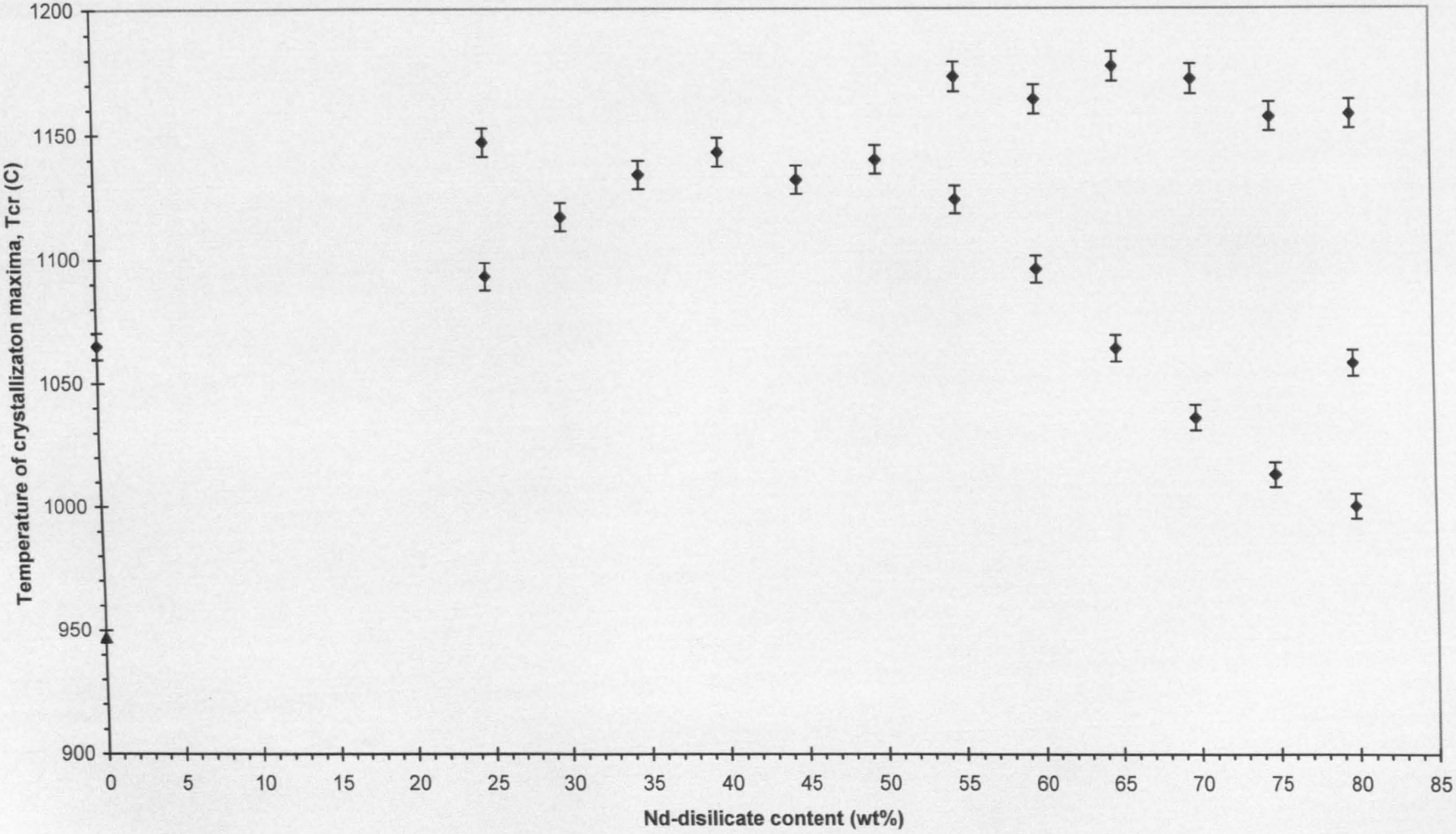

Fig.4.15. Crystallization temperatures of Si3N4-ground Mg-Nd-aluminosilicate glasses

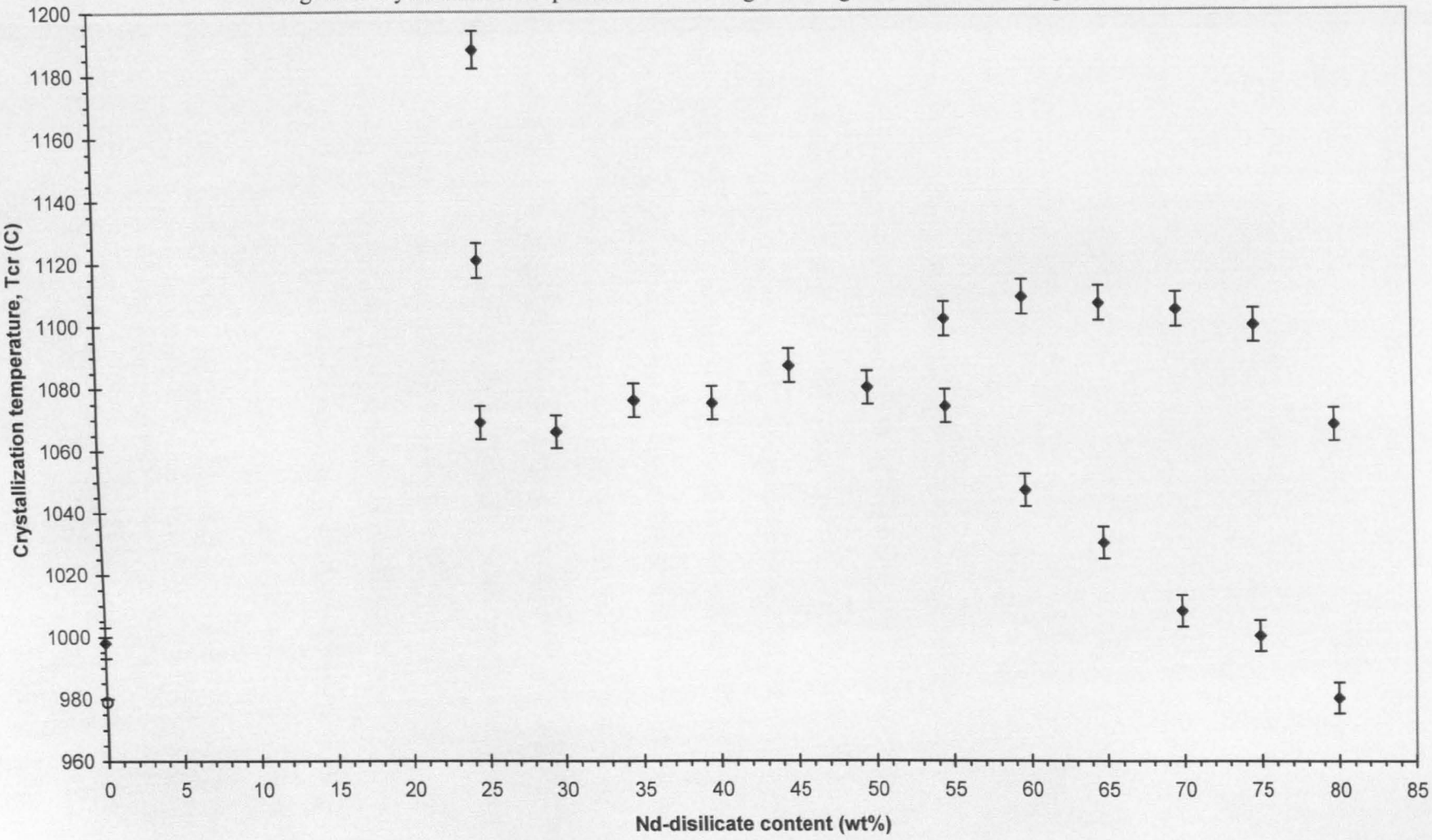

The crystallization ($T_{cr}$) and melting temperatures ($T_m$) of agate and $Si_3N_4$-ground Ca-Nd-aluminosilicate glasses are shown in Table 4.4. One crystallization peak was detected for nearly all glass compositions (except for the 55wt% Ca-Nd-silicate containing glass, where two peaks were observed), which suggest that the crystallization of both anorthite and Ca-Nd-silicate phases took place simultaneously. The $Si_3N_4$-ground glasses showed increased crystallization temperatures compared to the agate-ground ones. Similar comparison cannot be made for the melting temperatures, since the DTA experiments were stopped at the first sign of softening before the proper melting temperature in the case of the $Si_3N_4$-ground glasses, in order to avoid overflowing of the glass melt (the $Si_3N_4$-ground glass powder cannot be compacted as much as the agate ground one, and in order to use the same weight of powder for the experiments, the crucibles had to be filled nearly completely, which increased the possibility of glass melt overflow and damage of the equipment).

The glass transition ($T_g$) and softening temperatures ($M_g$) of agate-ground Mg-Nd-aluminosilicate glasses are shown in Fig.4.12. At the lower Nd-disilicate containing compositions $T_g$ and $M_g$ fluctuate around the same values, but they show a constant increasing trend above 50wt% Nd-disilicate content. Similar tendency was observed for the $T_g$ and $M_g$ of $Si_3N_4$-ground glasses, as shown in Fig.4.13 (the actual values were a few degrees higher than those of the agate-ground glasses). In the studied composition range (Table 4.2), the amount of $Si^{4+}$, the major network forming cation, is increasing (replacing $Al^{3+}$), also the amount of $Nd^{3+}$ is substantially increasing (mainly replacing $Mg^{2+}$), and both replacements are increasing the amount of stronger chemical bonds in the glass' structure. The effect of these tendencies is not so significant at the lower Nd-disilicate containing compositions, which explains the

levelling $T_g$ and $M_g$ values. However, the effect is more marked at the higher Nd-disilicate containing compositions, explaining the increasing $T_g$ and $M_g$ values.

The crystallization temperatures of the agate-ground Mg-Nd-aluminosilicate glasses are shown in Fig.4.14. Two crystallization peaks were observed at low and high Nd-disilicate concentrations and one crystallization peak was detected at the medium Nd-disilicate concentration. At low Nd-disilicate content the crystallization of cordierite precedes the crystallization of Nd-disilicate, whereas at high Nd-disilicate concentrations it is the other way around. At the middle range Nd-disilicate content the crystallization of both phases take place simultaneously. Similar tendency was observed for the crystallization temperatures of the $Si_3N_4$ ground glasses, though the actual values were lower than those of the agate ground ones. The crystallization behaviour observed is characteristic of eutectic systems. The melting temperatures of agate and $Si_3N_4$-ground glasses are shown in Table 4.4. Generally, the $Si_3N_4$-ground glasses showed higher melting temperatures than the agate-ground ones.

The observed differences between the agate-ground and $Si_3N_4$-ground Ca- and Mg-Nd-aluminosilicate glasses originate partly from different particle size distribution and partly from the difference in the surface chemistry caused by the applied grinding medium.

High glass transition ($T_g$), softening ($M_g$), and melting temperatures ($T_m$) are characteristic of the above described neodymium containing calcium- and magnesium aluminosilicate glasses, and these properties are due to their rare-earth content, since these rare-earth cations created relatively strong chemical bonds, compared to ordinary modifier cations. The Y and La containing calcium- and magnesium-aluminosilicate glasses, and the $TiO_2$ containing Ca-Nd-aluminosilicate glasses resulted in similar high $T_g$, $M_g$, and $T_m$ values (Table 4.3), also due to their rare-earth content.

### 4.3.5. Thermal expansion ($\alpha$)

The thermal expansion of glass is a result of anharmonic vibrations of atoms whose amplitude increases as a function of temperature. The amplitude of the vibrations depends on the symmetry of the close-range order of the glass [24], which is controlled by the glass' chemical composition and by structural aspects. The addition of modifier cations to the glass composition disrupts the glassy network structure by the formation of non-bridging oxygen bonds, which increase the degree of asymmetry in the $SiO_4$ tetrahedra and therefore increase the thermal expansion of the glass. In addition, the thermal expansion is modified by the thermal history of the glass (the temperature of melting, the rate of cooling and also the subsequent heat treatment e.g. annealing) [163]. It is also worth noting that, although the thermal expansion is almost constant, up to the glass transition temperature, its value is slightly increasing when measured over an increasing temperature range [24,316].

The thermal expansion of Ca-Nd-aluminosilicate glasses increases with increasing Ca-Nd-silicate content (Fig.4.16), although there is a slight tail-off at the highest Ca-Nd-silicate contents (50 & 55wt%). The thermal expansion of Mg-Nd-aluminosilicate glasses also showed an increasing trend (with some fluctuations) with increasing Nd-disilicate content (Fig.4.17). Increasing thermal expansion with increasing rare-earth oxide content was observed for Nd-aluminosilicate glasses [264], Y-aluminosilicate glasses [260], Er-aluminosilicate glasses [266] and Sm-aluminosilicate glasses [269]. The rare-earth cations in these glasses, due to their high field strength, increase the asymmetry of the $SiO_4$ tetrahedra, and are therefore responsible for the increase of these glasses' thermal expansion.

Fig.4.16. Thermal expansion values of Ca-Nd-aluminosilicate glasses

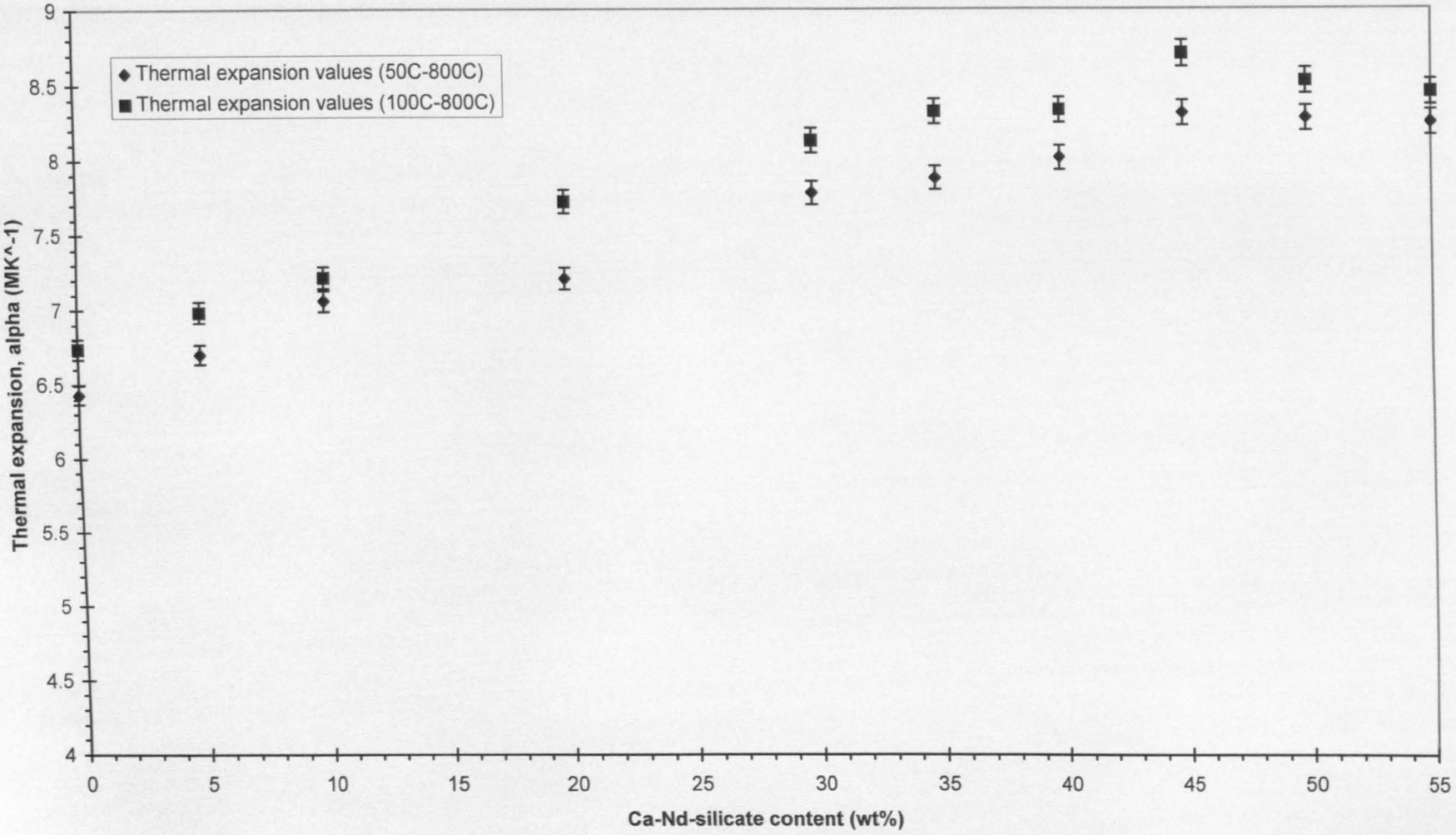

Fig.4.17. Thermal expansion values of Mg-Nd-aluminosilicate glassses

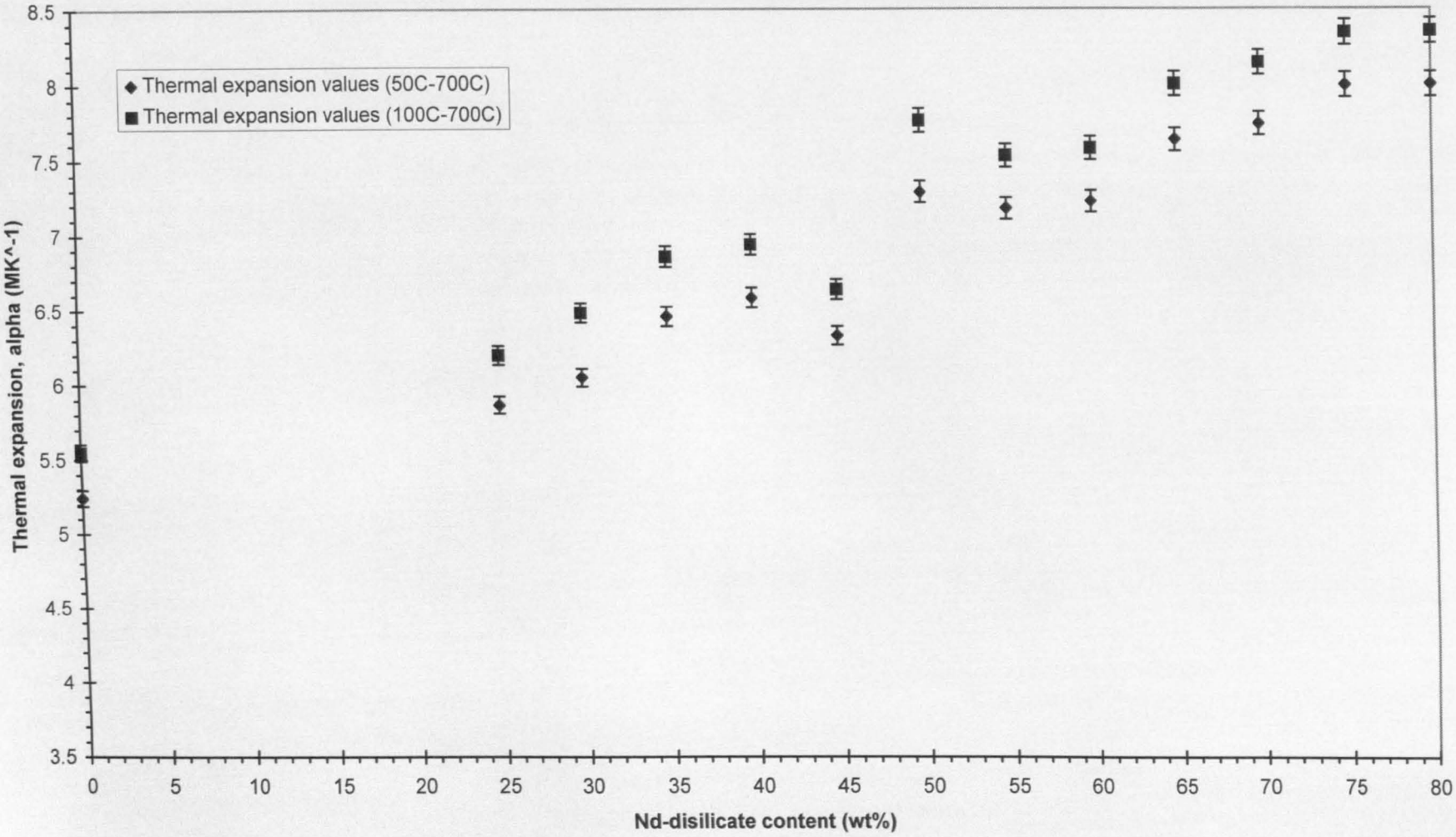

Similar, upper-medium range thermal expansion values were measured for the Y and La containing calcium- and magnesium-aluminosilicate glasses, as well as for the $TiO_2$ containing Ca-Nd-aluminosilicate glasses (Table 4.3), which is also due to their rare-earth oxide content.

### 4.4. Comparison with other aluminosilicate glasses

In order to evaluate the properties of the glasses prepared in this study, some physical and thermal properties of selected industrial glasses as well as some rare-earth containing experimental glasses are shown in Table 4.5.

The measured properties of the glasses prepared in this study were similar to the previous experimental rare-earth containing glasses, namely high refractive index, high Vickers hardness, high glass transition and softening temperatures and moderate thermal expansion. The relatively high density of rare-earth containing glasses is due to the high atomic weight of the rare-earth elements. Their high refractive index is due to the effect of high field strength rare-earth cations on the polarizability of oxygen anions. Their high hardness compared to ordinary glasses, can be described as the rare-earth cations having relatively high ionic charge and small radii and can fill the interstitial positions in the glassy network, this way increasing the packing density, therefore creating higher resistance to compression. The high glass transition and softening temperatures are due to the incorporation of rare-earth cations in the glass structure, which are still the weakest link in the glassy network, but create much stronger bonds than the ordinary modifier cations. The increase in thermal expansion is due to the effect of high field strength rare-earth cations on the degree of asymmetry of $SiO_4$ tetrahedra.

The combinations of these properties are outstanding, compared to the listed industrial glasses and propose some potential application areas. The high refractive index, the low dispersion and high elastic modulus of rare-earth containing glasses (though the last two properties were not measured in this study, one can suspect that they will behave similarly to the rare-earth aluminosilicate glasses) makes them ideal candidates for optical application e.g. fibre optics. Their thermal expansion is in the upper-medium range (it is fairly high for such refractive glasses), which suggests a use as glass-to-metal seals (especially when one counts the reported extra low He permeability of some rare-earth containing glasses [264,266]). Their high softening temperature and the reported high alkaline durability make them suitable candidates for high temperature applications in corrosive media.

Table 4.5. Properties of selected industrial and rare-earth containing experimental glasses

| glass type | Ln2O3 content (mol%) | density (g/cm^3) | thermal expansion alpha (MK^-1) | refractive index nD20 | Vickers hardness (GPa) | Youngs modulus (GPa) | indentation fracture toughness MPam^(1/2) | flexural strength (3 point bend) (MPa) | transition temp. (C) | softening point (C) | source |
|---|---|---|---|---|---|---|---|---|---|---|---|
| soda-lime | N/A | 2.5 | 9.2 (20-500C) | 1.512 | 5.5 | 70 | 0.75 | 120 | 510 | 696 | [6] [317] [46] |
| borosilicate (Pyrex) | N/A | 2.23 | 3.4 (0-300C) | 1.47 | 5 | 70 | 0.75 | | 515 | 780 | [20] [18] [159] |
| fused silica | N/A | 2.2 | 0.56 (0-300C) | 1.458 | 7.12 | | 0.7 | 50 | 1140 | 1667 | [20] [6] [159] [23] |
| aluminosilicate | N/A | 2.53 | 4.2 (0-300C) | 1.534 | | | | | 710 | 915 | [20] [23] |
| Li aluminosilicate | N/A | 2.4035 | 3.36 (0-300C) | | | | | | 682 | 1050 | [20] |
| Ca-aluminosilicate (20-20-60 mol%) | N/A | 2.6 | 5.0 (300-400C) | 1.56 | | | | | 818 | | [60] [52] |
| Mg-aluminosilicate (cordierite comp.) | N/A | | 3.7 (25-800C) | 1.555 | 6.6 | 96 | 0.9 | 100 | 810 | 860 | [82] [80] |
| La-aluminosilicate | 17.6-20.0 | 3.80-3.96 | | 1.680-1.704 | | 95-100 | | | | | [253] |
| Nd-aluminosilicate | 10-25<br>20<br>20<br>22.2-25.8 | 3.3-4.5<br><br><br>4.05-4.5 | 4.5-6.5 (200-500C)<br>6.22 (200-500C)<br><br>4.05-12.5 | 1.696 | <br><br>6.7<br>9.1-6.5 | | | | 870-857<br>866 | 910-886<br>898 | [264]<br>[259]<br>[266]<br>[240] |
| Y-aluminosilicate | 9 -28<br>17.6-22.0<br>5-25 | 2.86-3.81<br>3.38-3.57<br>2.93-3.72 | 3.1-7.0 (100-700C)<br><br>3.65-6.45 (200-500C) | 1.572-1.717<br>1.658-1.686<br>1.545-1.708 | 6.36-8.28 (0.98N)<br>7.86-8.07 (1.96N) | 112-114 | | | 884-895<br><br>897-911 | 933-947<br><br>933-948 | [268]<br>[253]<br>[260] |
| Ca-Y-aluminosilicate | 2.5-20<br>10 | 2.8-3.4 | 5.0-6.0 (50-350C) | | 6.4 (1.96N) | 85 | 0.6 | | | | [255] [254] |
| Nd-Si-Al-O-N | 8.6-25.0 | 3.51-4.8 | 5.0-8.0 | | 10.4-7.4 | | | | | | [240] |

## CHAPTER 5.

## GLASS-CERAMIC DERIVATIVES OF Ca-Ln-ALUMINOSILICATE GLASSES

### 5.1. Crystallization of a pure CAS (anorthite) glass

For comparison purposes, the crystallization of pure CAS glass (anorthite composition) was studied in parallel with the rare-earth containing calcium-aluminosilicate glasses. One crystallization exotherm was detected on the DTA trace of the CAS glass (Table 4.4). Polished-surface bulk glass and pelletized glass powder specimens were subjected to heat treatments at various temperatures (Table 5.1), at and above the crystallization temperature determined by DTA.

**Table 5.1.** Crystallization of CAS (anorthite) glass

| Sample type | Temp. of cryst. (°C) | Duration of cryst. | Crystalline phases detected by XRD (m: major, +: minor) |
|---|---|---|---|
| bulk glass | 1018 | 2 hr | no detectable crystallinity |
| bulk glass | 1039 | 2 hr | no detectable crystallinity |
| bulk glass | 1100 | 2 hr | no detectable crystallinity |
| bulk glass | 1150 | 2 hr | m: anorthite |
| bulk glass | 1200 | 2 hr | m: anorthite |
| bulk glass | 1300 | 2 hr | m: anorthite, +: mullite |
| glass powder | 1018 | 2 hr | m: o-Ca-Al-Si, m: anorthite |
| glass powder | 1039 | 2 hr | m: anorthite, +: mullite |
| glass powder | 1100 | 2 hr | m: anorthite, +: mullite |
| glass powder | 1150 | 2 hr | m: anorthite, +: mullite |
| glass powder | 1200 | 2 hr | m: anorthite, +: mullite |
| glass powder | 1300 | 2 hr | m: anorthite, +: mullite |
| hot pressed powder | 1300 | 2 hr | m: anorthite, +: mullite |

According to the XRD analysis (Table 5.1), the heat treatments of both types of samples resulted in anorthite ($CaAl_2Si_2O_8$, JCPDS 41-1486) as the major crystalline phase, which was occasionally accompanied by a minor phase of mullite (JCPDS 15-776). In addition, a major phase of orthorhombic $CaAl_2Si_2O_8$ (JCPDS 5-528) was also detected in a low temperature sintered powder pellet (Table 5.1). Anorthite and

mullite were identified on the XRD trace of the hot pressed CAS glass powder, as well (Table 5.1).

The bulk glasses showed surface crystallization, initiated from a limited number of nucleation sites. In spite of that, the high temperature crystallizations resulted in strong, compact, fully crystalline glass-ceramic bodies. Crystallizations of the pelletized and hot-pressed glass powders resulted in well-sintered, well-crystallized glass-ceramics, except for the lower temperature crystallized pellets, which showed a lower degree of crystallinity.

## 5.2. Crystallization and microstructure of Ca-La-aluminosilicate glass-ceramics

The composition of the Ca-La-aluminosilicate parent glass (CASL-2) used for the crystallization experiments was previously shown in Table 4.1. One crystallization exotherm was observed on the DTA trace of the glass (Table 4.3). The onset and the maximum of the crystallization exotherm were selected for the lower temperatures of crystallization. Since the lower temperature heat treatments resulted in only a thin crystalline layer on the surface of bulk glasses, higher temperature heat treatments were also applied, in order to get a higher degree of crystallinity and better microstructure. The lower temperature heat treatments were generally shorter (10/30min), in order to preferentially crystallize the primary phase, whereas the higher temperature ones were longer (30min/2hr), in order to achieve the crystallization of secondary and accompanying phases (if there are any). Similar concepts were applied during the selection of heat treatment temperature and duration for all glass compositions made during this study. The temperature and duration of the crystallization heat treatments applied, as well as the crystalline phases detected by XRD are shown in Table 5.2.

**Table 5.2.** Crystallization of Ca-La-aluminosilicate (CASL-2) glass

| Sample type | Temp. of cryst. (°C) | Duration of cryst. | Crystalline phases detected by XRD (m: major, +: minor) |
|---|---|---|---|
| bulk glass | 942 | 30 min | no detectable crystallinity |
| bulk glass | 978 | 10 min | no detectable crystallinity |
| bulk glass | 978 | 30 min | no detectable crystallinity |
| bulk glass | 1004 | 2 hr | no detectable crystallinity |
| bulk glass | 1150 | 30 min | m: anorthite, m: Ca-La-Si, +: Ca-La-Al-Si |
| bulk glass | 1150 | 2 hr | m: Ca-La-Si, m: anorthite, +: Ca-La-Al-Si |
| bulk glass | 1223 | 2 hr | m: Ca-La-Si, m: anorthite, +: Ca-La-Al-Si |
| powder pellet | 942 | 30 min | m: anorthite, +: Ca-La-Si |
| powder pellet | 978 | 10 min | m: anorthite, +: Ca-La-Si, +: Ca-La-Al-Si |
| powder pellet | 978 | 30 min | m: anorthite, +: Ca-La-Si, +: Ca-La-Al-Si |
| powder pellet | 1004 | 2 hr | m: anorthite, m: Ca-La-Si, +: Ca-La-Al-Si |
| powder pellet | 1150 | 30 min | m: anorthite, m: Ca-La-Si, +: t-La•2Si, +: Ca-La-Al-Si |
| powder pellet | 1150 | 2 hr | m: anorthite, m: Ca-La-Si, +: t-La•2Si, +: Ca-La-Al-Si |
| powder pellet | 1223 | 2 hr | m: anorthite, m: t-La•2Si, m: Ca-La-Si, +: Ca-La-Al-Si |

The crystallization of the polished and rough surfaced bulk glasses resulted in glass-ceramics bearing close similarities. The bulk samples showed the signs of a surface crystallization mechanism. In spite of that, the high temperature heat treatments resulted in compact, fully crystalline glass-ceramic bodies. The bulk glass-ceramics, originating from polished-surface parent glass slices, are used for SEM illustrations in Chapters 5&6. The rough glass slices crystallized faster, therefore the different stages of crystallization cannot be illustrated by them, and their surfaces were too rough even after crystallization, which resulted in less sharp contrast. It should be noted, that the SEM micrographs presented in Chapters 5&6 were made in backscattered electron mode (composition selective image), unless stated otherwise.

The lower temperature heat treatments of bulk Ca-La-aluminosilicate glasses resulted in a thin crystalline layer on the surface of the samples, and the amount of

crystallinity did not provided analysable XRD traces, therefore the identifications of these crystalline phases were done by SEM morphological studies and X-ray microanalysis. Up to 1004°C anorthite crystals were the primary and dominant phase, as shown in Fig.5.1/a&b. The small spherulites have complex morphology: the dark core is anorthite and the boundary region shows the early stage of spherulitic fibrillar growth.

Spherulitic growth was essentially studied by Keith & Padden [318-320], but their work was mainly concerned with organic polymers. Spherulitic crystallization of glasses and glass-ceramics was investigated by Freiman *et al.* [321] with Ba- and Li-silicate glasses, whereas Lewis *et al.* [322,323] published detailed TEM investigation on spherulitic crystallization of Ba-silicate glasses. Spherulites are spherical shaped polycrystalline aggregates, consist of radially oriented fibrillar crystals, where the fibres show low-angle, noncrystallographic branching, and the interfibrillar space is often occupied by glassy residue. Spherulitic growth is presumably initiated by crystal-liquid (i.e. glass) interface instabilities, which in turn are induced by impurity or second component segregation [323]. On Fig.5.1/a, the anorthite crystals were nucleated by active sites on the surface, and as the crystals grew, they rejected the rare-earth ions (in this case $La^{3+}$), whose concentration built up on the glass side of the interface. This enrichment in $La_2O_3$ can suppress the further crystallization of anorthite, unless the crystal-glass interface becomes irregular and forms fibrillar projections, which during their growth, will reject impurities into the interfibrillar area. According to Freiman *et al.* [321] spherulitic morphology can be frequently encountered during the initial stages of the crystallization of glass-ceramics.

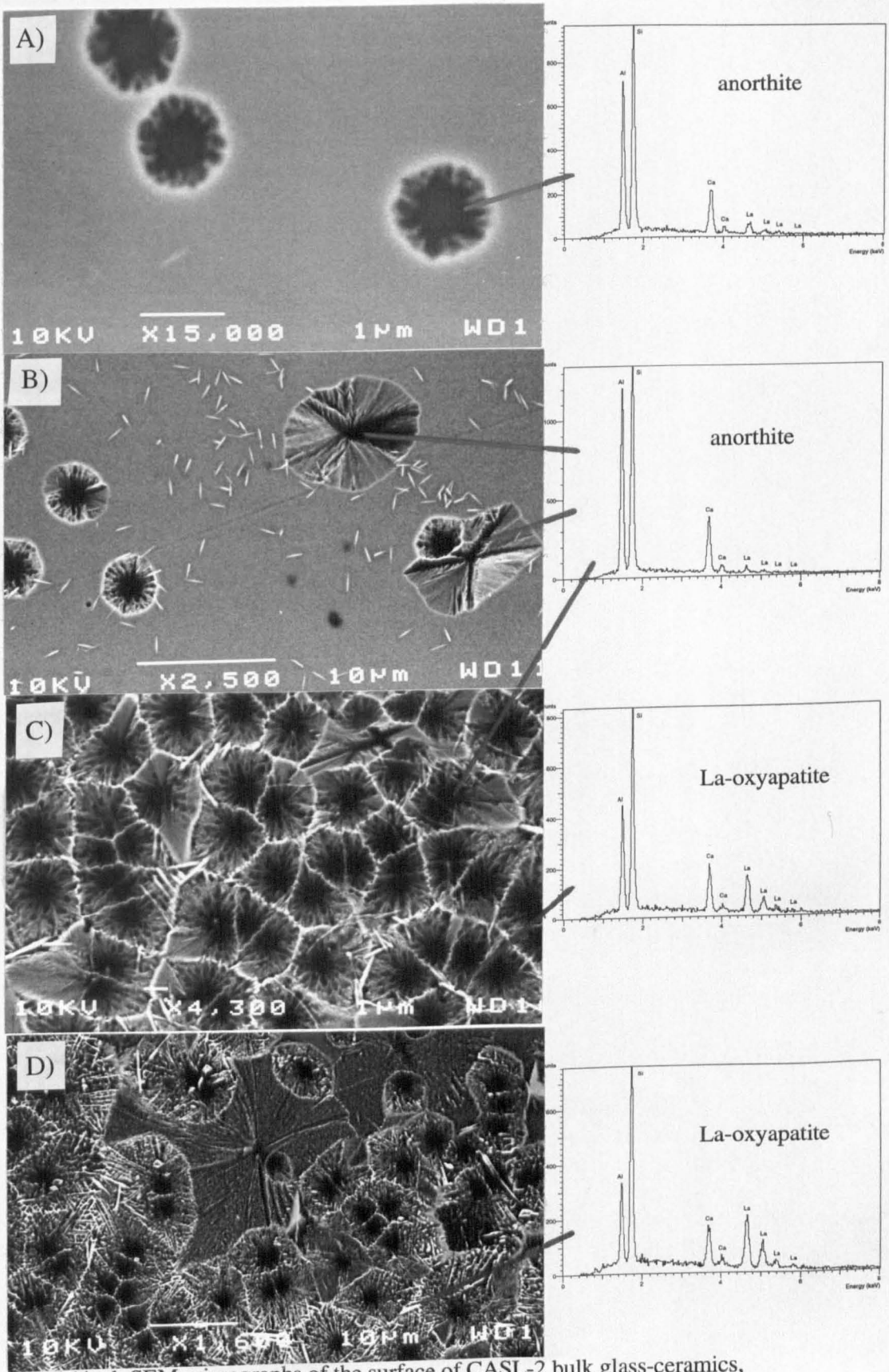


Fig.5.1/a-d. SEM micrographs of the surface of CASL-2 bulk glass-ceramics,
a) 942°C/30min; b) 978°C/2hr; c) 1004°C/2hr; d) 1150°C/2hr.

All authors quoted above agreed that spherulitic crystals represent an intermediate, metastable morphology, due to the large interfacial area of the fibrous crystals, and higher temperature heat treatments eventually lead to the recrystallization of the fine spherulitic arms into a more stable, lath-like morphology. Lewis & Smith [323] proposed, that controlled spherulitic growth and recrystallization can be a suitable process to produce glass-ceramics with microstructures consisting of fine-grained, randomly oriented crystals, without the need for nucleating agents.

At higher temperatures small, needle shaped $Ca_2La_8Si_6O_{26}$ (oxyapatite) crystals can be also detected, although their tiny size makes them hardly analysable by X-ray microanalysis. Large spherulitic and dendritic anorthite crystals can also be observed on the micrograph, their large size and small number suggest that they were nucleated by surface impurities. At 1004°C the impinging anorthite-centred spherulitic crystals completely covered the surface of the glass-ceramic (Fig.5.1/c). The micrograph reveals the advanced stage of interface instability-initiated spherulitic growth, and bears close similarities with its idealized image, drawn by Lewis *et al.* [322]. The previously crystallized, La-oxyapatite crystals show signs of secondary growth (coarsening). In addition, the crystallization of La-rich residual glassy phase can be observed at the spherulite interfaces.

The high temperature heat treatments increased the amount of the La-oxyapatite (JCPDS 29-337) phase (Table 5.2) at the expense of the glassy residual phase (Fig. 5.1/d). During that process the high temperature lowered the viscosity of the residual glass and lead to the recrystallization of the spherulitic microstructure, promoting the growth of crystals with fine grained, faceted morphology (Fig.5.2).

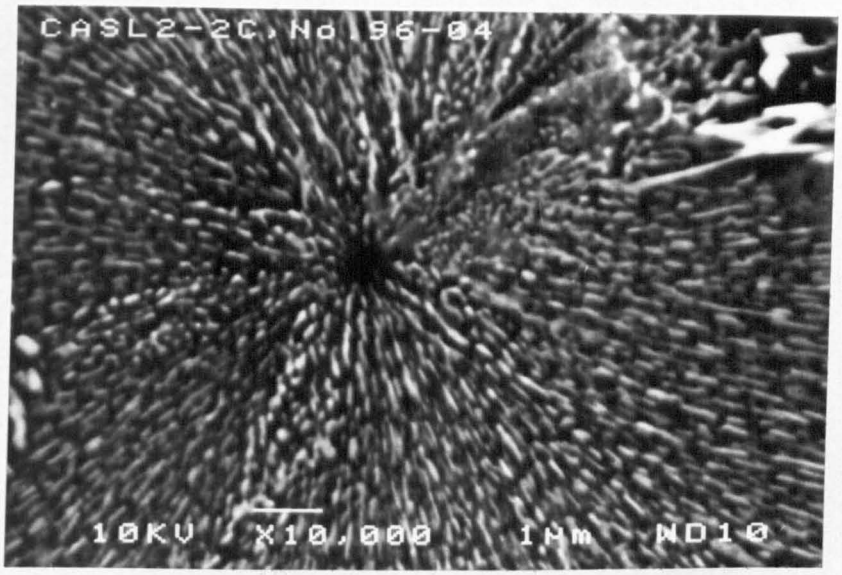


Fig.5.2. SEM micrograph of the surface of a CASL-2 bulk glass-ceramic after recrystallization (1150°C/2hr).

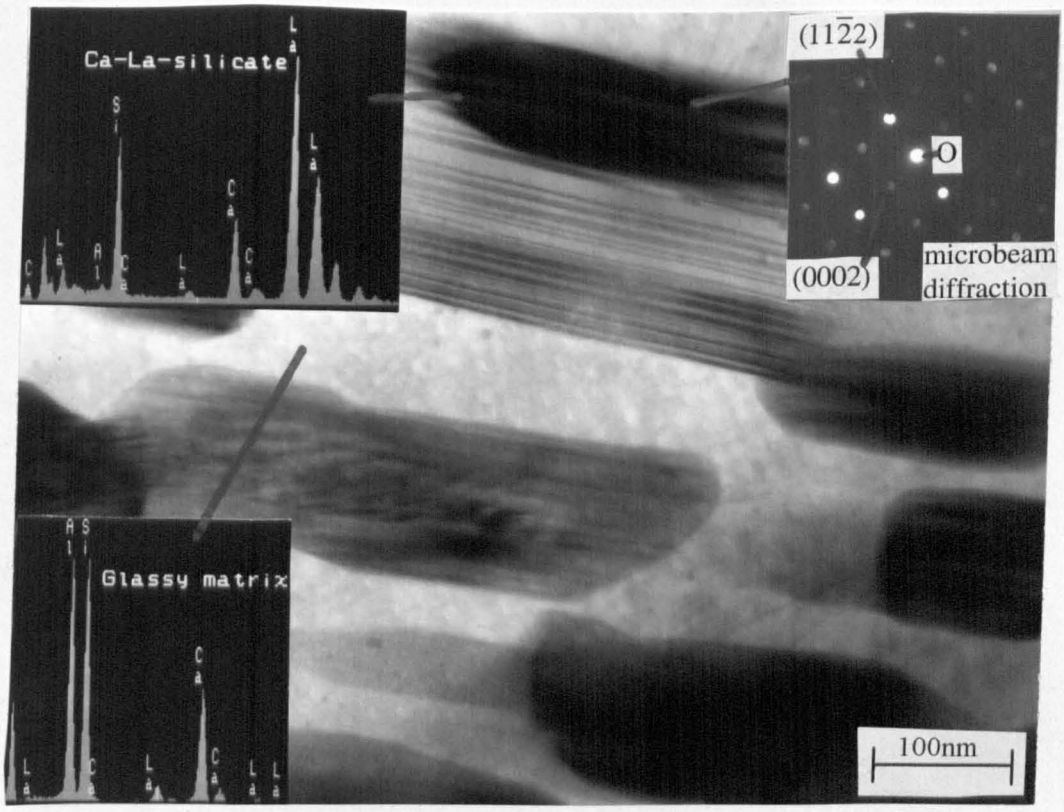


Fig.5.3. Bright field TEM micrograph of a CASL-2 bulk glass-ceramic

Some La-oxyapatite crystals are shown in a bright field TEM micrograph (Fig.5.3). In addition, after 2 hours at 1150°C, the bulk of the glass also crystallized with fine morphology (Fig.5.4/a&b). On the micrograph, a large amount of previously unknown quaternary rare-earth aluminosilicate crystalline phase (grey phase) can be identified by SEM/EDS, and the remaining XRD reflections were assigned to this new phase (Fig.II.1 - Appendix II). The X-ray powder data of the new phase is shown in Table 5.3. The oxide ratio ($CaO:La_2O_3:Al_2O_3:SiO_2$) of the new Ca-La-aluminosilicate phase, based on EDS analyses, is between 1:1:2:3 and 1:1.7:2:3.4. Moreover, a minor amount of low temperature, tetragonal $La_2Si_2O_7$ (XRD data source: [301]) was also detected in some samples by XRD (Table 5.2). The highest temperature heat treatment (1223°C/2hr) resulted in the recrystallization of spherulitic structures into small crystals, as well as causing some coarsening in the bulk of the glass (Fig.5.4/c), but the average crystal size still remained around 1 μm.

**Table 5.3.** X-ray Powder Diffraction data of the Ca-La-aluminosilicate phase

| d | Intensity | d | Intensity | d | Intensity |
|---|---|---|---|---|---|
| 5.848 | weak | 2.967 | weak | 2.084 | medium strong |
| 5.369 | medium strong | 2.926 | strong | 2.073 | medium strong |
| 5.076 | weak | 2.643 | weak | 1.980 | medium strong |
| 4.524 | weak | 2.584 | very strong | 1.916 | weak |
| 4.332 | weak | 2.550 | medium strong | 1.838 | strong |
| 3.939 | weak | 2.514 | weak | 1.822 | medium strong |
| 3.870 | medium strong | 2.491 | medium strong | 1.722 | weak |
| 3.450 | strong | 2.163 | medium strong | 1.702 | weak |
| 3.116 | very strong | 2.149 | medium strong | 1.593 | medium |
| 3.078 | strong | 2.096 | medium strong | 1.483 | medium |

The major difference between the polished and rough surface samples is that the rough surface provided numerous nucleation sites, which eventually lead to a thicker crystalline layer at the lower temperature heat treatments.

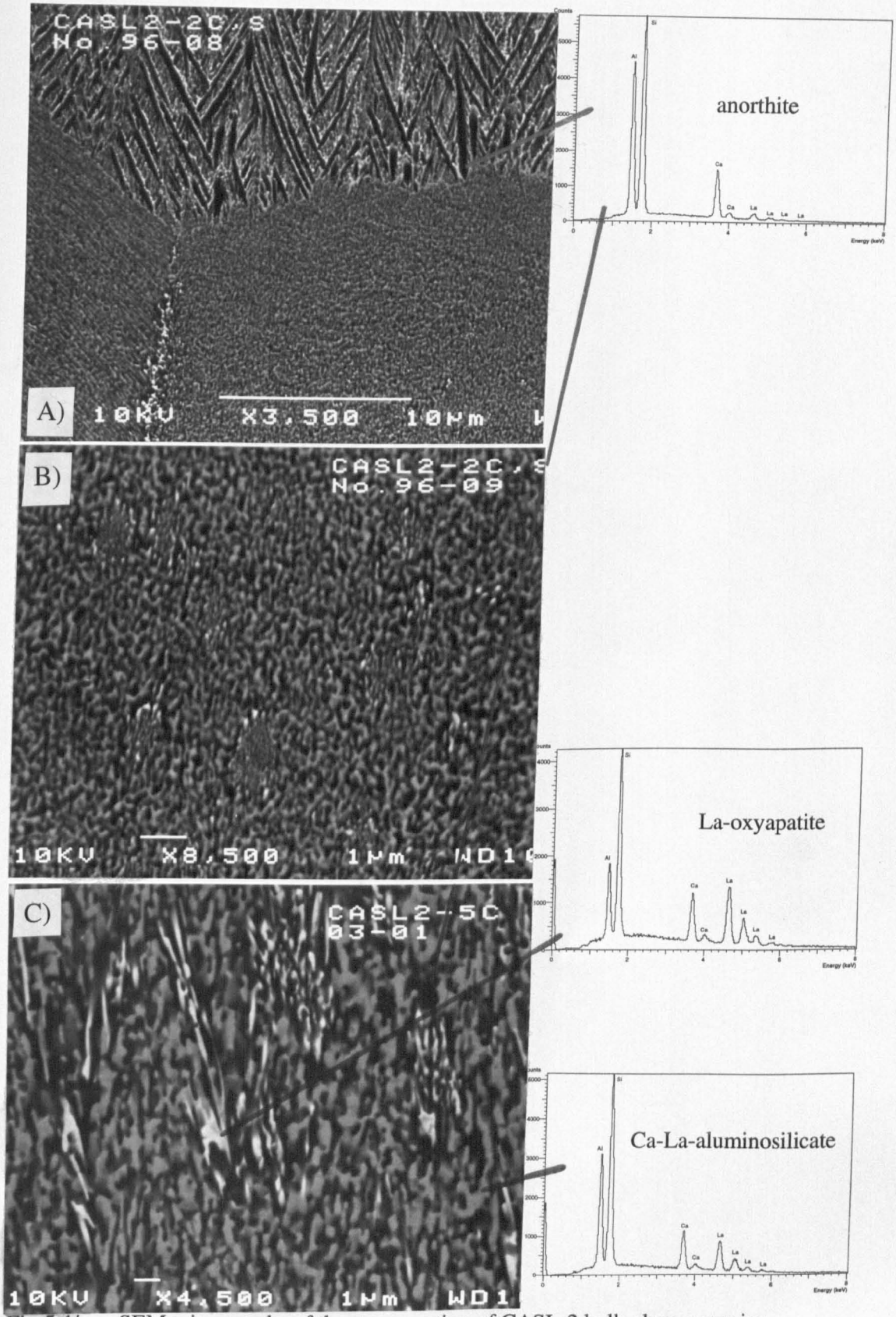


Fig.5.4/a-c. SEM micrographs of the cross-section of CASL-2 bulk glass-ceramics, a) 1150°C/30min; b) 1150°C/2hr; c) 1223°C/2hr.

In addition, the rough surface preferentially promoted the crystallization of anorthite, therefore hardly any La-oxyapatite crystals were detected on their surface. However, in the bulk, the microstructure of both types of samples was practically identical, and the XRD analysis gave almost identical results.

During the crystallization heat treatments, the pelletized specimens went through their glass compositions' softening range, which densified the pellets, reduced the size and the number of pores, due to the glass' viscous flow, which preceded crystallization. The crystallization mechanism in the case of pellets made from finely ground powders is almost entirely surface crystallization, but it cannot have any drawback on the properties, since the maximum crystal size is initially determined by the average size of the glass powder particles, whose largest dimension was 2-3 μm. The above comments are valid for the pelletized specimens of all glass compositions made during this study.

In the case of sintered powder pellets, anorthite was also the first phase to crystallize, but a minor amount of La-oxyapatite was also detected by XRD, even at the lowest crystallization temperature (Table 5.2). Up to 1004°C, the dominant phase was anorthite (Fig.5.5/a), and the amount of the La-oxyapatite phase increased with increasing crystallization temperature (Table 5.2), although its presence was not detectable by SEM. Above 1004°C, as the glassy residue between the anorthite grains started to crystallize (Fig.5.5/b) and a minor phase of low temperature, tetragonal La-disilicate was also detected by XRD (Table 5.2).

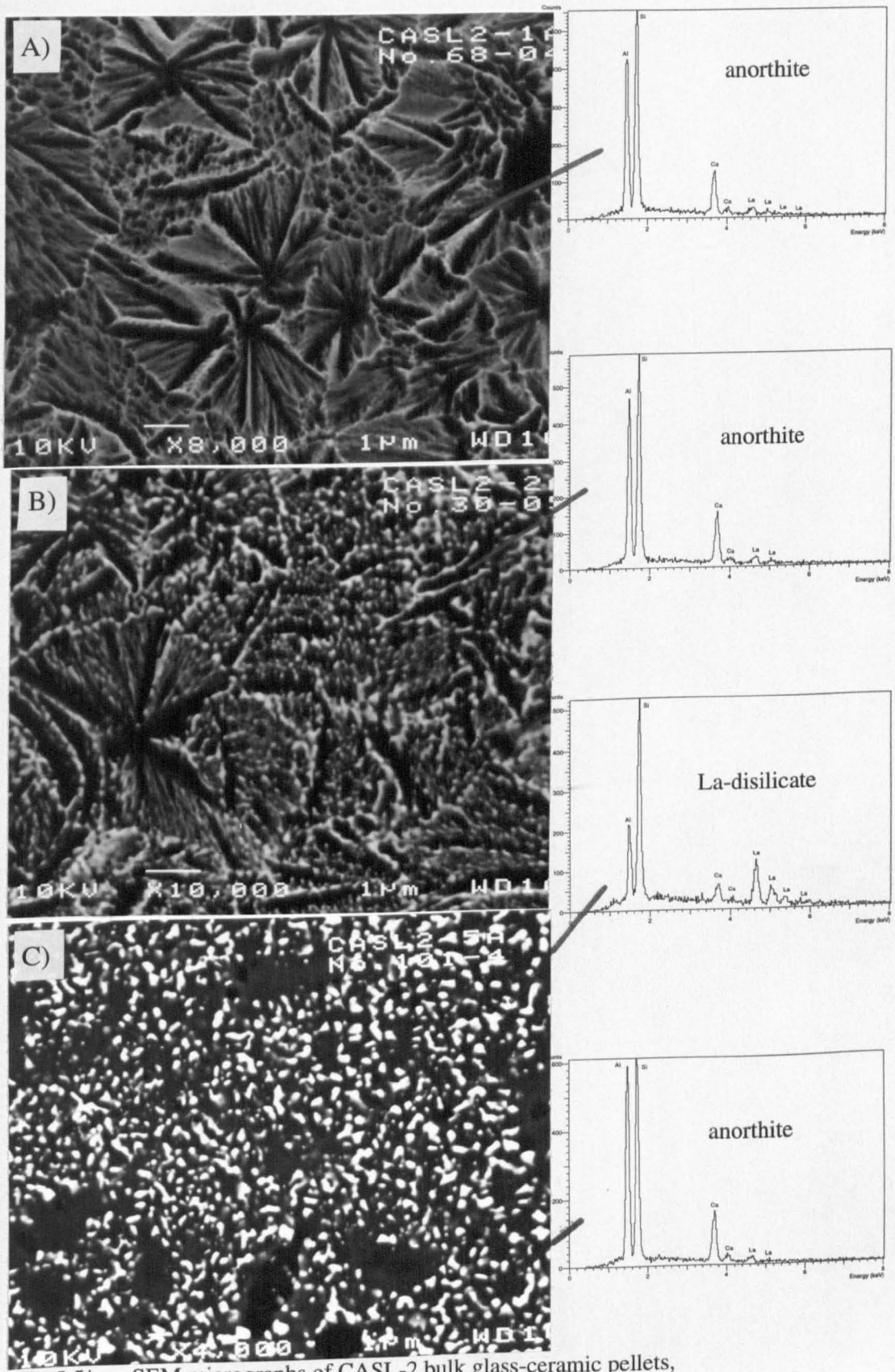


Fig.5.5/a-c. SEM micrographs of CASL-2 bulk glass-ceramic pellets,
a) 1004°C/30min; b) 1150°C/2hr; c) 1223°C/2hr.

As the temperature of the crystallization increased, the amount of La-disilicate was substantially increased at the expense of La-oxyapatite, and this process was accompanied by recrystallization and some coarsening of the crystalline grains (Fig.5.5/c), which were due to the lower viscosity of the glassy residue at high temperature. In addition, Ca-La-aluminosilicate, as a minor phase, always accompanied the major phases (Table 5.2).

## 5.3. Crystallization and microstructure of Ca-Y-aluminosilicate glass-ceramics

The composition of the Ca-Y-aluminosilicate glass (CASY-1) used for the crystallization experiments can be found in Table 4.1. The DTA analysis of the alumina-ground glass powder showed three crystallization exotherms (Table 4.3), and the heat treatments applied for crystallization and the crystalline phases detected by XRD are shown in Table 5.4.

**Table 5.4.** Crystallization of Ca-Y-aluminosilicate (CASY-1) glass

| Sample type | Temp. of cryst. (°C) | Duration of cryst. | Crystalline phases detected by XRD (m: major, +: minor) |
|---|---|---|---|
| bulk glass | 1008 | 30 min | no detectable crystallinity |
| bulk glass | 1033 | 2 hr | no detectable crystallinity |
| bulk glass | 1170 | 30 min | m: anorthite, m: Ca-Y-Si, +: y-Y•2Si, +: α-Y•2Si |
| bulk glass | 1170 | 2 hr | m: Ca-Y-Si, m: anorthite +: y-Y•2Si, +: α-Y•2Si |
| bulk glass | 1243 | 2 hr | m: y-Y•2Si, m: anorthite, m: Ca-Y-Si |
| powder pellet | 1008 | 30 min | m: anorthite, +:α-Y•2Si, +: o-Ca-Al-Si, +:Ca-Y-Si |
| powder pellet | 1033 | 2 hr | m: anorthite, +:α-Y•2Si, +: o-Ca-Al-Si, +:Ca-Y-Si |
| powder pellet | 1170 | 30 min | m: anorthite, +:α-Y•2Si, +: o-Ca-Al-Si, +:Ca-Y-Si |
| powder pellet | 1170 | 2 hr | m: anorthite, +:α-Y•2Si, +: o-Ca-Al-Si, +:Ca-Y-Si |
| powder pellet | 1243 | 2 hr | m: anorthite, m: β-Y•2Si |

The glass-ceramics crystallized from polished and rough surfaced bulk Ca-Y-aluminosilicate glasses also showed the signs of surface crystallization, and were almost identical, except for the thickness of the crystalline layer of the low-

temperature crystallized samples. The heat treatments up to 1033°C resulted in samples with low level of crystallinity. The SEM/EDS analyses of these samples detected anorthite, and $Ca_4Y_6Si_6O_{25}$ (Y-oxyapatite) crystals, with anorthite being the primary and dominant phase. Fig.5.6/a shows the slightly advanced stage of the process: the crystalline layer completely covered the surface of the sample. The long, needle shaped crystals are Y-oxyapatite (their twinned structure can be observed at higher magnification), and most of the surface is covered by anorthite centred spherulitic crystalline complexes (Fig.5.6/b). In addition, some surface impurity or defect initiated dendritic anorthite crystals can also be observed.

Higher temperature heat treatment resulted in coarsening of the crystalline microstructure (Fig.5.6/c). It was the result of secondary growth of Y-oxyapatite crystals and the crystallization of the Y-rich glassy interfibrillar area. The XRD traces show, among the major phases of anorthite and Y-oxyapatite (JCPDS 27-93), minor phases of y-$Y_2Si_2O_7$ (XRD data source: [296]) & α-$Y_2Si_2O_7$ (JCPDS 38-223). According to the XRD traces, as the duration of the heat treatment increased, the amount of Y-oxyapatite increased first, then at higher temperature, the amount of the y-Y-disilicate increased considerably at the expense of Y-oxyapatite (Table 5.4). The signs of complete recrystallization can be observed on the surface of the glass-ceramic, where the fibrous type microstructure is converted into fine grained lath-like microstructure (Fig.5.6/d) due to the high temperature which reduced the viscosity of the residue and promoted the growth of the energetically more stable faceted morphology.

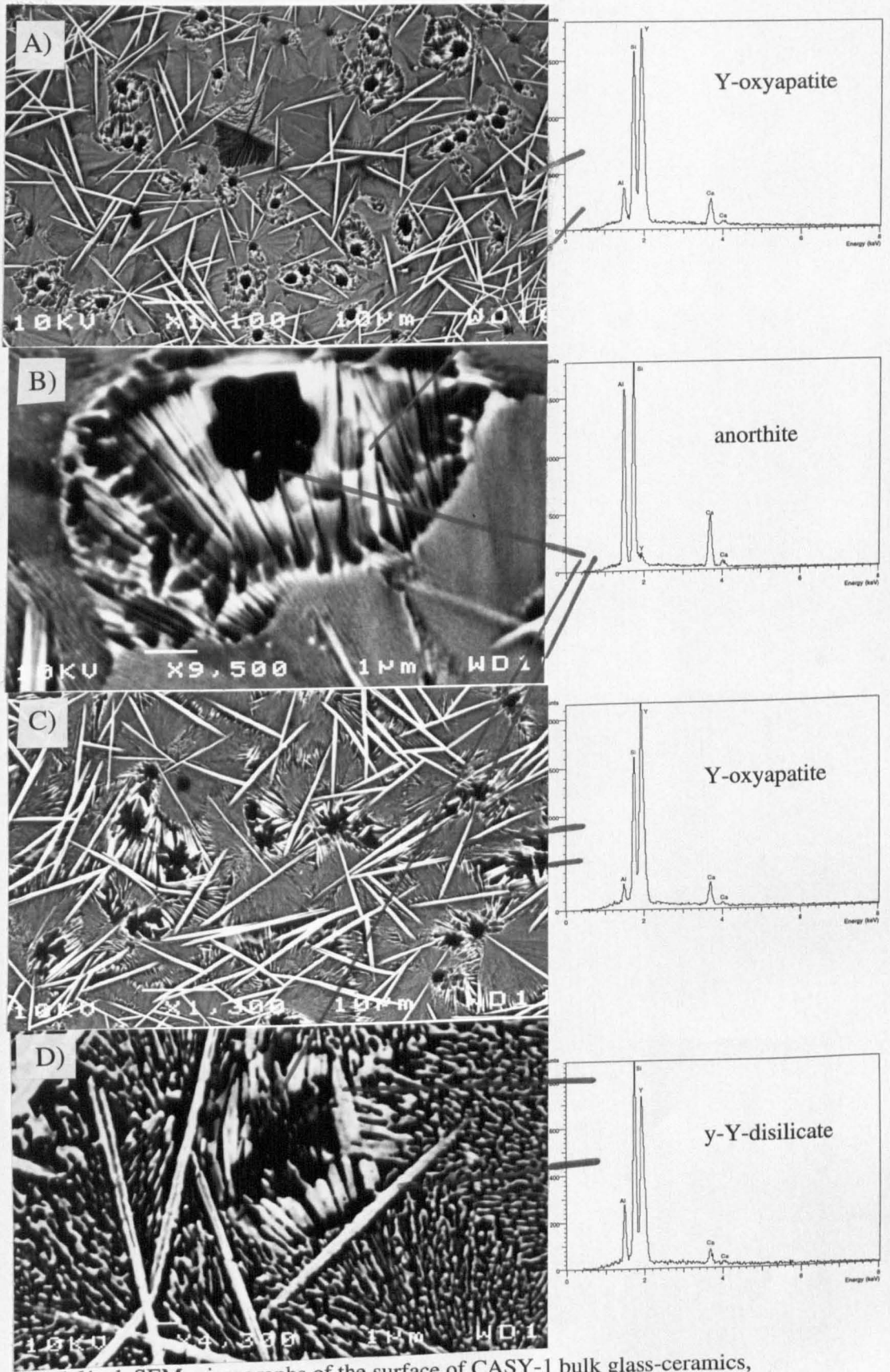


Fig.5.6/a-d. SEM micrographs of the surface of CASY-1 bulk glass-ceramics, a) 1033°C /2hr; b) 1033°C/2hr; c) 1170°C/30min; d) 1243°C/2hr.

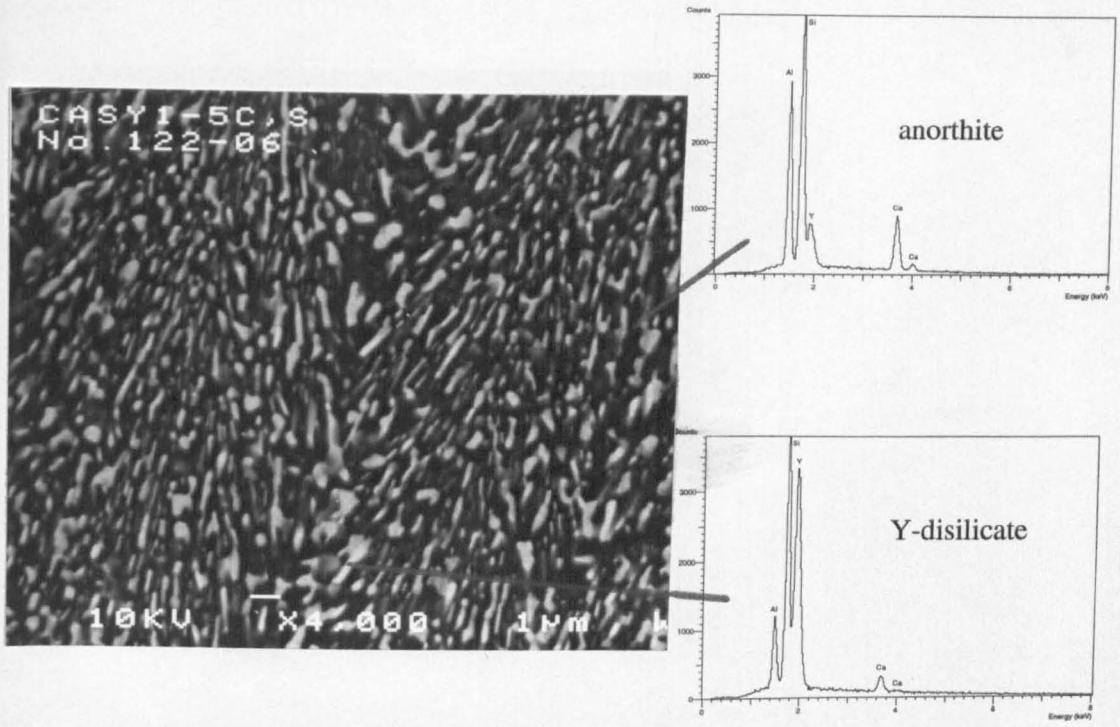


Fig.5.7. SEM micrograph of a cross section of a CASY-1 bulk glass-ceramic (1243°C/2hr).

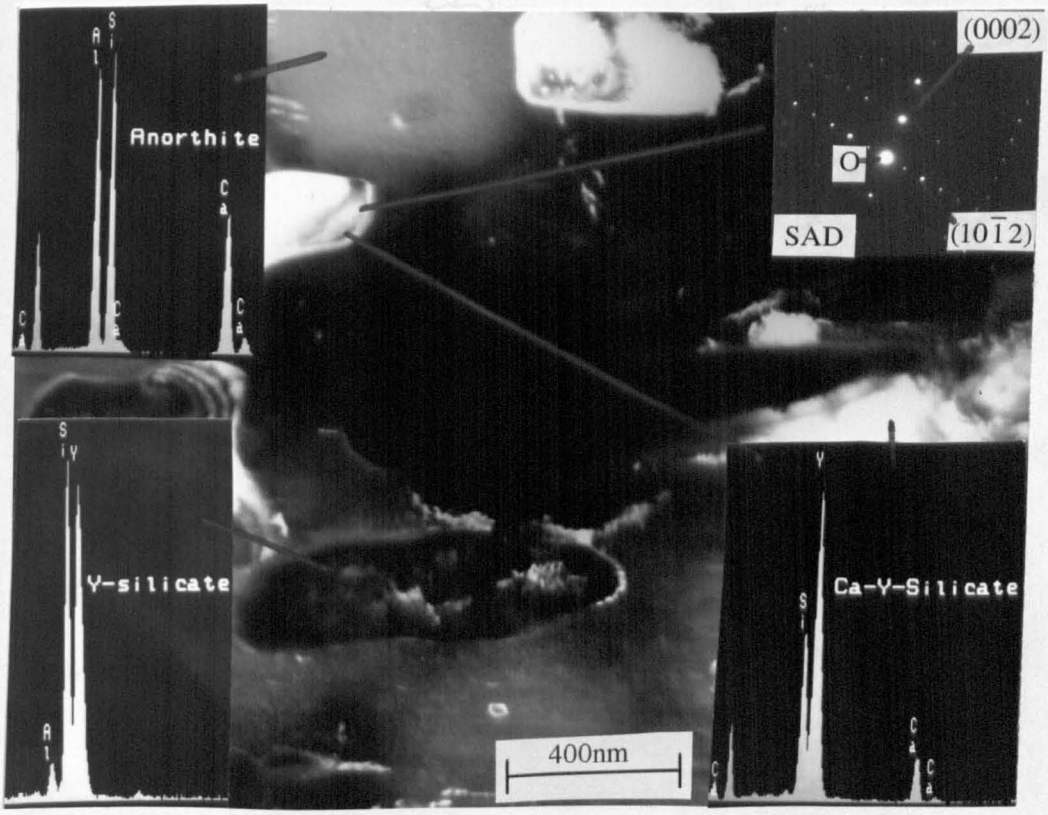


Fig.5.8. Dark field TEM micrograph of a CASY-1 bulk glass-ceramic (1243°C/2hr).

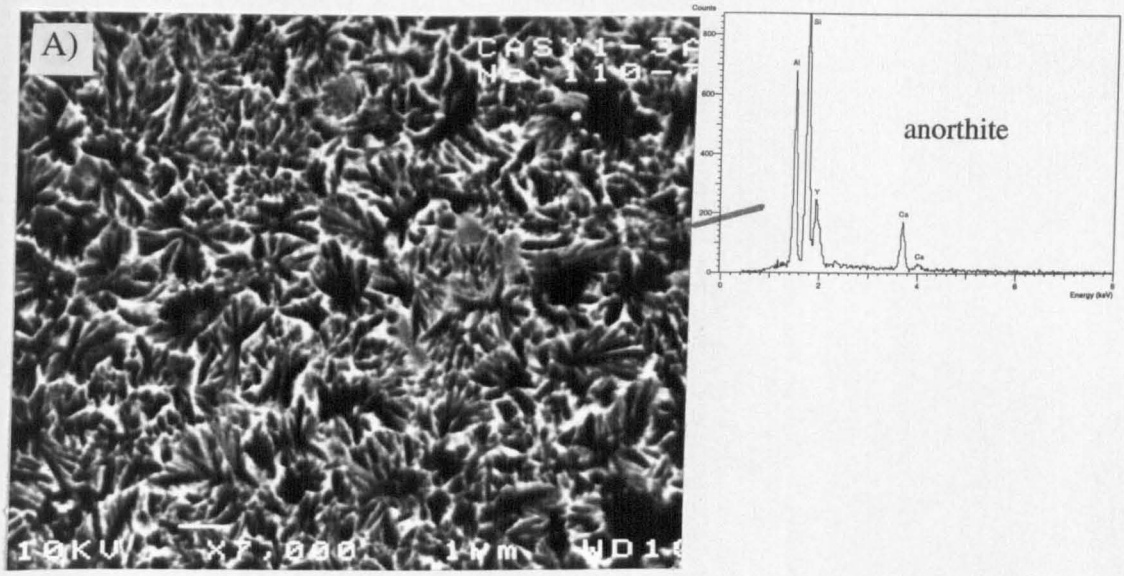


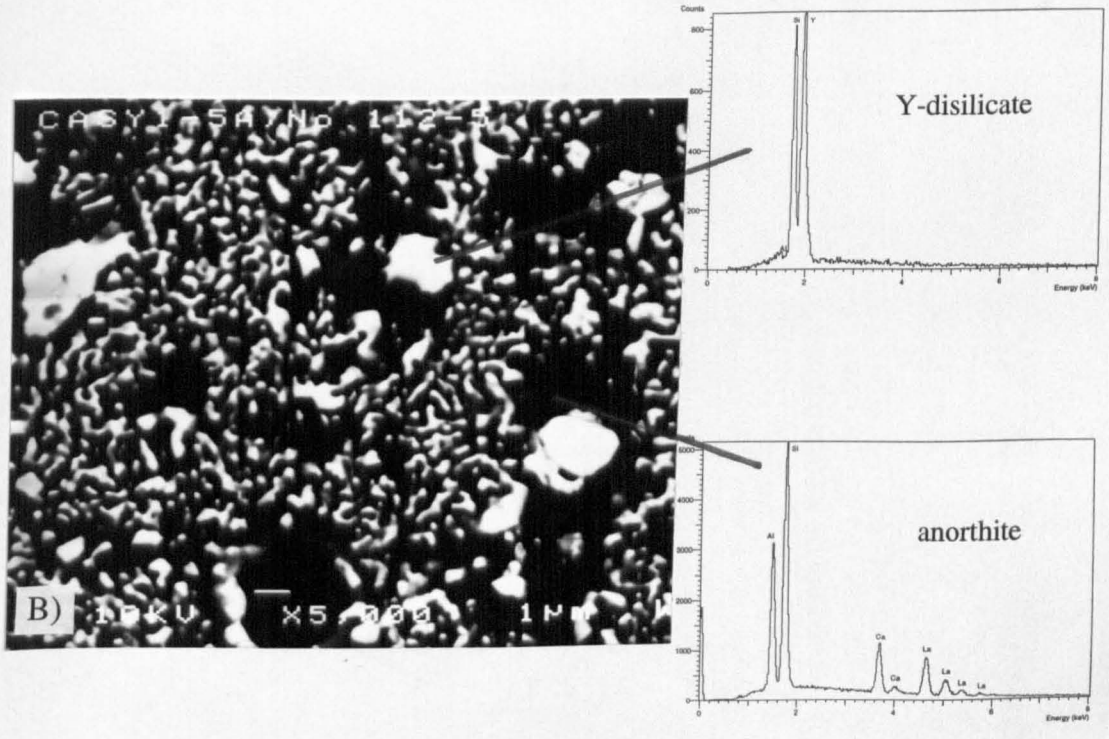


Fig.5.9/a-b. SEM micrographs of CASY-1 glass-ceramic pellets, a) 1008°C/30min; b) 1223°C/2hr.

The recrystallized microstructure can also be detected in the bulk of the glass-ceramic (Fig.5.7). In Fig.5.8, the dark field TEM micrograph shows Y-oxyapatite crystals and y-Y-disilicate crystals.

The sintered pellets showed a relatively high level of crystallinity even after the lowest temperature heat treatment (Fig.5.9/a). The bright areas between the dark anorthite grains are mainly Y-enriched glassy residue, and only few, tiny $\alpha$-$Y_2Si_2O_7$ can be detected. In addition, minor amounts of orthorhombic $CaAl_2Si_2O_8$ and Y-oxyapatite were also detected by the XRD analysis of the glass-ceramics sintered up to 1033°C (Table 5.4). At 1170°C, the amount of $\alpha$-Y-disilicate increased, whereas at 1243°C all $\alpha$-Y-disilicate and Y-oxyapatite crystals were converted into $\beta$-$Y_2Si_2O_7$ (JCPDS 38-440), which became the dominant phase (Table 5.4). The recrystallized microstructure of $\beta$-Y-disilicate crystals is shown in Fig.5.9/b.

## 5.4. Crystallization of Ca-Nd-aluminosilicate glasses

The compositions of the Ca-Nd-aluminosilicate glasses used for the crystallization experiments are shown in Table 4.1. One crystallization exotherm appeared on the DTA traces of the CASN glasses, except for the highest $Nd_2O_3$ containing composition where two of them were observed (Table 4.4). The temperature and duration of heat treatments used for the crystallization, as well as the crystalline phases detected by XRD are summarized in Tables 5.5/a-g. Some representative XRD traces are shown in Fig.II.2 (Appendix II).

**Table 5.5/a.** Crystallization of Ca-Nd-aluminosilicate bulk glasses (CASN-13,11,10)

| Sample type | Temp. of cryst. (°C) | Duration of cryst. | Crystalline phases detected by XRD (m: major, +: minor) |
|---|---|---|---|
| **CASN-13 glass** | | | |
| bulk glass | 1008 | 2 hr | no detectable crystallinity |
| bulk glass | 1200 | 2 hr | m: anorthite, +: Ca-Nd-Si, +: mullite |
| bulk glass | 1300 | 2 hr | m: anorthite, +: Ca-Nd-Si, +: mullite |
| **CASN-11 glass** | | | |
| bulk glass | 1002 | 2 hr | no detectable crystallinity |
| bulk glass | 1200 | 2 hr | m: anorthite, +: Ca-Nd-Si, +: mullite |
| bulk glass | 1300 | 2 hr | m: anorthite, +: Ca-Nd-Si, +: mullite |
| **CASN-10 glass** | | | |
| bulk glass | 996 | 2 hr | no detectable crystallinity |
| bulk glass | 1200 | 2 hr | m: anorthite, +: Ca-Nd-Si, +: mullite |
| bulk glass | 1300 | 2 hr | m: Ca-Nd-Si, m: anorthite, +: mullite |

### 5.4.1. Crystallization and microstructure of Ca-Nd-aluminosilicate bulk glass-ceramics

Both polished and rough surfaced bulk glass slices were used for the crystallization experiments in the case of the CASN-1 glass composition, whereas only polished samples were used in the case of the other glass compositions. The bulk glasses mostly crystallized by surface nucleation mechanism, but compositions CASN-1, CASN-9, CASN-12 also showed signs of bulk nucleation. Regardless of the crystallization mechanism, the high temperature heat treatments (1300°C/2hr) generally resulted in well crystallized, compact crystalline bodies.

It is interesting to separate the studied parent glass compositions into three groups. The first group consists of the low-$Nd_2O_3$ compositions, which are closer to the anorthite end of the studied pseudobinary system (CASN-13, CASN-11, CASN-10; 0.8-3.4mol% $Nd_2O_3$). The second group covers the middle range CASN-8, CASN-7, CASN-6, CASN-5 & CASN-1 (5.5-9.1mol% $Nd_2O_3$). Finally, the third

group consists of the $Nd_2O_3$-rich compositions (CASN-9 & CASN-12; 10.5-12mol% $Nd_2O_3$).

During the crystallization of CASN-13,11,10 bulk glasses, anorthite was the primary and major crystalline phase. The amount of crystalline phase after the low temperature heat treatments (up to 1000°C) resulted in limited crystallinity and identification of the crystals was only achievable by SEM/EDS analysis. Fig.5.10/a shows the familiar, anorthite-centred spherulitic crystals. At higher temperature (1200°C/2hr), the XRD analysis detected anorthite as the major phase, as well as $Ca_2Nd_8Si_6O_{26}$ (oxyapatite, JCPDS 28-228) and mullite as a minor phase (Table 5.5/a). The highest temperature heat treatment (1300°C/2hr) resulted in the recrystallization of the fine, fibrillar crystals into small, lath-shaped ones on the surface (Fig.5.10/b), as well as the crystallization of Nd-enriched residual glass as Nd-oxyapatite (Table 5.5/a). The reasons for recrystallization were the same as in the case of La- and Y-calcium aluminosilicate glass-ceramics: the lower viscosity of the glassy residue at high temperatures allowed the recrystallization of the spherulitic microstructure (which represented a higher energy state due to the large interfacial area) into the more stable, energetically more favoured lath-like morphology.

The low temperature heat treatments (around 1000°C) of CASN-8,7,6,1,5 glass compositions, similar to group one, resulted in a low level of crystallinity and the analyses of the crystalline phases were done by SEM/EDS. Since the parent glass compositions are in the middle range of the pseudobinary system, anorthite and Nd-oxyapatite both appeared at low temperatures (Fig.5.11/a). Higher magnification images (Fig.5.11/b) show the fine structure of the spherulitic, anorthite centred crystal.

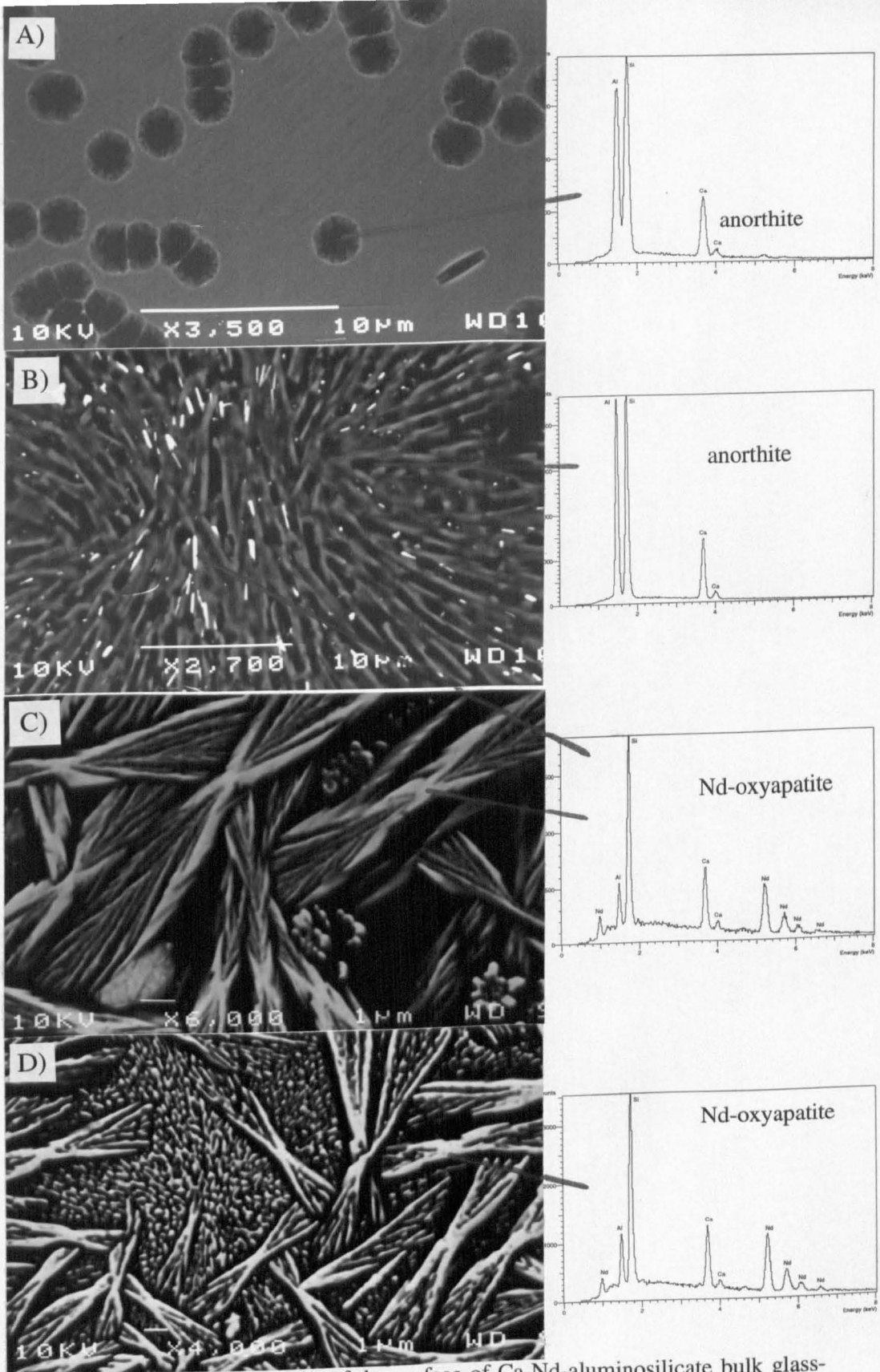


Fig.5.10/a-d. SEM micrographs of the surface of Ca-Nd-aluminosilicate bulk glass-ceramics, a) CASN-10, 996°C/2hr; b) CASN-13, 1300°C/2hr; c) CASN-12, 1170°C/2hr; d) CASN-9, 1300°C/2hr.

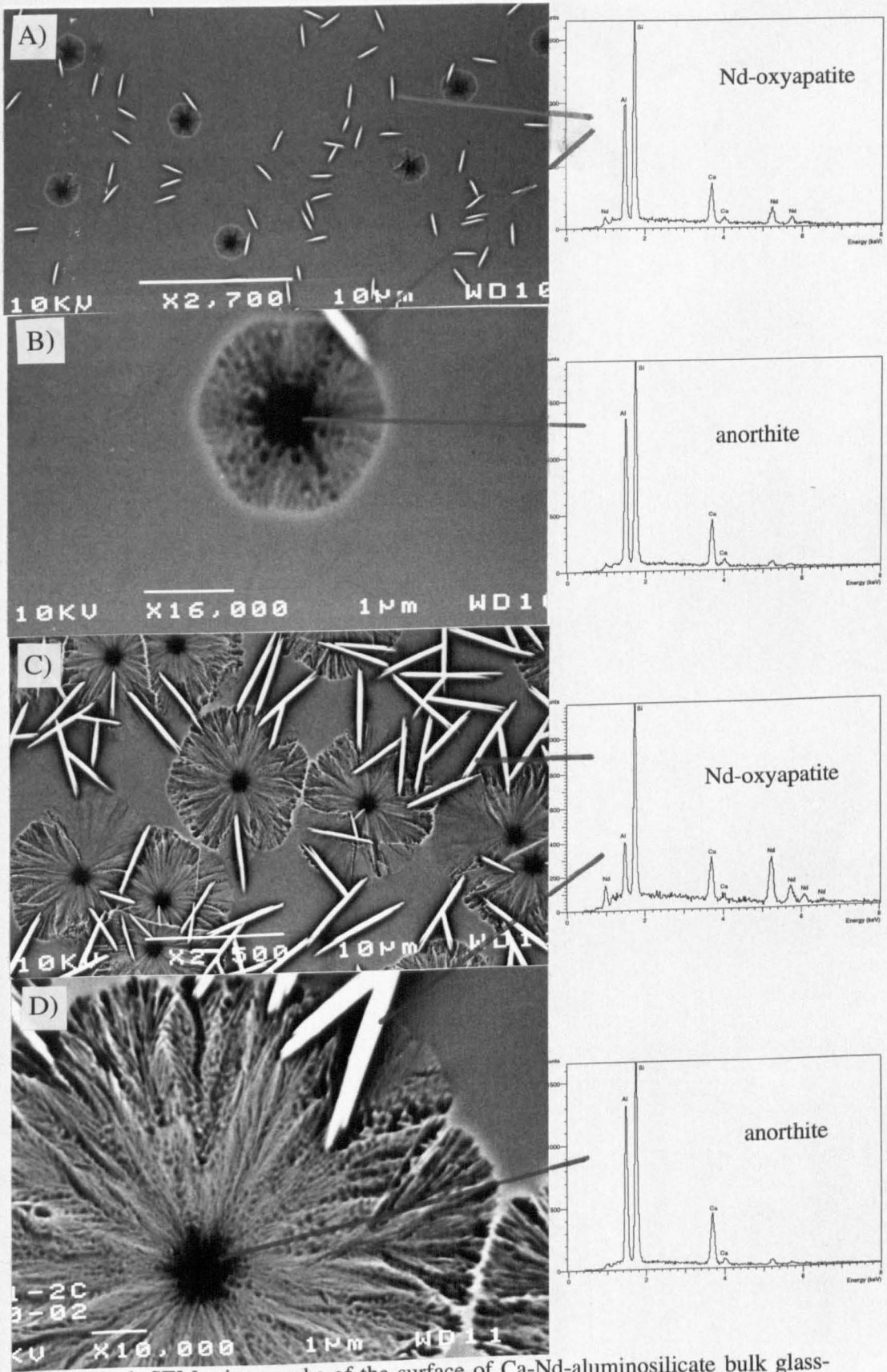


Fig.5.11/a-d. SEM micrographs of the surface of Ca-Nd-aluminosilicate bulk glass-ceramics (CASN-1), a) & b) 973°C/30min; c) & d) 973°C/2hr.

Increasing the duration of the heat treatment resulted in substantial growth of both spherulites and needle shaped crystals (Fig.5.11/c). The serrated surface profile of spherulites and the flat interface between the impinging spherulites, shown on the picture, are characteristic of impurity segregation (i.e. rejection of neodymium) during the growth of spherulites. The higher magnification view (Fig.5.11/d) shows a coarser fibrillar structure at the periphery of the spherulite, which arose due to the build up of high Nd concentration in the glassy residual phase. It is also worth noting the opening of the edges of the needle shaped, bright crystals of Nd-oxyapatite, since these crystals also have some tendency towards spherulite formation. Crystals having similar morphology (Fig.5.12) were detected in the bulk of the crystallized glass of the composition close to the suspected eutectic point of the pseudobinary system (CASN-6). The large spherulite, considering its homogeneous centre and cellular periphery, has to be an anorthite centred spherulitic crystal, whereas the dark sheaf-shaped crystals, which showed small-angle branching at their both ends, are presumably Nd-oxyapatite.

The first analysable XRD traces showed the major phases of anorthite and Nd-oxyapatite (Table 5.5/b). In addition, the 1170°C heat treatments resulted in bulk nucleated crystals in CASN-5 & CASN-1 glass compositions (Fig.5.13/b&c). The crystalline agglomerates are built up from bright crystals of Nd-oxyapatite with small crystals inside and slightly larger ones at the edges. All individual bright crystals showed pseudohexagonal morphology, and the agglomerates also showed hexagonal symmetry to some extent. The area between the bright crystals is either crystallized as anorthite or remained glassy.

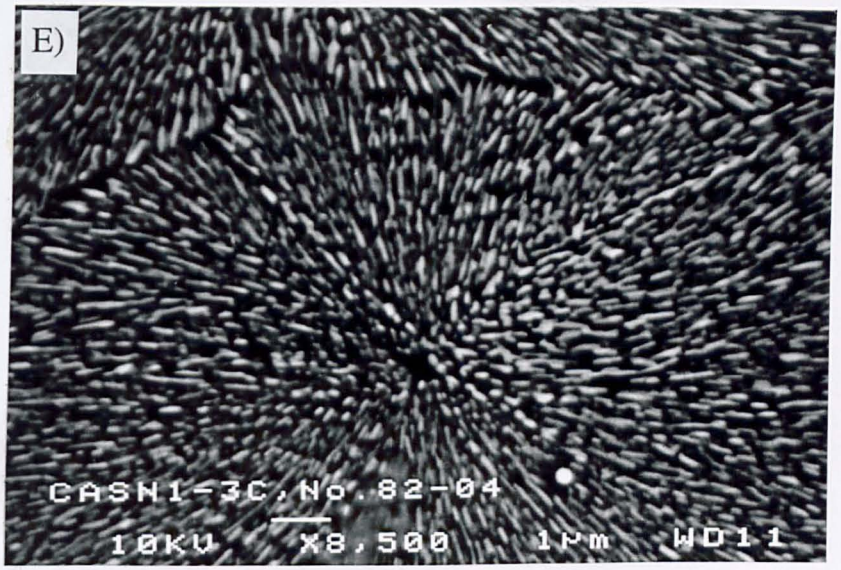


Fig.5.11/e. SEM micrograph of the surface of a Ca-Nd-aluminosilicate bulk glass-ceramic after recrystallization (CASN-1, 1170°C/2hr).


Fig.5.12. Transmission optical micrograph of a Ca-Nd-alumnosilicate bulk glass-ceramic (CASN-6, 1170°C/2hr).

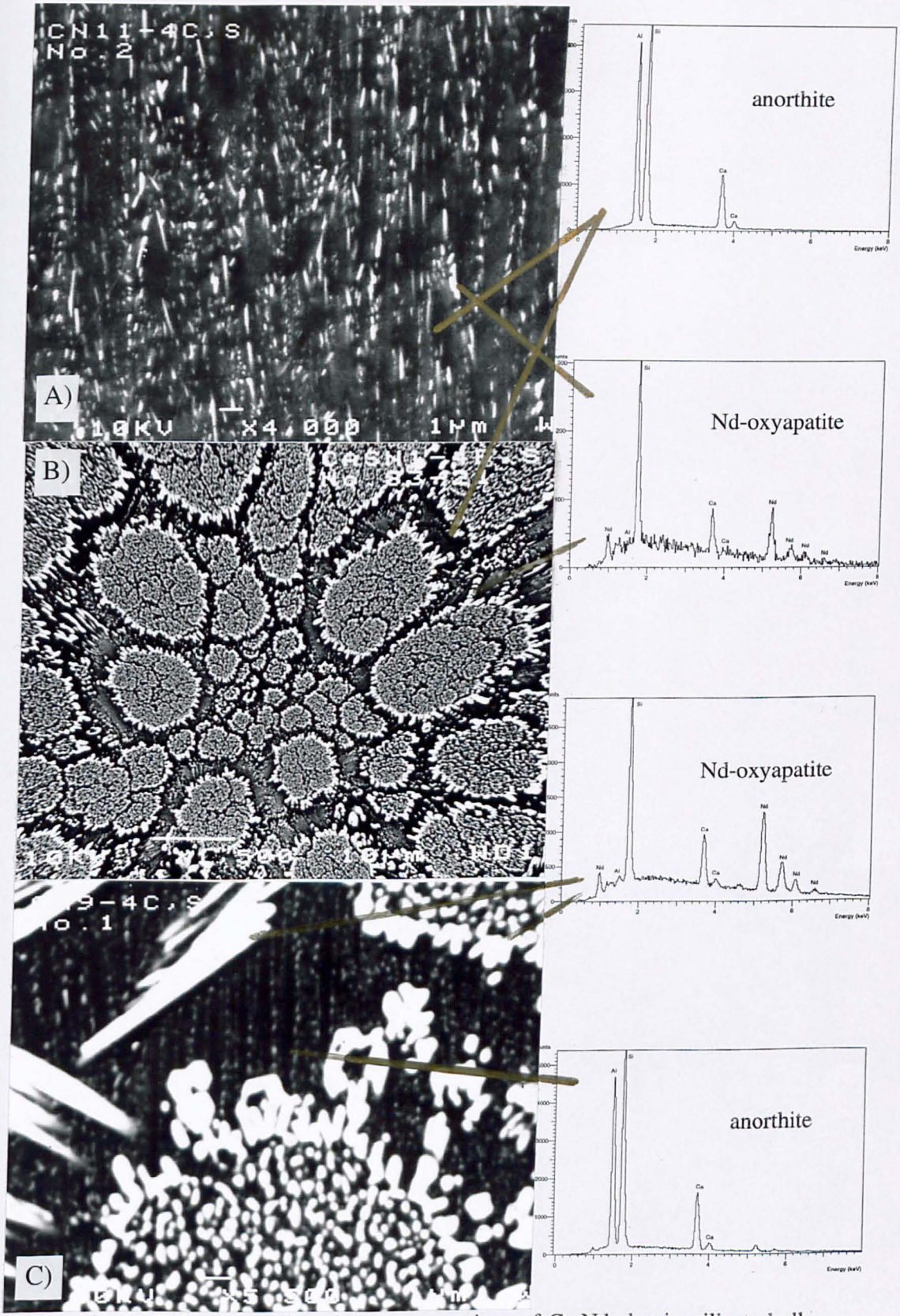


Fig.5.13/a-c. SEM micrographs of the cross-sections of Ca-Nd-aluminosilicate bulk glass-ceramics, a) CASN-11, 1300°C/2hr; b) CASN-1, 1170°C/2hr; c) CASN-9, 1170°C/2hr.

The preferred temperature range of the bulk nucleated crystalline aggregate formation is between 1050°C and 1170°C, and the range is also valid to all the other compositions which showed similar signs of bulk nucleation. In addition, a minor amount of mullite was also detected, along with the major phases, by XRD for nearly all crystallized glass compositions (Table 5.5/b).

**Table 5.5/b.** Crystallization of Ca-Nd-aluminosilicate bulk glasses (CASN-8,7,6,1,5)

| Sample type | Temp. of cryst. (°C) | Duration of cryst. | Crystalline phases detected by XRD (m: major, +: minor) |
|---|---|---|---|
| **CASN-8 glass** | | | |
| bulk glass | 1012 | 2 hr | no detectable crystallinity |
| bulk glass | 1170 | 2 hr | m: anorthite, +: Ca-Nd-Si, +: mullite |
| bulk glass | 1300 | 2 hr | m: Ca-Nd-Si, m: anorthite |
| **CASN-7 glass** | | | |
| bulk glass | 1012 | 2 hr | no detectable crystallinity |
| bulk glass | 1170 | 2 hr | m: anorthite, m: Ca-Nd-Si, +: mullite |
| bulk glass | 1300 | 2 hr | m: Ca-Nd-Si, +: anorthite |
| **CASN-6 glass** | | | |
| bulk glass | 1010 | 2 hr | no detectable crystallinity |
| bulk glass | 1170 | 2 hr | m: anorthite, m: Ca-Nd-Si, +: mullite |
| bulk glass | 1200 | 2 hr | m: Ca-Nd-Si, m: anorthite, +: mullite |
| bulk glass | 1300 | 2 hr | m: Ca-Nd-Si, +: anorthite |
| **CASN-1 glass** | | | |
| bulk glass | 973 | 30 min | no detectable crystallinity |
| bulk glass | 973 | 2 hr | no detectable crystallinity |
| bulk glass | 992 | 2 hr | no detectable crystallinity |
| bulk glass | 1050 | 30 min | no detectable crystallinity |
| bulk glass | 1050 | 2 hr | m: Ca-Nd-Si, m: anorthite, +: mo-Nd•2Si |
| bulk glass | 1110 | 2 hr | m: Ca-Nd-Si, m: anorthite, +: mo-Nd•2Si |
| bulk glass | 1170 | 30 min | m: Ca-Nd-Si, +: anorthite, +: mo-Nd•2Si |
| bulk glass | 1170 | 2 hr | m: Ca-Nd-Si, +: anorthite, +: mo-Nd•2Si |
| **CASN-5 glass** | | | |
| bulk glass | 1001 | 2 hr | no detectable crystallinity |
| bulk glass | 1170 | 2 hr | m: Ca-Nd-Si, +: anorthite |
| bulk glass | 1170 | 10 hr | m: Ca-Nd-Si, +: anorthite |
| bulk glass | 1300 | 2 hr | m: Ca-Nd-Si, +: anorthite |

Moreover, high temperature, monoclinic $Nd_2Si_2O_7$ (JCPDS 38-1456) was always present in CASN-1 glass-ceramics (Table 5.5/b), since its parent glass composition was not exactly on the anorthite-Nd-oxyapatite tie line. The bright field TEM micrograph (Fig.5.14) shows a monoclinic Nd-disilicate crystal, having a low-angle boundary. The low-angle grain boundary is more visible in the insert, which shows the lattice fringe image of the (110) planes of the Nd-disilicate crystal. In addition, Fig.5.15 shows a bright field TEM micrograph of a well-shaped Nd-oxyapatite crystal. At higher temperature (1300°C/2hr) the amount of Nd-oxyapatite increased, and it became the dominant crystalline phase for all glass compositions in this group (Table 5.5/b). The high temperature resulted in the complete crystallization of the interfibrillar glassy residue and the recrystallization of the fibrous crystals into small, lath-shaped morphology (Fig.5.11/e).

The XRD traces of the CASN-9,12 glasses crystallized at low temperatures (around 1000°C), revealed Nd-oxyapatite as the primary crystalline phase, although a minor amounts of anorthite, tetragonal $Nd_2Si_2O_7$ (JCPDS 22-1177), and mullite were also detected for the CASN-12 composition (Table 5.5/c).

**Table 5.5/c.** Crystallization of Ca-Nd-aluminosilicate bulk glasses (CASN-9,12)

| Sample type | Temp. of cryst. (°C) | Duration of cryst. | Crystalline phases detected by XRD (m: major, +: minor) |
|---|---|---|---|
| **CASN-9 glass** | | | |
| bulk glass | 1018 | 2 hr | just detectable: Ca-Nd-Si |
| bulk glass | 1170 | 2 hr | m: Ca-Nd-Si, +: anorthite, +: mullite |
| bulk glass | 1300 | 2 hr | m: Ca-Nd-Si, +: anorthite, +: mullite |
| **CASN-12 glass** | | | |
| bulk glass | 1000 | 2 hr | m: Ca-Nd-Si, +: t-Nd•2Si, +: anorthite, +: mullite |
| bulk glass | 1170 | 2 hr | m: Ca-Nd-Si, +: anorthite, +: mullite |
| bulk glass | 1300 | 2 hr | m: Ca-Nd-Si, +: anorthite, +: mullite |

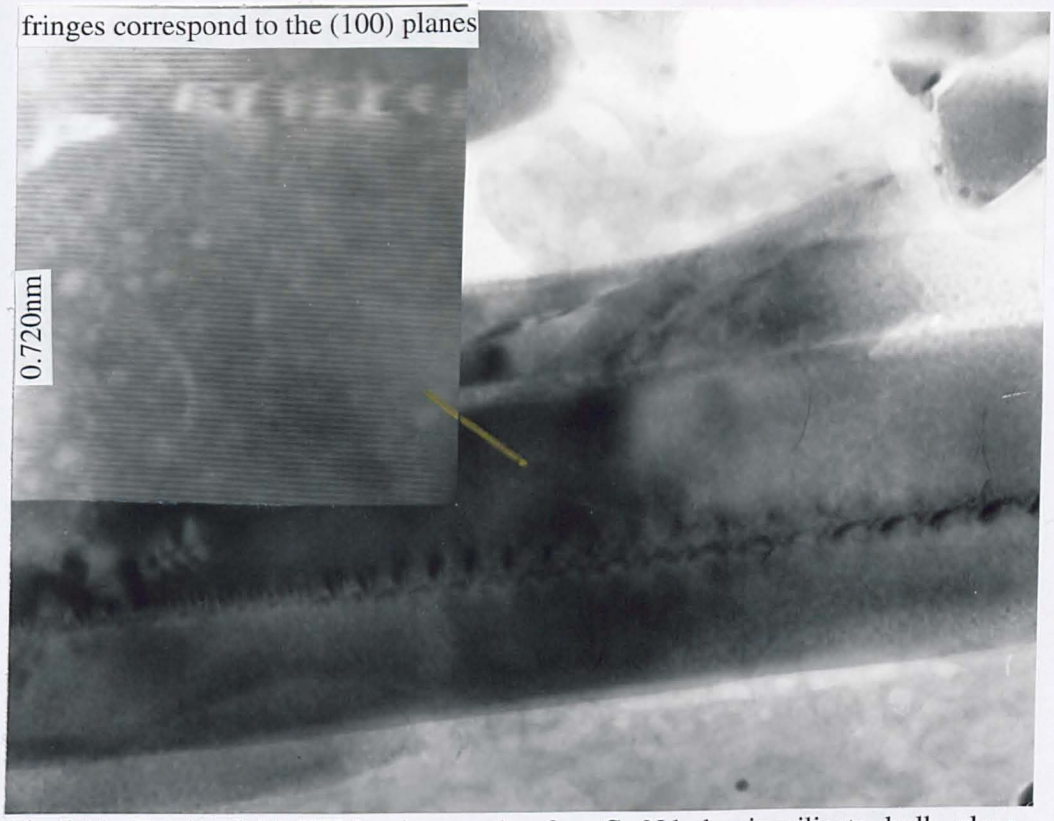


Fig.5.14. Bright field TEM micrograph of a Ca-Nd-aluminosilicate bulk glass-ceramic showing a monoclinic $Nd_2Si_2O_7$ crystal with a low angle boundary (CASN-1, 1170°C/2hr).

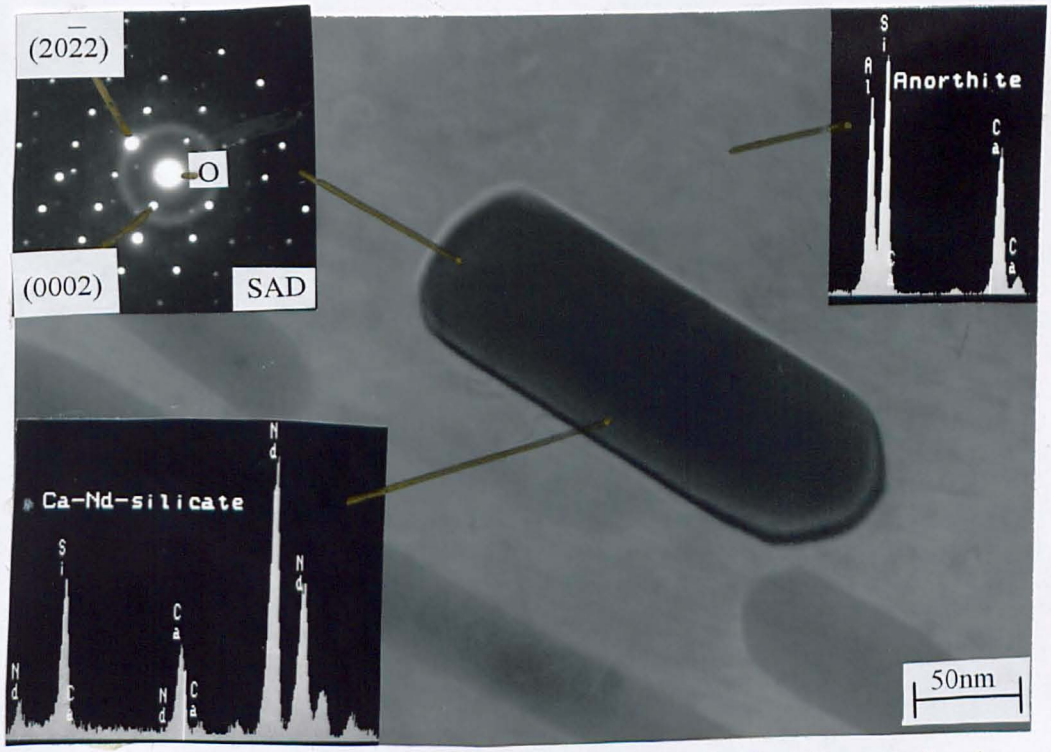


Fig.5.15. Bright field TEM micrograph of a Ca-Nd-aluminosilicate bulk glass-ceramic (CASN-1, 1170°C/2hr).

Higher temperature heat treatments (1170°C/2hr) resulted in the growth of the anorthite phase, as well as leading to advanced small-angle branching of the Nd-oxyapatite crystals (Fig.5.10/c), creating well-developed sheaf-shaped crystals. These glass compositions also showed signs of bulk nucleated crystallization (Fig.5.13/c). The previously described aggregates of pseudohexagonal Nd-oxyapatite crystals were detected, and the matrix was mainly crystalline anorthite. The 1300°C/2hr heat treatment resulted in recrystallization of the thin fibrous crystals into fine grains, although it did not completely brake up the sheaf-shaped morphology (Fig.5.10/d)

### 5.4.2. Crystallization and microstructure of Ca-Nd-aluminosilicate glass-ceramic pellets

Small, spherulitic grains of anorthite are dominant in the CASN-13,11,10 glass-ceramic pellets, crystallized at lower temperatures (around 1000°C). In addition, minor phases of orthorhombic $CaAl_2Si_2O_8$, Nd-oxyapatite and mullite were also detected (Table 5.5/d). Most of the compositions (except for CASN-13) showed low degree of crystallinity after the low temperature heat treatments. Higher temperature heat treatments resulted in the increase of the Nd-oxyapatite, while anorthite remained the dominant phase. In addition, after 1300°C/2hr, the microstructure showed fine grained morphology due to recrystallization (Fig.5.16/a).

The CASN-8,7,6,1,5 glass-ceramic pellets showed an acceptable degree of crystallinity after the low temperature heat treatments (around 1000°C), though the levels of crystallinity decreased with decreasing $Nd_2O_3$ content. According to the XRD analysis (Table 5.5/e-f), the major phases were Nd-oxyapatite and anorthite, and Nd-oxyapatite was the dominant phase at most compositions. In addition, a minor phase of mullite was also detected on most of the XRD traces.

**Table 5.5/d.** Crystallization of Ca-Nd-aluminosilicate glass powders (CASN-13,11,10)

| Sample type | Temp. of cryst. (°C) | Duration of cryst. | Crystalline phases detected by XRD (m: major, +: minor) |
|---|---|---|---|
| **CASN-13 glass** | | | |
| powder pellet | 1008 | 2 hr | m: anorthite, +: o-Ca-Al-Si, +: Ca-Nd-Si, +: mullite |
| powder pellet | 1200 | 2 hr | m: anorthite, +: Ca-Nd-Si |
| powder pellet | 1300 | 2 hr | m: anorthite, +: Ca-Nd-Si, +: mullite |
| hot pressed | 1300 | 2 hr | m: anorthite, +: Ca-Nd-Si, +: mullite |
| **CASN-11 glass** | | | |
| powder pellet | 1002 | 2 hr | m: anorthite, +: o-Ca-Al-Si, +: Ca-Nd-Si |
| powder pellet | 1200 | 2 hr | m: anorthite, +: Ca-Nd-Si |
| powder pellet | 1300 | 2 hr | m: anorthite, +: Ca-Nd-Si, +: mullite |
| hot pressed | 1300 | 2 hr | m: anorthite, +: Ca-Nd-Si, +: mullite |
| **CASN-10 glass** | | | |
| powder pellet | 996 | 2 hr | m: anorthite, +: o-Ca-Al-Si, +: Ca-Nd-Si, +: mullite (weak XRD trace) |
| powder pellet | 1200 | 2 hr | m: anorthite, m: Ca-Nd-Si |
| powder pellet | 1300 | 2 hr | m: Ca-Nd-Si, m: anorthite, +: mullite |
| hot pressed | 1300 | 2 hr | m: Ca-Nd-Si, m: anorthite, +: mullite |

Fig.5.16/b shows a cross sectional view of a pseudohexagonal, bright crystal of Nd-oxyapatite (CASN-1). The crystal's hexagonal, tubular morphology closely resembles that of a $Ca_2Y_8Si_6O_{26}$ (oxyapatite) crystal, which is the major and key crystalline phase of a machinable glass-ceramic material bearing high temperature stability, as reported by Makishima et al. [254,255]. The unusually large size of the crystal might be due to the presence of crystal seeds in the glass precursor after quenching (crystalline residue was found in the crucible after the melting of this composition). The Ca-Nd-silicate crystals grew preferentially along their 'c' axis, whereas their lateral growth rate was much smaller.

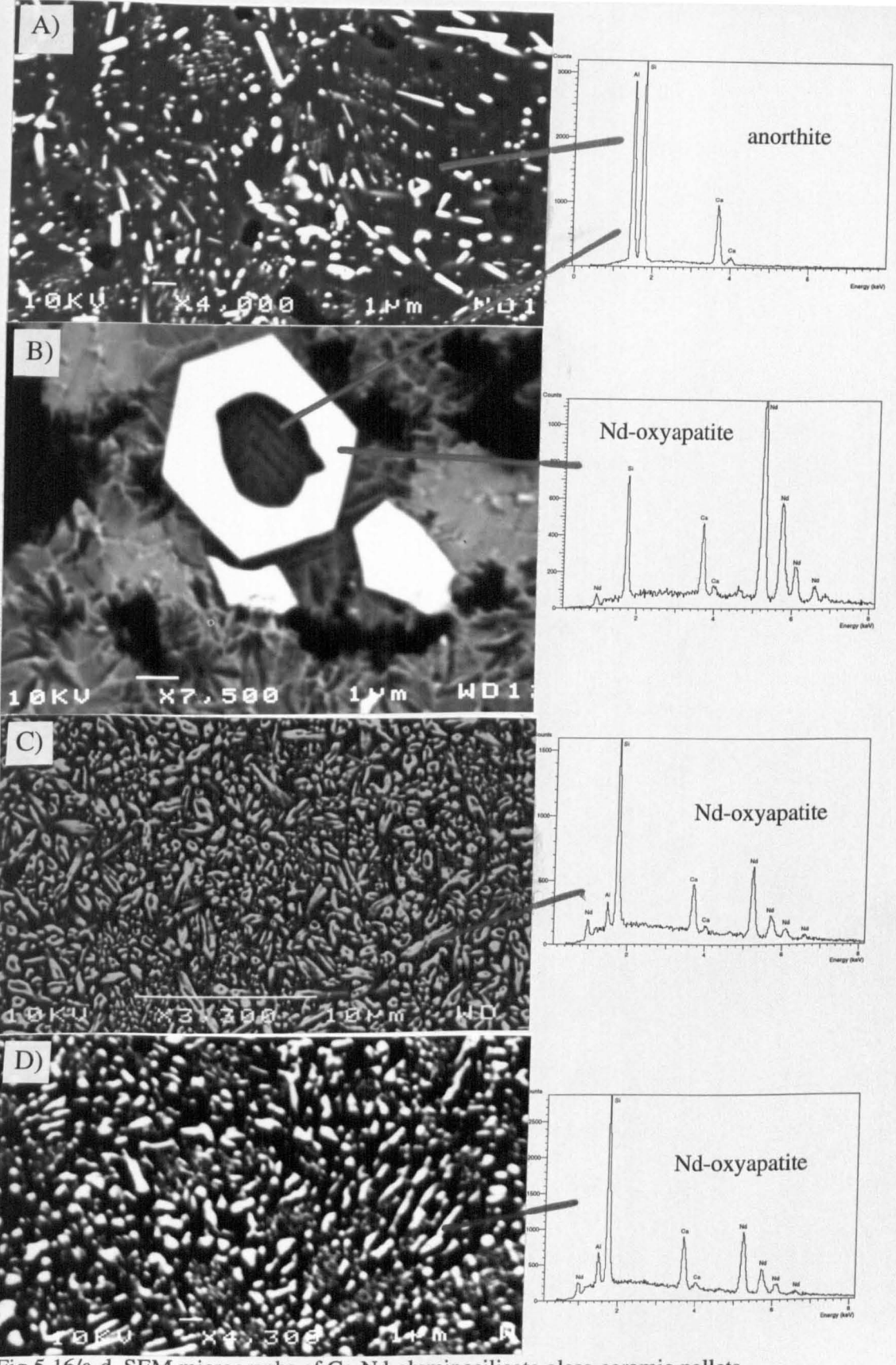


Fig.5.16/a-d. SEM micrographs of Ca-Nd-aluminosilicate glass-ceramic pellets, a) CASN-11, 1300°C/2hr; b) CASN-1, 992°C/2hr; c) CASN-12, 1300°C/2hr; d) CASN-7 (hot pressed), 1300°C /2hr.

The growth rate along the 'c' axis was fastest around the edges of the hexagon, but the diffusion rate of the rejected elements was probably smaller, and the components eventually became trapped by the fast growing crystal. The dark core presumably contains crystalline anorthite: it shows visually detectable crystalline grains and it has a composition close to anorthite. The dark phases on the picture are fragmented pieces of alumina, originating from the milling process (Section 3.1).

**Table 5.5/e.** Crystallization of Ca-Nd-aluminosilicate glass powders (CASN-8,7,6)

| Sample type | Temp. of cryst. (°C) | Duration of cryst. | Crystalline phases detected by XRD (m: major, +: minor) |
|---|---|---|---|
| **CASN-8 glass** | | | |
| powder pellet | 1012 | 2 hr | m: anorthite, m: Ca-Nd-Si, +: mullite |
| powder pellet | 1170 | 2 hr | m: anorthite, m: Ca-Nd-Si |
| powder pellet | 1300 | 2 hr | m: Ca-Nd-Si, +: anorthite, +: mullite |
| hot pressed | 1300 | 2 hr | m: Ca-Nd-Si, +: anorthite, +: mullite |
| **CASN-7 glass** | | | |
| powder pellet | 1012 | 2 hr | m: Ca-Nd-Si, m: anorthite, +: mullite |
| powder pellet | 1170 | 2 hr | m: Ca-Nd-Si, m: anorthite |
| powder pellet | 1300 | 2 hr | m: Ca-Nd-Si, +: anorthite |
| hot pressed | 1300 | 2 hr | m: Ca-Nd-Si, +: anorthite, +: mullite |
| **CASN-6 glass** | | | |
| powder pellet | 1010 | 2 hr | m: Ca-Nd-Si, m: anorthite, +: mullite |
| powder pellet | 1170 | 2 hr | m: Ca-Nd-Si, +: anorthite, +: mullite |
| powder pellet | 1200 | 2 hr | m: Ca-Nd-Si, +: anorthite, +: mullite |
| powder pellet | 1300 | 2 hr | m: Ca-Nd-Si, +: anorthite |
| hot pressed | 1300 | 2 hr | m: Ca-Nd-Si, +: anorthite |

Higher temperature heat treatments of the CASN-8,7,6,1,5 pellets resulted in well crystallized glass-ceramics, the amount of both major phases is increased and Nd-oxyapatite became the dominant phase in all glass-ceramic compositions (Table 5.5/e-f). Some heat treatments of CASN-5 and CASN-6 compositions were studied using hand-ground glasses in parallel with the generally used ball-milled powders. The same crystalline phases were detected in each case, and the only difference was

the lower level of crystallinity of the hand-ground glass powders, which suggests that the ball-milling process activated the surface of the powdered particles.

**Table 5.5/f.** Crystallization of Ca-Nd-aluminosilicate glass powders (CASN-1,5)

| Sample type | Temp. of cryst. (°C) | Duration of cryst. | Crystalline phases detected by XRD (m: major, +: minor) |
|---|---|---|---|
| **CASN-1 glass** | | | |
| powder pellet | 973 | 30 min | m: anorthite, m: Ca-Nd-Si, +: o-Ca-Al-Si, +: mo-Nd•2Si, +: t-Nd•2Si |
| powder pellet | 973 | 2 hr | m: anorthite, m: Ca-Nd-Si, +: o-Ca-Al-Si, +: mo-Nd•2Si, +: t-Nd•2Si |
| powder pellet | 992 | 2 hr | m: Ca-Nd-Si, m: anorthite, +: mo-Nd•2Si, +:t-Nd•2Si |
| powder pellet | 1050 | 30 min | m: Ca-Nd-Si, m: anorthite, +: mo-Nd•2Si, +:t-Nd•2Si |
| powder pellet | 1050 | 2 hr | m: Ca-Nd-Si, m: anorthite, +: mo-Nd•2Si, +:t-Nd•2Si |
| powder pellet | 1110 | 2 hr | m: Ca-Nd-Si, m: anorthite, +: t-Nd•2Si, +:mo-Nd•2Si |
| powder pellet | 1170 | 30 min | m: Ca-Nd-Si, m: anorthite, +: t-Nd•2Si, +:mo-Nd•2Si |
| powder pellet | 1170 | 2 hr | m: anorthite, m: t-Nd•2Si, m:Ca-Nd-Si, +:mo-Nd•2Si |
| powder pellet | 1300 | 2 hr | m: Ca-Nd-Si, m: anorthite |
| **CASN-5 glass** | | | |
| powder pellet | 1001 | 2 hr | m: Ca-Nd-Si, +: anorthite, +: mullite |
| powder pellet | 1170 | 2 hr | m: Ca-Nd-Si, +: anorthite |
| powder pellet | 1170 | 10 hr | m: Ca-Nd-Si, +: anorthite |
| powder pellet | 1300 | 2 hr | m: Ca-Nd-Si, +: anorthite |
| hot pressed | 1300 | 2 hr | m: Ca-Nd-Si, +: anorthite |

Since the CASN-1 composition was slightly off the tie-line of anorthite and Nd-oxyapatite, minor phases of monoclinic and tetragonal Nd-disilicate phases were detected by XRD traces of these glass-ceramics (Table 5.5/f). Above 1100°C, the amount of tetragonal phase was increased with temperature at the expense of Nd-oxyapatite, while at the highest temperature heat treatment it disappeared, presumably recrystallized into Nd-oxyapatite. The high temperature heat treatment (1300°C/2hr) caused partial melting (suggested by the unusual amount of glassy residue), which eventually lead to the re-crystallization of Nd-oxyapatite.

The CASN-9,12 compositions provided well-crystallized glass-ceramic pellets even after the low temperature crystallizations. The XRD traces of the glass-ceramic pellets showed a major phase of Nd-oxyapatite and a major phase of anorthite, regardless of the crystallization temperature (Table 5.5/g), as well as occasionally a minor phase of mullite. The microstructure of the $Nd_2O_3$-rich glass-ceramic pellets is shown in Fig. 16/c.

**Table 5.5/g.** Crystallization of Ca-Nd-aluminosilicate glass powders (CASN-9,12)

| Sample type | Temp. of cryst. (°C) | Duration of cryst. | Crystalline phases detected by XRD (m: major, +: minor) |
|---|---|---|---|
| **CASN-9 glass** | | | |
| powder pellet | 1018 | 2 hr | m: Ca-Nd-Si, +: anorthite |
| powder pellet | 1170 | 2 hr | m: Ca-Nd-Si, +: anorthite |
| powder pellet | 1300 | 2 hr | m: Ca-Nd-Si, +: anorthite |
| hot pressed | 1300 | 2 hr | m: Ca-Nd-Si, +: anorthite |
| **CASN-12 glass** | | | |
| powder pellet | 1000 | 2 hr | m: Ca-Nd-Si, +: anorthite, +: mullite |
| powder pellet | 1170 | 2 hr | m: Ca-Nd-Si, +: anorthite |
| powder pellet | 1300 | 2 hr | m: Ca-Nd-Si, +: anorthite |

The hot pressing schedule was 1300°C/2hr for all compositions, and the hot pressed samples behaved similarly to their sintered derivatives. The XRD analyses of the low-$Nd_2O_3$ compositions showed anorthite as the major phase, and minor phases of Nd-oxyapatite and mullite (Table 5.5/a,d). The hot pressing of medium- and high-$Nd_2O_3$ compositions resulted in Nd-oxyapatite as a major phase, as well as anorthite and occasionally mullite minor phases (Table 5.5/b,c,e,f,g). The fine grained microstructure of hot pressed Ca-Nd-aluminosilicate glass ceramics is shown in Fig.5.16/d.

## 5.5. The effect of $TiO_2$ on the crystallization and microstructure of Ca-Nd-aluminosilicate glass-ceramics

The addition of titania to Ca-Nd-aluminosilicate glasses (CASN9-T1, CASN12-T1, their compositions can be found in Table 4.1) enhanced the crystallization of these glasses, but did not provide bulk nucleation, which would be expected from a nucleating agent. The bulk glasses, similar to the pure Ca-Nd-aluminosilicate glasses, showed signs of surface nucleation only. Despite that, the high temperature crystallizations provided well crystallized, compact glass-ceramic bodies. There were two crystallization exotherms on the DTA trace of CASN9-T1 glass composition, whereas only one was detected on the trace of CASN12-T1 (Table 4.3). The temperature and duration of crystallizations of the Ti containing Ca-Nd-aluminosilicate glass-ceramics as well as the crystalline phases detected by XRD are shown in Table 5.6.

The crystallizations of CASN9-T1 glass below 1000°C, provided insufficient crystallinity for XRD analysis, therefore they were analysed by SEM/EDS, whereas CASN12-T1 glass-ceramics were already analysable by XRD from 957°C. The primary phase in case of both glasses was Nd-oxyapatite, its tiny, sheaf-shaped crystals can be seen in Fig.5.17/a. At higher temperature the Nd-oxyapatite crystals grew in size and showed more advanced branching (Fig.5.17/b.).

Above 1000°C the XRD traces showed Nd-oxyapatite as the major phase, anorthite as a minor phase and two other phases (Table 5.6). One of phases (named "α") had similar reflections to $(Ca,Ln)(Ti,Al,Fe)O_3$ (JCPDS 15-158), although a few reflections were missing (d=2.4; 2.11; 1.95), and it was the second largest phase at that temperature. The reflections of the other phase (named "β"), which was only a minor phase at those temperatures, became stronger especially at high temperatures.

The X-ray powder diffraction data of the β-phase is shown in Table 5.7. These XRD reflections are also shown in Fig.II.3 (Appendix II).

**Table 5.6.** Crystallization of $TiO_2$ containing Ca-Nd-aluminosilicate glasses

| Sample type | Temp. of cryst. (°C) | Duration of cryst. | Crystalline phases detected by XRD (m: major, +: minor) |
|---|---|---|---|
| **CASN9-T1** | | | |
| bulk glass | 944 | 2 hr | no detectable crystallinity |
| bulk glass | 1000 | 2 hr | just detectable: anorthite, Ca-Nd-Si, α-Ti, β-Ti |
| bulk glass | 1170 | 2 hr | m: Ca-Nd-Si, +: α-Ti, +: anorthite, +: β-Ti |
| bulk glass | 1300 | 2 hr | m: Ca-Nd-Si, m: β-Ti, m: anorthite, +: α-Ti |
| powder pellet | 944 | 2 hr | just detectable: α-Ti, Ca-Nd-Si |
| powder pellet | 979 | 2 hr | m: anorthite, m: Ca-Nd-Si, +: α-Ti, +: β-Ti |
| powder pellet | 990 | 2 hr | m: anorthite, m: Ca-Nd-Si, +: α-Ti, +: β-Ti |
| powder pellet | 1000 | 2 hr | m: anorthite, m: Ca-Nd-Si, +: α-Ti, +: β-Ti |
| powder pellet | 1170 | 2 hr | m: Ca-Nd-Si, m: anorthite, +: β-Ti, +: α-Ti |
| powder pellet | 1300 | 2 hr | m: Ca-Nd-Si, m: β-Ti, +: anorthite |
| **CASN12-T1** | | | |
| bulk glass | 957 | 2 hr | m: Ca-Nd-Si, m: α-Ti, +: anorthite, +: β-Ti |
| bulk glass | 1100 | 2 hr | m: Ca-Nd-Ti, +: anorthite, +: α-Ti, +: β-Ti |
| bulk glass | 1200 | 2 hr | m: Ca-Nd-Si, +: α-Ti, +: anorthite, +: β-Ti |
| bulk glass | 1300 | 2 hr | m: Ca-Nd-Si, m: β-Ti, +: anorthite, +: α-Ti |
| powder pellet | 946 | 2 hr | just detectable: Ca-Nd-Si, α-Ti, β-Ti, anorthite |
| powder pellet | 957 | 2 hr | m: Ca-Nd-Si, +: α-Ti, +: anorthite, +: β-Ti |
| powder pellet | 1100 | 2 hr | m: Ca-Nd-Si, +: anorthite, +: α-Ti, +: β-Ti |
| powder pellet | 1200 | 2 hr | m: Ca-Nd-Si, +: β-Ti, +: anorthite, +: α-Ti |
| powder pellet | 1300 | 2 hr | m: Ca-Nd-Si, m: β-Ti, +: anorthite |

Surprisingly, only one extra phase was detected by SEM/EDS analysis, therefore α and β phases are considered as two different temperature modifications of the same crystal. The analysed oxide ratios ($CaO:Al_2O_3:SiO_2:Nd_2O_3:TiO_2$) were 1:1.5:2.5:2:1.8. Considering the X-ray microanalysis results, the phases are believed to be a Nd and Al substituted modification of titanite ($CaTiSiO_5$). Rare-earth cations readily substitute for $Ca^{2+}$ in various minerals (e.g. apatite, Section 2.3.6), and the same applies to titanite [294]. In addition, Al can substitute for Ti in the titanite

structure [294]. The suspected substitutions lead to the following formula: $(Ca,Nd)(Ti,Al)SiO_5$.

High temperature heat treatments resulted in an increase in the amount of Nd-oxyapatite crystals, and the surface of a glass-ceramic crystallised at 1170°C/2hr is shown in Fig.5.17/c. In addition, the highest temperature heat treatment resulted in the transformation of α-Nd-titanite phase into the β-modification (Table 5.6). The phase transformation was part of a complete recrystallization process, shown in Fig.5.17/d (combined secondary & backscattered electron image).

**Table 5.7.** X-ray Powder Diffraction data of β-$(Ca,Nd)(Ti,Al)SiO_5$ phase

| d | Intensity | d | Intensity | d | Intensity |
|---|---|---|---|---|---|
| 6.185 | weak | 2.938 | very strong | 2.039 | medium strong |
| 5.691 | weak | 2.909 | very strong | 2.011 | medium weak |
| 5.485 | weak | 2.792 | strong | 1.923 | medium strong |
| 5.324 | medium strong | 2.691 | medium | 1.814 | medium |
| 5.099 | medium strong | 2.653 | strong | 1.779 | weak |
| 4.920 | medium | 2.590 | weak | 1.734 | medium |
| 4.322 | medium | 2.545 | weak | 1.727 | medium |
| 4.046 | medium | 2.531 | medium | 1.704 | weak |
| 3.800 | medium | 2.470 | medium strong | 1.684 | weak |
| 3.784 | medium | 2.431 | medium | 1.637 | medium |
| 3.648 | medium | 2.355 | medium strong | 1.606 | weak |
| 3.617 | medium | 2.212 | medium | 1.590 | weak |
| 3.511 | medium strong | 2.190 | medium | 1.573 | medium |
| 3.408 | medium strong | 2.141 | strong | 1.552 | weak |
| 3.088 | medium | 2.126 | medium strong | 1.394 | medium |
| 3.002 | medium strong | 2.103 | weak | | |

Fig.5.18/a-c show the development of microstructure in the cross-sections of bulk glass-ceramics. The microstructure of CASN12-T1 glass-ceramics after heat treatment at 957°C/2hr is shown in Fig.5.18/a. The glass-ceramic was almost fully crystalline at that temperature, containing sheaf-shaped crystals and large bright crystals of Nd-oxyapatite, fibrous grey crystals of Nd-titanite and anorthite.

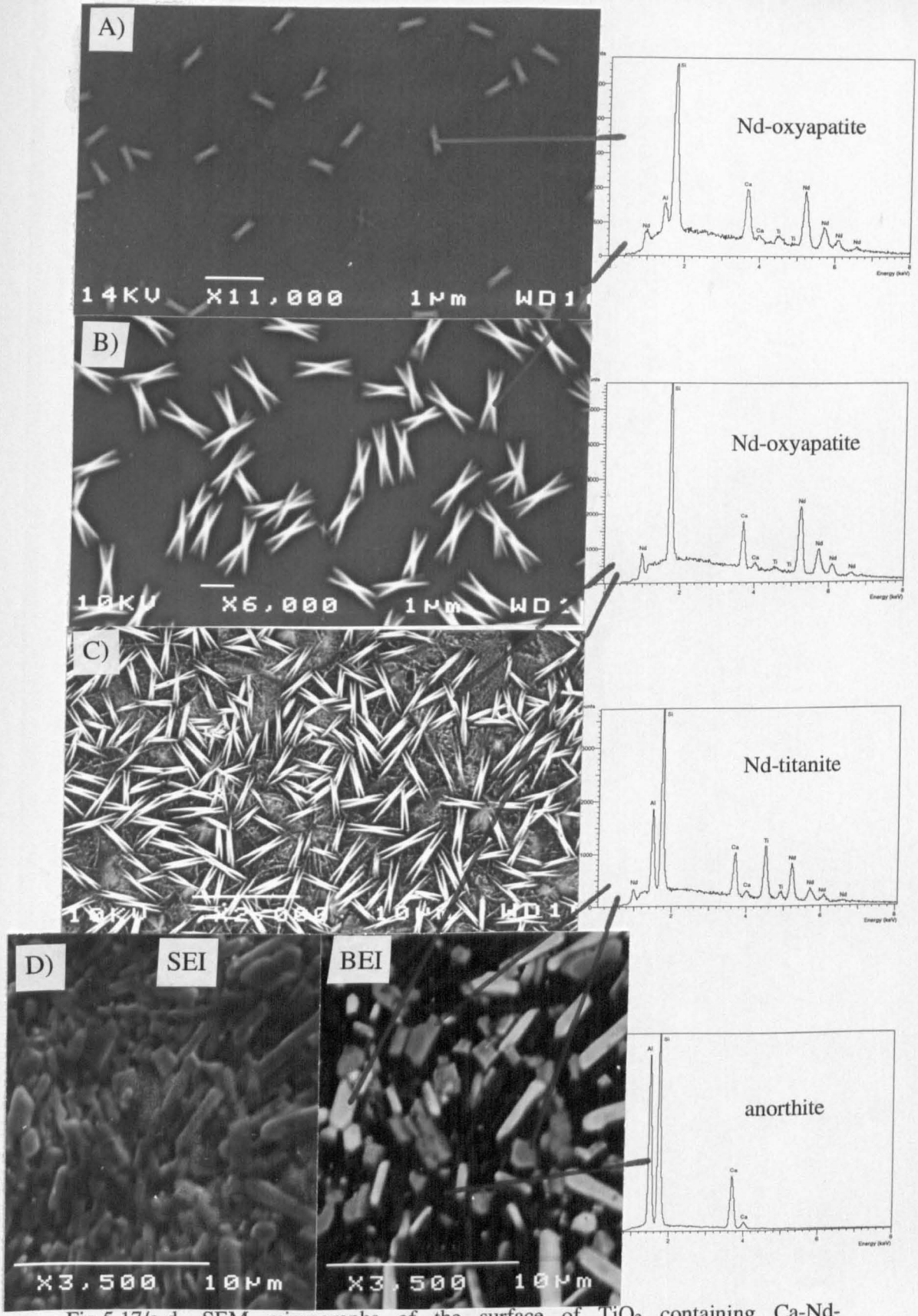


Fig.5.17/a-d. SEM micrographs of the surface of $TiO_2$ containing Ca-Nd-aluminosilicate bulk glass-ceramics (CASN9-T1), a) 927°C/2hr; b) 944°C/2hr; c) 1170°C/2hr; d) combined secondary & backscattered image,1300°C /2hr.

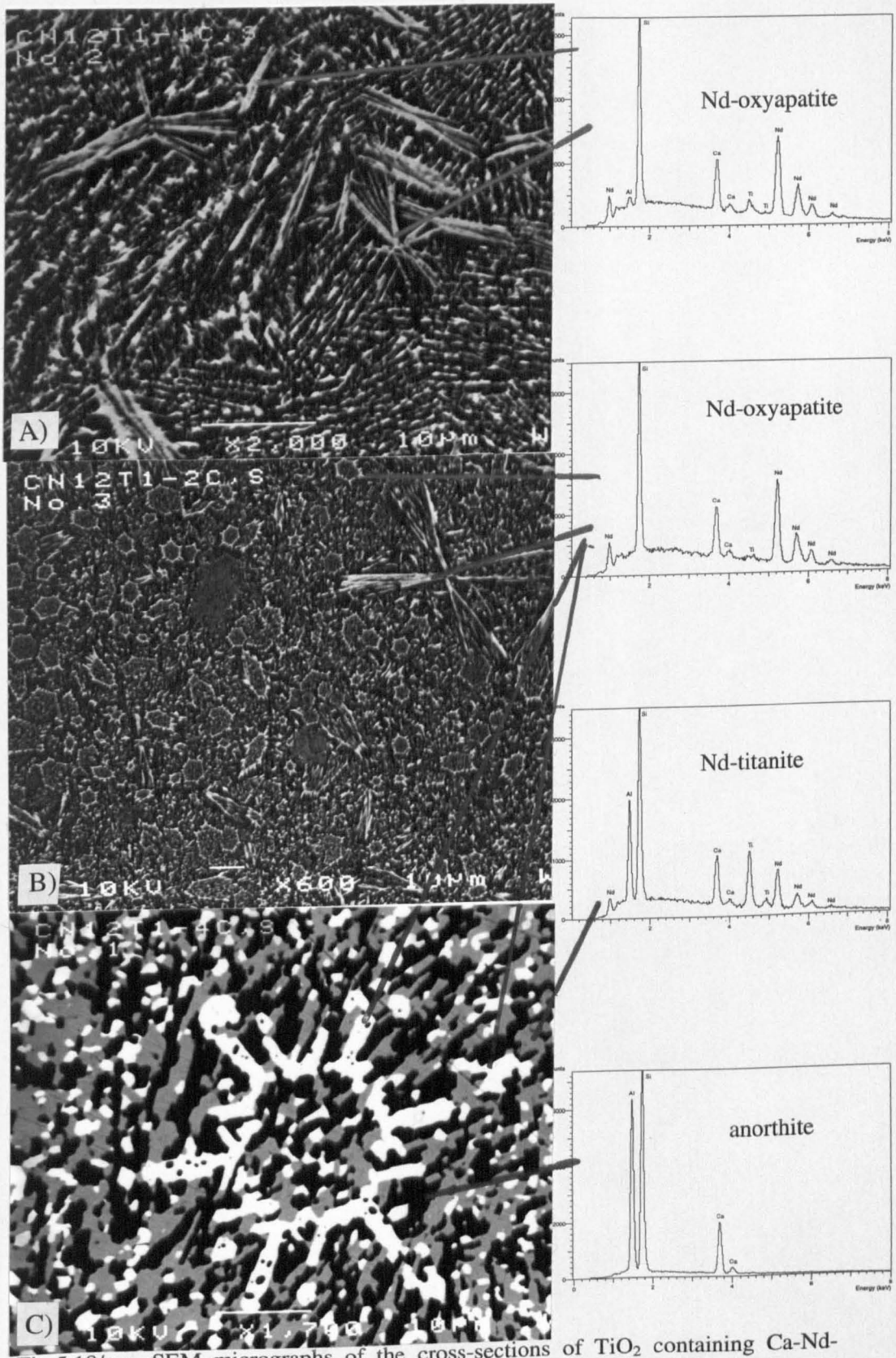


Fig.5.18/a-c. SEM micrographs of the cross-sections of $TiO_2$ containing Ca-Nd-aluminosilicate bulk glass-ceramics (CASN12-T1), a) 957°C/2hr; b) 1200°C/2hr; c) 1300°C/2hr.

At higher temperature the cross-section is fully crystalline, and the microstructure is dominated by crystalline aggregates of pseudohexagonal Nd-oxyapatite crystals as well as their sheaf-shaped morphology (Fig.5.18/b). A recrystallized microstructure is shown in Fig.5.18/c, the slight coarsening of the grains is presumably due to a minor amount of molten phase formation during crystallization. An interesting feature on the micrograph, are the remains of a Nd-oxyapatite crystalline aggregate. The larger, surrounding Nd-oxyapatite crystals almost kept their original pseudohexagonal shape, but their inner structure is recrystallized into anorthite, β-Nd-titanite, and Nd-oxyapatite.

The low temperature heat treatments (around 1000°C) resulted in a low degree of crystallinity in glass-ceramic pellets of both compositions. Among large lateral and sheaf shaped crystals of Nd-oxyapatite and fibrillar crystals of Nd-titanite, grey glassy residual areas can also be detected in Fig.5.19/a. The large Nd-oxyapatite crystals were presumably nucleated on crystalline seeds, which originated from the improper melting of the CASN12-T1 composition (Section 4.2). Higher temperature heat treatments resulted in the growth of overlapping fibrous crystallites of Nd-oxyapatite, Nd-titanite and anorthite (Fig.5.19/b.) The XRD analysis of pelletized samples crystallized up to 1000°C, showed Nd-oxyapatite as the major phase, as well as anorthite and both modifications of Nd-titanite in considerable amount. Higher temperature heat treatments increased the amount of the β-Nd-titanite phase at the expense of the α modification, which eventually lead to the complete conversion of α into β-Nd-titanite at 1300°C (Table 5.6).

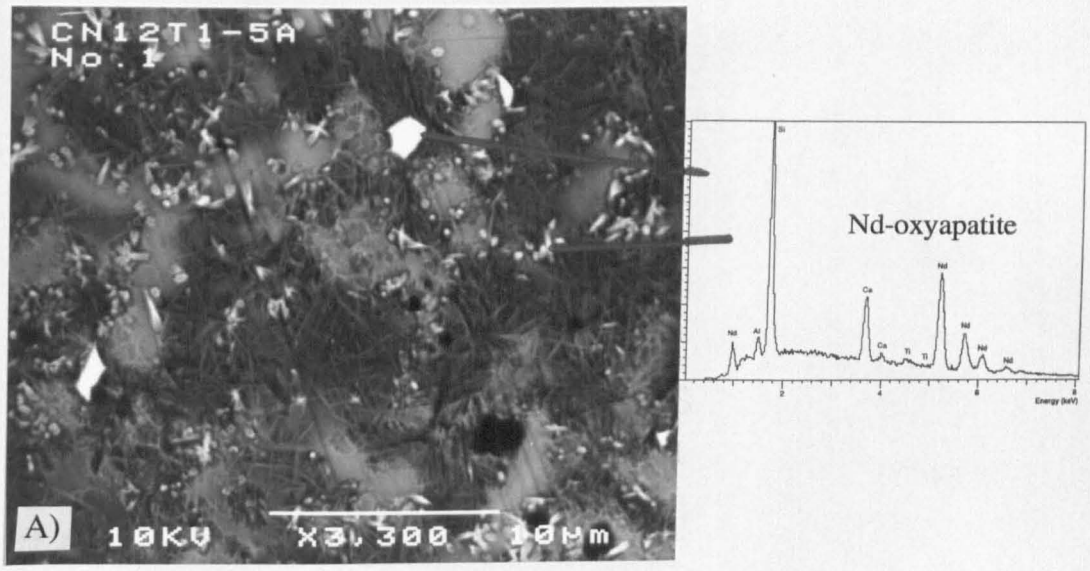



Fig.5.19/a-b. SEM micrographs of $TiO_2$ containing Ca-Nd-aluminosilicate glass-ceramic pellets (CASN12-T1), a) 946°C/2hr; b) 957°C/2hr.

## 5.6. Summary of the crystallization of Ln containing CAS glasses

The rare-earth containing quaternary aluminosilicate glasses generally crystallized as pure binary systems, resulting in diphasic glass ceramics containing anorthite and the appropriate $Ca_2Ln_8Si_6O_{21}$ oxyapatite structured phase ($Ca_4Y_6Si_6O_{25}$ in the case of Y). At the aluminosilicate rich end of the glass forming region (CASN series) the primary crystalline phase was anorthite, whereas at the rare-earth rich end the primary phase was the Ca-Nd-oxyapatite phase, and in the middle area of the glass forming region where the suspected eutectic point of this pseudobinary system lies, simultaneous crystallization of both phases was observed. This crystallization behaviour is characteristic of binary eutectic systems. The higher temperature crystallizations resulted in fully crystalline glass-ceramics, which among the two major phases, contained minor phases also. The dominant crystallization mechanism was surface crystallization for the bulk glasses, although signs of bulk nucleation were also detected in the Nd-rich glass-ceramics. Spherulites were the dominant crystalline morphology at lower temperature crystallizations, which then recrystallized at higher temperatures, providing glass-ceramics with fine grained lath-like morphology.

The $TiO_2$ addition to selected compositions did not introduce phase separation or bulk nucleation as classical nucleating agents, but enhanced the crystallization and provided fine grained microstructure even after lower temperature heat treatments.

Previously uncharacterized crystalline phases were identified, one in the CASL system (Ca-La-aluminosilicate crystals), and a further two in the $TiO_2$ containing CASN system ($\alpha$ & $\beta$-Nd-titanite).

## CHAPTER 6.

## GLASS-CERAMIC DERIVATIVES OF Mg-Ln-ALUMINOSILICATE GLASSES

### 6.1. Crystallization of a pure MAS (cordierite) glass

The crystallization of pure MAS glass (cordierite composition, $Mg_2Al_4Si_5O_{18}$) was studied in parallel with the rare-earth containing magnesium-aluminosilicate glasses. Two crystallization exotherms were detected on the DTA trace of the pure MAS glass (Fig.4.14&15). According to the literature [80,81,95], the lower temperature exotherm belongs to the crystallization of μ-cordierite, whereas the higher temperature one belongs to the crystallization of indialite. Polished-surface bulk glasses and glass powder pellets were crystallized at and above the crystallization temperatures determined by DTA. The heat treatment schedules and the crystalline phases determined by XRD are listed in Table 6.1.

**Table 6.1.** Crystallization of MAS (cordierite) glass

| Sample type | Temp. of cryst. (°C) | Duration of cryst. | Crystalline phases detected by XRD (m: major, +: minor) |
|---|---|---|---|
| bulk glass | 947 | 2 hr | no detectable crystallinity |
| bulk glass | 979 | 2 hr | no detectable crystallinity |
| bulk glass | 1000 | 2 hr | no detectable crystallinity |
| bulk glass | 1065 | 2 hr | m: indialite, +: μ-cordierite |
| bulk glass | 1100 | 2 hr | m: indialite |
| bulk glass | 1200 | 2 hr | m: indialite |
| powder pellet | 947 | 2 hr | m: μ-cordierite |
| powder pellet | 979 | 2 hr | m: μ-cordierite, +: indialite |
| powder pellet | 1000 | 2 hr | m: μ-cordierite, m: indialite |
| powder pellet | 1065 | 2 hr | m: indialite |
| powder pellet | 1100 | 2 hr | m: indialite |
| powder pellet | 1170 | 2 hr | m: indialite |
| powder pellet | 1200 | 2 hr | m: indialite |
| powder pellet | 1200 | 10 hr | m: indialite |
| hot pressed | 1170 | 2 hr | m: indialite |

The bulk glasses are crystallized by a surface nucleation mechanism, and after the low temperature heat treatments resulted in only limited amount of crystals on the surface of the specimens. The amount of crystallinity in the bulk samples reached the suitable level for XRD analysis from the 1065°C heat treatment. Indialite (JCPDS 13-293) was detected as a major phase, and it was accompanied by a minor phase of μ-cordierite (JCPDS 14-249). The μ-cordierite phase was completely converted into indialite by higher temperature heat treatments. Surprisingly, the high temperature crystallized, fully crystalline glass-ceramic specimens were distorted, and showed degradation in strength, which was presumably due to the volume change associated with the transformation of large μ-cordierite grains into indialite.

According to the XRD analysis, μ-cordierite was the first crystalline phase in the glass-ceramic pellet crystallized at low temperature (Table 6.1). Slightly higher temperature crystallization increased the amount of μ-cordierite phase, and also resulted in the appearance of indialite, as a minor phase. Higher temperature treatments resulted in gradual transformation of μ-cordierite into indialite, and the transformation reached completion at 1065°C/2hr (Table 6.1). In addition, the only crystalline phase detected by XRD for the hot pressed powder specimen was indialite. Both the hot-pressed specimen and the high temperature crystallized pellets were well-sintered, fully crystalline glass-ceramics, and did not show any loss in strength.

The differences between the bulk and sintered glass-ceramics originate from the different crystallite size, since the size of μ-cordierite crystals was limited by the mean particle size of the parent glass powder. On the other hand, the abraded surface of the powdered particles provided numerous nucleation sites, and resulted in fine microstructure. The transformation of small μ-cordierite crystallites into indialite

generated much smaller stresses, than the transformation of the large μ-cordierite grains in the bulk samples.

In addition, there were difference between the bulk glasses and the pellets in the crystallization temperatures of the two phases. The abraded surface of glass powder promoted the crystallization of μ-cordierite at lower temperatures, and as a consequence, the transformation of μ-cordierite into indialite started and completed at lower temperatures, than in the case of bulk glass-ceramics.

## 6.2. Crystallization and microstructure of Mg-La-aluminosilicate glass-ceramics

The composition of the Mg-La-aluminosilicate glass (MASL-1) used for the crystallization experiments is shown in Table 4.2. Three crystallization exotherms were detected on the DTA trace of the alumina-ground parent glass (Table 4.3). Polished and rough surfaced bulk glass specimens and glass powder pellets were used for the crystallization experiments. The heat treatment schedules and the crystalline phases detected by XRD are summarized in Table 6.2.

The bulk samples showed a surface nucleated crystallization mechanism, and the low temperature heat treatments resulted in a thin crystalline layer on the surface of the specimens, therefore the identification of crystalline species was mainly done by X-ray microanalysis and morphological studies, although the main phases could just be detected on the XRD traces as well. The large, dark, dendritic crystals of indialite on the surface of a crystallized bulk glass samples, are presumably nucleated by surface imperfections (Fig.6.1/a). The bright areas, between the dendritic arms consist of mainly La-rich glassy residue, but minute sized $La_2Si_2O_7$ crystals were also detected. In addition, tiny, dark magnesium-aluminate spinel crystals, and dark, oval crystals of pyrope were also observed.

**Table 6.2.** Crystallization of Mg-La-aluminosilicate (MASL-1) glass

| Sample type | Temp. of cryst. (°C) | Duration of cryst. | Crystalline phases detected by XRD (m: major, +: minor) |
|---|---|---|---|
| bulk glass | 1050 | 10 min | (rough): just detectable indialite |
| bulk glass | 1050 | 30 min | m: indialite (weak XRD trace) |
| bulk glass | 1068 | 30 min | m: indialite, +: mo-La•2Si, (weak XRD trace) |
| bulk glass | 1160 | 30 min | m: indialite, +: mo-La•2Si, +: t-La•2Si |
| bulk glass | 1160 | 3 hr | m: indialite, +: mo-La•2Si, +: t-La•2Si |
| bulk glass | 1180 | 2 hr | m: indialite, +: mo-La•2Si, +: t-La•2Si |
| powder pellet | 1050 | 10 min | m: mullite, +: indialite, +: mo-La•2Si |
| powder pellet | 1050 | 30 min | m: indialite, m: mullite, +: mo-La•2Si, +:t-La•2Si |
| powder pellet | 1068 | 30 min | m: indialite, m: mullite, +: mo-La•2Si, +: t-La•2Si |
| powder pellet | 1160 | 30 min | m: indialite, +: t-La•2Si, +: mo-La•2Si |
| powder pellet | 1160 | 3 hr | m: indialite, +: t-La•2Si, +: mo-La•2Si |
| powder pellet | 1180 | 2 hr | m: indialite, +: t-La•2Si, +: mo-La•2Si |

According to the XRD analysis of bulk glass-ceramics crystallized at 1068°C (Table 6.2), the primary and major phase was indialite, and it was accompanied by minor phase of high temperature, monoclinic $La_2Si_2O_7$ (XRD data source: [301]). At this temperature the surface of the specimen was covered by large dendritic crystalline complexes, as shown in Fig.6.1/b. The microstructure of a dendritic complex is shown at higher magnification in Fig.6.1/c. The La-enriched interdendritic area is partially crystallized as La-disilicate. It should be noted, that the small, dark spinel crystals shown in Fig.6.1/a&c, were only detected on the sample surface, their presence has not been confirmed in the bulk. In addition, they were more abundant on the surface of the polished specimens, which suggest that the polishing process somehow activated the surface, which in turn initiated the formation of spinel crystals.

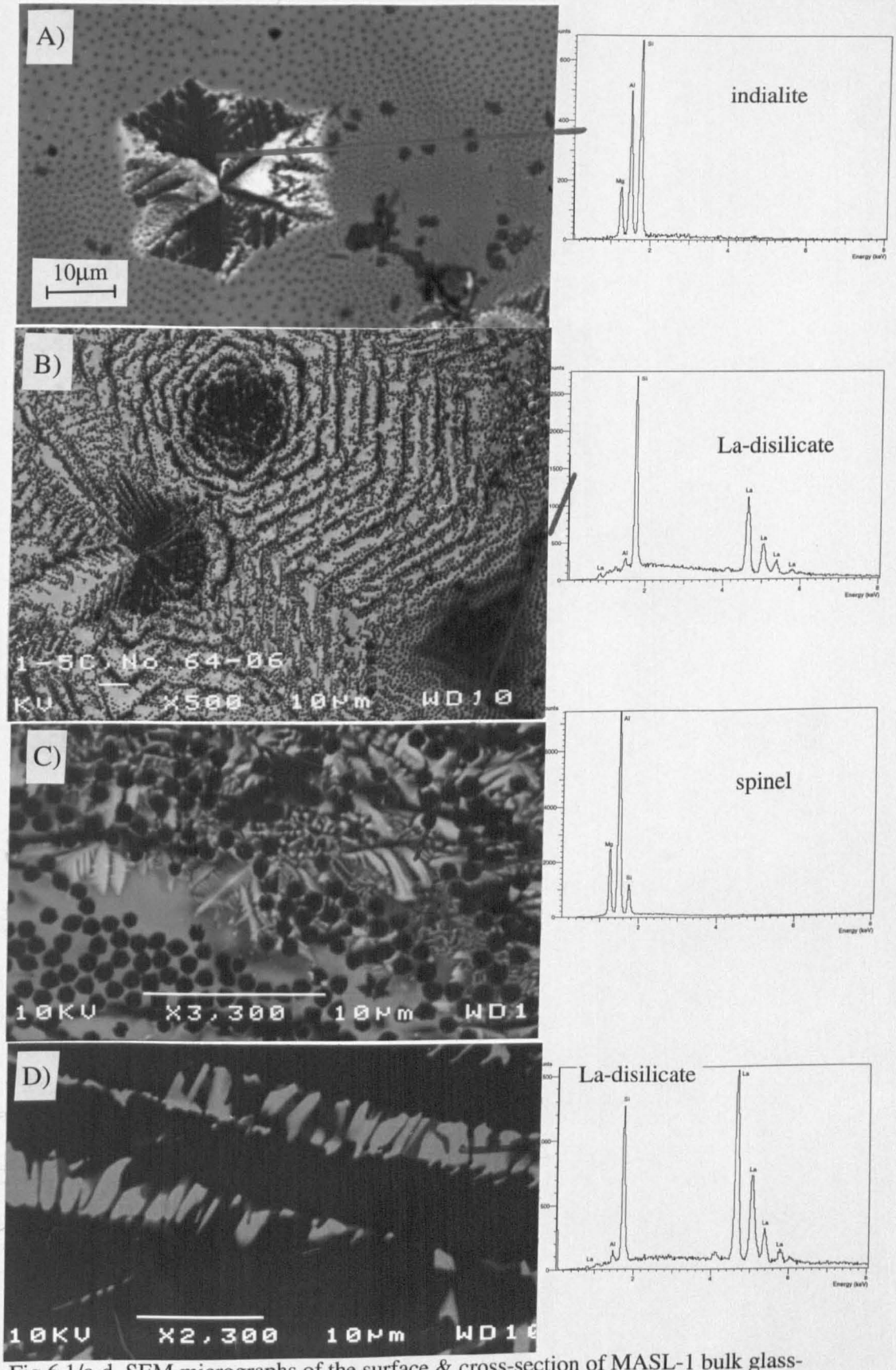


Fig.6.1/a-d. SEM micrographs of the surface & cross-section of MASL-1 bulk glass-ceramics, a) 1050°C/10min; b) 1068°C/30min; c) 1068°C/30min; d) 1160°C/3hr.

The bulk specimens seemed fully crystalline after high temperature heat treatments, and the XRD traces showed indialite as a major crystalline phase, monoclinic and tetragonal $La_2Si_2O_7$ (XRD data source: [301]) as minor phases, and the amount of the latter gradually increased with increasing temperature. The cross section of an almost fully crystalline bulk glass-ceramic is shown in Fig.6.1/d. The microstructure is dominated by large dendritic grains of indialite. The areas between the indialite crystals are mainly occupied by small, bright La-disilicate crystals, although a small amount of glassy residue can still be detected.

The major difference between the two types of crystallized bulk glasses was, that the rough surfaced specimens showed a higher degree of crystallinity and thicker crystalline layer, than the polished surfaced ones, which was due to the numerous nucleation sites and also to the lower activation energy required for crystallization on the abraded surface. Regardless of the surface condition of the parent glasses, the high temperature crystallization of the bulk samples provided almost fully crystalline, strong, compact glass-ceramic bodies.

The sintered pellets provided XRD analysable amounts of crystallinity even after the lowest temperature of crystallization (Table 6.2). The major phase was mullite ($Al_6Si_2O_{13}$, JCPDS 15-776), and minor phases of indialite and $\alpha$-$La_2Si_2O_7$ (JCPDS 35-223) were also detected. The microstructure of a low temperature sintered glass-ceramic pellet is shown in Fig.6.2/a. The large dark indialite crystal in the middle is surrounded by tiny, bright crystals of La-disilicate. Mullite crystals have tiny, whisker-shaped morphology and all of the crystals were embedded in a glassy matrix.

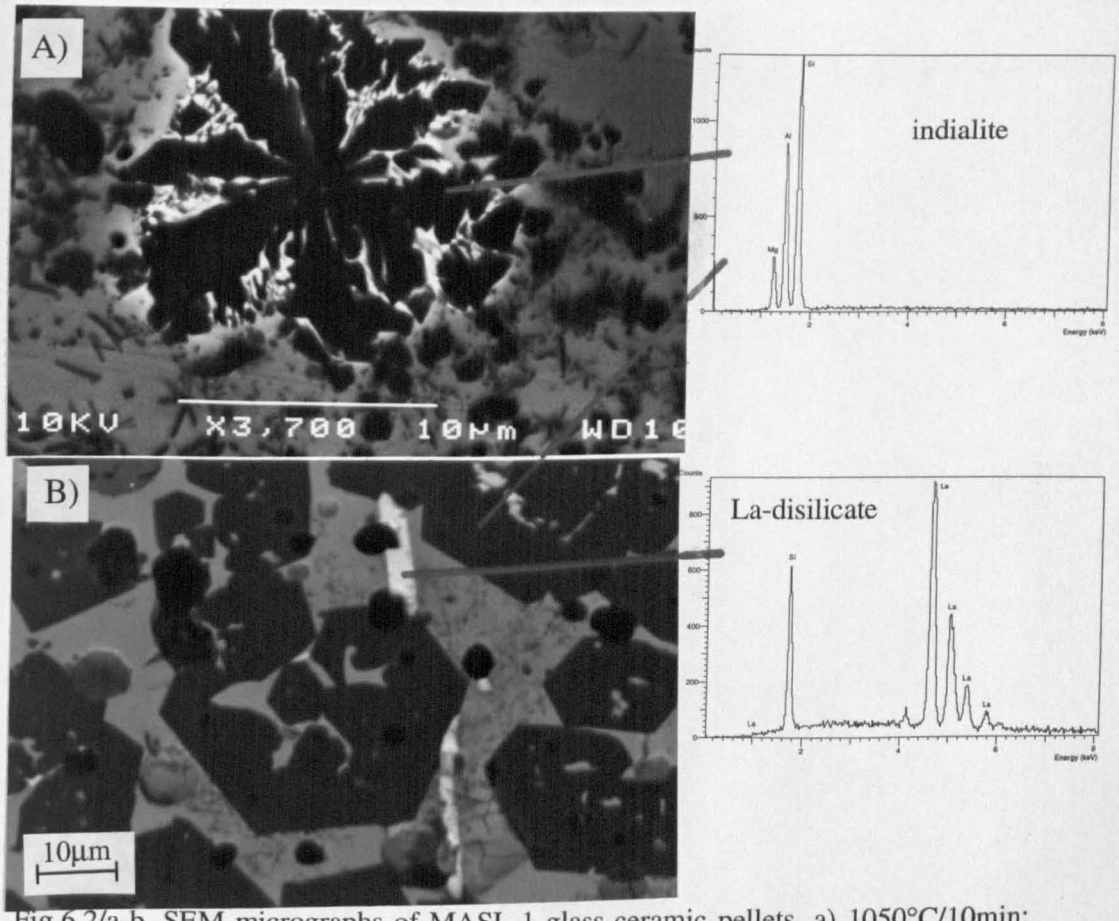


Fig.6.2/a-b. SEM micrographs of MASL-1 glass-ceramic pellets, a) 1050°C/10min; b) 1180°C/2hr.

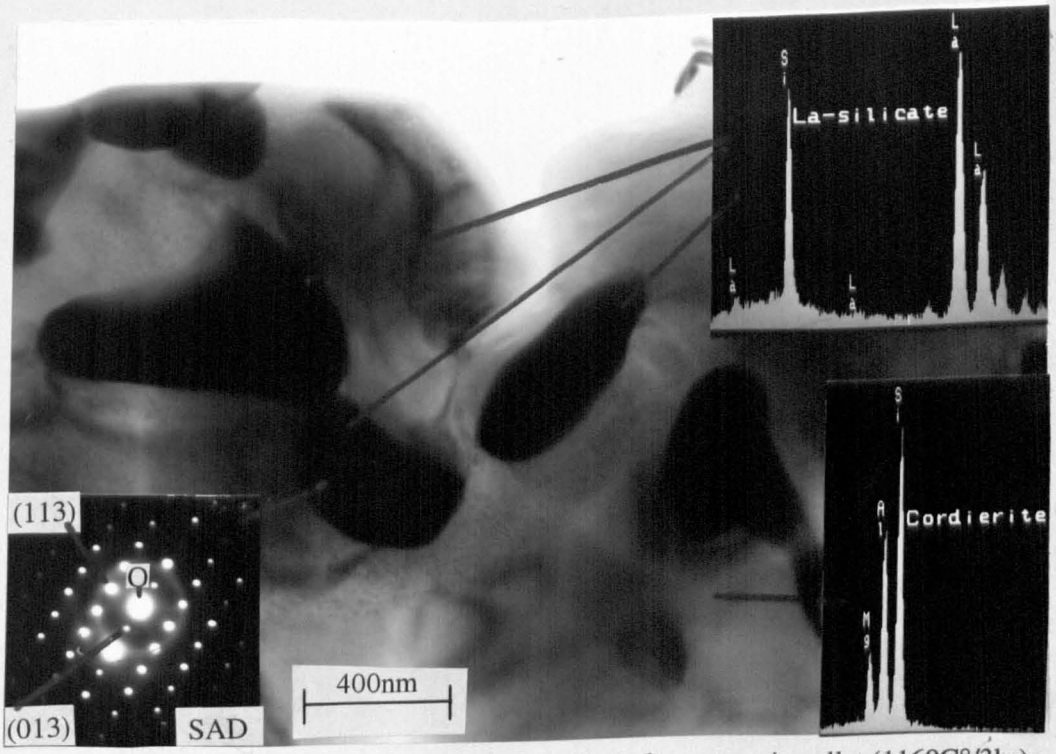


Fig.6.3. Bright field TEM micrograph of a MASL-1 glass-ceramic pellet (1160C°/3hr).

The medium temperature heat treatments (1068°C) resulted in a marked increase in the amount of the indialite phase, at the expense of the mullite and the glassy residue (Table 6.2). In addition, two other minor phases were identified by XRD: tetragonal and monoclinic La-disilicate. A bright field TEM micrograph of dark La-disilicate crystals found in a glass-ceramic pellet is shown in Fig.6.3.

Indialite was the major phase in the glass-ceramic pellets crystallized at high temperatures, and among the minor phases of the monoclinic and tetragonal La-disilicate, the latter modification became dominant (Table 6.2). The coarse microstructure of the highest temperature crystallized pellets (Fig.6.2/b) and the presence of an unusually large amount of glassy residue, suggests partial melting at the applied temperature. The presence of the liquid phase promoted the recrystallization and growth of indialite crystals into a pseudohexagonal faceted morphology and also resulted in elongated crystals of La-disilicate. Regardless of the signs of partial melting at the highest crystallization temperature, the high temperature crystallized pellets of the MASL-1 composition were well-sintered, highly crystalline, strong glass-ceramic bodies.

### 6.3. Crystallization and microstructure of Mg-Y-aluminosilicate glass-ceramics

The composition of the Mg-Y-aluminosilicate parent glass (MASY-1), used for the crystallization experiments is shown in Table 4.2. Three crystallization exotherms were detected on the DTA trace of the alumina-ground glass powder, similar to the MASL-1 glass composition. Polished and rough surfaced bulk glass slices, as well as glass powder pellets were crystallized. The heat treatment schedules and the crystalline phases detected by XRD are shown in Table 6.3.

**Table 6.3.** Crystallization of Mg-Y-aluminosilicate (MASY-1) glass

| Sample type | Temp. of cryst. (°C) | Duration of cryst. | Crystalline phases detected by XRD (m: major, +: minor) |
|---|---|---|---|
| bulk glass | 975 | 2 hr | no detectable crystallinity |
| bulk glass | 1075 | 10 min | rough sample: just detectable indialite |
| bulk glass | 1075 | 30 min | rough sample: just detectable indialite |
| bulk glass | 1075 | 2 hr | m: indialite, +: α-Y•2Si |
| bulk glass | 1100 | 2 hr | m: indialite, +: α-Y•2Si, +: y-Y•2Si |
| bulk glass | 1115 | 2 hr | m: indialite, +: α-Y•2Si, +: y-Y•2Si |
| bulk glass | 1160 | 30 min | m: indialite, +: α-Y•2Si, +: y-Y•2Si |
| bulk glass | 1160 | 2 hr | m: indialite, +: α-Y•2Si, +: y-Y•2Si |
| powder pellet | 975 | 2 hr | m: μ-cordierite, +: α-Y•2Si, +: indialite, +: mullite, +: y-Y•2Si, |
| powder pellet | 1075 | 10 min | m: indialite, +: α-Y•2Si, +: y-Y•2Si |
| powder pellet | 1075 | 30 min | m: indialite, +: α-Y•2Si, +: y-Y•2Si |
| powder pellet | 1075 | 2 hr | m: indialite, +: α-Y•2Si, +: y-Y•2Si |
| powder pellet | 1100 | 2 hr | m: indialite, +: α-Y•2Si, +: y-Y•2Si |
| powder pellet | 1115 | 2 hr | m: indialite, +: α-Y•2Si, +: y-Y•2Si |
| powder pellet | 1160 | 30 min | m: indialite, +: α-Y•2Si, +: y-Y•2Si |
| powder pellet | 1160 | 2 hr | m: indialite, +: α-Y•2Si, +: y-Y•2Si |

The bulk glass specimens were crystallized by surface initiated crystallization mechanism, and had a thin crystalline layer on their surface after the low temperature heat treatments. The XRD traces of the low temperature crystallized samples were hardly analysable, therefore the identifications of crystalline phases were mainly done by SEM/EDS. Indialite was the primary and dominant phase to crystallize, as it is shown in Fig.6.4/a. In addition, tiny crystals of $Y_2Si_2O_7$ were detected in the Y-enriched interdendritic area. The well distributed, dark spots on the picture are spinel crystals. Slightly higher temperature heat treatment resulted in enhanced growth of the dendritic crystalline complexes (Fig.6.4/b), and promoted the crystallization of the Y-rich glassy residue in the form of dendritic and fine grained eutectic Y-disilicate crystals.

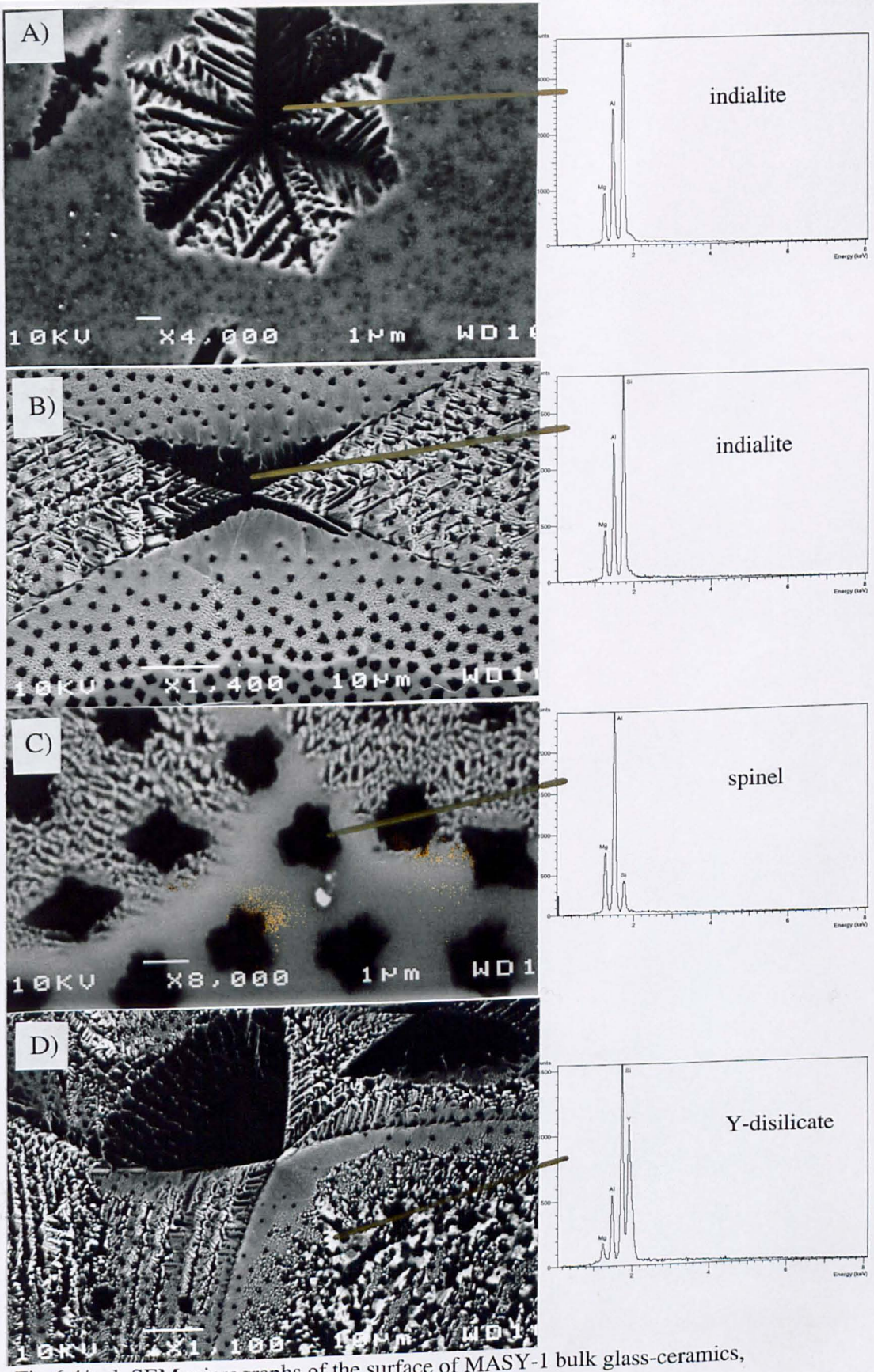


Fig.6.4/a-d. SEM micrographs of the surface of MASY-1 bulk glass-ceramics,
a) 975°C/2hr; b) 1075°C/2hr; c) 1075°C/2hr; d) 1160°C/2hr.

In addition, it also promoted the growth of the spinel crystals, which are shown at high magnification in Fig.6.4/c, partly surrounded by eutectic type fine-grained crystal mixture of indialite & Y-disilicate.

The XRD traces of crystallized bulk glasses became analysable after the 1050°C/30min heat treatment, in the case of the rough surfaced samples. The major phase was indialite, and minor phase of $\alpha$-$Y_2Si_2O_7$ (JCPDS 38-223) was also detected (Table 6.3). Higher temperature heat treatments increased the amount of the indialite, and the $\alpha$-Y-disilicate minor phase. In addition, minor phase of y-$Y_2Si_2O_7$ (XRD data source: [296]) was also detected. The fast growing crystalline front of dark indialite crystals shows dendritic growth in Fig.6.5. Characteristic dendritic side branches and fine cellular morphology can be observed, which originate from the instability on the lateral surface of the growing indialite crystal. In addition, the Y-enriched glassy phase started to crystallize as Y-disilicate at the dendritic side branches, but some glassy residue became entrapped between the fast growing dendritic grains.

The high temperature heat treatments resulted in the crystallization of the remaining glassy residue (Fig.6.4/d). The XRD traces of the high temperature crystallized bulk glasses showed an increase in the amount of indialite, and showed considerable increase in the amount of y-Y-disilicate phase at the expense of $\alpha$-Y-disilicate, in the case of rough surfaced samples. These results suggested, that the rough surface promotes the formation of the "y" modification at high temperatures. The microstructure was dominated by the surface nucleated, large indialite grains, whose side branches showed some coarsening after the high temperature heat treatments. The high temperature crystallized bulk glasses provided well crystallized, strong glass-ceramic bodies.

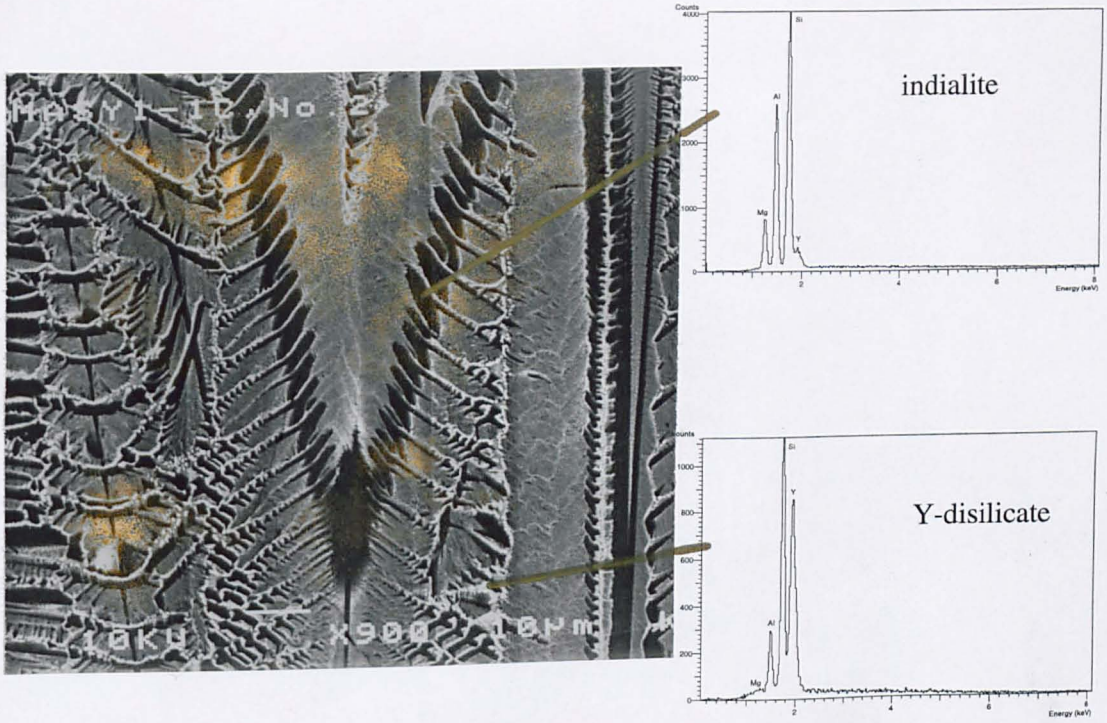


Fig.6.5. SEM micrograph of the cross-section of a MASY-1 bulk glass-ceramic (1115°C/2hr).

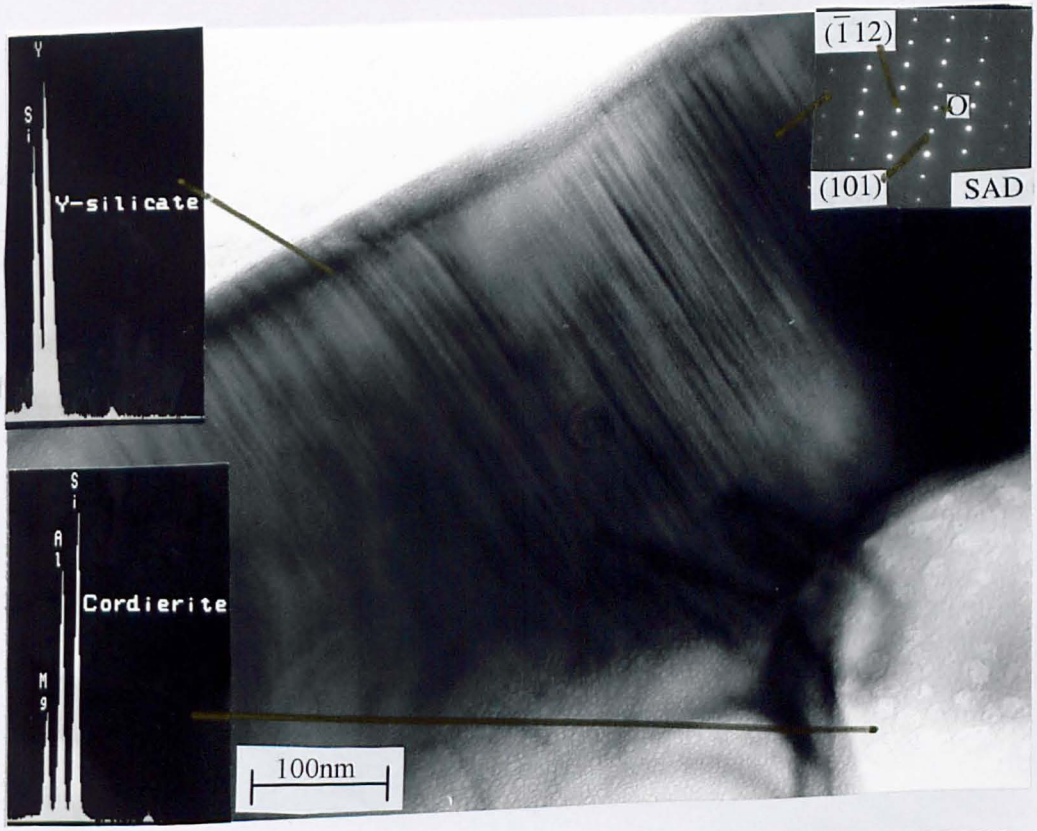


Fig.6.7. Bright field TEM micrograph of a MASY-1 glass-ceramic pellet (1160C°/30min).

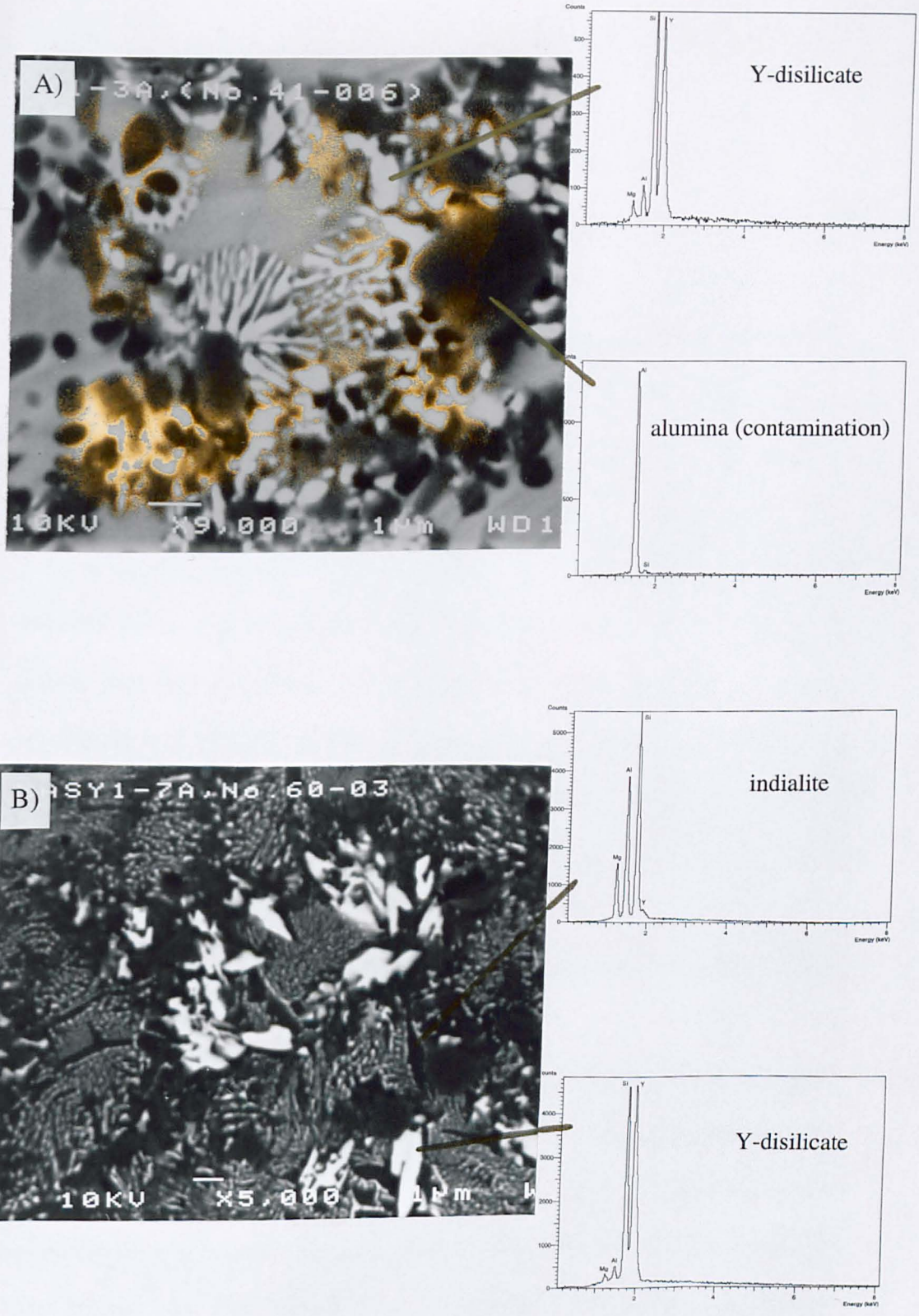


Fig.6.6/a-b. SEM micrographs of MASY-1 glass-ceramic pellets, a) 975°C/2hr; b) 1160°C/30min.

The glass powder pellets provided reasonably well crystallized specimens even after low temperature heat treatments (Fig.6.6/a). The XRD analysis of the low temperature crystallized sample showed a surprising result: μ-cordierite was the dominant phase, and it was accompanied by minor phases of α-Y-disilicate, indialite, mullite, and y-Y-disilicate (Table 6.3). The μ-cordierite phase was not expected to crystallize in glass compositions other than the pure MAS system. After medium temperature heat treatments the μ-cordierite phase was completely converted into indialite. The heat treatments at high temperatures resulted in an overall increase in crystallinity, and the microstructure of a high temperature crystallized glass-ceramic pellet is shown in Fig.6.6/b. The dark crystals are indialite, the bright ones are Y-disilicate, and the bulk of the sample mainly contains tiny crystals of the previous two phases, showing a fine grained eutectic type microstructure. The high temperature crystallization of MASY-1 pellets provided well sintered, well crystallized, fine microstructure glass-ceramic bodies. A bright field TEM micrograph of a large α-Y-disilicate crystal, showing stacking faults, can be seen in Fig.6.7.

## 6.4. Crystallization and microstructure of Mg-Nd-aluminosilicate glass-ceramics

The compositions of Mg-Nd-aluminosilicate glasses, used for the crystallization experiments are shown in Table.4.2. Generally one or two crystallization exotherms were detected on the DTA traces of the ground glass powders, depending on the composition (Fig.4.14 & 15), except for the alumina ground MASN-1 composition, which showed three crystallization peaks. Polished and rough surfaced bulk glasses and glass powder pellets were crystallized from the MASN-1 composition, whereas only polished surfaced bulk glasses and glass powder pellets were used in the case of

all other MASN parent glass composition. The applied heat treatment schedules and the crystalline phases detected by XRD are shown in Table 6.4/a-d. & Table 6.6/a-d. Some representative XRD traces are shown in Fig.II.4 (Appendix II).

### 6.4.1. Crystallization and microstructure of Mg-Nd-aluminosilicate bulk glass-ceramics

It is worth separating the studied range of Mg-Nd-aluminosilicate glass compositions into four regions according to the crystallization behaviour of bulk glasses. The four groups are: the low-$Nd_2O_3$ compositions (MASN 1-3; 4.2-6.2mol% $Nd_2O_3$), the medium-$Nd_2O_3$ compositions (MASN 4-7; 7.4-11.4mol% $Nd_2O_3$), the high-$Nd_2O_3$ compositions (MASN 8-9; 13.0-14.7mol% $Nd_2O_3$), and finally the extra high-$Nd_2O_3$ glass compositions (MASN 10-12; 16.6-20.0mol% $Nd_2O_3$).

The MASN 1-3 bulk glasses showed surface initiated crystallization, as most of the MASN glass compositions. Low temperature heat treatments resulted in the formation of large dendritic complexes (Fig.6.8/a), where the crystallization of the indialite is initiated by surface imperfections. The crystalline derivatives of both polished and rough glass slices showed an even distribution of tiny spinel crystals on their surface (Fig.6.8/a), although the spinel crystals were more abundant on the surface of polished specimens, similar to the crystallized MASL & MASY glasses. In addition, mullite and pyrope crystals were also detected. Moreover, $Nd_2Si_2O_7$ started to crystallize in the Nd-rich glassy residual area of the large crystalline complexes. Major phase of indialite and minor phases of high temperature, monoclinic $Nd_2Si_2O_7$ (JCPDS 38-1456) and mullite were detected in the low temperature crystallized samples by XRD (Table 6.4/a).

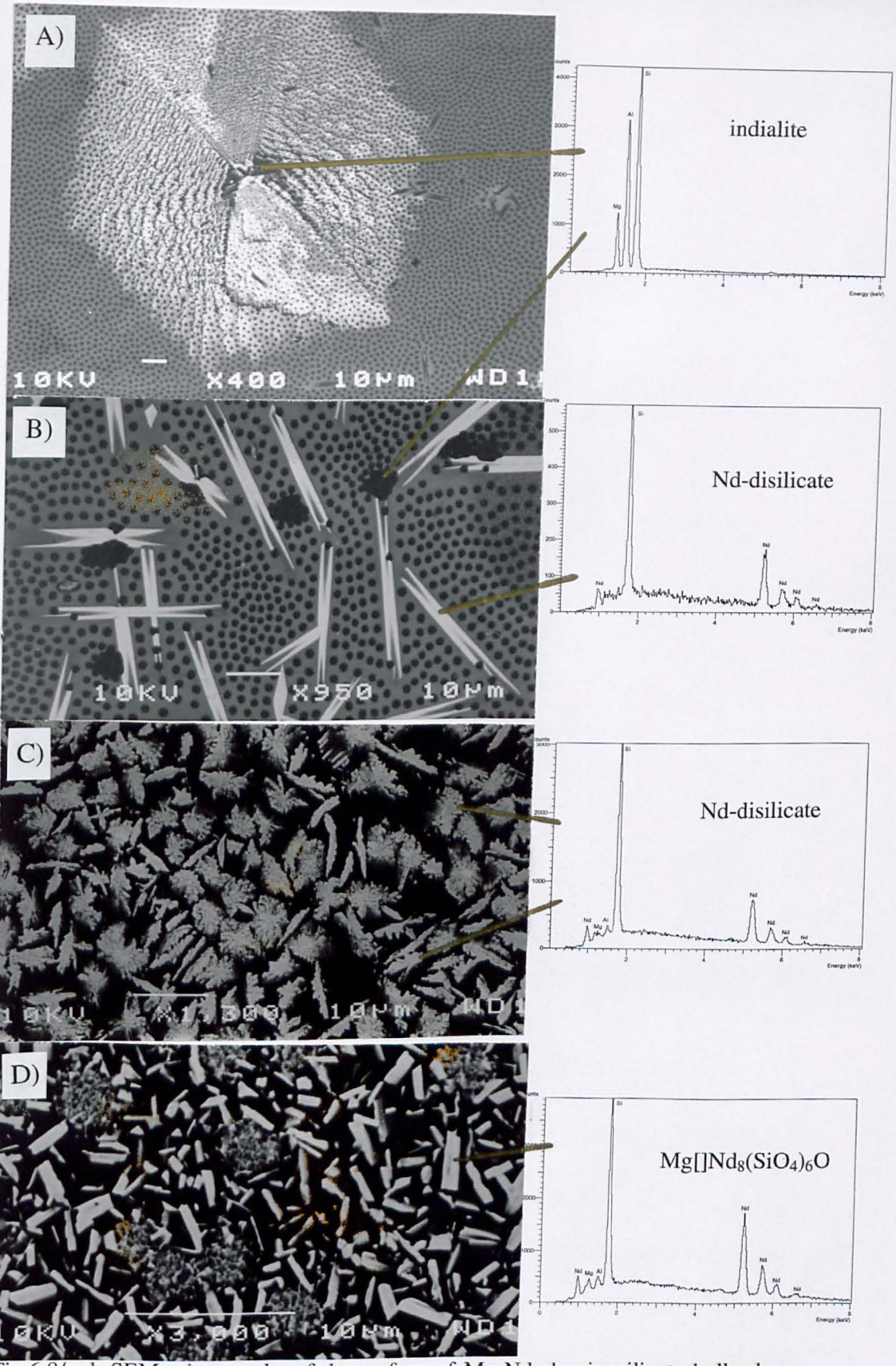


Fig.6.8/a-d. SEM micrographs of the surface of Mg-Nd-aluminosilicate bulk glass-ceramics, a) MASN-1, 1075°C/30min; b) MASN-6, 1140°C/2hr; c) MASN-7, 1124°C/2hr; d) MASN-10, 1200°C/2hr.

In addition, the presence of a ternary Mg-Nd-silicate phase was detected, which was previously reported [183,299], but the phase had no JCPDS file. The XRD reflections of the Mg-Nd-silicate phase will be described later on in this section. The other phases, which were identified on the surface by SEM/EDS, were not detectable on the XRD traces.

**Table 6.4/a.** Crystallization of Mg-Nd-aluminosilicate bulk glasses (MASN 1-3)

| Sample type | Temp. of cryst. (°C) | Duration of cryst. | Crystalline phases detected by XRD (m: major, +: minor) |
|---|---|---|---|
| **MASN-1 glass** | | | |
| bulk glass | 1070 | 30 min | (rough) just detectable: indialite |
| bulk glass | 1075 | 10 min | (rough) m: indialite, +: mo-Nd•2Si |
| bulk glass | 1075 | 30 min | (rough) m: indialite, +: mullite, +: Mg-Nd-Si, +: mo-Nd•2Si |
| bulk glass | 1120 | 30 min | m: indialite, +: Mg-Nd-Si, +: mo-Nd•2Si, +: t-Nd•2Si |
| bulk glass | 1120 | 2 hr | m: indialite, +: mo-Nd•2Si, +: t-Nd•2Si, +: Mg-Nd-Si |
| bulk glass | 1130 | 2 hr | m: indialite, +: mo-Nd•2Si, +: t-Nd•2Si, +: Mg-Nd-Si |
| bulk glass | 1188 | 2 hr | m: indialite, +: mo-Nd•2Si, +: t-Nd•2Si, +: Mg-Nd-Si |
| **MASN-2 glass** | | | |
| bulk glass | 1100 | 2 hr | no detectable crystallinity |
| bulk glass | 1117 | 2 hr | no detectable crystallinity |
| bulk glass | 1170 | 2 hr | m: indialite, +: mo-Nd•2Si (weak XRD trace) |
| bulk glass | 1200 | 2 hr | m: indialite, +: mo-Nd•2Si, +: t-Nd•2Si |
| **MASN-3 glass** | | | |
| bulk glass | 1100 | 2 hr | no detectable crystallinity |
| bulk glass | 1134 | 2 hr | just detectable: indialite |
| bulk glass | 1180 | 2 hr | m: indialite, +: mo-Nd•2Si |

Higher temperature heat treatments resulted in a marked increase in the amount of indialite, and also increased the amount of the minor phases of Mg-Nd-silicate and monoclinic Nd-disilicate. In addition, a minor amount of low temperature, tetragonal $Nd_2Si_2O_7$ (JCPDS 22-1177) was also detected. Fig.6.9/a shows the microstructure of the cross-section of a bulk glass-ceramic specimen. The surface nucleated large indialite grains dominate the microstructure of the bulk glass-ceramics. Some of the

Nd-rich glassy residue, which became entrapped between the large indialite grains, crystallized as Nd-disilicate, although some glassy residue still remained. The bright field TEM micrograph in Fig.6.10/a shows pseudohexagonal indialite crystals, and dark Nd-disilicate crystals between the indialite grains. Similar features are shown on the dark field TEM micrograph in Fig.6.10/b. Crystallizations at even higher temperature, resulted in further increase of the amount of indialite, as well as the increase of the amount of both tetragonal and monoclinic Nd-disilicate modifications. The increase of the latter was at the expense of the Mg-Nd-silicate phase. The dominance of the indialite crystalline phase at every crystallization temperature was characteristic to this group of bulk glasses (Table 6.4/a). It should be noted, that bulk glass specimens of MASN-2 and MASN-3 compositions showed limited amount of crystallinity below the highest temperature heat treatments. After the highest temperature heat treatments their XRD traces showed high degree of crystallinity, and the fibrous interdendritic area seemed fully crystalline, but some uncrystallized glassy areas were still detected in the bulk of the samples (Fig.6.9/b).

The heat treatments below 1200°C resulted in a modest amount of crystallinity, in the case of MASN 4-7 bulk glasses (Fig.6.8/b). In spite of that, the crystallizations at 1200°C resulted in well crystallized glass-ceramics (Fig.6.8/c). The dominant phase in the glass-ceramics in this group was monoclinic Nd-disilicate, regardless of the heat treatment temperature (Table 6.4/b). The major phase was accompanied by minor phases of indialite and tetragonal Nd-disilicate. The amount of the latter phase increased with increasing duration of crystallization at high temperature. In addition, a minor phase of Mg-Nd-silicate was also detected on some of the XRD traces.

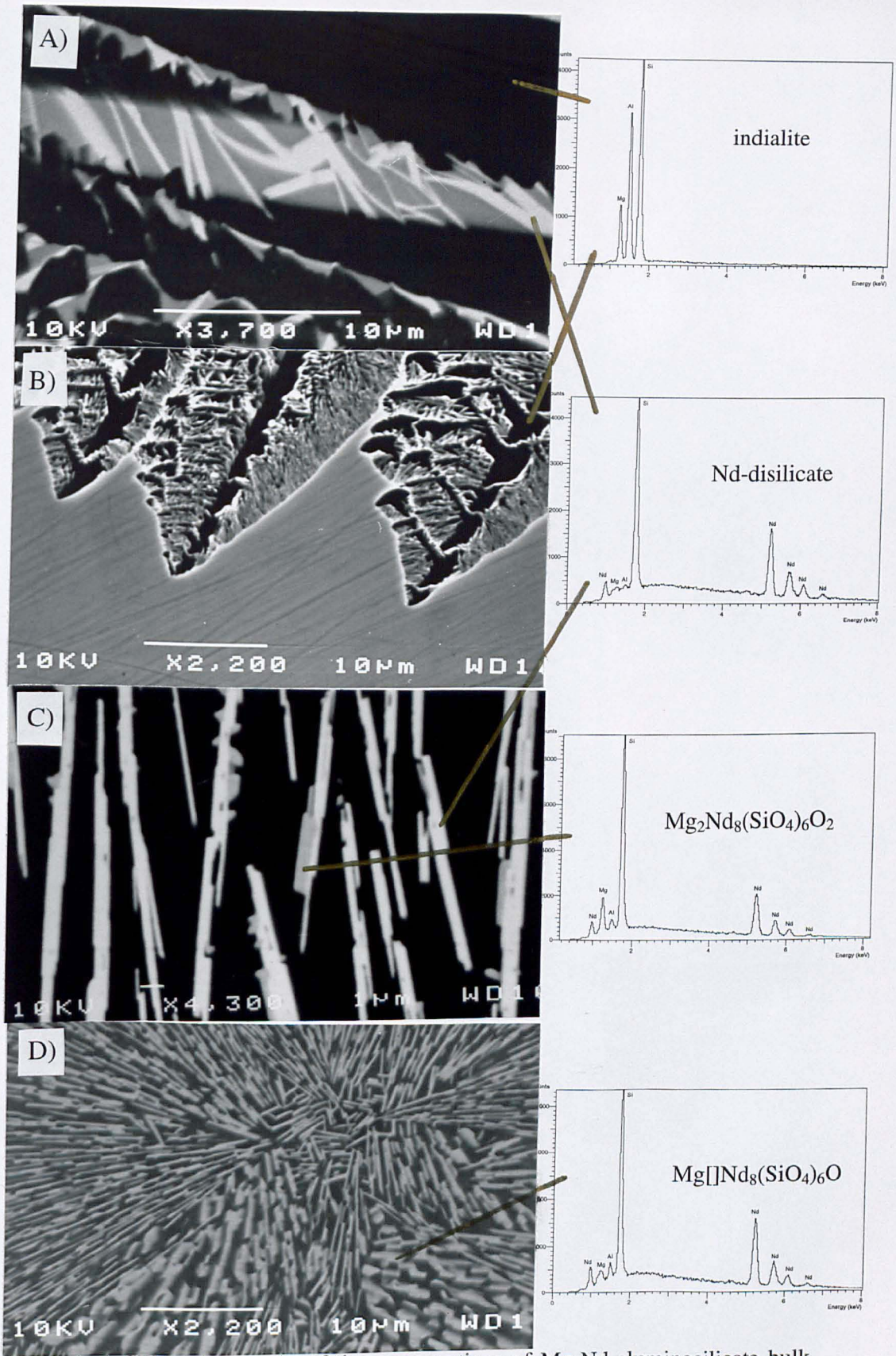


Fig.6.9/a-d. SEM micrographs of the cross-sections of Mg-Nd-aluminosilicate bulk glass-ceramics, a) MASN-1, 1120°C/2hr; b) MASN-2, 1200°C/2hr; c) MASN-7, 1200°C/2hr; d) MASN-12, 1200°C/2hr.

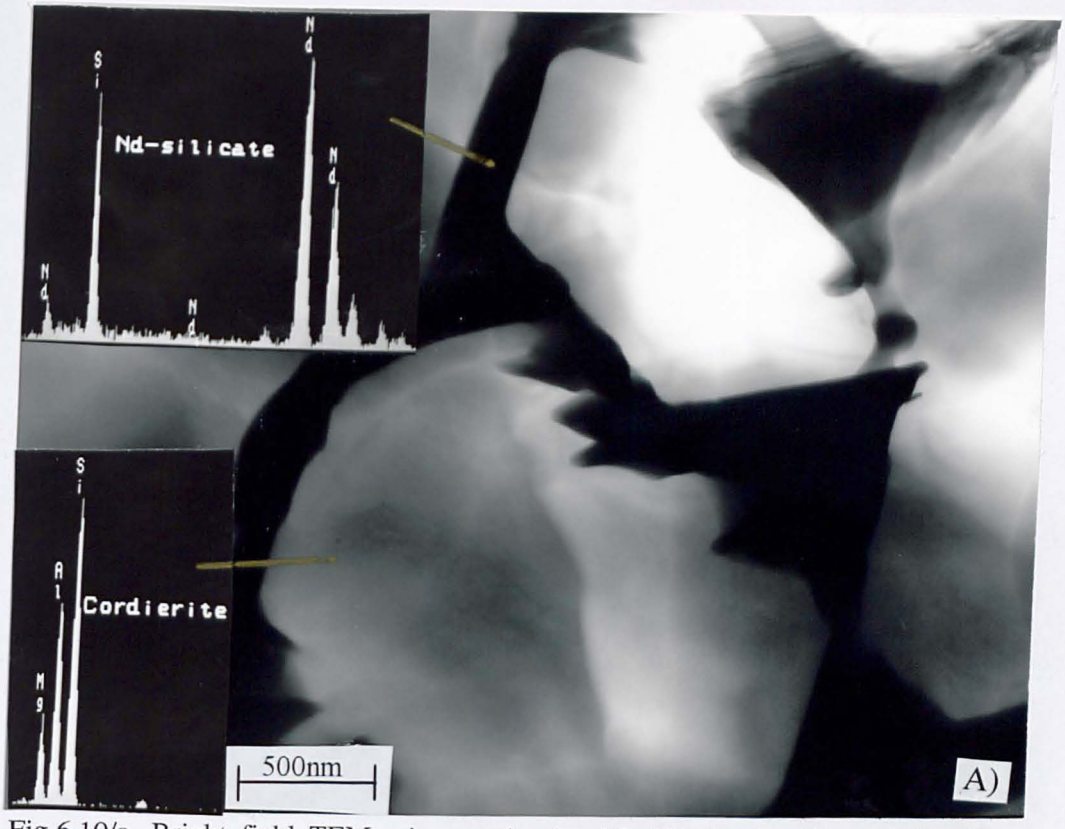


Fig.6.10/a. Bright field TEM micrograph of a Mg-Nd-aluminosilicate bulk glass-ceramic (MASN-1, 1120°C/2hr).

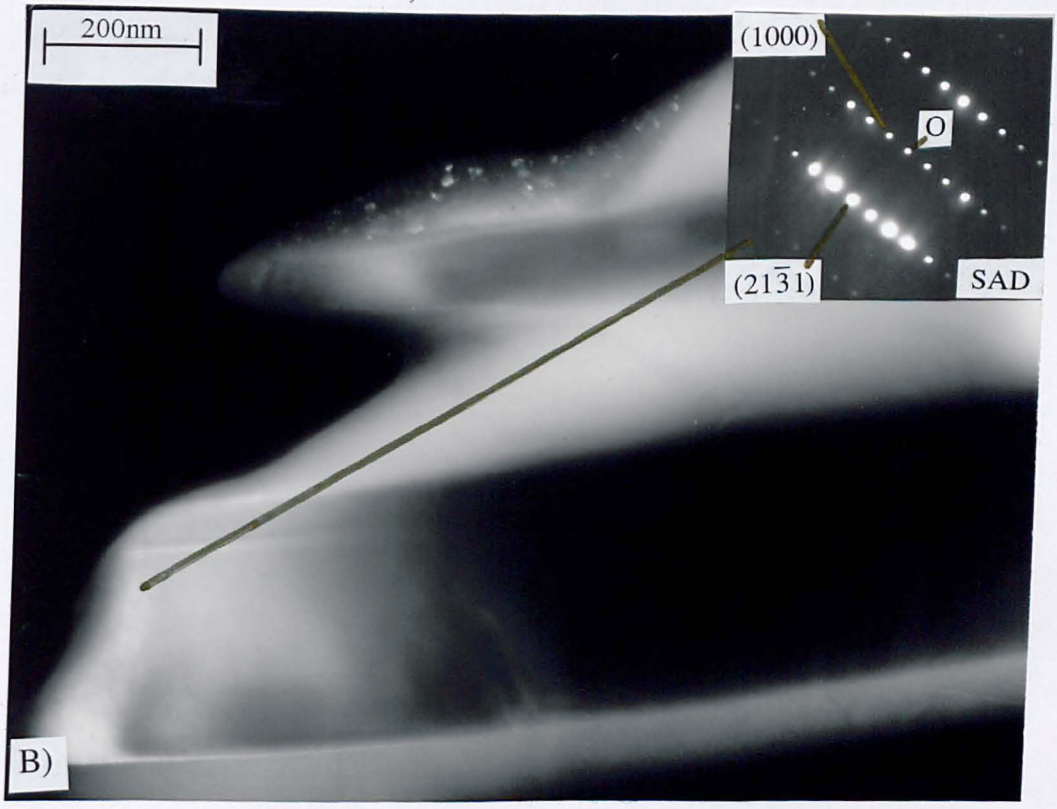


Fig.6.10/b. Dark field TEM micrograph of a Mg-Nd-aluminosilicate bulk glass-ceramic (MASN-1, 1120°C/2hr).

The well-crystallized cross section of a bulk glass-ceramic is shown in Fig.6.9/c. The small, greyish crystallites of Mg-Nd-silicate are attached to the long bright grains of Nd-disilicate, whereas the large dark grains are indialite.

**Table 6.4/b.** Crystallization of Mg-Nd-aluminosilicate bulk glasses (MASN 4-7)

| Sample type | Temp. of cryst. (°C) | Duration of cryst. | Crystalline phases detected by XRD (m: major, +: minor) |
|---|---|---|---|
| **MASN-4 glass** | | | |
| bulk glass | 1100 | 2 hr | no detectable crystallinity |
| bulk glass | 1143 | 2 hr | m: mo-Nd•2Si, m: indialite (weak XRD trace) |
| bulk glass | 1200 | 2 hr | m: mo-Nd•2Si, m: indialite, +: t-Nd•2Si |
| **MASN-5 glass** | | | |
| bulk glass | 1100 | 2 hr | no detectable crystalline phase |
| bulk glass | 1132 | 2 hr | m: mo-Nd•2Si, m: indialite (weak XRD trace) |
| bulk glass | 1200 | 2 hr | m: mo-Nd•2Si, m: indialite, +: t-Nd•2Si |
| **MASN-6 glass** | | | |
| bulk glass | 1100 | 2 hr | no detectable crystallinity |
| bulk glass | 1140 | 2 hr | m: mo-Nd•2Si, +: indialite, +: t-Nd•2Si |
| bulk glass | 1200 | 2 hr | m: mo-Nd•2Si, +: indialite |
| **MASN-7 glass** | | | |
| bulk glass | 1124 | 2 hr | no detectable crystallinity |
| bulk glass | 1173 | 2 hr | just detectable: mo-Nd•2Si, indialite, Mg-Nd-Si |
| bulk glass | 1200 | 2 hr | m: mo-Nd•2Si, m: indialite, +: t-Nd•2Si, +: Mg-Nd-Si |
| bulk glass | 1200 | 10 hr | m: mo-Nd•2Si, m: indialite, m: t-Nd•2Si |

The low temperature heat treatments of the MASN 8-9 glasses also resulted in only a thin crystalline layer on the surface. Higher temperature heat treatments eventually led to complete crystallization of the bulk samples. The dominant crystalline phase in these glass ceramics was tetragonal Nd-disilicate, regardless of the crystallization temperature (Table 6.4/c). The major phase was accompanied by minor phases of monoclinic Nd-disilicate and indialite. The amount of all crystalline phases increased with increasing heat treatment temperature, although their ratio has not changed. Longer duration high temperature heat treatment increased the amount

of the monoclinic Nd-disilicate at the expense of the tetragonal modification.

**Table 6.4/c.** Crystallization of Mg-Nd-aluminosilicate bulk glasses (MASN 8-9)

| Sample type | Temp. of cryst. (°C) | Duration of cryst. | Crystalline phases detected by XRD (m: major, +: minor) |
|---|---|---|---|
| **MASN-8 glass** | | | |
| bulk glass | 1096 | 2 hr | no detectable crystallinity |
| bulk glass | 1164 | 2 hr | m: t-Nd•2Si, +: mo-Nd•2Si, +: indialite |
| bulk glass | 1200 | 2 hr | m: t-Nd•2Si, +: mo-Nd•2Si, +: indialite |
| bulk glass | 1200 | 10 hr | m: t-Nd•2Si, +: indialite, +: mo-Nd•2Si |
| **MASN-9 glass** | | | |
| bulk glass | 1064 | 2 hr | no detectable crystallinity |
| bulk glass | 1177 | 2 hr | m: t-Nd•2Si, +: mo-Nd•2Si, +: indialite |
| bulk glass | 1200 | 2 hr | m: t-Nd•2Si, +: mo-Nd•2Si, +: indialite |
| bulk glass | 1200 | 10 hr | m: t-Nd•2Si, +: mo-Nd•2Si, +: indialite |

The extra high-$Nd_2O_3$ bulk glass-ceramics (MASN 10-12) were fairly well crystalline even after heat treatments at 1058°C (Table 6.4/d). The new, Mg-Nd-silicate phase was the major crystalline phase at low and medium crystallization temperatures. Although the major phase was usually accompanied by minor phases of monoclinic Nd-disilicate and indialite, the XRD analysis of the MASN-12 glass ceramic crystallized at 1058°C, provided a good XRD trace of the new phase (Fig.II.5 - Appendix II). The XRD data of the Mg-Nd-silicate phase are shown Table 6.5. Although the XRD reflections of the Mg-Nd-silicate phase were similar in the whole studied composition range (MASN 1-12), according to the SEM/EDS analysis results, its Mg-content varied with parent glass composition leading to $Mg_2Nd_8(SiO_4)_6O_2$ formula in the lower amount of $Nd_2O_3$ containing glass-ceramics and $Mg[]Nd_8(SiO_4)_6O$ in the $Nd_2O_3$-rich ones ([] indicates cation deficiency).

Higher temperature heat treatments resulted in the growth of monoclinic Nd-disilicate and indialite phases, and eventually led to the almost complete

disappearance of the Mg-Nd-silicate phase (Table 6.4/d). Considering its crystallization behaviour and temperature range of stability, the Mg-Nd-silicate phase is believed to be a metastable, intermediate phase, which crystallizes in larger amounts only in $Nd_2O_3$-rich glass compositions, and at higher temperatures recrystallizes into orthorhombic Nd-disilicate and indialite. The surface of a fully crystalline bulk glass-ceramic is shown in Fig.6.8/d.

**Table 6.4/d.** Crystallization of bulk Mg-Nd-aluminosilicate glasses (MASN 10-12)

| Sample type | Temp. of cryst. (°C) | Duration of cryst. | Crystalline phases detected by XRD (m: major, +: minor) |
|---|---|---|---|
| **MASN-10 glass** | | | |
| bulk glass | 1036 | 2 hr | no detectable crystallinity |
| bulk glass | 1172 | 2 hr | m: Mg-Nd-Si, +: t-Nd•2Si, +: mo-Nd•2Si, +: indialite |
| bulk glass | 1200 | 2 hr | m: Mg-Nd-Si, m: t-Nd•2Si, +: mo-Nd•2Si, +: indialite |
| bulk glass | 1200 | 10 hr | m: mo-Nd•2Si, +: indialite, +: t-Nd•2Si |
| **MASN-11 glass** | | | |
| bulk glass | 1013 | 2 hr | no detectable crystallinity |
| bulk glass | 1157 | 2 hr | m: Mg-Nd-Si, +: t-Nd•2Si, +: mo-Nd•2Si, +: indialite |
| bulk glass | 1200 | 2 hr | m: Mg-Nd-Si, +: t-Nd•2Si, +: mo-Nd•2Si, +: indialite |
| bulk glass | 1200 | 10 hr | m: mo-Nd•2Si, +: t-Nd•2Si, +: Mg-Nd-Si, +: indialite |
| **MASN-12 glass** | | | |
| bulk glass | 1000 | 2 hr | no detectable crystallinity |
| bulk glass | 1058 | 2 hr | m: Mg-Nd-Si |
| bulk glass | 1158 | 2 hr | m: Mg-Nd-Si, +: indialite, +: mo-Nd•2Si |
| bulk glass | 1200 | 2 hr | m: Mg-Nd-Si, +: mo-Nd•2Si, +: indialite |
| bulk glass | 1200 | 10 hr | m: mo-Nd•2Si, +: indialite, +: Mg-Nd-Si |

The bulk glass-ceramics of MASN 10-12 compositions were the only ones, which showed signs of bulk nucleation. A bulk nucleated area of a glass-ceramic specimen is shown in Fig.6.9/d. The fine crystal whiskers of Mg-Nd-silicate show radial orientation, and their morphology is similar to a recrystallized spherulitic structure. In spite of the generally dominating surface initiated crystallization mechanism, the high temperature crystallizations of bulk MASN glasses provided

fully or almost fully crystalline (except for the MASN-2&3), strong glass-ceramic bodies.

**Table 6.5.** X-ray Powder Diffraction data of the Mg-Nd-silicate phase

| d | Intensity | d | Intensity | d | Intensity |
|---|---|---|---|---|---|
| 5.283 | 28 | 3.096 | 46 | 2.084 | 19 |
| 4.835 | 20 | 3.064 | 13 | 2.004 | 24 |
| 4.568 | 11 | 2.955 | 100 | 1.964 | 9 |
| 4.347 | 5 | 2.798 | 11 | 1.924 | 9 |
| 3.990 | 21 | 2.666 | 42 | 1.870 | 13 |
| 3.770 | 5 | 2.634 | 27 | 1.833 | 13 |
| 3.573 | 32 | 2.558 | 8 | 1.78 | 19 |
| 3.431 | 16 | 2.357 | 7 | 1.74 | 10 |
| 3.385 | 13 | 2.285 | 12 | 1.631 | 10 |
| 3.278 | 13 | 2.194 | 10 | | |
| 3.182 | 40 | 2.125 | 13 | | |

### 6.4.2. Crystallization and microstructure of Mg-Nd-aluminosilicate glass-ceramic pellets

The MASN glass compositions can be divided into four categories according to the crystallization behaviour of glass powder pellets. The four groups are similar to those applied for bulk glass-ceramics, although some glass compositions were assigned to different groups. The low-$Nd_2O_3$ group this time covers the MASN 1-4 range (4.2-7.4mol% $Nd_2O_3$), the medium-$Nd_2O_3$ group consists of MASN 5-6 (8.6-10.0mol% $Nd_2O_3$), the high-$Nd_2O_3$ group covers the MASN 7-10 range (11.4-16.6mol% $Nd_2O_3$), whereas the most $Nd_2O_3$ rich group contains MASN 11-12 (18.7-21.0mol% $Nd_2O_3$).

The glass-ceramic pellets of the MASN 1-4 compositions were reasonably well crystallized even after the lowest temperature heat treatments. The major phase was indialite at all crystallization temperatures, and it was accompanied even at the lowest

temperatures by minor phases of monoclinic- and tetragonal Nd-disilicate, and Mg-Nd-silicate (Table 6.6/a).

**Table 6.6/a.** Crystallization of Mg-Nd-aluminosilicate glass powders (MASN 1-4)

| Sample type | Temp. of cryst. (°C) | Duration of cryst. | Crystalline phases detected by XRD (m: major, +: minor) |
|---|---|---|---|
| **MASN-1 glass** | | | |
| powder pellet | 1070 | 30 min | m: indialite, +: t-Nd•2Si, +: mo-Nd•2Si, +: Mg-Nd-Si |
| powder pellet | 1075 | 10 min | m: indialite, +: t-Nd•2Si, +: mo-Nd•2Si, +: Mg-Nd-Si |
| powder pellet | 1075 | 30 min | m: indialite, +: t-Nd•2Si, +: mo-Nd•2Si |
| powder pellet | 1100 | 2 hr | m: indialite, +: t-Nd•2Si, +: mo-Nd•2Si |
| powder pellet | 1120 | 30 min | m: indialite, +: t-Nd•2Si, +: Mg-Nd-Si |
| powder pellet | 1120 | 2 hr | m: indialite, +: t-Nd•2Si, +: Mg-Nd-Si |
| powder pellet | 1130 | 2 hr | m: indialite, +: t-Nd•2Si, +: Mg-Nd-Si |
| powder pellet | 1188 | 2 hr | m: indialite, +: t-Nd•2Si, +: Mg-Nd-Si |
| hot pressed | 1170 | 2 hr | m: indialite, +: t-Nd•2Si, +: mo-Nd•2Si |
| **MASN-2 glass** | | | |
| powder pellet | 1072 | 2 hr | m: indialite, +: t-Nd•2Si, +: mo-Nd•2Si, +: Mg-Nd-Si |
| powder pellet | 1100 | 2 hr | m: indialite, +: t-Nd•2Si |
| powder pellet | 1117 | 2 hr | m: indialite, +: t-Nd•2Si, +: mo-Nd•2Si |
| powder pellet | 1170 | 2 hr | m: indialite, +: t-Nd•2Si |
| powder pellet | 1200 | 2 hr | m: indialite, +: t-Nd•2Si |
| hot pressed | 1080 | 2 hr | m: indialite, +: t-Nd•2Si |
| **MASN-3 glass** | | | |
| powder pellet | 1060 | 2 hr | m: indialite, +: Mg-Nd-Si, +: mo-Nd•2Si, +: t-Nd•2Si |
| powder pellet | 1076 | 2 hr | m: indialite, +: mo-Nd•2Si, +: t-Nd•2Si, +: Mg-Nd-Si |
| powder pellet | 1100 | 2 hr | m: indialite, +: t-Nd•2Si, +: mo-Nd•2Si, +: Mg-Nd-Si |
| powder pellet | 1134 | 2 hr | m: indialite, +: t-Nd•2Si, +: mo-Nd•2Si, +: Mg-Nd-Si |
| powder pellet | 1170 | 2 hr | m: indialite, +: t-Nd•2Si, +: mo-Nd•2Si |
| powder pellet | 1180 | 2 hr | m: indialite, +: t-Nd•2Si |
| hot pressed | 1070 | 2 hr | m: indialite, +: t-Nd•2Si, +: mo-Nd•2Si |
| **MASN-4 glass** | | | |
| powder pellet | 1060 | 2 hr | m: indialite, +: Mg-Nd-Si, +: mo-Nd•2Si, +: t-Nd•2Si |
| powder pellet | 1075 | 2 hr | m: indialite, +: mo-Nd•2Si, +: Mg-Nd-Si, +: t-Nd•2Si |
| powder pellet | 1100 | 2 hr | m: indialite, +: mo-Nd•2Si, +: t-Nd•2Si, +: Mg-Nd-Si |
| powder pellet | 1143 | 2 hr | m: indialite, +: mo-Nd•2Si, +: t-Nd•2Si |
| powder pellet | 1170 | 2 hr | m: indialite, +: mo-Nd•2Si, +: t-Nd•2Si |
| powder pellet | 1200 | 2 hr | m: indialite, +: mo-Nd•2Si, +: t-Nd•2Si |
| hot pressed | 1060 | 2 hr | m: indialite, +: mo-Nd•2Si, +: t-Nd•2Si |

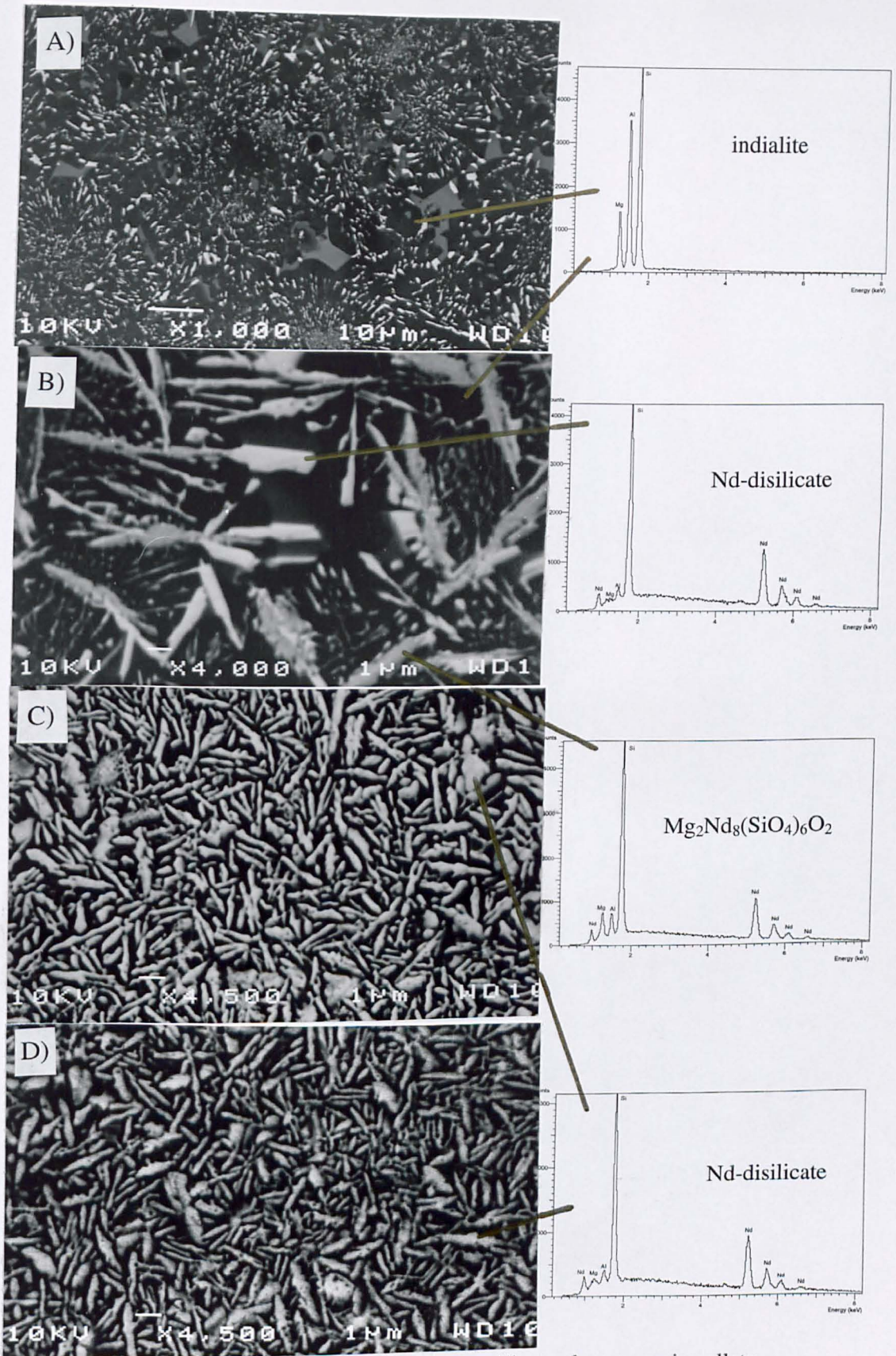


Fig.6.11/a-d. SEM micrographs of Mg-Nd-aluminosilicate glass-ceramic pellets, a) MASN-1, 1188°C/2hr; b) MASN-7, 1200°C/2hr; c) MASN-12, 1200°C/2hr; d) MASN-12, hot pressed, 1170°C/2hr.

As the heat treatment temperature increased an increase in the amount of the major phase of indialite, as well as in the amount of the tetragonal phase was observed. The general fine grained morphology of the high temperature sintered, MASN 1-4 glass-ceramic pellets is shown in Fig.6.11/a.

The XRD traces of the MASN 5-6 glass ceramic pellets suggest a considerable amount of residual glassy phase after the low temperature heat treatments. After the low temperature heat treatment the major phase was indialite, and minor phases of monoclinic Nd-disilicate, Mg-Nd-silicate and tetragonal Nd-disilicate were also present (Table 6.6/b). The amount of both Nd-disilicate modifications increased with increasing heat treatment temperature.

**Table 6.6/b.** Crystallization of Mg-Nd-aluminosilicate glass powders (MASN 5-6)

| Sample type | Temp. of cryst. (°C) | Duration of cryst. | Crystalline phases detected by XRD (m: major, +: minor) |
|---|---|---|---|
| **MASN-5 glass** | | | |
| powder pellet | 1060 | 2 hr | m: indialite, +: mo-Nd•2Si, +: Mg-Nd-Si, +: t-Nd•2Si |
| powder pellet | 1087 | 2 hr | m: indialite, +: mo-Nd•2Si, +: t-Nd•2Si, +: Mg-Nd-Si |
| powder pellet | 1100 | 2 hr | m: indialite, +: mo-Nd•2Si, +: t-Nd•2Si, +: Mg-Nd-Si |
| powder pellet | 1132 | 2 hr | m: indialite, +: mo-Nd•2Si, +: t-Nd•2Si, +: Mg-Nd-Si |
| powder pellet | 1170 | 2 hr | m: indialite, +: t-Nd•2Si, +: mo-Nd•2Si |
| powder pellet | 1200 | 2 hr | m: indialite, +: t-Nd•2Si, +: mo-Nd•2Si, +: Mg-Nd-Si |
| **MASN-6 glass** | | | |
| powder pellet | 1080 | 2 hr | m: indialite, +: mo-Nd•2Si, +: t-Nd•2Si, +: Mg-Nd-Si |
| powder pellet | 1100 | 2 hr | m: indialite, +: mo-Nd•2Si, +: t-Nd•2Si, +: Mg-Nd-Si |
| powder pellet | 1140 | 2 hr | m: indialite, +: mo-Nd•2Si, +: t-Nd•2Si, +: Mg-Nd-Si |
| powder pellet | 1170 | 2 hr | m: indialite, +: mo-Nd•2Si, +: t-Nd•2Si |
| powder pellet | 1200 | 2 hr | m: indialite, +: mo-Nd•2Si, +: t-Nd•2Si |

The MASN 7-10 glass-ceramic pellets showed a reasonable amount of crystallinity after the low temperature crystallizations resulting in a major phase of indialite, and minor phases of monoclinic- and tetragonal Nd-disilicate and Mg-Nd-silicate (Table 6.6/c).

**Table 6.6/c.** Crystallization of Mg-Nd-aluminosilicate glass powders (MASN 7-10)

| Sample type | Temp. of cryst. (°C) | Duration of cryst. | Crystalline phases detected by XRD (m: major, +: minor) |
|---|---|---|---|
| **MASN-7 glass** | | | |
| powder pellet | 1074 | 2 hr | m: indialite, +: mo-Nd•2Si, +: t-Nd•2Si, +: Mg-Nd-Si |
| powder pellet | 1102 | 2 hr | m: indialite, +: mo-Nd•2Si, +: t-Nd•2Si, +: Mg-Nd-Si |
| powder pellet | 1124 | 2 hr | m: indialite, m: mo-Nd•2Si, +: t-Nd•2Si, +: Mg-Nd-Si |
| powder pellet | 1173 | 2 hr | m: indialite, +: t-Nd•2Si, +: mo-Nd•2Si, +: Mg-Nd-Si |
| powder pellet | 1200 | 2 hr | m: indialite, +: t-Nd•2Si, +: mo-Nd•2Si, +: Mg-Nd-Si |
| powder pellet | 1200 | 10 hr | m: indialite, +: t-Nd•2Si, +: mo-Nd•2Si |
| hot pressed | 1070 | 2 hr | m: indialite, +: t-Nd•2Si, +: mo-Nd•2Si, +: Mg-Nd-Si |
| **MASN-8 glass** | | | |
| powder pellet | 1047 | 2 hr | m: indialite, +: mo-Nd•2Si, +: t-Nd•2Si, +: Mg-Nd-Si |
| powder pellet | 1096 | 2 hr | m: indialite, +: mo-Nd•2Si, +: t-Nd•2Si, +: Mg-Nd-Si |
| powder pellet | 1109 | 2 hr | m: indialite, +: t-Nd•2Si, +: mo-Nd•2Si |
| powder pellet | 1164 | 2 hr | m: indialite, +: t-Nd•2Si, +: mo-Nd•2Si |
| powder pellet | 1200 | 2 hr | m: indialite, m: t-Nd•2Si, +: mo-Nd•2Si |
| powder pellet | 1200 | 10 hr | m: t-Nd•2Si, m: indialite, +: mo-Nd•2Si |
| hot pressed | 1170 | 2 hr | m: t-Nd•2Si, m: indialite, +: mo-Nd•2Si, +: Mg-Nd-Si |
| **MASN-9 glass** | | | |
| powder pellet | 1030 | 2 hr. | m: mo-Nd•2Si, +: Mg-Nd-Si, +: t-Nd•2Si, +: indialite |
| powder pellet | 1064 | 2 hr. | m: mo-Nd•2Si, +: indialite, +: Mg-Nd-Si, +: t-Nd•2Si |
| powder pellet | 1107 | 2 hr. | m: mo-Nd•2Si, +: indialite, +: t-Nd•2Si, +: Mg-Nd-Si |
| powder pellet | 1177 | 2 hr. | m: t-Nd•2Si, m: indialite, +: mo-Nd•2Si, +: Mg-Nd-Si |
| powder pellet | 1200 | 2 hr. | m: t-Nd•2Si, m: indialite, +: mo-Nd•2Si, +: Mg-Nd-Si |
| powder pellet | 1200 | 10 hr. | m: t-Nd•2Si, m: indialite, +: mo-Nd•2Si |
| hot pressed | 1170 | 2 hr. | m: t-Nd•2Si, m: indialite, +: mo-Nd•2Si |
| **MASN-10 glass** | | | |
| powder pellet | 1008 | 2 hr. | m: Mg-Nd-Si, +: mo-Nd•2Si, +: t-Nd•2Si |
| powder pellet | 1036 | 2 hr. | m: Mg-Nd-Si, m: mo-Nd•2Si, +: t-Nd•2Si, +: indialite |
| powder pellet | 1105 | 2 hr. | m: indialite, m: mo-Nd•2Si, +: t-Nd•2Si, +: Mg-Nd-Si |
| powder pellet | 1172 | 2 hr. | m: t-Nd•2Si, m: mo-Nd•2Si, +: indialite |
| powder pellet | 1200 | 2 hr. | m: t-Nd•2Si, m: mo-Nd•2Si, +: indialite |
| powder pellet | 1200 | 10 hr. | m: t-Nd•2Si, m: mo-Nd•2Si, +: indialite |
| hot pressed | 1170 | 2 hr. | m: t-Nd•2Si, +: mo-Nd•2Si, +: indialite, +: Mg-Nd-Si |

Higher temperature heat treatments resulted in the increase of the tetragonal Nd-disilicate modification, at the expense of the monoclinic phase and Mg-Nd-silicate (Table 6.6/c). The microstructure of the glass-ceramic pellets in this group was slightly coarser (Fig.6.11/b), than the other glass compositions.

The MASN 11-12 glass-ceramic pellets showed an acceptable amount of crystallinity even after the low temperature heat treatments. According to the XRD analysis, the low temperature crystallized samples contained a major phase of monoclinic Nd-disilicate, and its tetragonal modification as minor phase (Table 6.6/d). The higher temperature heat treatments resulted in high degree of crystallinity, and growth of both Nd-disilicate modifications as well as the crystallization of indialite from the residual glassy phase. The glass-ceramic pellets of the MASN-12 composition were slightly different. The monoclinic Nd-disilicate was the dominant phase at all crystallization temperatures (Table 6.6/d). The only accompanying phase was a minor amount of indialite, which started to crystallize at relatively low temperatures. The high temperature crystallized specimens had a fine grained microstructure, as shown in Fig.6.11/c. The high temperature crystallizations of the glass powder pellets provided well-sintered, well crystallized, generally fine microstructure glass-ceramic bodies.

The hot pressed MASN glass-ceramics showed the same crystalline phases as their pressureless sintered derivatives (Table 6.6/a-d). They were well-sintered, had relatively low porosity, and generally showed fine grained crystalline structure (Fig.6.11/d). Although most of the hot pressed specimens appeared almost fully crystalline by SEM (Fig.6.11/d), their XRD traces, suggest the presence of a considerable amount of glassy residue. The amount of the residual glassy phase, as well as the amount of remaining porosity of the hot-pressed glass-ceramics can be

markedly reduced by optimizing the hot pressing temperature and pressure schedule for each composition, which would have a beneficial effect on the properties of these glass-ceramics.

**Table 6.6/d.** Crystallization of Mg-Nd-aluminosilicate glass powders (MASN 11-12)

| Sample type | Temp. of cryst. (C) | Duration of cryst. | Crystalline phases detected by XRD (m: major, +: minor) |
|---|---|---|---|
| **MASN-11 glass** | | | |
| powder pellet | 1000 | 2 hr. | m: mo-Nd•2Si, +: t-Nd•2Si, +: Mg-Nd-Si |
| powder pellet | 1013 | 2 hr. | m: mo-Nd•2Si, +: t-Nd•2Si |
| powder pellet | 1100 | 2 hr. | m: mo-Nd•2Si, +: t-Nd•2Si, +: indialite, +: Mg-Nd-Si |
| powder pellet | 1157 | 2 hr. | m: mo-Nd•2Si, +: t-Nd•2Si, +: indialite, +: Mg-Nd-Si |
| powder pellet | 1170 | 2 hr. | m: mo-Nd•2Si, +: t-Nd•2Si, +: indialite, +: Mg-Nd-Si |
| powder pellet | 1200 | 2 hr. | m: mo-Nd•2Si, +: t-Nd•2Si, +: indialite, +: Mg-Nd-Si |
| powder pellet | 1200 | 10 hr. | m: mo-Nd•2Si, m: t-Nd•2Si, +: indialite |
| hot pressed | 1170 | 2 hr. | m: t-Nd•2Si, m: mo-Nd•2Si, +: indialite |
| **MASN-12 glass** | | | |
| powder pellet | 980 | 2 hr. | just detectable: t-Nd•2Si, indialite |
| powder pellet | 1000 | 2 hr. | m: mo-Nd•2Si |
| powder pellet | 1058 | 2 hr. | m: mo-Nd•2Si, +: indialite |
| powder pellet | 1068 | 2 hr. | m: mo-Nd•2Si, +: indialite |
| powder pellet | 1158 | 2 hr. | m: mo-Nd•2Si, +: indialite |
| powder pellet | 1170 | 2 hr. | m: mo-Nd•2Si, +: indialite |
| powder pellet | 1200 | 2 hr. | m: mo-Nd•2Si, +: indialite |
| powder pellet | 1200 | 10 hr. | m: mo-Nd•2Si, +: indialite, +: t-Nd•2Si |
| hot pressed | 1170 | 2 hr. | m: t-Nd•2Si, +: mo-Nd•2Si, +: indialite |

### 6.5. Summary of the crystallization of Mg-Ln-aluminosilicate glasses

The rare-earth containing quaternary Mg-aluminosilicate glasses generally crystallized as pseudo-binary systems, similar to the Ca-Ln-aluminosilicate glasses. The primary phase in the aluminosilicate-rich compositions was indialite, and Nd-disilicate at the rare-earth-rich compositions (MASN series), whereas the two phases co-crystallized around the suspected eutectic region of the pseudobinary system (MASN 5-6). The crystallization of the primary phase was followed by the

crystallization of the relevant secondary phase at higher crystallization temperatures, creating diphasic glass-ceramic structures. Most of the bulk glasses studied crystallized by surface crystallization mechanism, but bulk nucleation was also observed in the $Nd_2O_3$-rich compositions. Regardless of the crystallization mechanism involved, both bulk glasses and powder pellets after high temperature crystallization resulted in strong, fully crystalline glass-ceramic bodies. The microstructure of the sintered pellets was fine grained, regardless of the parent glass composition. The bulk glass-ceramics were fine grained in the $Nd_2O_3$-rich compositions, whereas excessive growth of dendritic indialite crystals dominated the aluminosilicate-rich compositions (containing Y, La or Nd), which resulted in a coarser microstructure. Although at high temperatures the dendritic crystals showed secondary growth of their side branches accompanied by the crystallization of rare-earth disilicates, the dendritic microstructures were less susceptible towards recrystallization than the spherulitic structures observed in the Ca-Ln-aluminosilicate glass-ceramics (Chapter 5). In addition, a previously reported, but not fully characterized ternary Mg-Nd-silicate phase was detected, whose Mg-content was the function of the Mg-content of the parent glass.

## CHAPTER 7.

## THE PROPERTIES OF Nd CONTAINING Ca- AND Mg- ALUMINOSILICATE GLASS-CERAMICS

The direct crystallization of bulk glass specimens is not advisable, since only a few glass compositions showed a tendency to bulk nucleation, and although some work has been done with suitable candidates for nucleating agents (Chapter 5), the selection of a prospective one for each of the two major systems investigated, the optimising of its quantity and the heat treatment schedule, as well as the complete understanding of its effect on the crystallization sequence and behaviour, would have needed considerable extra time of study. Therefore pressure sintering of glass powder seemed to be a suitable method to get sizeable glass-ceramic specimens, since in this case surface nucleation is the dominating mechanism during crystallization. The processing route closely followed that used for ceramic fibre reinforced glass-ceramic matrix composites [138], aiming at a potential future application of high temperature structural materials. A small number of test bars was prepared from the hot pressed glass-ceramic plates (Chapter 3), and investigated in order to get information on their crystallization behaviour and microstructure (Chapter 5&6), as well as on some of their physical and mechanical properties, which in turn can give at least an indication on these materials' performance and can also suggest other potential application areas.

Glass-ceramics contain arbitrarily oriented fine crystals, which create a uniform crystalline structure, therefore their properties are normally isotropic [4,5]. The properties of glass-ceramics depend on the properties of the crystalline phases (which is determined by their chemical composition and crystalline structure) and that of the residual glassy phase (which is determined by its chemical composition), as well as

their relative amount. In addition, there are other important determining factors such as the microstructure (i.e. the size and morphology of crystals and the distribution of the glassy phase), and the interface between the crystals and the glassy residue. However, the glass-ceramic materials investigated in this study were prepared by pressure sintering, therefore the amount and distribution of the unwanted, but unavoidable residual porosity also has an influence on the density, mechanical strength, elastic modulus, and other important mechanical and physical properties of the sintered glass-ceramic.

## 7.1. Density

The density of a glass-ceramic material is an additive function of the densities of the crystalline phases present and the residual glassy phase (their contribution is weighted according to their volume fraction). Glass-ceramics generally have higher density than their parent glass and the density difference according to Strnad [5] is usually less than 3%. When comparing the measured density values of this study with the calculated crystallographic density values it should be noted that the measured density is a bulk density, which includes all lattice defects and the residual porosity of the pressure sintered glass-ceramic as well. The results presented are the average of at least 7 density measurements of glass-ceramic test bars and the standard deviations of the measurements were in the range $\pm 0.0017$-$0.0052 g/cm^3$.

a) The density of Ca-Nd-aluminosilicate glass-ceramics

The measured density values of Ca-Nd-aluminosilicate glass-ceramics as a function of the calculated Nd-oxyapatite ($Ca_2Nd_8Si_6O_{26}$) content (of their parent

glass composition) are shown in Fig.7.1. The density values showed a linear increase with increasing Nd-oxyapatite content. The increase is due to the increasing amount of neodymium which has a much higher atomic weight than the other components. The calculated crystallographic density values, presuming a fully crystalline, diphasic, anorthite - Nd-oxyapatite glass-ceramic, containing perfect crystals are also presented for comparison in Fig.7.1. The measured density values of the glass-ceramics were lower than the calculated ones, which is partly due to the residual porosity (Fig.7.5) of the glass-ceramic test bars, and partly the residual glassy phase (as was indicated by XRD). The density values of the hot-pressed Ca-Nd-aluminosilicate glass-ceramics are generally 0.02-0.03g/cm$^3$ larger than that of the parent glass of corresponding composition, except for the 40-50wt% Nd-oxyapatite containing compositions, where the differences are small and negative, which is also an indication of a relatively higher level of residual porosity.

b) The density of Mg-Nd-aluminosilicate glass-ceramics

The measured bulk density values of Mg-Nd-aluminosilicate glass-ceramics as a function of the Nd-disilicate ($Nd_2Si_2O_7$) content (of their parent glass composition) are shown in Fig.7.2. The density values showed an almost linear increase with increasing Nd-disilicate content, similar to the Ca-Nd-aluminosilicate glass-ceramics. The calculated crystallographic density of ideal indialite - Nd-disilicate (high temperature, monoclinic) glass-ceramics are also shown in Fig.7.2.

Fig.7.1. Density of Ca-Nd-aluminosilicate glass-ceramics

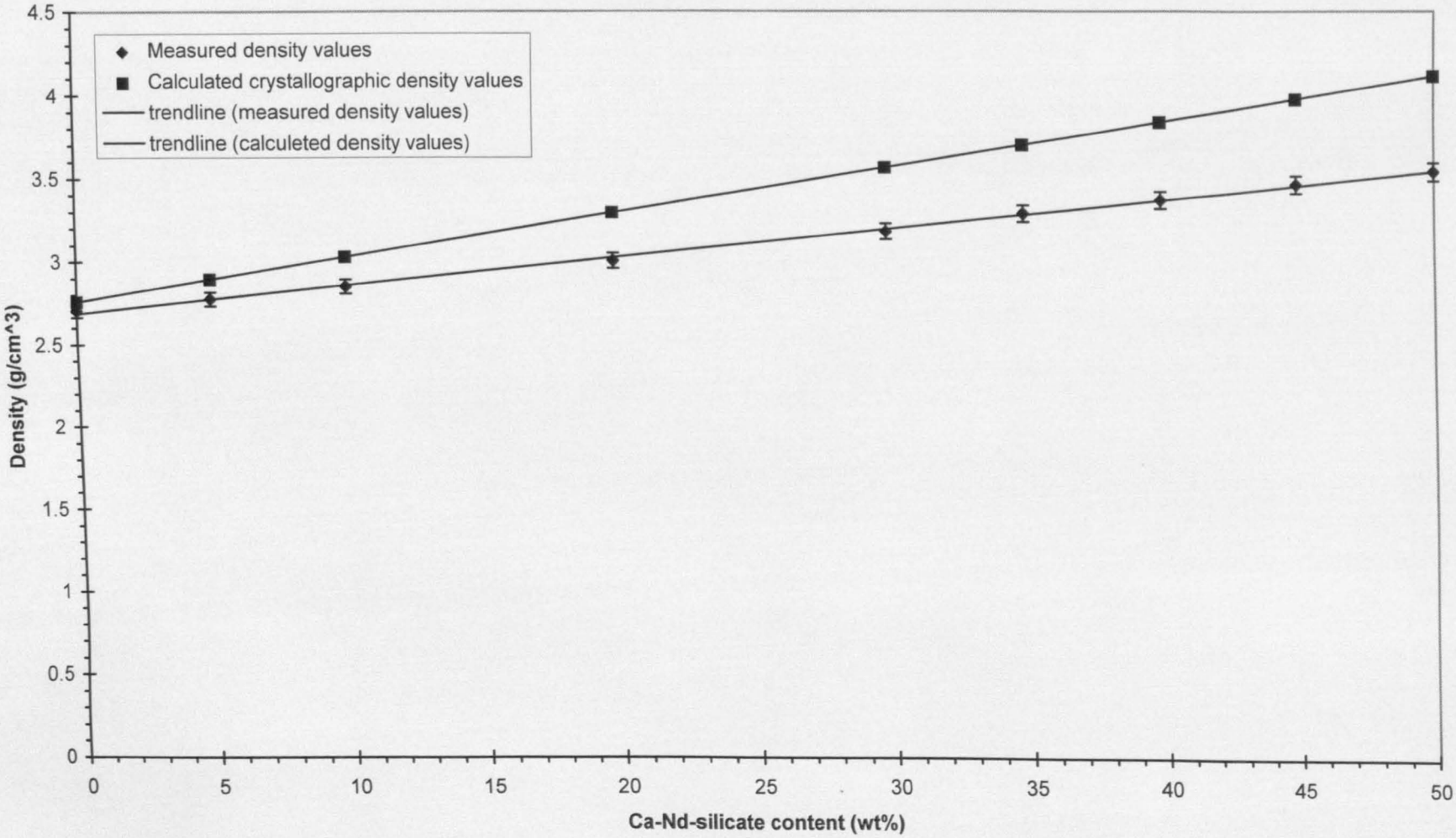

Fig.7.2. Density of Mg-Nd-aluminosilicate glass-ceramics

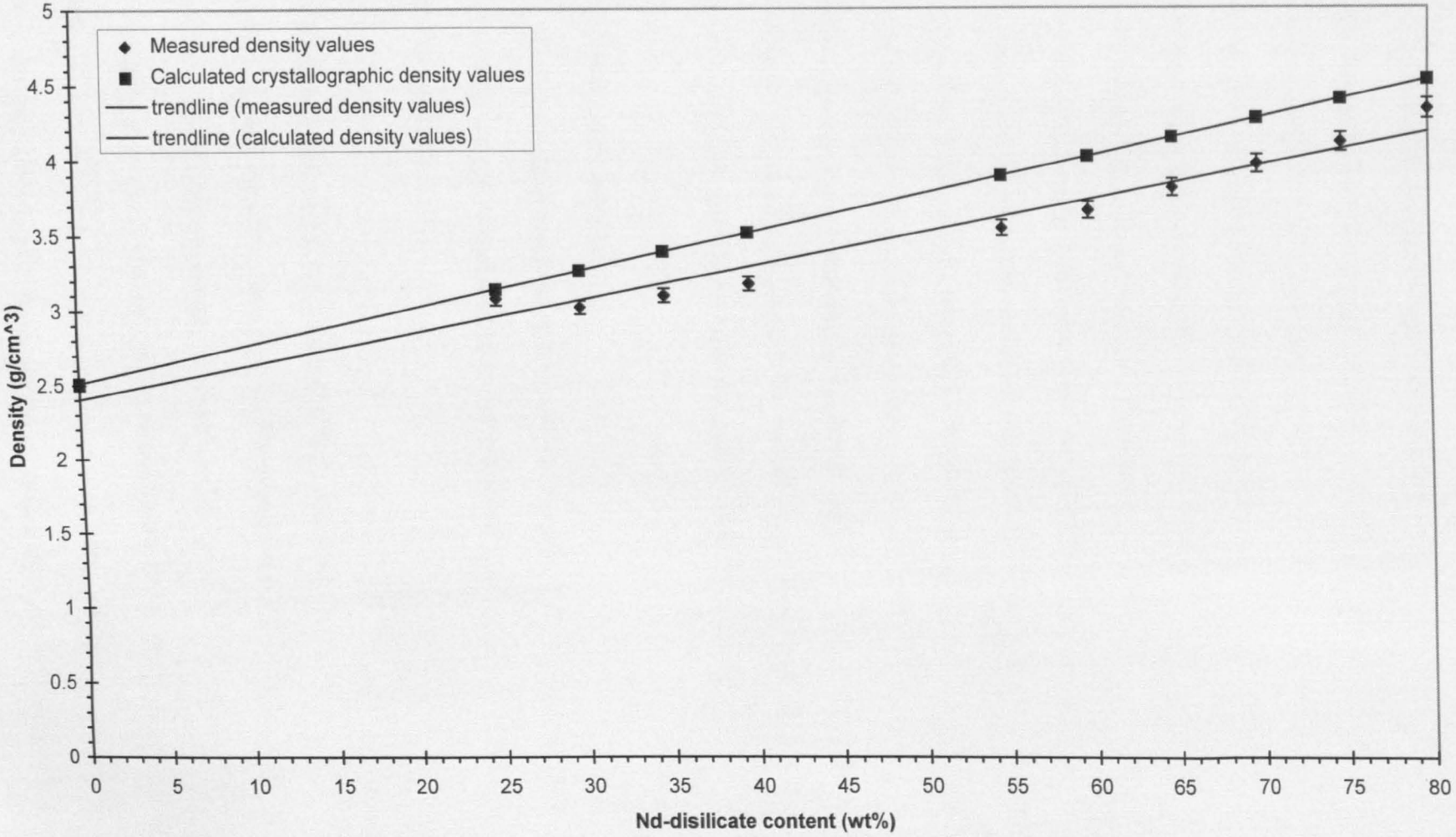

The measured bulk density values were generally lower than the calculated ones, which are due to fabrication porosity, residual glassy phase, and the co-existence of the minor phase of low temperature, tetragonal Nd-disilicate. Nevertheless, the calculated and measured density values were almost identical for the cordierite composition glass-ceramic and were close to each other in the case of the 25wt% Mg-Nd-silicate containing glass-ceramic. The latter can originate from the different raw material processing conditions, since that particular glass was milled in an alumina mill with alumina balls, which left fragmented alumina particles in the glass powder. When comparing the densities of Mg-Nd-silicate glass-ceramics to those of their parent glasses, they generally show a decrease of 0.05-0.09g/cm$^3$, except for the 25wt% Mg-Nd-silicate containing glass-ceramic which showed an increase of 0.1288g/cm$^3$. The reason can be partly the residual porosity, partly the fact that the indialite crystal has a lower density than the glass of cordierite composition.

## 7.2. Thermal expansion ($\alpha$)

The thermal expansion is roughly an additive property of the thermal expansion of crystalline and glassy phases present (their contribution is weighted according to their volume fraction).

a) The thermal expansion of Ca-Nd-aluminosilicate glass-ceramics

The thermal expansion values of Ca-Nd-aluminosilicate glass-ceramics as a function of Nd-oxyapatite content is shown in Fig.7.3. Two values of thermal expansion are presented for each composition: one for the 50°C-1200°C temperature range and another for the 100°C-1200°C temperature range. The thermal expansion values showed an increase with increasing Nd-oxyapatite content. The increase is due

to the increasing amount of the rare-earth containing crystalline phase, which has a higher thermal expansion than anorthite.

It is a difficult task to make comparison between the thermal expansion of glass-ceramics and their parent glasses since the temperature ranges of measurement were different (it was 50°C-800°C and 100°C-800°C for the glasses), but the general trend is that the Nd-oxyapatite glass-ceramics showed lower thermal expansion than their parent glasses.

b) The thermal expansion of Mg-Nd-aluminosilicate glass-ceramics

The thermal expansion values of Mg-Nd-aluminosilicate glass-ceramics as a function of Nd-disilicate content are shown in Fig.7.4. Similar to the Ca-Nd-aluminosilicate glass-ceramics, two values of thermal expansion are presented for each composition: one for the 50°C-1100°C temperature range and another for the 100°C-1100°C temperature range. The thermal expansion values showed an almost linear increase with increasing Nd-disilicate content above 40wt%. The trend of increasing thermal expansion is due to the increasing amount of Nd-disilicate crystalline phase, having markedly higher thermal expansion than that of the cordierite phase. The scattered results below 40wt% Nd-disilicate content are due to alumina contamination in the case of the 25wt% Nd-disilicate containing composition, as well as the different heat treatment schedule of the 30 & 35wt% Nd-disilicate containing composition (the crystallization temperatures were 1080°C and 1070°C, respectively, instead of the generally used 1170°C).

Fig.7.3. Thermal expansion of Ca-Nd-aluminosilicate glass-ceramics

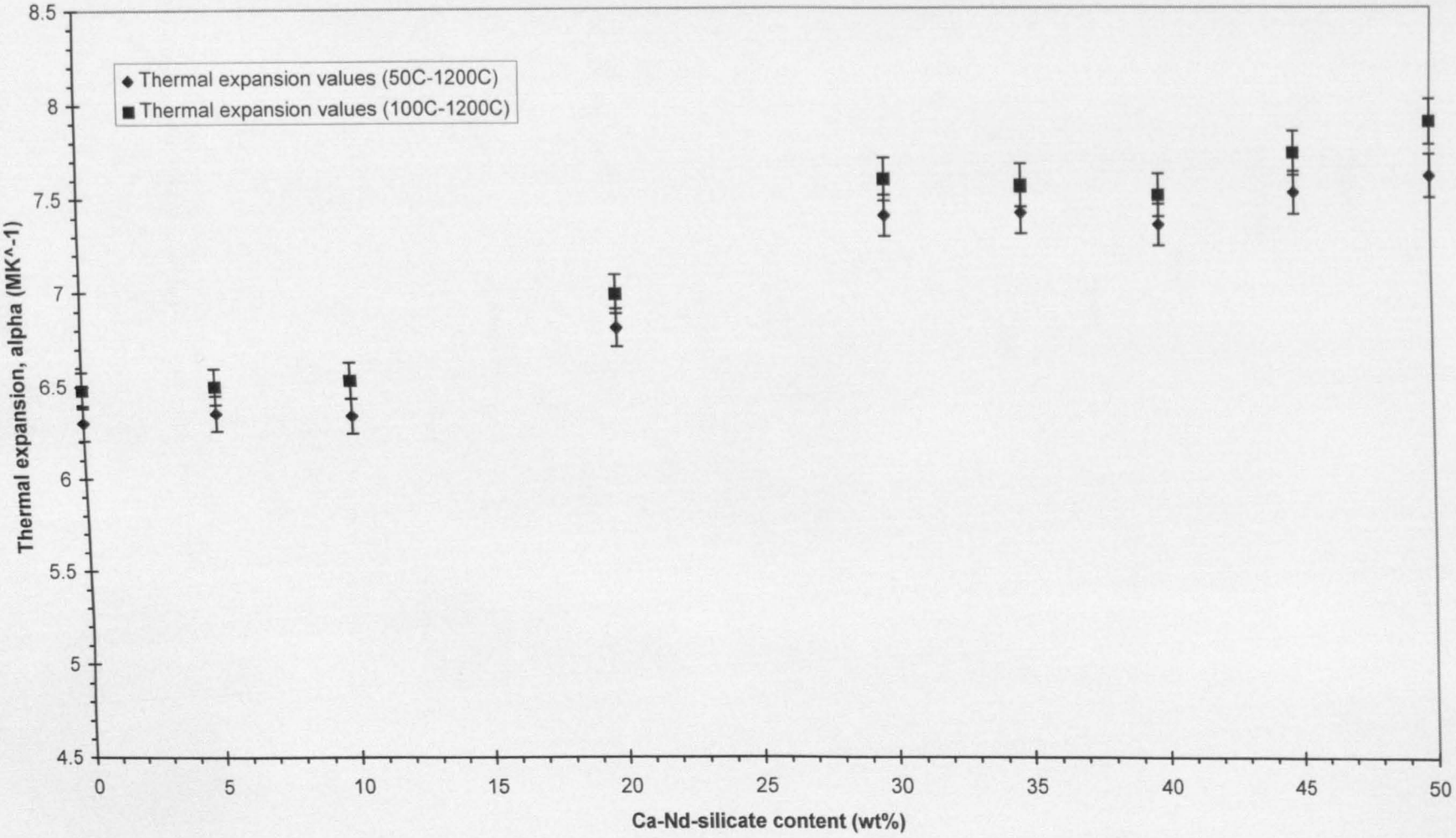

Fig.7.4. Thermal expansion of Mg-Nd-aluminosilicate glass-ceramics

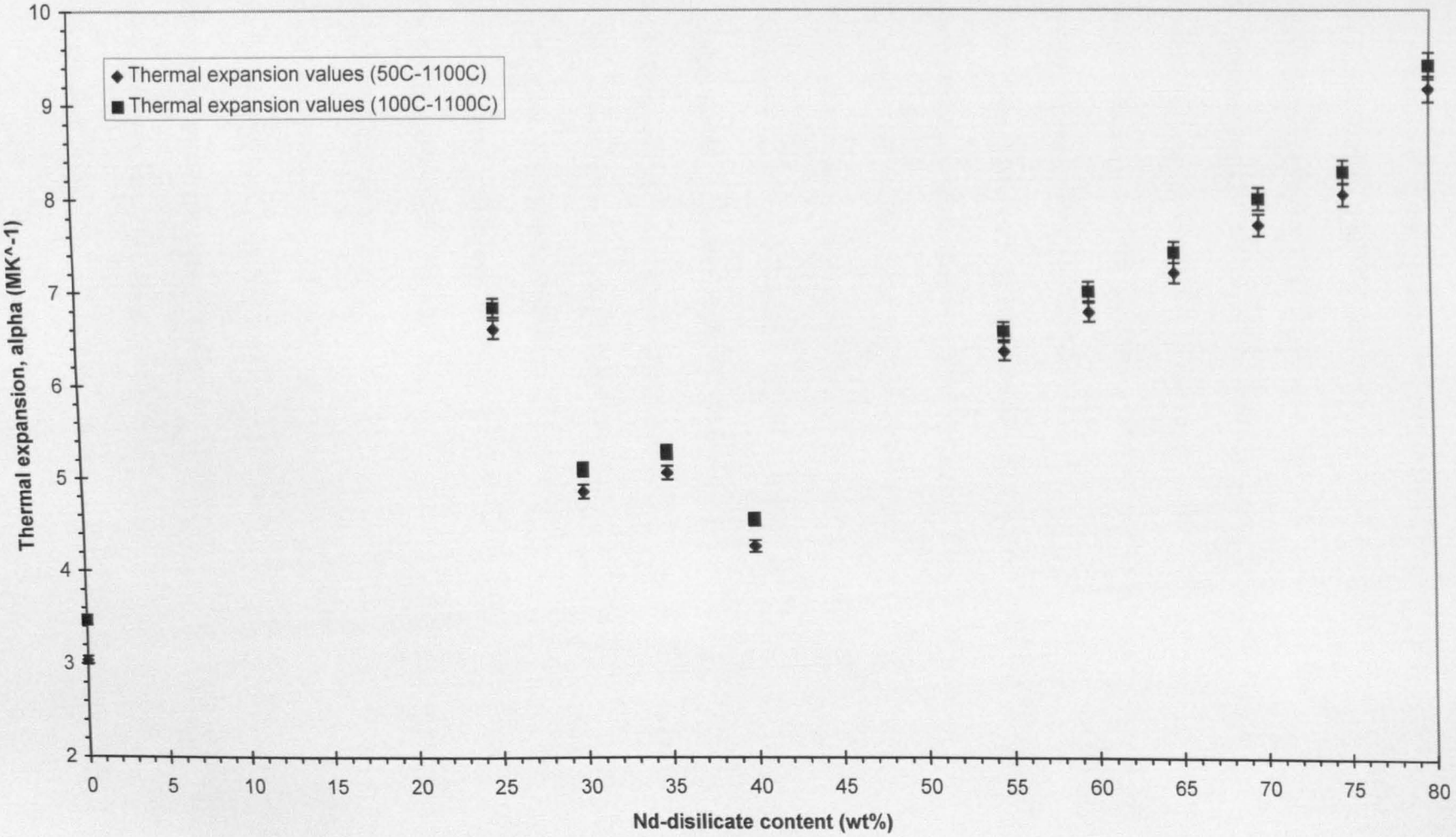

Comparing the thermal expansions of the glass-ceramics and those of their parent glasses, the former generally showed lower thermal expansion over a wider temperature range (it was 50°C-700°C and 100°C-700°C for the glasses), except for two compositions: the 25wt% Nd-disilicate containing one which showed a slight increase due to the previously described alumina contamination, and the 80wt% Nd-disilicate containing one, which showed a larger increase due to the appearance of a new crystalline phase ($Mg[]Nd_8(SiO_4)_6O$).

Due to the presence of the higher thermal expansion rare-earth silicate phase, the thermal expansions of the Ca-Nd-aluminosilicate glass-ceramics cover the $\alpha$=6.5-7.9 $MK^{-1}$ range, and those of the Mg-Nd-aluminosilicate glass-ceramics include the $\alpha$=5.1-9.4 $MK^{-1}$ range, whereas the thermal expansion of pure CAS and MAS glass-ceramics are around 4.5 $MK^{-1}$ and 2.6-3.4 $MK^{-1}$, respectively.

Refractoriness is another important thermal property of glass-ceramics, which mainly depends on the amount and chemical composition of the residual glassy phase. The upper temperatures in the temperature ranges of the presented thermal expansion values indicate the recommended highest temperatures of application of the glass-ceramics prepared in this study, since they have not shown any sign of softening up to those temperatures during the dilatometric experiments. It should be noted however, that it is valid for glass-ceramics processed by the given heat treatment temperature and pressure schedule and it almost certainly can be improved by optimising these parameters. The improved refractoriness of these glass-ceramics is due to the presence of rare-earth ions incorporated not only in the rare-earth containing crystalline phases, but in the structure of the residual glassy phase. The rare-earth ions create stronger bonds than the ordinary modifier cations and therefore result in

residual glass having high glass transition and softening temperatures, thus enhance the overall refractoriness of the glass-ceramics.

### 7.3. Hardness and fracture toughness

The hardness is an intrinsic property, which refers to the materials' resistance to plastic deformation. The hardness depends on the strength of the chemical bonds in the crystalline phases and glassy residue and on the microstructure (the size and morphology of crystals as well as the amount and distribution of glassy phase). In addition, the applied load of indentation also affects the measured hardness to some extent.

The mechanical strength and the fracture toughness of glass-ceramic materials depend on several factors: the heat treatment schedule (which determines the type and proportion of crystalline phases), the microstructure (fine grained, uniform microstructure of interlocking crystals enhances the strength, because propagating cracks can be diverted, slowed down or even stopped as they cross glassy and crystalline grain boundaries), the surface conditions (edge chipping and coarse surface finish reduce the strength), the interfacial bondstrength, the differences of the crystalline phases and the glassy residue in elastic modulus and thermal expansion (mismatch forms microstresses at the boundary of glassy and crystalline phases), as well as the specimen size.

A typical Vickers indent is shown in Fig.7.5. The SEM micrograph was made in backscattered electron mode with two quadrants of the solid-state annular detector switched in opposite polarity [324], which instead of the normal, composition selective image, gave a purely topographic, relief like appearance to the indent, as well as made the residual porosity highly visible. The picture of the same area using

normal backscattered electron mode is shown in Fig.7.6 for comparison. The presented hardness and indentation fracture toughness results are the average of 10 Vickers tests with each glass-ceramic composition.

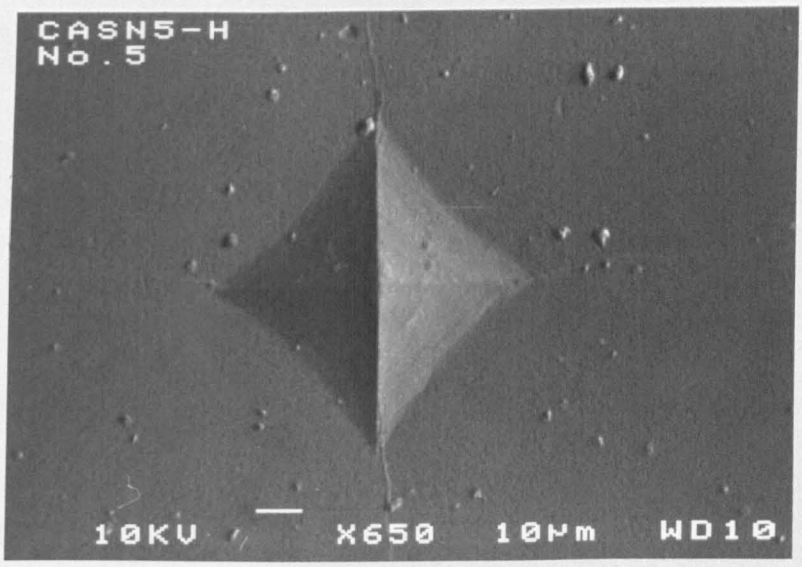


Fig.7.5. SEM micrograph of a Vickers indent on the surface of a hot pressed Ca-Nd-aluminosilicate glass-ceramic test bar; a modified backscattered electron image which made all surface impressions highly visible.

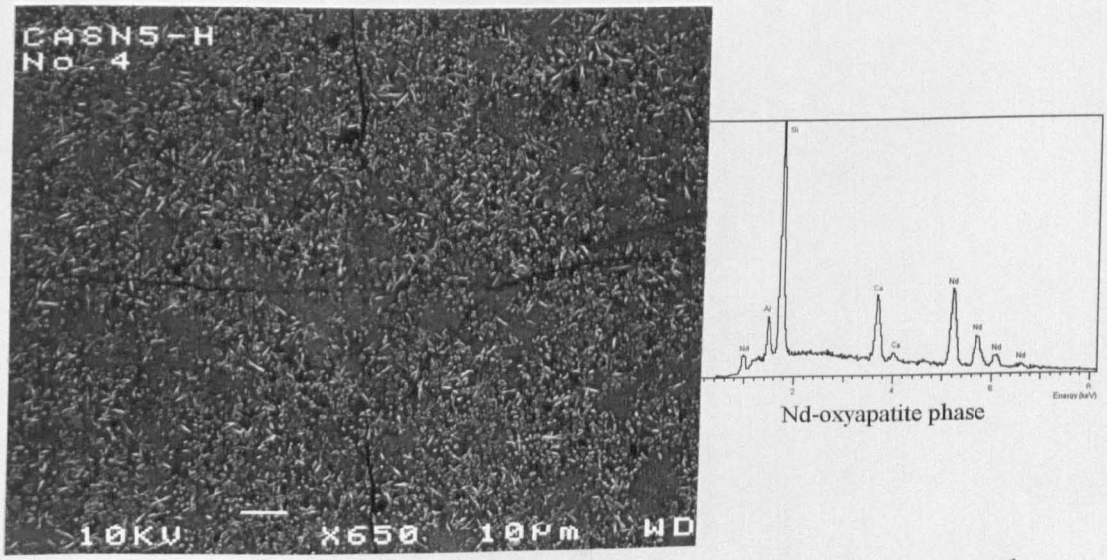


Fig.7.6. SEM micrograph of the Vickers indent shown in Fig.7.5., in normal backscattered electron mode.

In addition to the Vickers test, fracture toughness was also determined by the 4-point bend test. In order to make the best utilization of the small number of samples

available, indentation is applied to develop a controlled, dominant flaw on the carefully polished (Chapter 3) tensile surface of the test bars prior to a 4-point bend test. The presented results are the average of 12 measurements with each glass-ceramic.

a) The Vickers hardness and fracture toughness of Ca-Nd-aluminosilicate glass-ceramics

The Vickers hardness and indentation fracture toughness values of Ca-Nd-aluminosilicate glass-ceramics are shown in Fig.7.7. The Vickers hardness shows almost constant values and a slight increase in the case of the compositions of 40-50wt% Nd-oxyapatite content. The indentation fracture toughness showed nearly constant values at lower Ca-Nd-silicate contents and decreased at higher Nd-oxyapatite contents (>30%). The constancy of both hardness and fracture toughness at lower Nd-oxyapatite contents can be due the effect of residual glassy phase and porosity. The slight increase in hardness at Nd-oxyapatite rich compositions can be a result of an increased amount of Nd-oxyapatite crystals ($Ca_2Nd_8Si_6O_{26}$) in those glass-ceramics. Moreover, that particular crystalline phase is believed to bear the property of machinability due to having cleavage plane(s) in its apatite type crystal structure. When comparing the Vickers hardness values of Ca-Nd-aluminosilicate glass-ceramics and those of their parent glasses, little difference can be seen, except for the glass-ceramics of 40-50wt% Nd-oxyapatite content, which showed 0.38-0.96GPa increase. It also suggests a considerable amount of residual glassy phase at the glass-ceramics of lower Nd-oxyapatite content.

Fig.7.7. Vickers hardness and indentation fracture toughness of Ca-Nd-aluminosilicate glass-ceramics

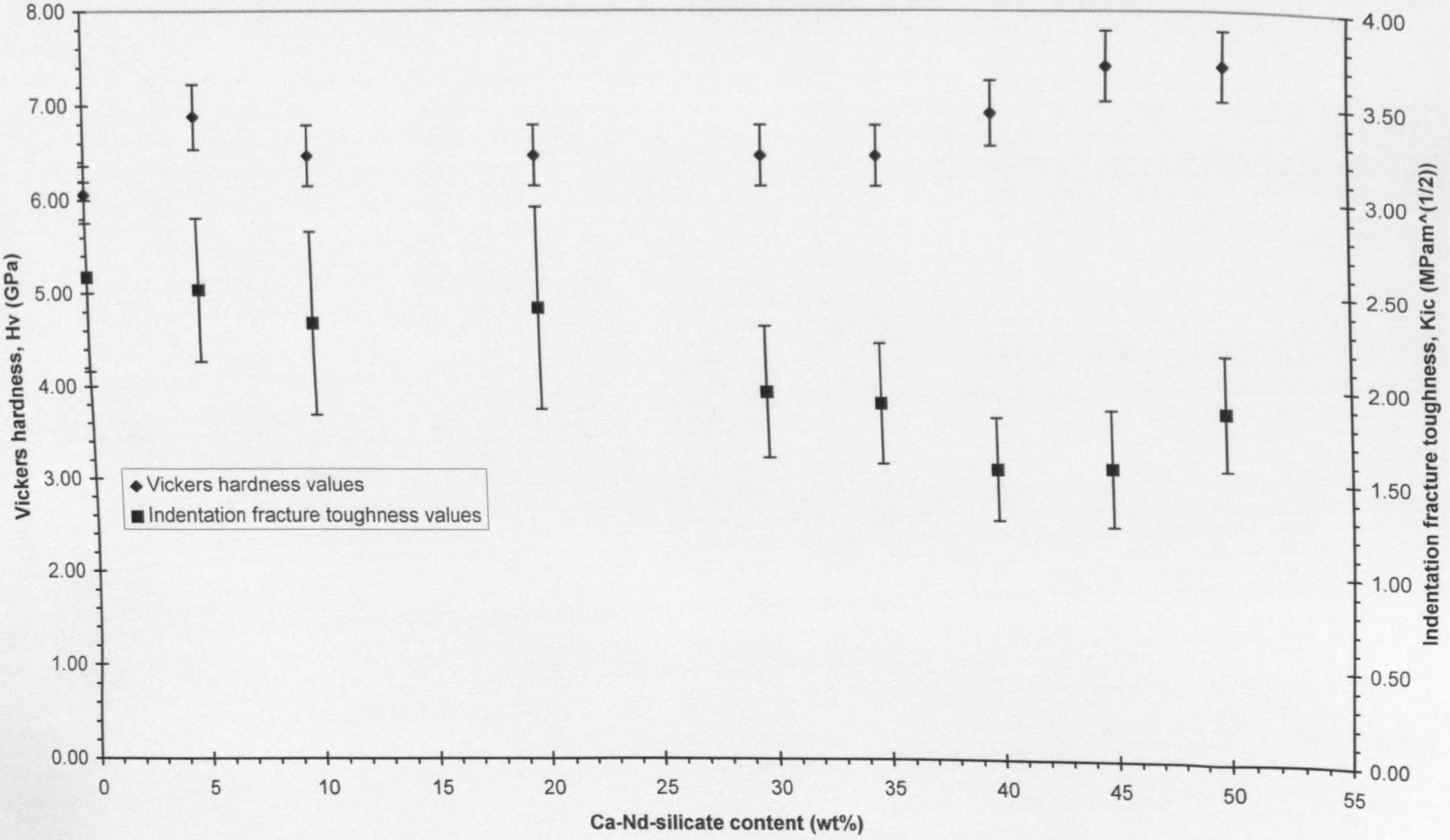

Fig.7.8. Fracture toughness of Ca-Nd-aluminosilicate glass-ceramics, measured by indent initiated four-point bend test

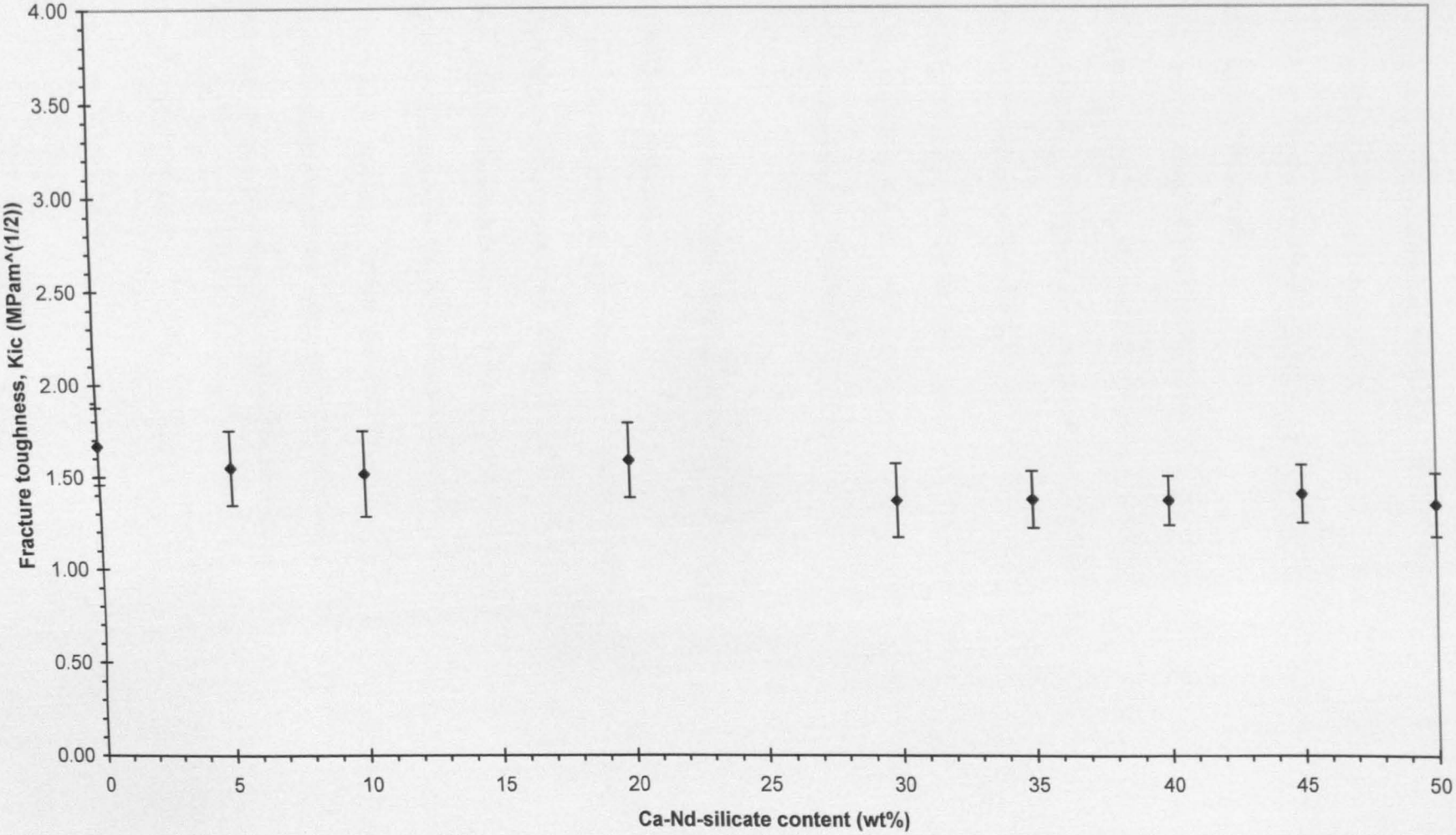

Nevertheless, the indentation fracture toughness values of the glass-ceramics showed a significant increase compared to their parent glasses (0.57-1.38MPam$^{(1/2)}$), which can be due to the crack diverting and crack propagation inhibiting effect of the numerous grain boundaries.

The fracture toughness of Ca-Nd-aluminosilicate glass-ceramics determined by 4-point bend test (Fig.7.8), showed two relatively constant values: a higher one at the low Nd-oxyapatite compositional range and a lower one at the higher amount (≤30wt%) of Nd-oxyapatite containing compositions. The reason for this tendency can be the influence on the fracture toughness of the relatively higher amount of anorthite crystal at the low Nd-oxyapatite compositions, and the relatively higher amount of machinable $Ca_2Nd_8Si_6O_{26}$ crystals at the high Nd-oxyapatite compositions.

b) The Vickers hardness and indentation fracture toughness of Mg-Nd-aluminosilicate glass-ceramics

The Vickers hardness and indentation fracture toughness values of Mg-Nd-aluminosilicate glass-ceramics are shown in Fig.7.9. The hardness values showed an almost constant value regardless of the Nd-disilicate content, except for the alumina particle contaminated 25wt% Nd-disilicate composition. The constant hardness level can be a result of glassy residue, and also the effect of the residual porosity. The indentation fracture toughness values were also fluctuating around a certain value, but showed a decreasing tendency at the highest Nd-disilicate concentrations.

Fig.7.9. Vickers hardness and indentation fracture toughness of Mg-Nd-aluminosilicate glass-ceramics

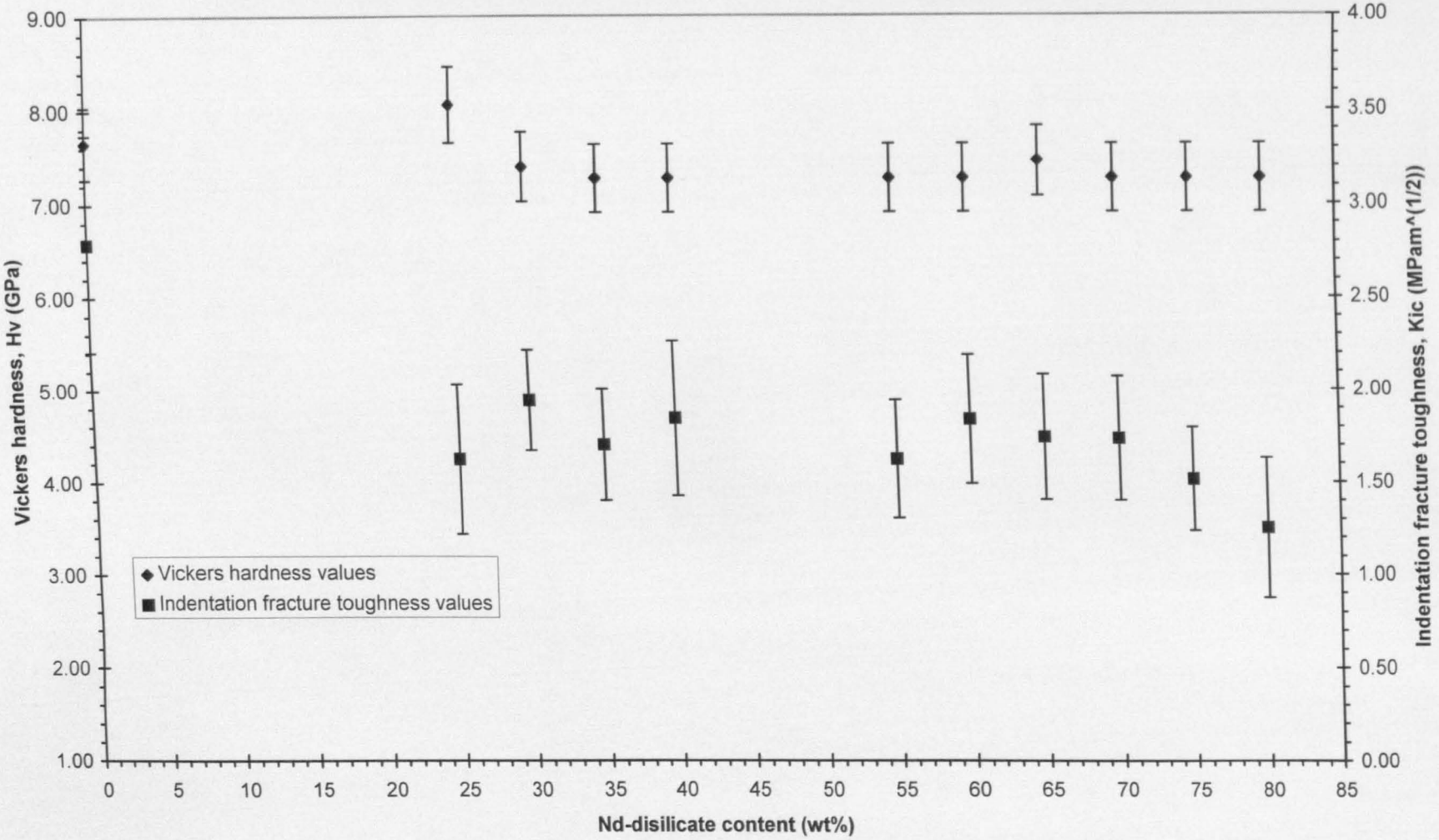

Fig.7.10. Fracture toughness of Mg-Nd-aluminosilicate glass-ceramics, measured by indent initiated four-point bend test

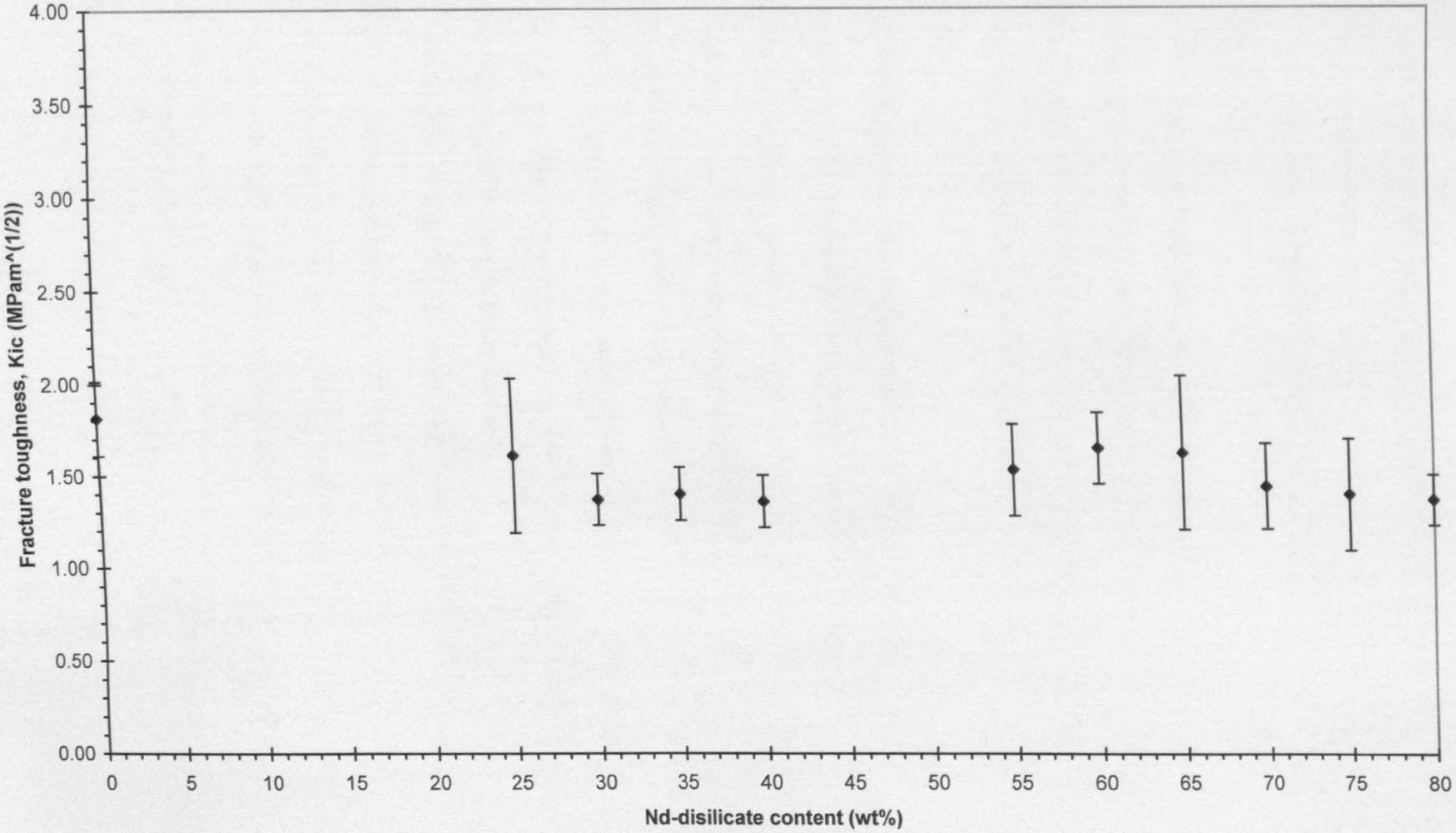

When comparing these results with those of the parent glasses, the glass-ceramics showed a general increase of 0.3-0.5GPa in hardness and a more significant 0.65-1.05MPam$^{(1/2)}$ increase in indentation fracture toughness due to the appearance of the crystalline phases.

The fracture toughness values of Mg-Nd-silicate glass-ceramics (determined by 4-point bend test; Fig.7.10), were more random, with a detectable decrease at the highest amount of (≤70wt%) Nd-disilicate containing compositions, which again can be explained by relatively high level of glassy residue.

## 7.5. Comparison with other ceramic and glass-ceramic materials

Until now only limited work has been done on the crystallization of rare-earth aluminosilicate glasses, therefore the data available on the properties of rare-earth aluminosilicate glass-ceramics are even more scarce. In order to be able to evaluate the properties of the glass-ceramics prepared in this study some physical and mechanical properties of a few aluminosilicate ceramics and glass-ceramics are summarized in Table 7.1 for comparison, with particular emphasis on *Macor*, a commercially available machinable glass-ceramic.

The density of both Ca-Nd-aluminosilicate and Mg-Nd-aluminosilicate glass-ceramics is in the medium range, and higher than the lithium and magnesium aluminosilicate glass-ceramics due to the high molar weight of the rare-earth elements in their structure. This restricts their applications as structural materials since there are areas where low density is an important selection criterion.

Table 7.1. Properties of some ceramic and glass-ceramic materials

| material | major crystalline phase | density (g/cm^3) | thermal expansion alpha (MK^-1) | Vickers hardness (GPa) | Youngs modulus (GPa) | indentation fracture toughness MPam^(1/2) | flexural strength (3 point bend) (MPa) | softening point (C) | source |
|---|---|---|---|---|---|---|---|---|---|
| Al2O3 hot pressed ceramic | corundum | 3.6-3.9 | 7.8 (20C-500C) | 19 | 406 | 3.5 (2.0N load) | 250-350 | | [6] [159] |
| Pyroceram 9606 (Mg-Al-Si glass-ceramic) | cordierite | 2.61 | 5.7 (20C-320C) | 8.4 | 120 | 2.5 (0.98N load) | 137-220 | 1350 | [5] [159] [16] |
| Pyroceram 9608 (Li-Al-Si glass-ceramic) | B-spodumen | 2.50 | 0.4-2.0 (20C-320C) | 5.76 (Knoop, 4.9N load) | | | 110-158 | 1250 | [5] |
| Macor (Corning, Code 9658) machinable glass-ceramic | fluorophologopite mica | 2.52 | 12.3 (25C-800C) | 2.45 | 64 | 2.0 (20.0N load) | | 1000 (max. working temperature) | [5] [254] [330] |
| Ca-Y-Al-Si machinable glass ceramic | Ca4Y6O(SiO4)6 | 3.24-3.1 | 5.3-5.7 (50C-350C) | 7.2-6.6 (1.96N load) | 106-100 | 0.98 | | 1550 (melting temp.) | [254] |
| La-silicate glass-ceramic | La2Si2O7 | | | 6.87 | | | | | [159] |
| Nd-Si-Al-O-N glass-ceramic | Nd3Si3Al3O12N2 | 3.44-4.65 | 5.0-7.3 | 9.3-15.4 | | | | | [240] |

The thermal expansion values of Ca-Nd-aluminosilicate and Mg-Nd-aluminosilicate glass-ceramics, due to the incorporation of the rare-earth containing crystalline phases, were in the medium- upper-medium range, and were higher than those of the aluminosilicate glass-ceramics, therefore closer to those of metals and higher thermal expansion ceramics. In addition, the thermal expansion of the developed glass-ceramics can be adjusted to the requirement of certain applications, by selecting suitable parent glass composition along the tie line in the glass forming region revealed in this study.

The obtainable ranges of thermal expansion suggest a potential application of ceramic-to-metal or ceramic-to-ceramic seals. The thermal expansions of the higher rare-earth containing Ca-Nd-aluminosilicate and Mg-Nd-aluminosilicate glass-ceramics are close to that of sintered alumina ($\alpha$ = 8.8 $MK^{-1}$ [18]), as well as to that of niobium ($\alpha$ = 7 $MK^{-1}$ [309]), therefore these glass-ceramics can be potentially used for joining niobium and alumina. For example, this kind of joining is used in high-pressure sodium lamps, where the currently used "sealing glass" is an Y-Ca-Sr-aluminate glass-ceramic material [325,326]. The heart of a high-pressure sodium lamp is the discharge tube, which is made of sintered polycrystalline alumina and closed at both ends by alumina end plugs. The sealing glass is used for sealing the plugs to the alumina tube, as well as to seal the niobium electric feedthrough into the plugs (Fig.7.11).

The requirements for a good sealing material are [327,328]:

1) high temperature structural stability & acceptable melting temperature (<1600°C),

2) relatively close match with the thermal expansion of both niobium and alumina,

3) good wetting of both niobium and alumina & good adhesion to them,

4) resistance to thermal shock during lamp-start and switch-off,

5) good chemical resistance against high temperature sodium & mercury vapours.

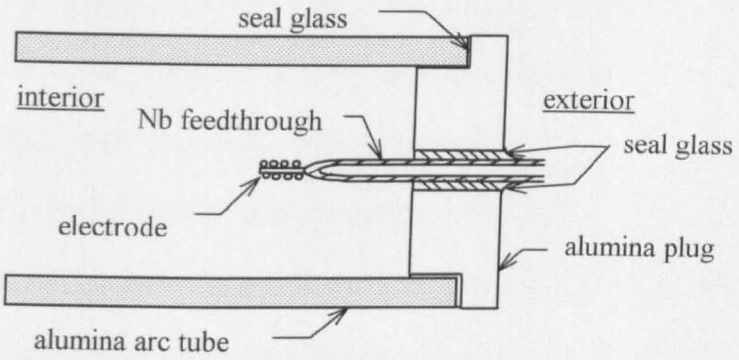


Fig.7.11. Schematic drawing of the longitudinal cross section of a high pressure sodium lamp arc tube [327].

The glass-ceramic materials developed during this work would provide good candidates for similar applications, since they fulfil most of the criteria: being stable at high temperature, melting below 1600°C, having thermal expansion in the desired range, bearing good chemical resistance against both acids and alkalis, and wetting alumina well (as demonstrated by the sintering experiments). Though, when considering this kind of application, the glass-ceramics behaviour against the aggressive vapours, as well as their wetting of, and adhesion to niobium will need to be checked. A similar kind of application exists in the recently developed ceramic metal-halide lamps [329], where the currently used sealing material is a dysprosium-aluminosilicate glass-ceramic. In this lamp the corrosive effect of halide vapours at the high operating temperature is even stronger than in the high-pressure sodium lamp, therefore good chemical resistance of the sealing glass-ceramic against the aggressive vapours is even more important. However, when considering lamp arc tube application, the La and Y containing modifications of the currently developed glass-ceramics would be preferred, because of their white colour.

The thermal expansion of Ca-Nd-aluminosilicate glass-ceramics was smaller than *Macor*, and slightly larger than that of the Ca-Y-aluminosilicate machinable glass-ceramic. Moreover, the potential upper temperature of use of Ca-Nd-aluminosilicate glass-ceramics (1200°C) is higher than that of the *Macor*.

The hardness of the Ca-Nd-aluminosilicate was in the medium range, smaller than that of the magnesium aluminosilicate glass-ceramic, but larger than that of the lithium-aluminosilicate ceramic and *Macor*, and were in the same range with the Ca-Y-aluminosilicate and La-silicate glass ceramics. The Mg-Nd-aluminosilicate glass ceramics were slightly harder and therefore their hardness was closer to that of the Mg-aluminosilicate glass-ceramics. The indentation fracture toughness of Ca-Nd-aluminosilicate and Mg-Nd-aluminosilicate glass-ceramics was smaller than that of the Mg-aluminosilicate glass-ceramic and was close to that of *Macor*, except for the low amount of Nd-oxyapatite containing compositions, which showed fracture toughness values close to that of the Mg-aluminosilicate glass-ceramics.

The Ca-Nd-aluminosilicate glass-ceramics if they are proven to be machinable, can provide an alternative machinable glass-ceramic to *Macor* with smaller thermal expansion, higher hardness and maximum temperature of application.

It should be noted, however, that the hot-pressed glass-ceramics prepared in this work still contained residual porosity and glassy phase and the amount of these residual phases can be reduced, therefore the properties of these glass-ceramics can be further improved by optimization of the heat treatment and pressure schedule.

## CHAPTER 8.

## SUMMARY, CONCLUSIONS, AND FUTURE WORK

Previously uncharacterized quaternary, rare-earth containing calcium- and magnesium aluminosilicate glasses were investigated in the current study. The glass compositions, selected on pseudo-binary tie-lines, were relatively good glass formers, provided low viscosity glass melts, and resulted in clear glasses after quenching, although the higher rare-earth containing compositions were susceptible to crystallization during cooling.

The highest amount of rare-earth oxide ($Nd_2O_3$) incorporated in CAS & MAS glasses was dependent on the amount of accompanying alkaline-earth oxide; the sum of the two types of oxide was a maximum ~25mol% (by normalizing the amount of alkaline-earth to 3+ cation charge), which is consistent with the highest amount of $Nd_2O_3$ in aluminosilicate glasses [252]. This fact suggests that $Nd^{3+}$ and presumably all the other applied rare-earths, occupy similar positions in the glass structure to $Mg^{2+}$ and $Ca^{2+}$, therefore they can be considered as modifier cations. Their beneficial effects on the properties of these glasses showed that rare-earths have to be considered separately from ordinary modifiers, due to their small ionic radius and high field strength.

The rare-earth containing Ca-, and Mg-aluminosilicate glasses have high density, high refractive index, high hardness, high glass transition and softening temperatures, as well as moderate thermal expansion, due to the incorporation of rare-earth oxides in the glass structure. Similar properties were previously reported for ternary rare-earth aluminosilicate glasses. Among the properties listed above, density, refractive index, and thermal expansion increased with increasing rare-earth content. In addition, the appearance of phase separation, which was reported in certain rare-earth

aluminosilicate glass systems, was not observed in the quaternary rare-earth containing glass compositions studied.

The quaternary glass-ceramic systems studied are generally crystallized as pure binary systems. The crystallization of rare-earth containing Mg-aluminosilicate glasses resulted in major phases of indialite (hexagonal cordierite) and $Ln_2Si_2O_7$ polymorphs. Crystallization of rare-earth containing Ca-aluminosilicate glasses resulted in major phases of $Ca_2Ln_8(SiO_4)_6O_2$ (oxyapatite) and anorthite, except for the Ca-Y-aluminosilicate system where the composition of the oxyapatite phase was $Ca_4Y_6(SiO_4)_6O$ and the two phases of anorthite and oxyapatite were accompanied by a third major phase of $Y_2Si_2O_7$. Although, a minor phase of $Ln_2Si_2O_7$ was also detected in the La and Nd containing CAS systems, the amount was markedly smaller. These results suggest that the parent glass compositions were selected in the La and Nd containing CAS systems on existing binary joins, whereas there is no pure binary between the anorthite and $Ca_4Y_6(SiO_4)_6O$ phases. In addition, the glass-ceramics prepared from the Ca-Ln-aluminosilicate glass compositions are presumed to be machinable, due to their $Ca_2Ln_8(SiO_4)_6O_2$ (or $Ca_4Y_6(SiO_4)_6$) content, although this property was not tested during this study.

The high temperature crystallized pelletized glass-ceramic specimens were generally fine-grained in the rare-earth containing Ca-, and Mg-aluminosilicate systems. The bulk specimens of Ln-CAS glasses also resulted in fine-grained glass-ceramics after high temperature heat treatments, due to recrystallization of the previously formed spherulitic crystals. The dendritic grains observed in bulk Ln-MAS glass-ceramics are not as susceptible to recrystallization at high temperatures, which resulted in coarse grained microstructures.

Most of the glasses studied are crystallized by a surface nucleation mechanism, except for some $Nd_2O_3$ rich glasses, which showed evidence of bulk nucleation as well. In order to study the effect of nucleating agents on the glasses developed, 10wt% $TiO_2$ was added to certain selected glass compositions. In the case of Nd-MAS glasses, $TiO_2$ additions resulted in uncontrolled phase separation, whereas in the Nd-CAS glasses it enhanced crystallization, and resulted in a finer grained fibrous microstructure, although direct bulk nucleation was not detected. In addition, two new Ti containing phases were detected, having the $(Ca,Nd)(Ti,Al)SiO_5$ composition. Moreover, a previously unreported crystalline phase was detected in the Ca-La-aluminosilicate glass-ceramics, with compositions between $CaLa_2Al_4Si_3O_{16}$ and $Ca_4La_6Al_8Si_{14}O_{53}$. Furthermore, the presence of the Mg-Nd-silicate phase was confirmed by EDS & XRD in Mg-Nd-aluminosilicate glass-ceramics, having composition of $Mg[]Nd_8(SiO_4)_6$ - $Mg_2Nd_8(SiO_4)_6$.

Glass-ceramic plates were prepared by hot pressing of glass powders, in order to allow a study of the properties of these newly developed glass-ceramics. They have fine-grained microstructure, although the amount of porosity and residual glassy phase could be further reduced by optimizing the pressure and heat treatment schedule. The glass-ceramics prepared have medium density, medium/upper medium ranged thermal expansion, and medium hardness, which are due to the presence of the rare-earth containing crystalline phases. The thermal expansion of the developed glass-ceramics can be tailored to the specific applications by choosing suitable parent glass composition on the pseudobinary tie-line, which after heat treatment, provides the phase ratio of the two major phases required to achieve the targeted average thermal expansion. The thermal expansion of the developed Ln-CAS glass-ceramics

cover the $\alpha$=6.5-7.9 $MK^{-1}$ range, whereas that of the Ln-MAS glass-ceramics include the $\alpha$=5.1-9.4 $MK^{-1}$ range.

The developed glasses, and glass-ceramics offers suitable candidates for high temperature structural applications in corrosive media. They can be utilized as glass-to-metal, ceramic-to-metal, and ceramic-to-ceramic seals, or as heat resistant, chemically durable coatings on metals. In addition, the Ca-Nd-aluminosilicate glass-ceramics if they are proven to be machinable, may provide an alternative machinable glass-ceramic to *Macor*, with smaller thermal expansion, higher hardness and higher maximum temperature of application.

Despite the amount of work done on these newly developed glasses and glass-ceramics, there are certain aspects of the current study, which can be investigated in more detail, and can be a theme of future research.

The investigation of new glass compositions in these quaternary systems, off the studied tie-lines, would reveal the complete glass-forming region in these systems. In addition, measurement of unstudied properties of the developed glasses, such as DC resistivity, dielectric properties, magneto-optical properties would reveal further potential application areas. Since the structure of rare-earth containing glasses is still not fully understood, application of sophisticated methods such as MAS-NMR and neutron scattering could provide valuable data on rare-earth co-ordination, and their local structure in the glass, which would lead to better understanding of their role in the glass structure.

On the glass-ceramic side, a widened survey may reveal valuable properties, leading to new prospective applications. In addition, full characterization of the previously unreported crystalline phases would be recommended. The preparation of glass-ceramics from bulk specimens of the developed glasses requires the selection of

suitable nucleating agents for both systems. $ZrO_2$ would be a potential candidate for this role, although application of a smaller amount of $TiO_2$ (less than 10wt%) in the Ln-MAS system can also be suggested. Furthermore, the developed glass-ceramic materials offer potential refractory matrices for ceramic fibre reinforced composites, with variable expansion coefficient and matrix fracture toughness.

## REFERENCES


1. J. King, "Materials science", *Graduate Scientist & Engineer*, **13** [6] pp.27-28 (1992)
2. J. C. Agrawal, "Process economics and strategies in the advanced ceramics industry", *Advanced Ceramic Materials*, **1** [4] pp.332-34 (1986)
3. V. Smith, B. Deckman & D. Brueck, "Advanced ceramics: Where do we go from here?", *Am. Ceram. Soc. Bull.*, **73** [12] pp.49-52 (1994)
4. P. W. McMillan, "Glass Ceramics", 2nd ed., Academic Press, London (1979)
5. Z. Strnad, "Glass Ceramic Materials", Glass Science and Technology, Vol.8, Elsevier, Oxford (1986)
6. G. Partridge, "An overview of glass ceramics. Part 1. Development and principal bulk applications", *Glass Technol.*, **35** [3] pp.116-26 (1994)
7. G. Partridge, "An overview of glass ceramics. Part 2. Joining, minor applications and the future", *Glass Technol.*, **35** [4] pp.171-82 (1994)
8. G. Yoldjian, "The use of rare-earths in ceramics", *J.Less-Comm. Metals*, **111** pp.17-22 (1985)
9. M. Z. A. Munshi & P. S. Nicholson, "Polycrystalline $H_3O^+$-yttrium silicate: Synthesis, characterization, and utilization in steam electrolysis cells", *Solid State Ionics*, **42** pp.47-52 (1990)
10. J. P. M. Van Vliet & G. Blasse, "Luminescence from $Pr^{3+}$ in barium lanthanum silicate oxyapatite", *Mat. Res. Bull.*, **25** pp.391-94 (1990)
11. W. J. Weber, "Radiation damage in a rare-earth silicate with the apatite structure", *J. Am. Ceram. Soc.*, **65** [11] pp.544-48 (1982)
12. M. H. O'Brien & M. Akinc, "Reduction in aluminium alloy attack on aluminosilicate refractories by addition of rare-earth oxides", *J. Am. Ceram. Soc.*, **73** [3] pp.491-95 (1990)
13. M. H. O'Brien & M. Akinc, "Role of ceria in enhancing the resistance of aluminosilicate refractories to attack by molten aluminum alloy", *J Am. Ceram. Soc.*, **72** [6] pp.896-904 (1989)
14. H. Hornberger & P. M. Marquis, "Mechanical properties and microstructure of *In-Ceram*, a ceramic-glass composite for dental crowns", *Glastechn. Ber. Glass Sci. Technol.*, **68** [6] pp.188-94 (1995)
15. W. Chengyu, T. Ying, Q. Youyuan & T. Nailing, "The manufacture and application of glass fertilizer containing rare-earth element", *Bol. Soc. Esp. Ceram. Vid.*, **31-C** Vol. 6, pp.541-46 (1992)
16. A. I. Berezhnoi, "Glass-Ceramics and Photo-Sitalls", Plenum Press, New York (1970)
17. M. H. Lewis, ed., "Glasses and Glass Ceramics", Chapman & Hall, London (1989)
18. W. D. Kingery, H. K. Bowen & D. R. Uhlmann, "Introduction to Ceramics", John Wiley & Sons, London (1976)
19. R. H. Doremus, "Glass Science", John Wiley & Sons, London (1973).
20. W. Vogel, "Structure and Crystallization of Glasses", Pergamon Press, Oxford (1971)
21. W. Vogel, "Chemistry of Glass", The American Ceramic Society, Columbus, Ohio (1985)
22. J. Hlavac, "The Technology of Glass and Ceramics", Glass Science and Technology Vol.4, Elsevier, Amsterdam (1983)
23. A. Paul, "Chemistry of Glasses", 2nd ed., Chapman & Hall, London (1990)

24. H. Scholze, "Glass, Nature, Structure, and Properties", Springer-Verlag, Berlin (1991)
25. J. J. Hammel, "Nucleation in glass - A review", pp.1-9 in L. L. Hench & S. W. Freiman, eds., *"Advances in Nucleation and Crystallization in Glasses"*, The American Ceramic Society, Columbus, Ohio (1971)
26. A. R. Cooper, "Crystal growth in network liquids by structure rearrangement", pp.123-30 in L. L. Hench & S. W. Freiman, eds., *"Advances in Nucleation and Crystallization in Glasses"*, The American Ceramic Society, Columbus, Ohio (1971)
27. D. R. Uhlmann, "Crystal growth in glass-forming systems - A review", pp.91-115 in L. L. Hench & S. W. Freiman, eds., *"Advances in Nucleation and Crystallization in Glasses"*, The American Ceramic Society, Columbus, Ohio (1971)
28. D. R. Uhlmann, "Nucleation and crystallization in glass forming systems", pp.1-20 in A. F. Wright & J. Dupuy, *"Glass ... Current Issues"*, Martinus Nijhoff Publ., Dordrecht (1985)
29. P. W. McMillan, "The crystallization of glasses", *J. Non-Cryst. Solids*, **52** pp.67-76 (1982)
30. G. H. Beall & D. A. Duke, "Glass ceramic technology", pp.403-45 in D. R. Uhlmann & N. J. Kreidl, eds., *"Glass Forming Systems"*, Glass Science and Technology Vol. 1, Academic Press, London (1983)
31. D. R. Bridge, D. Holland & P. W. McMillan, "Development of the alpha-cordierite phase in glass ceramics for use in electronic devices", *Glass Technol.*, **26** [6] pp.286-92 (1985)
32. S. H. Knickerbocker; A. H. Kumar & L. W. Herron, "Cordierite glass-ceramics for multilayer ceramic packaging", *Am. Ceram. Soc. Bull.*, **72** [1] pp.90-95 (1993)
33. B. Ryu & I. Yasui, "Sintering and crystallization behaviour of a glass powder and block with a composition of anorthite and the microstructure dependence of its thermal expansion", *J. Mater. Sci.*, **29** pp.3323-28 (1994)
34. M. H. Lewis, A. M. Daniel, A. Chamberlain, M. W. Pharaoh & M. G. Cain, "Microstructure-property relationship in silicate-matrix composites", *J. Microscopy*, **169** [2] pp.109-18 (1993)
35. A. Chamberlain, M. W. Pharaoh & M. H. Lewis, "Novel silicate matrices for fibre reinforced ceramics", *Ceram. Eng. Sci. Proc.*, **14** [9-10] pp.939-46 (1993)
36. I. Wandsworth & R. Stevens, "Strengthening and toughening of cordierite by the addition of silicon carbide whiskers, platelets and particles", *J. Mater. Sci.*, **26** pp.6800-8 (1991)
37. M. Y. Chen, J. M. Battison & T.-I. Mah, "Interface analysis of Si-C-O fibre/magnesium aluminosilicate matrix composites", *J. Mater. Sci.*, **24** pp.3213-20 (1989)
38. K. M. Prewo, J. J. Brennan & G. K. Layden, "Fiber reinforced glasses and glass-ceramics for high performance applications", *Am. Ceram. Soc. Bull.*, **65** [2] pp.305-22 (1986)
39. A. M. Daniel & M. H. Lewis, "Measurement of interfacial micromechanics in fibre reinforced ceramic matrix composites", *Ceram. Eng. Sci. Proc.*, **14** [7-8] pp.131-38 (1993)
40. M. H. Lewis & V. S. R. Murthy, "Microstructural characterization of interfaces in fibre reinforced ceramics", *Composite Sci. Technol.*, **42** pp.221-49 (1991)

41. K. P. Gadkaree, "Whisker reinforcement of glass-ceramics", *J. Mater. Sci.*, **26** pp.4845-54 (1991)
42. R. F. Cooper & K. Chyung, "Structure and chemistry of fibre-matrix interfaces in silicon carbide fibre-reinforced glass-ceramic composites: An electron microscopy study", *J. Mater. Sci.*, **22** pp.3148-60 (1987)
43. L. A. Bonney & R. F. Cooper, "Reaction layer interfaces in SiC-fiber-reinforced glass-ceramics: A high resolution Scanning Transmission Electron Microscopy analysis", *J. Am Ceram. Soc.*, **73** [10] pp.2916-21 (1990)
44. I. Wadsworth & R. Stevens, "The influence of whisker dimension on the mechanical properties of cordierite/SiC whisker composites", *J. Eur. Ceram. Soc.*, **9** pp.153-63 (1992)
45. G. Partridge & P. W. McMillan, "Strengthening of glass by surface crystallization", *Glass Technol.*, **15** [5] pp.127-33 (1974)
46. G. Partridge, "A review of surface crystallization in vitreous systems", *Glass Technol.*, **28** [1] pp.9-18 (1987)
47. P. F. James, "Review: Liquid phase separation in glass forming systems", *J. Mater. Sci.*, **10** pp.1802-25 (1975)
48. P. W. McMillan, "The constitution, microstructure and properties of glass-ceramics", pp.224-50 in L. L. Hench & S. W. Freiman, eds., *"Advances in Nucleation and Crystallization in Glasses"*, The American Ceramic Society, Columbus, Ohio (1971)
49. N. Kreidl, "Phase separation in glasses", *J. Non-Cryst. Solids*, **129** pp.1-11 (1991)
50. O. V. Mazurin & E. A. Porai-Koshits, "Phase Separation in Glass", North-Holland Publ., Oxford (1984)
51. P. F. James, "Volume nucleation in silicate glasses", pp.59-105 in M. H. Lewis, ed., *"Glasses and Glass-Ceramics"*, Chapman & Hall, London (1989)
52. J. E. Shelby, "Formation and properties of calcium aluminosilicate glasses", *J. Am. Ceram. Soc.*, **68** [3] pp.155-58 (1985)
53. G. Engelhardt, M. Nofz, K. Forkel, F. G. Wishmann, M. Mägi, A. Samonson & E. Lippmaa, "Structural studies of calcium aluminosilicate glasses by high resolution solid state $^{29}Si$ and $^{27}Al$ Magic Angle Spinning Nuclear Magnetic Resonance", *Phys. Chem. Glasses*, **26** [5] pp.157-65 (1985)
54. P. L. Higby, R. J. Ginther, I. D. Aggarwal & E. J. Friebele, "Glass formation and thermal properties of low-silica calcium aluminosilicate glasses", *J. Non-Cryst. Solids*, **126** pp.209-15 (1990)
55. R. C. C. Monteiro, F. P. Glasser & E. E. Lachowski, "Crystallization of CaO-$Al_2O_3$-$SiO_2$ and CaO-MO-$Al_2O_3$-$SiO_2$ (M=Mg, Zn) glasses", *J. Mater. Sci.*, **24** pp.2839-44 (1989)
56. R. C. C. Monteiro, F. I. F. Silva & M. R. A. Lima, "Effect of the addition of $TiO_2$ and $ZrO_2$ on the crystallization of calcium aluminosilicate glasses", *Bol. Soc. Esp. Ceram. Vid.*, **31-C** Vol.5. pp.89-94 (1992)
57. S. K. Chopra & C. A. Taneja, "Co-ordination state of aluminium ions in CaO-$Al_2O_3$-$SiO_2$ glasses", *J. Appl. Chem.*, **15** [4] pp.157-61 (1965)
58. C. I. Merzbacher, B. L. Sheriff, J. S. Hartman & W. B. White, "A high resolution $^{29}Si$ and $^{27}Al$ NMR study of alkaline earth aluminosilicate glasses", *J. Non-Cryst. Solids*, **124** pp.194-206 (1990)

59. B. Cote, D. Massiot, P. F. McMillan, B. Poe & J. P. Coutures, "$^{27}$Al NMR spectroscopy of $CaO$-$Al_2O_3$-$SiO_2$ melts and glasses", *Bol. Soc. Esp. Ceram. Vid.*, **31-C** Vol.3. pp.365-69 (1992)
60. C. Huang & E. C. Behrman, "Structure and properties of calcium aluminosilicate glasses", *J. Non-Cryst. Solids*, **128** pp.310-21 (1991)
61. P. McMillan, B. Piriou & A. Navrotsky, "A Raman spectroscopic study of glasses along the joins silica-calcium aluminate, silica-sodium aluminate and silica-potassium aluminate", *Geochim. Cosmochim. Acta*, **46** pp.2021-37 (1982)
62. R. K. Sato, P. F. McMillan, P. Dennison & R. Dupree, "A structural investigation of high alumina glasses in the $CaO$-$Al_2O_3$-$SiO_2$ system via Raman and Magic Angle Spinning Nuclear Magnetic Resonance Spectroscopy", *Phys. Chem. Glasses*, **32** [4] pp.149-56 (1991)
63. F. Siefert, B. O. Mysen & D. Virgo, "Three dimensional network structure of quenched melts (glass) in the systems $SiO_2$-$NaAlO_2$, $SiO_2$-$CaAl_2O_4$ and $SiO_2$-$MgAl_2O_4$", *Am. Miner.*, **67** pp.696-717 (1982)
64. D. A. Dutt, P. L. Higby & D. L. Griscom, "A structural model for low silica content calcium aluminosilicate glasses", *Phys. Chem. Glasses*, **33** [2] pp.51-55 (1992)
65. E. M. Lewin, C. R. Robbins & M. F. McMurdie, "Phase Diagram for Ceramists", The American Ceramic Society, Columbus, Ohio (1964)
66. R. Oestrike & R. J. Kirkpatrick, "$^{27}$Al and $^{29}$Si MASS NMR Spectroscopy of glasses in the system anorthite-diopside-forsterite", *Am. Miner.*, **73** [5-6] pp.534-46 (1988)
67. D. T. Griffen, "Silicate Crystal Chemistry", Oxford Univ. Press, Oxford (1992)
68. H. D. Megaw, "Notation on feldspar structures", *Acta Cryst.*, **9** pp.56-60 (1956)
69. C. J. E. Kempster, H. D. Megaw & E. W. Radoslovich, "The structure of anorthite, $CaAl_2Si_2O_8$, I. Structure analysis", *Acta Cryst.*, **15** pp.1005-117 (1962)
70. H. D. Megaw, C. J. E. Kempster & E. W. Radoslovich, "The structure of anorthite, $CaAl_2Si_2O_8$, II. Description and discussion", *Acta Cryst.*, **15** pp.1017-35 (1962)
71. J. E. Wainwright & J. Starkey, "A refinement of the structure of anorthite", *Z. Kristallogr.*, **133** pp.75-84 (1971)
72. G. L. Davis & O. F. Tuttle, "Two new crystalline phases of the anorthite composition, $CaO{\bullet}Al_2O_3{\bullet}SiO_2$", *Am. J. Sci.*, (Bowen Volume) p.107 (1952)
73. G. Donnay, "Hexagonal $CaAl_2Si_2O_8$", *Acta Cryst.*, **5** p.153 (1952)
74. Y. Takeuchi & G. Donnay, "The crystal structure of hexagonal $CaAl_2Si_2O_8$", *Acta Cryst.*, **12** pp.465-70 (1959)
75. R. A. Gdula, "Anorthite ceramic dielectrics", *Am. Ceram. Soc. Bull.*, **50** [6] pp.555-57 (1971)
76. R. Cioffi, P. Pernice, A. Aronne, A. Marotta & G. Quattroni, "Nucleation and crystal growth in a fly ash derived glass", *J. Mater. Sci.*, **28** pp.6591-94 (1993)
77. J. A. Topping, "Glass ceramics from the system $CaO$-$Al_2O_3$-$SiO_2$", *Am. Ceram. Soc. Bull.*, **56** pp.574-77 (1977)
78. I. A. Bondar & N. A. Toropov, "Establishment of phase separation in systems composed of fluorine containing slags and rare-earth silicates", pp.35-36 in E. A. Porai-Koshits, ed., *"Catalyzed Crystallization of Glass"*, Consultants Bureau, New York (1964)
79. R. G. Hill, C. Goat & D. Wood, "Thermal analysis of a $SiO_2$-$Al_2O_3$-$CaO$-$CaF_2$ glass", *J. Am. Ceram. Soc.*, **75** [4] pp.778-85 (1992)

80. W. Schreyer & J. F. Schairer, "Compositions and structural states of anhydrous Mg-cordierites: A re-investigation of the central part of the system $MgO-Al_2O_3-SiO_2$", *J. Petrology*, **2** [3] pp.324-406 (1961)
81. W. Schreyer & J. F. Schairer, "Metastable solid solutions with quartz type structures on the join $SiO_2MgAl_2O_4$", *Z. Kristallogr.*, **116** pp.60-82 (1961)
82. B. H. Mussler & M. W. Schafer, "Preparation and properties of mullite-cordierite composites", *Am. Ceram. Soc. Bull.*, **63** [5] pp.705-14 (1984)
83. P. F. McMillan & R. J. Kirkpatrick, "Al co-ordination in magnesium aluminosilicate glasses", *Am. Miner.*, **77** pp.898-900 (1992)
84. G. V. Gibbs, "The polymorphism of cordierite I.: The crystal structure of low cordierite", *Am. Miner.*, **51** pp.1068-87 (1966)
85. A. Miyashiro, T. Iiyama, M. Yamasaki & T. Miyashiro, "The polymorphism of cordierite and indialite", *Am. J. Sci.*, **253** pp.158-208 (1955)
86. A. Miyashiro, "Cordierite-indialite relations", *Am. J. Sci.*, **255** [1] pp.43-62 (1957)
87. T. Zoltai, "Classification of silicates and other minerals with tetragonal structures", *Am. Miner.*, **45** pp.960-73 (1960)
88. M. F. Hochella, Jr. & G. E. Brown, Jr., "Structural mechanisms of anomalous thermal expansion of cordierite-beryl and other framework silicates", *J. Am. Ceram. Soc.*, **69** [1] pp.13-18 (1986)
89. M. F. Hochella, G. E. Brown, F. K. Ross & G. V. Gibbs, "High temperature crystal chemistry of hydrous Mg- and Fe cordierites", *Am. Miner.*, **64** pp.337-51 (1979)
90. T. Armbruster & F. D. Bloss, "Orientation and effects of channel $H_2O$ and $CO_2$ in cordierite", *Am. Miner.*, **67** pp.284-91 (1982)
91. J. P. Cohen, F. K. Koss & G. V. Gibbs, "An X-ray and neutron diffraction study of hydrous low cordierite", *Am. Miner.*, **62** [1-2] pp.67-78 (1977)
92. R. D. Shannon, A. N. Mariano & G. R. Rossman, "Effect of $H_2O$ and $CO_2$ on dielectric properties of single-crystal cordierite and comparison with polycrystalline cordierite", *J. Am. Ceram. Soc.*, **75** [9] pp.2395-99 (1992)
93. D. S. Goldman, G. R. Rossman & W. A. Dollase, "Channel constituents in cordierite", *Am. Miner.*, **62** pp.1144-57 (1977)
94. E. P. Meagher & G. V. Gibbs, "The polymophism of cordierite: II. The crystal structure of indialite", *Can. Miner.*, **15** pp.43-49 (1977)
95. K. Langer & W. Schreyer, "Infrared and powder X-ray diffraction studies on the polymorphism of cordierite $Mg_2(Al_4Si_5O_{18})$", *Am. Miner.*, **54** [9-10] pp.1442-49 (1969)
96. A. Putnis, "Order modulated structures and the thermodynamics of cordierite reactions", *Nature*, **287** [11] pp.128-31 (1980)
97. A. Putnis & D. L. Bish, "The mechanism and kinetics of Al, Si ordering in Mg-cordierite", *Am. Miner.*, **68** [1] pp.60-65 (1983)
98. P. Daniels, "What is the true space group of high-cordierite?", *Z. Kristallogr.*, **190** pp.271-76 (1990)
99. T. Epicier, C. Esnouf, J. Guille & J. Werckman, "High resolution electron microscopy of α-cordierite (indialite)", *Mater. Lett.*, **11** [10-12] pp.389-95 (1991)
100. D. L. Evans, G. R. Fischer, J. E. Geiger & F. W. Martin, "Thermal expansions and chemical modifications of cordierite", *J. Am. Ceram. Soc.*, **63** [11-12] pp.629-34 (1980)

101. H. Ikawa, T. Otagiri, O. Imai, M. Suzuki, K. Urabe & S. Udagawa, "Crystal structures and mechanism of thermal expansion of high cordierite and its solid solutions", *J. Am. Ceram. Soc.*, **69** [6] pp.492-98 (1986)
102. P. Predecki, J. Haas, J. Faber, Jr. & R. L. Hitterman, "Structural aspects of the lattice thermal expansion of hexagonal cordierite", *J. Am. Ceram. Soc.*, **70** [3] pp.175-82 (1987)
103. W. Schreyer & J. F. Schairer, "Metastable osumilite- and petalite type phases in the system $MgO-Al_2O_3-SiO_2$", *Am. Miner.*, **47** [1-2] pp.90-104 (1962)
104. A. G. Gregory & T. J. Veasey, "Review: The crystallization of cordierite glass, Part 1.", *J. Mater. Sci.*, **6** pp.1312-21 (1971)
105. A. G. Gregory & T. J. Veasey, "Review: The crystallization of cordierite glass, Part 2.", *J. Mater. Sci.*, **7** pp.1327-41 (1972)
106. A. G. Gregory & T. J. Veasey, "Review: The crystallization of cordierite glass, Part 3.", *J. Mater. Sci.*, **8** pp.324-32 (1973)
107. A. G. Gregory & T. J. Veasey, "Review: The crystallization of cordierite glass, Part 4.", *J. Mater. Sci.*, **8** pp.333-39 (1973)
108. R. Roy, "Silica O, a new common form of silica", *Z. Kristallogr.*, **111** pp.185-89 (1959)
109. H. Schultz, G. M. Muchow, W. Hoffmann & G. Bayer, "X-ray study of Mg-Al silicate high quartz phases", *Z. Kristallogr.*, **133** pp.91-109 (1971)
110. H. Schultz, W. Hoffmann & G. M. Muchow, "The average structure of $Mg[Al_2Si_3O_{10}]$ a stuffed derivative of the high-quartz structure", *Z. Kristallogr.*, **134** pp.1-27 (1971)
111. G. A. Rankin & H. E. Mervin, "The ternary system $MgO-Al_2O_3-SiO_2$", *Am. J. Sci.*, 4th ser. **45** pp.301-25 (1918)
112. M. D. Karkhanavala & F. A. Hummel, "The polymorphism of cordierite", *J. Am. Ceram. Soc.*, **36** [12] pp.389-92 (1953)
113. A. Miyashiro, "Osumilite, a new silicate mineral and its crystal structure", *Am. Miner.*, **41** pp.104-16 (1956)
114. W. Winter, C. Bogdanow, G. Müller & W. Pannhorst, "Crystallization sequence of barium osumilite and MAS osumilite glass-ceramics with low thermal expansion", *Glastech. Ber. Glass Sci. Technol.*, **66** [5] pp.109-17 (1993)
115. W. Winter, A. Berger, G. Müller & W. Pannhorst, "Crystallization mechanism of MAS-osumilite with composition $Mg_2Al_4Si_{11}O_{30}$ from glass", *J. Am. Ceram. Soc.*, **76** [7] pp.1837-43 (1993)
116. S. B. Holmquist, "A note on a Mg-petalite phase", *Z. Kristallogr.*, **118** pp.477-78 (1963)
117. S. Reinsch, R. Müller & W. Pannhorst, "Active Nucleation sites at cordierite glass surfaces", *Glastech. Ber. Glass Sci. Technol.*, **67C** pp.432-35 (1994)
118. K. Heide, G. Völksch & C. Hanay, "Characterization of crystallization in cordierite glass by means of optical and electron microscopy", *Bol. Soc. Esp. Ceram. Vid.*, **31-C** Vol.5, pp.111-16 (1992)
119. N. D. Mora, E. C. Ziemath & E. D. Zanotto, "Heterogeneous crystallization in cordierite glasses", *Bol. Soc. Esp. Ceram. Vid.*, **31-C** Vol.5, pp.117-18 (1992)
120. R. Müller, D. Thamm & W. Pannhorst, "On the nature of nucleation sites at cordierite glass surfaces", *Bol. Soc. Esp. Ceram. Vid.*, **31-C** Vol.5, pp.105-10 (1992)

121. I. Szabó, W. Pannhorst & M. Rappensberger, "Investigation on the effect of surface treatment and annealing on the surface crystallization of the $MgO-Al_2O_3-SiO_2$ glass", *Bol. Soc. Esp. Ceram. Vid.*, **31-C** Vol.5, pp.119-24 (1992)
122. I. Szabó & M. Rappensberger, "Crystallization of μ-cordierite, Mg-osumilite and indialite in cordierite glass", *Glastech. Ber. Glass Sci. Technol.*, **67C** pp.137-42 (1994)
123. N. S. Yuritsin, V. M. Fokin, A. M. Kalinina & V. N. Filipovich, "Kinetics of nucleation on the surface of cordierite glass", *Bol. Soc. Esp. Ceram. Vid.*, **31-C** Vol.5. pp.21-26 (1992)
124. N. S. Yuritsin, V. M. Fokin, A. M. Kalinina & V. N. Filipovich, "Crystal nucleation and growth in the surface crystallization of cordierite glass", *Glass Physics and Chemistry* (Fizika i Khimiya Stekla), **20** [2] pp.116-24 (1994)
125. V. M. Fokin, N. S. Yuritsin, A. M. Kalinina, V. N. Filipovich & D. N. Filipova, "The temperature dependence of the μ-cordierite crystals nucleation rate on the polished surface of cordierite glass", *Glastech. Ber. Glass Sci. Technol.*, **67C** pp.392-95 (1994)
126. H. G. Wang, G. S. Fischman & H. Hermann, "Plasma-spayed cordierite: structure and transformations", *J. Mater. Sci.*, **24** pp.811-15 (1989)
127. R. Müller, "On the kinetics of sintering and crystallization of glass powders", *Glastech. Ber. Glass Sci. Technol.*, **67C** pp.93-98 (1994)
128. D. Holland & E. A. Logan, "Thermal expansion control in metal-cored glass-ceramic substrates", *Bol. Soc. Esp. Ceram. Vid.*, **31-C** Vol.4, pp.61-66 (1992)
129. Y. Hirose, H. Doi & O. Kamigaito, "Thermal expansion of hot pressed cordierite glass ceramics", *J. Mater. Sci. Lett.*, **3** pp.153-55 (1984)
130. T. Rudolph, D. V. Szabó & W. Pannhorst, "Microstructural development of a $P_2O_5$ modified glass-ceramic during sintering, Part 1. Microscopic characterization", *Glastech. Ber.*, **64** [8] pp.218-24 (1991)
131. T. Rudolph, K.-L. Weisskopf, W. Pannhorst & G. Petzow, "Microstructural development of a $P_2O_5$-modified cordierite glass ceramic during sintering, Part 2. Densification experiments", *Glastech. Ber.*, **64** [12] pp.305-9 (1991)
132. E. A. Giess, C. F. Guerci, G. F. Walker & S. H. Wen, "Isothermal sintering of spheroidized cordierite-type glass powders", *J. Am. Ceram. Soc.*, **68** [12] C-328-29 (1985)
133. H. E. Exner & E. A. Giess, "Anisotrophic shrinkage of cordierite type glass powder cylindrical compacts", *J. Mater. Res.*, **3** [1] pp.122-25 (1988)
134. E. A. Giess, J. P. Fletcher & L. W. Herron, "Isothermal sintering of cordierite-type glass powders", *J. Am. Ceram. Soc.*, **67** [8] pp.549-52 (1984)
135. K. Watanabe & E. A. Giess, "Coalescence and crystallization in powdered high-cordierite ($2MgO{\cdot}2Al_2O_3{\cdot}5SiO_2$) glass", *J. Am. Ceram. Soc.*, **68** [4] C-102-3 (1985)
136. K. Watanabe & E. A. Giess, "Crystallization kinetics of high-cordierite glass", *J. Non-Cryst. Solids*, **169** pp.306-10 (1994)
137. R. C. C. Monteiro, M. M. R. A. Lima & F. I. F. Silva, "Sintering and crystallization of cordierite glass powders", *Bol. Soc. Esp. Ceram. Vid.*, **31-C** Vol.2, pp.259-64 (1992)
138. A. Chamberlain, "Novel silicate matrix composites", Ph.D. Thesis, University of Warwick, Coventry (1995)
139. W. Zdaniewski, "Crystallization and structure of a $MgO-Al_2O_3-SiO_2-TiO_2$ glass-ceramic", *J. Mater. Sci.*, **8** pp.192-202 (1973)

140. W. Zdaniewski, "DTA and X-ray analysis study of nucleation and crystallization of $MgO-Al_2O_3-SiO_2$ glasses containing $ZrO_2$, $TiO_2$ and $CeO_2$", *J. Am. Ceram. Soc.*, **58** [5-6] pp.163-69 (1975)
141. W. A. Zdaniewski, "Microstructure and kinetics of crystallization of $MgO-Al_2O_3-SiO_2$ glass-ceramics", *J. Am. Ceram. Soc.*, **61** [5-6] pp.199-204 (1978)
142. S. M. Ohlberg, H. R. Golob & D. W. Strickler, "Crystal nucleation by glass in glass phase separation", pp.55-62 in M. K. Reser, ed., *"Symposium on Nucleation and Crystallization in Glasses and Melts"*, The American Ceramic Society, Columbus, Ohio (1962)
143. R. D. Maurer, "Crystallization of a titania-nucleated glass", pp.5-9 in M. K. Reser, ed., *"Symposium on Nucleation and Crystallization in Glasses and Melts"*, The American Ceramic Society, Columbus, Ohio (1962)
144. I. O. Owate & R. Freer, "The electrical properties of some cordierite glass ceramics in the system $MgO-Al_2O_3-SiO_2-TiO_2$", *J. Mater. Sci.*, **25** pp.5291-97 (1990)
145. E. M. Rabinovich, "Cordierite glass-ceramics produced by sintering", pp.327-33 in J. H. Simmons *et al.*, eds., *"Nucleation and crystallization in glasses"*, Advances is Ceramics Vol.4, The American Ceramic Society, Columbus, Ohio (1982)
146. A. F. Wright, A. N. Fitch, J. B. Hayter & B. E. F. Fender, "Nucleation and crystallization of cordierite-$TiO_2$ glass ceramic. Part 1. Small angle neutron scattering measurements and simulations", *Phys. Chem. Glasses*, **26** [4] pp.113-18 (1985)
147. W. Vogel & W. Höland, "Nucleation and crystallization kinetics of an $MgO-Al_2O_3-SiO_2$ base glass with various dopants", pp.125-45 in J. H. Simmons *et al.*, eds., *"Nucleation and crystallization in glasses"*, Advances is Ceramics Vol.4, The American Ceramic Society, Columbus, Ohio (1982)
148. R. C. De Vekey & A. J. Majumdar, "The effect of fabrication variables on the properties of cordierite based glass-ceramics, Part 1. The effect of variations in heat treatment", *Glass Technol.*, **14** [5] pp.125-34 (1973)
149. G. F. Neilson, "Nucleation and crystallization in $ZrO_2$-nucleated glass-ceramic systems", pp.73-82 in L. L. Hench & S. W. Freiman, eds., *"Advances in Nucleation and Crystallization in Glasses"*, The American Ceramic Society, Columbus, Ohio (1971)
150. G. F. Neilson, "Small angle X-ray scattering study of complex particle growth in an $MgO-Al_2O_3-ZrO_2-SiO_2$ glass", *J. App. Phys.*, **43** [9] pp.3728-35 (1972)
151. M. McCoy, W. E. Lee & A. H. Heuer, "Crystallization of $MgO-Al_2O_3-SiO_2-ZrO_2$ glasses", *J. Am. Ceram. Soc.*, **69** [3] pp.292-96 (1986)
152. M. A. McCoy & A. H. Heuer, "Microstructural characterization and fracture toughness of cordierite - $ZrO_2$ glass ceramics", *J. Am. Ceram. Soc.*, **71** [8] pp.673-77 (1988)
153. T. I. Barry, J. M. Cox & R. Morell, "Cordierite glass-ceramics - Effect of $TiO_2$ and $ZrO_2$ content on phase sequence during heat treatment", *J. Mater. Sci.*, **13** pp.594-610 (1978)
154. T. Dumas & J. Petiau, "EXAFS study of titanium and zinc environments during nucleation in a cordierite glass", *J. Non-Cryst. Solids*, **81** pp.201-20 (1986)
155. T. Rudolph, W. Pannhorst & G. Petzow, "Determination of activation energies for the crystallization of a cordierite type glass", *J. Non-Cryst. Solids*, **155** pp.273-81 (1993)

156. K. Watanabe, E. A. Giess & M. W. Shafer, "The crystallization mechanism of high cordierite glass", *J. Mater. Sci.*, **20** pp.508-15 (1985)
157. A. Katzschmann & P. Wange, "Crystallization behaviour of aluminosilicate glasses and glass ceramics with different content of MgO", *Glastech. Ber. Glass Sci. Technol.*, **67C** pp.412-15 (1994)
158. A. Katzschmann & P. Wange, "Processability, crystallization and mechanical strength of $P_2O_5$ modified glasses and glass-ceramics in the system $MgO$-$Al_2O_3$-$SiO_2$-$TiO_2$", *Glastech. Ber. Glass Sci. Technol.*, **68** [4] pp.111-16 (1995)
159. I. J. McColm, "Ceramic Hardness", Plenum Press, New York (1990)
160. C. J. Fairbanks, H. L. Lee & D. P. H. Hasselman, " Effect of crystallites on thermal shock resistance of cordierite glass-ceramics", *J. Am. Ceram. Soc.*, **67** [11] C-236-37 (1984)
161. I. M. Lachman, R. D. Bagley & R. M. Lewis, "Thermal expansion of extruded cordierite ceramics", *Am. Ceram. Soc. Bull.*, **60** [2] pp.202-5 (1981)
162. M. B. Volf, "Chemical Approach to Glass", Glass Science and Technology Vol.7, Elsevier, Oxford (1984)
163. H. Rawson, "Properties and Application of Glass", Glass Science and Technology Vol.3, Elsevier, Oxford (1980)
164. H.-D. Witzke, R. Takke, S. Thomas & W. Englisch, "Absorption and luminescence properties of Ce-/Ti-doped fused quartz", *Glastech. Ber. Glass Sci. Technol.*, **67C** pp.346-49 (1994)
165. A. T. Stanley, E. A. Harris, T. M. Searle & J. M. Parker, "Upconversion in neodymium doped fluoride glasses", *J. Non-Cryst. Solids*, **161** pp.235-40 (1993)
166. B. Jacquier, A. Remillieux, M. F. Joubert, P. Christensen & H. Poignant, "Upconversion and relaxation of high lying states in rare-earth-doped ZBLAN bulk and fibers", *J. Non-Cryst. Solids*, **161** pp.241-44 (1993)
167. C. X. Cardoso, Y. Messaddeq, L. A. O. Nunes & M. A. Aegerter, "Optical properties of pure $Nd^{3+}$-doped and $Pr^{3+}$-doped fluoroindate glasses", *J. Non-Cryst. Solids*, **161** pp.277-81 (1993)
168. E. Macho, R. Balda, M. J. Elejalde, J. Fernandez & J. L. Adam, "Luminescence thermal quenching of $Nd^{3+}$ doped fluoride BIGaZYTZr glass", *J. Non-Cryst. Solids*, **161** pp.245-48 (1993)
169. M. J. Weber, E. Hildum, S. Leung & R. Morgret, "Rare-earth Faraday rotator materials for lasers", *J. Less-Comm. Metals*, **93** pp.276-77 (1983)
170. M. R. Shahriari, T. Iqbal, P. Hajcak & G. H. Sigel, Jr., "The effect of rare-earth ions on the thermal stability of $AlF_3$-based glasses", *J. Non-Cryst. Solids*, **161** pp.77-80 (1993)
171. R. J. Mears, L. Reekie, S. B. Poole & D. N. Payne, "Neodymium-doped silica single mode fibre lasers", *Electr. Lett.*, **21** [17] pp.738-40 (1985)
172. S. B. Poole, D. N. Payne & M. E. Fermann, "Fabrication of low-loss optical fibres containing rare-earth ions", *Electr. Lett.*, **21** [17] pp.737-38 (1985)
173. F. Gan & Y. Chen, "Superfluorescence in Re-doped silica fiber", *Bol. Soc. Esp. Ceram. Vid.*, **31-C** Vol.4, pp.497-502 (1992)
174. V. McGahay & M. Tomozawa, "Phase separation in rare-earth doped $SiO_2$ glasses", *J. Non-Cryst. Solids*, **159** pp.246-52 (1993)
175. Y. Nageno, H. Takebe & K. Morinaga, "Correlation between radiative transition probabilities of $Nd^{3+}$ and composition in silicate, borate, and phosphate glasses", *J. Am. Ceram. Soc.*, **76** [12] pp.3081-86 (1993)

176. K. Arai, H. Namikawa, K. Kumata, T. Honda, Y. Ishii & T. Handa, "Aluminum or phosphorus co-doping effects on the fluorescence and structural properties of neodymium doped silica glass", *J. App. Phys.*, **59** [10] pp.3430-36 (1986)
177. S. G. Lunger, G. T. Petrovskii, A. G. Plukhin & Yu. K. Fedorov, "Nd laser glasses based upon several glass forming substances", *Bol. Soc. Esp. Ceram. Vid.*, **31-C** Vol.3. pp.475-80 (1992)
178. S. J. Gurman, R. J. Newport, M. Oversluizen & E. J. Tarbox, "An extended X-ray absorption fine structure of the rare-earth sites in a neodymium doped glass", *Phys. Chem. Glasses*, **33** [1] pp.30-32 (1992)
179. A. G. Clare, "Rare-earth in glasses for laser applications", *Key Eng. Mater.*, **94-95** pp.161-80 (1994)
180. K. H. Jack, "Review: SiAlONs and related nitrogen ceramics", *J. Mater. Sci.*, **11** pp.1135-58 (1976)
181. K. H. Jack, "SiAlONs and related nitrogen ceramics: Their crystal chemistry, phase relationship, properties and industrial potential", pp.204-21 in F. P. Glasser & P. E. Potter, eds., *"High temperature chemistry of inorganic and ceramic materials"*, The Chemical Society, London (1977)
182. N. Hirosaki, A. Okada & K. Matoba, "Sintering of $Si_3N_4$ with the addition of rare-earth oxides", *J. Am. Ceram. Soc.*, **71** [3] C-144-47 (1988)
183. S. Hampshire, M. Leigh, V. J. Morrissey, M. J. Pomeroy & B. Saruhan, "Crystallization heat treatments of silicon nitride ceramics and glass-ceramics containing neodymia", pp.432-42 in V. J. Tennery, ed., *"Ceramic Materials and Components for Engines"*, Proc. 3rd Int. Symp., Las Vegas, Nevada (1988)
184. F. F. Lange, "High temperature deformation and fracture phenomena of polyphase $Si_3N_4$ materials", pp.467-90 in F. L. Riley, ed., *"Progress in Nitrogen Ceramics"*, Martinus Nijhoff Publ., Boston (1983)
185. M. Redington, K. P. J. O'Reilly & S. Hampshire, "α' SiAlON ceramics containing mixed modifying cations", pp.127-38 in V. J. Tennery, ed., *"Ceramic Materials and Components for Engines"*, Proc. 3rd Int. Symp., Las Vegas, Nevada (1988)
186. M. Mimoto, "Fabrication and properties of SiAlON Ceramics", pp.197-205 in S. Saito, ed., *"Fine Ceramics"*, Elsevier, London (1988)
187. K. S. Mazdiyashi & C. M. Cooke, "Consolidation, microstructure and mechanical properties of $Si_3N_4$ doped with rare-earth oxides", *J. Am. Ceram. Soc.*, **57** [12] pp.536-37 (1974)
188. K. Komeya, "Fabrication and properties of silicon nitride ceramics", pp.175-88 in S. Saito, ed., *"Fine Ceramics"*, Elsevier, London (1988)
189. W. A. Sanders & D. M. Miekowski, "Strength and microstructure of sintered $Si_3N_4$ with rare-earth oxide additions", *Am. Ceram. Soc. Bull.*, **64** [2] pp.304-9 (1985)
190. E. Tani, S. Umebayashi, K. Kishi, K. Kobayashi & M. Nishijima, "Gas-pressure sintering of $Si_3N_4$ with concurrent addition of $Al_2O_3$ and 5wt% rare-earth oxide: High fracture toughness $Si_3N_4$ with fiber like structure", *Am. Ceram. Soc. Bull.*, **65** [9] pp.1311-15 (1986)
191. D. R. Clarke & G. Thomas, "Microstructure of $Y_2O_3$ fluxed hot-pressed silicon nitride", *J. Am. Ceram. Soc.*, **61** [3-4] pp.114-18 (1978)
192. J. Heinrich, E. Backer & M. Böhmer, "Hot isostatic pressing of $Si_3N_4$ powder compacts and reaction-bonded $Si_3N_4$", *J. Am. Ceram. Soc.*, **71** [1] C-28-31 (1988)

193. S. M. Wiederhorn & N. J. Tighe, "Structural reliability of yttria-doped hot-pressed silicon nitride at elevated temperatures", *J. Am. Ceram. Soc.*, **66** [12] pp.884-89 (1983)
194. T. Ekstrom, "Fabrication and properties of yttrium SiAlON ceramics", pp.605-10 in C. C. Sorrell & B. Ben-Nissan, eds., Proc. Int. Ceram. Conf. Austceram 88, Trans Tech Publ. (1988)
195. M. Peuckert, C. Boberski & P. Selgert, "Microstructure development of silicon nitride ceramics", pp.400-8 in V. J. Tennery, ed., *"Ceramic Materials and Components for Engines"*, Proc. 3rd Int. Symp., Las Vegas, Nevada (1988)
196. R. R. Wills, R. W. Stewart, J. A. Cunningham & J. M. Wimmer, "The silicon lanthanide oxynitrides", *J. Mater. Sci.*, **11** pp.749-59 (1976)
197. M. K. Cinibulk, G. Thomas & S. M. Johnson, "Fabrication and secondary-phase crystallization of rare-earth disilicate-silicon nitride ceramics", *J. Am. Ceram. Soc.*, **75** [8] pp.2037-43 (1992)
198. M. K. Cinibulk, G. Thomas & S. M. Johnson, "Oxidation behavior of rare-earth disilicate-silicon nitride ceramics", *J. Am. Ceram. Soc.*, **75** [8] pp.2044-49 (1992)
199. M. K. Cinibulk, G. Thomas & S. M. Johnson, "Strength and creep behaviour of rare-earth disilicate-silicon nitride ceramics", *J. Am. Ceram. Soc.*, **75** [8] pp.2050-55 (1992)
200. J. T. Smith & C. L. Quackenbush, "Phase effects in $Si_3N_4$ containing $Y_2O_3$ or $CeO_2$ I, Strength", *Am. Ceram. Soc. Bull.*, **59** [5] pp.529-32, 537 (1980)
201. C. L. Quackenbush & J. T. Smith, "Phase effects in $Si_3N_4$ containing $Y_2O_3$ or $CeO_2$: II. Oxidation", *Am. Ceram. Soc. Bull.*, **59** [5] pp.533-37 (1980)
202. G. N. Babini, A. Bellosi & P. Vincenzini, "Oxidation of silicon nitride hot pressed with ceria", J. Am. Ceram. Soc., 64 [10] pp.578-84 (1981)
203. F. F. Lange, "$Si_3N_4$-$CeO_2$-$SiO_2$ materials: Phase relations and strength", *Am. Ceram. Soc. Bull.*, **59** [2] pp.239-49 (1980)
204. M. Mimoto, F. Izumi, S. Moriuchi & Y. Matsui, "Phase relationship in the system $Si_3N_4$-$SiO_2$-$La_2O_3$", *J. Mater. Sci.*, **17** pp.2359-64 (1982)
205. D. M. Miekowski & W. A. Sanders, "Oxidation of silicon nitride sintered with rare-earth oxide additions", *J. Am. Ceram. Soc.*, **68** [7] C-160-63 (1985)
206. J. K. Patel & D. P. Thompson, "Further studies of the low-temperature oxidation problem in yttria densified silicon nitride ceramics", pp.987-96 in V. J. Tennery, ed., *"Ceramic Materials and Components for Engines"*, Proc. 3rd Int. Symp., Las Vegas, Nevada (1988)
207. M. H. Lewis, G. Leng-Ward & C. Jasper, "Sintering additive chemistry in controlling microstructure and properties of nitride ceramics", *Ceram. Trans.*, **1** pp.1019-33 (1988)
208. I. P. Tuersley, G. Leng-Ward & M. H. Lewis, "Silicon nitride-based ceramics for gas turbine applications", pp.856-70 in V. J. Tennery, ed., *"Ceramic Materials and Components for Engines"*, Proc. 3rd Int. Symp., Las Vegas, Nevada (1988)
209. R. K. Govila, "Strength characterization of yttria-doped sintered silicon nitride", *J. Mater. Sci.*, **20** pp.4345-53 (1985)
210. R. R. Wills, J. A. Cunningham, J. M. Wimmer & R. W. Stewart, "Stability of the silicon yttrium oxynitrides", *J. Am. Ceram. Soc.*, **69** [5-6] pp.269-70 (1976)
211. R. R. Wills, S. Holmquist, J. M. Wimmer & J. A. Cunningham, "Phase relationships in the system $Si_3N_4$-$Y_2O_3$-$SiO_2$", *J. Mater. Sci.*, **11** pp.1305-09 (1976)

212. F. F. Lange, S. C. Singhal & R. C. Kuznicki, "Phase relations and stability studies in the $Si_3N_4$-$SiO_2$-$Y_2O_3$ pseudoternary system", *J. Am. Ceram. Soc.*, **60** [5-6] pp.249-52 (1977)
213. G. N. Babini, A. Bellosi, P. Vincenzini, "Factors influencing structure evolution in the oxide of hot-pressed $Si_3N_4$-$Y_2O_3$-$SiO_2$ materials", *J. Mater. Sci.*, **19** pp.3487-97 (1984)
214. U. Ernstberger, G. Grathwohl & F. Thümmler, "High temperature durability and limits of sintered and hot-pressed silicon nitride materials", *Int. J. High Technol. Ceram.*, **3** pp.43-61 (1987)
215. C. H. Drummond III, "Glass formation and crystallization in high-temperature glass-ceramics and $Si_3N_4$", *J. Non-Cryst. Solids*, **123** pp.114-28 (1990)
216. M. H. Lewis, "Ceramics applications and limitations", pp.1-20 in *"Materials at their Limits"*, Institute of Metals, London (1986)
217. W. E. Lee, C. H. Drummond III, G. E. Hilmas & S. Kumar, "Microstructural evolution in near-eutectic yttrium silicate compositions fabricated from a bulk melt and as an intergranular phase in silicon nitride", *J. Am. Ceram. Soc.*, **73** [12] pp.3575-79 (1990)
218. M. H. Lewis & G. Leng-Ward, "Advanced engineering ceramics", *Met. Mater. (Inst. Met.)*, **7** [6] pp.356-61 (1991)
219. M. K. Cinibulk, G. Thomas & S. M. Johnson, "Grain-boundary-phase crystallization and strength of silicon nitride sintered with a YSiAlON glass", *J. Am. Ceram. Soc.*, **73** [6] pp.1606-12 (1990)
220. J.-B. Veyret, M. Van de Voorde & M. Billy, "Oxidation behaviour of silicon yttrium oxynitride", J. Am. Ceram. Soc., 75 [12] pp.3289-92 (1992)
221. L. Wang, C. He & J. G. Wu, "Oxidation of sintered silicon nitride materials", pp.604-11 in V. J. Tennery, ed., *"Ceramic Materials and Components for Engines"*, Proc. 3rd Int. Symp., Las Vegas, Nevada (1988)
222. H. M. Trigg & J. Drennan, "Devitrification of glassy phases in yttrium O'-SiAlON materials", pp.629-32 in C. C. Sorrell & B. Ben-Nissan, eds., Proc. Int. Ceram. Conf. Austceram 88, Trans Tech Publ. (1988)
223. M. H. Lewis, G. Leng-Ward & S. Mason, "Microstructural design of high-temperature ceramics", pp.1-13 in R. Freer *et al.*, eds., *"Engineering with Ceramics 2"*, Br. Ceram. Proc. No.39 (1987)
224. P. A. Walls & M. Ueki, "Analysis of the $\alpha$ to $\beta$ transformation in Y-Si-Al-O-N ceramics", *J. Mater. Sci.*, **28** pp.2967-74 (1993)
225. M. H. Lewis, A. R. Bhatti, R. J. Lumby & B. North, "The microstructure of sintered Si-Al-O-N ceramics", *J. Mater. Sci.*, **15** pp.103-13 (1980)
226. R. S. Aujla, G. Leng-Ward, M. H. Lewis, E. F. W. Seymour, G. A. Styles & G. W. West, "An NMR-study of silicon co-ordination in Y-Si-Al-O-N glasses", *Phil. Mag.*, **B54** [2] L51 (1986)
227. D. Kruppa, R. Dupree & M. H. Lewis, "$^{15}N$ MAS-NMR in the YSiAlON system", *Mater. Lett.*, **11** [5-6-7] pp.195-98 (1991)
228. K. R. Shillito, R. R. Wills & R. B. Bennett, "Silicon metal oxynitride glasses", *J. Am. Ceram. Soc.*, **61** [11-12] p.537 (1978)
229. A. Makishima, M. Mimoto, N. Ii & M. Tsutsumi, "Microhardness and transparency of an La-Si-O-N oxynitride glass", *J. Am. Ceram. Soc.*, **66** [3] C-55-56 (1983)

230. S. Hampshire, R. A. L. Drew & K. H. Jack, "Viscosities, glass transition temperatures, and microhardness of Y-Si-Al-O-N glasses", *J. Am. Ceram. Soc.*, **67** [3] C-46-47 (1984)
231. T. Rouxel, J. L. Besson, C. Gault, P. Gours, M. Leigh & S. Hampshire, "Viscosity and Young's modulus of an oxynitride glass", *J. Mater. Sci. Lett.*, **8** pp.1158-60 (1989)
232. D. R. Messier & A. Broz, "Microhardness and elastic moduli of Si-Al-O-N glasses", *J. Am. Ceram. Soc.*, **65** [8] C-123 (1982)
233. R. Pastuszak & P. Verdier, "M-Si-Al-O-N glasses (M=Mg, Ca, Ba, Mn, Nd), existence range and comparative study of some properties", *J. Non-Cryst. Solids*, **56** pp.141-46 (1983)
234. M. Ohashi, K. Nakamura, K. Hirao, S. Kanzaki & S. Hampshire, "Formation and properties of Ln-Si-O-N glasses (Ln= Lanthanides or Y)", *J. Am. Ceram. Soc.*, **78** [1] pp.71-76 (1995)
235. R. E. Loehman, "Oxynitride glasses", *J. Non-Cryst. Solids*, **42** pp.433-46 (1980)
236. R. E. Loehman, "Preparation and properties of oxynitride glasses", *J. Non-Cryst. Solids*, **56** pp.123-34 (1983)
237. R. E. Loehman, "Preparation and properties of yttrium-silicon-aluminum oxynitride glasses", *J. Am. Ceram. Soc.*, **62** [9-10] pp.491-94 (1979)
238. R. A. L. Drew, S. Hampshire & K. H. Jack, "The preparation and properties of oxynitride glasses", pp.323-30 in F. L. Riley, ed., *"Progress in Nitrogen Ceramics"*, Martinus Nijhoff Publ., Boston (1983)
239. S. Hampshire, E. Nestor, R. Flynn, J.-L. Besson, T. Rouxel, H. Lemercier, P. Goursat, M. Sebai, D. P. Thompson & K. Liddell, "Yttrium oxynitride glasses: properties and potential for crystallization to glass-ceramics", *J. Eur. Ceram. Soc.*, **14** pp.261-73 (1994)
240. J. A. Fernie, "Oxynitride glasses and glass ceramics", Ph.D. Thesis, University of Warwick, Coventry (1992)
241. G. Leng-Ward & M. H. Lewis, "Oxynitride glasses and their glass-ceramic derivatives", pp.106-55 in M. H. Lewis, ed., *"Glasses and Glass-Ceramics"*, Chapman and Hall, London (1989)
242. G. Leng-Ward & M. H. Lewis, "Crystallization in Y-Si-Al-O-N glasses", *Mater. Sci. Eng.*, **71** pp.101-11 (1985)
243. J. A. Fernie, M. H. Lewis & G. Leng-Ward, "Crystallization of Nd-Si-Al-O-N glasses", *Mater. Lett.*, **9** [1] pp.29-32 (1989)
244. D. S. Perera, D. P. Thompson & J. S. Thorp, "Nitrogen glass ceramics in the Mg-Si-Al-O-N and Y-Si-Al-O-N systems", pp.633-37 in C. C. Sorrell & B. Ben-Nissan, eds., Proc. Int. Ceram. Conf. Austceram 88, Tans Tech Publ., (1988)
245. T. Rouxel, J.-L. Besson, E. Rzepka & P. Goursat, "Raman spectra of SiYAlON glasses and ceramics", *J. Non-Cryst. Solids*, **122** pp.298-304 (1990)
246. T. R. Dinger, R. S. Rai & G. Thomas, "Crystallization behaviour of a glass in the $Y_2O_3$-$SiO_2$-AlN system", *J. Am. Ceram. Soc.*, **71** [4] pp.236-44 (1988)
247. R. Wusirika, "Problems associated with the melting of oxynitride glasses", *J. Am. Ceram. Soc.*, **67** [11] C-232-33 (1984)
248. R. R. Wusirika & C. K. Chyung, "Oxynitride glasses and glass ceramics", *J. Non-Cryst. Solids*, **38-39** pp.39-44 (1980)
249. C. H. Drummond III, W. E. Lee, W. A. Sanders & J. D. Kiser, "Crystallization and characterization of $Y_2O_3$-$SiO_2$ glasses, *Ceram. Eng. Sci. Proc.*, **9** [9-10] pp.1343-54 (1988)

250. A. Makishima, "Characterization of aluminosilicate glass containing rare-earth oxides", pp.104-12 in S. Saito, ed., *"Fine Ceramics"*, Elsevier, London (1988)
251. A. Makishima & T. Shimohira, "Alkaline durability of high elastic modulus alumino-silicate glasses containing $Y_2O_3$, $La_2O_3$ & $TiO_2$", *J. Non-Cryst. Solids,* **38-39** pp.661-66 (1980)
252. A. Makishima, M. Kobayashi, T. Shimohira & T. Nagata, "Formation of aluminosilicate glasses containing rare-earth oxides", *J. Am. Ceram. Soc.,* **65** [12] C-210 (1982)
253. A. Makishima, Y. Tamura & T. Sakaino, "Elastic moduli and refractive indices of aluminosilicate glasses containing $Y_2O_3$, $La_2O_3$ and $TiO_2$", *J. Am. Ceram. Soc.,* **61** [5-6] pp.247-49 (1978)
254. A. Makishima, M. Asami & Y. Ogura, "A machinable calcia-alumina-yttria-silica glass-ceramic", *J. Am. Ceram. Soc.,* **72** [6] pp.1024-26 (1989)
255. A. Makishima, H. Kubo & T. Shimohira, "Formation and crystallization of yttrium aluminosilicate glasses containing calcium oxide", *J. Am. Ceram. Soc.,* **69** [6] C-130-31 (1986)
256. A. Makishima, H. Kubo, K. Kotani, M. Tsutsumi & M. Asami, "Formation and crystallization in the yttrium aluminosilicate glasses containing zinc oxide", *J. Am. Ceram. Soc.,* **69** [12] C-294-96 (1986)
257. A. Makishima & T. Hara, "Thermal expansions and chemical durabilities of yttrium-aluminosilicate glasses containing $Na_2O$ and $ZrO_2$", *J. Am. Ceram. Soc.,* **74** [2] pp.428-30 (1991)
258. K. Morita, A. Umezawa, S. Yamato & A. Makishima, "Surface roughness of yttria-containing aluminosilicate glass-ceramics as indicative of their machinability", *J. Am. Ceram. Soc.,* **76** [7] pp.1861-64 (1993)
259. J. E. Shelby & J. T. Kohli, "Rare-earth aluminosilicate glasses", *J. Am. Ceram. Soc.,* **73** [1] pp.39-42 (1990)
260. J. E. Shelby, S. M. Minton, C. E. Lord & M. R. Tuzzolo, "Formation and properties of yttrium aluminosilicate glasses", *Phys. Chem. Glasses,* **33** [3] pp.93-98 (1992)
261. J. T. Kohli & J. E. Shelby, "Magneto-optical properties of rare-earth aluminosilicate glasses", *Phys. Chem. Glasses,* **32** [3] pp.109-14 (1991)
262. J. T. Kohli, J. E. Shelby & J. S. Frye, "A structural investigation of yttrium aluminosilicate glasses using $^{29}Si$ and $^{27}Al$ Magic Angle Spinning Nuclear Magnetic Resonance", *Phys. Chem. Glasses,* **33** [3] pp.73-78 (1992)
263. J. T. Kohli, R. A. Condrate, Sr., & J. E. Shelby, "Raman and infrared spectra of rare-earth aluminosilicate glasses", *Phys. Chem. Glasses,* **34** [3] pp.81-87 (1993)
264. J. T. Kohli & J. E. Shelby, "Formation and properties of rare-earth aluminosilicate glasses", *Phys. Chem. Glasses,* **32** [2] pp.67-71 (1991)
265. J. E. Shelby, "Rare-earths as modifiers in oxide glasses", *Key Eng. Mat.,* **94-95** pp.43-80 (1994)
266. J. E. Shelby, "Rare-earths as major components in oxide glasses", *Key Eng. Mat.,* **94-95** pp.1-42 (1994)
267. D. E. Day, "Rare-earth aluminosilicate glasses as radiation delivery vehicles", pp.243-51 in Proc. XVIIth Int. Cong. Glass, Vol.1, Chinese Ceramic Society, Beijing (1995)
268. M. J. Hyatt & D. E. Day, "Glass properties in the yttria-alumina-silica system", *J. Am. Ceram. Soc.,* **70** [10] C-283-87 (1987)

269. E. M. Erbe & D. E. Day, "Properties of $Sm_2O_3$-$Al_2O_3$-$SiO_2$ glasses for in vivo applications", *J. Am. Ceram. Soc.*, **73** [9] pp.2708-13 (1990)
270. J. E. White & D. E. Day, "Rare-earth aluminosilicate glasses for in vivo radiation delivery", *Key Eng. Mat.*, **94-95** pp.181-208 (1994)
271. I. H. Arita, D. S. Wilkinson & G. R. Purdy, "Crystallization of yttria-alumina-silica glasses", *J. Am. Ceram. Soc.*, **75** [12] pp.3315-20 (1992)
272. J. Wang, W. S. Brocklesby, J. R. Lincoln, J. E. Townsend & D. N. Payne, "Local structures of rare-earth ions in glasses: The crystal-chemistry approach", *J. Non-Cryst. Solids*, **163** pp.261-67 (1993)
273. S. Tanabe, K. Hirao & N. Soga, "Elastic properties and molar volume of rare-earth aluminosilicate glasses", *J. Am. Ceram. Soc.*, **75** [3] pp.503-06 (1992)
274. A. Buri, D. Caferra, F. Branda & A. Marotta, "Relationship between composition and glass transition temperature in $Na_2O$-$M_2O_3$-$SiO_2$ glasses (M=Ga, In, Sc, Y, La)", *Phys. Chem. Glasses*, **23** [1] pp.37-40 (1982)
275. F. Branda, A. Buri, D. Caferra & A. Marotta, "The glass transition temperatures of soda-silica glasses containing $M_2O_3$ oxides (M=Al, Ga, In, Sc, Y, La)", *Phys. Chem. Glasses*, **22** [3] pp.68-69 (1981)
276. R. A. Condrate, Sr., "Infrared and Raman spectra of glasses containing rare-earth ions", *Key Eng. Mat.*, **94-95** pp.209-32 (1994)
277. H. Raeder, P. Möller, M. Nofz & R. Stösser, "On the incorporation of $Gd^{3+}$, $Eu^{3+}$ and $Eu^{2+}$ ions in anorthite and related glasses", *Bol. Soc. Esp. Ceram. Vid.*, **31-C** Vol.3. pp.329-34 (1992)
278. A. G. Clare & A. C. Wright, "Neutron scattering studies of glasses containing rare-earths", *Key Eng. Mat.*, **94-95** pp.141-60 (1994)
279. S. Tanabe, N. Soga, K. Hirao & T. Hanada, "Physical properties and structure of silica-alumina-europium oxide glasses", *J. Am. Ceram. Soc.*, **73** [6] pp.1733-36 (1990)
280. G. N. Greaves, "EXAFS and the structure of glass", *J. Non-Cryst. Solids*, **71** pp.203-13 (1985)
281. M. R. Heslin & J. E. Shelby, "Formation and properties of lithium neodymium silicate glasses", *J. Non-Cryst. Solids*, **167** pp.172-79 (1994)
282. P. W. Angel & R. E. Hann, "Glass formation, properties and structure of soda-yttria-silica glasses", *J. Am. Ceram. Soc.*, **75** [12] pp.3278-82 (1992)
283. F. C. Lee, J. Marr, R. P. Gunawardane & F. P. Glasser, "Phase relations at liquidus temperatures in the $Na_2$-$Y_2O_3$-$SiO_2$ system", *Br. Ceram. Trans. J.*, **90** pp.8-11 (1991)
284. J. E. Shelby, C. M. Shaw, S. M. Minton & C. E. Lord, "Yttrium gallosilicate glasses", *Phys. Chem. Glasses*, **31** [2] pp.49-53 (1990)
285. J. M. Jewell, P. L. Higby & I. D. Aggarwal, "Properties of BaO-$R_2O_3$-$Ga_2O_3$-$GeO_2$ (R= Y, Al, La, and Gd) glasses", *J. Am. Ceram. Soc.*, **77** [3] pp.697-700 (1994)
286. J. T. Kohli & J. E. Shelby, "Rare-earth aluminogermanate glasses", *J. Am. Ceram. Soc.*, **74** [5] pp.1031-35 (1991)
287. I. N. Chakraborty, J. E. Shelby & R. A. Condrate, Sr., "Properties and structure of lanthanum borate glasses", *J. Am. Ceram. Soc.*, **67** [12] pp.782-85 (1984)
288. I. N. Chakraborty & D. E. Day, "Effect of $R^{3+}$ ions on the structure and properties of lanthanum borate glasses", *J. Am. Ceram. Soc.*, **68** [12] pp.641-45 (1985)

289. H. L. Rutz, D. E. Day & C. F. Spencer, Jr., "Properties of yttria-aluminoborate glasses", *J. Am. Ceram. Soc.*, **73** [6] pp.1788-90 (1990)
290. I. N. Chakraborty, D. E. Day, J. C. Lapp & J. E. Shelby, "Structure-property relations in lanthanide borate glasses", *J. Am. Ceram. Soc.*, **68** [7] pp.368-71 (1985)
291. C. B. Ping, M. Z. A. Malek & I. Kitano, "Rare-earth aluminosilicate glasses and their related glass-ceramics", from: Asean-Japan Region Seminar on Fine Ceramics, Oct. 1-2. (1991)
292. V. Saraswati, S. Raoot, K. V. S. R. Anjaneyulu & N. V. Visveswararao, "Evaluation of processing methods for calcia-yttria-alumina-silica glass-ceramic", *J. Mater. Sci.*, **28** pp.1867-73 (1993)
293. J. Felsche, "The Crystal chemistry of rare-earth silicates", pp.99-197 in *"Structure and Bonding", Vol.13. Rare-Earths,* Springer-Verlag, Berlin (1973)
294. D. M. Burt, "Compositional and phase relations among rare-earth element minerals", pp.259-307 in B. R. Lipin & G. A. McKay, eds., *"Reviews in Mineralogy"*, Vol.21, The Mineralogical Society of America, Washington D.C. (1989)
295. K. Liddell & D. P. Thompson, "X-ray diffraction data for yttrium silicates", *Br. Ceram. Trans. J.*, **85** pp.17-22 (1986)
296. J. Ito & H. Johnson, "Synthesis and study of yttrialite", *Am. Miner.*, **53** [11-12] pp.1940-52 (1968)
297. I. A. Bondar & N. A. Toropov, "Preparation and properties of rare-earth silicates and aluminates", *Mater. Res. Bull.*, **2** pp.479-89 (1967)
298. I. A. Bondar, "Rare-earth silicates", *Ceram. Int.*, **8** [3] pp.83-89 (1982)
299. J. Ito, "Silicate apatites and oxyapatites", *Am. Miner.*, **53** pp.890-907 (1968)
300. K. Liddell, Ph.D. Thesis, University of Newcastle-upon-Tyne, Newcastle-upon-Tyne (1984)
301. J. Felsche & W. Hirsinger, "The polymorphs of the rare-earth pyrosilicates $RE_2Si_2O_7$ [RE: La, Ce, Pr, Nd, Sm]", *J. Less-Comm. Met.*, **18** pp.131-37 (1969)
302. J. Felsche, "Polymorphism and crystal data of the rare-earth disilicates of type $RE_2Si_2O_7$", *J. Less-Comm. Met.*, **21** pp.1-14 (1970)
303. J. Felsche, "Rare-earth silicates with the apatite structure", *J. Solid State Chem.*, **5** pp.266-75 (1972)
304. M. Leskelä & L Niinistö, "Inorganic complex compounds I.", pp.203-334 in K. A. Gschneider, Jr., & L. Eyring, eds., *"Handbook of the Physics and Chemistry of Rare-Earths"*, Vol.8., Elsevier, Amsterdam (1986)
305. A. C. Tas & M. Akinc, "Crystal structure of the high-temperature forms of $Ln_2Si_2O_7$ (Ln= La, Ce, Pr, Nd, Sm) revisited", *J. Am. Ceram. Soc.*, **77** [11] pp.2968-70 (1994)
306. J. M. Hughes, M. Cameron & A. N. Mariano, "Rare-earth-element ordering and structural variations in natural rare-earth-bearing apatites", *Am. Miner.*, **76** pp.1165-73 (1991)
307. J. G. Ronsbo, "Coupled substitutions involving REEs and Na and Si in apatites in alkaline rocks from the Ilimanssaq intrusion, South Greenland, and the petrological implications", *Am. Miner.*, **74** pp.896-901 (1989)
308. P. L. Roeder, D. MacArthur, X.-P. Ma, G. R. Palmer & A. N. Mariano, "Cathodoluminescence and microprobe study of rare-earth elements in apatite", *Am. Miner.*, **72** pp.801-11(1987)

309. D. R. Lide, ed., "Handbook of Chemistry and Physics", 71st edition, CRC Press, Boston (1990-91)
310. A. G. Evans & E. A. Charles, *"Fracture toughness determination by indentation", J. Am. Ceram. Soc.*, **59** [7-8] pp.371-72 (1976)
311. D. W. Richerson, "Modern Ceramic Engineering", 2nd ed., Marcel Dekker Inc., New York (1992)
312. I. Fanderlik, "Optical Properties of Glass", Glass Science and Technology Vol.5, Elsevier Oxford (1983)
313. H. E. Kissinger, "Variation of peak temperature with heating rate in Differential Thermal Analysis", *J. Res. Nat. Bur. Stand.*, **57** pp.217-21 (1956)
314. H. E. Kissinger, "Reaction kinetics in Differential Thermal Analysis", *Anal. Chem.*, **29** [11] pp.1702-06 (1957)
315. K. Matusita & S. Sakka, "Kinetic study on crystallization of glass by Differential Thermal Analysis - criterion on application of Kissinger plot", *J. Non-Cryst. Solids*, **38-39** pp.741-46 (1980)
316. L. H. Van Vlack, "Elements of Materials Science and Engineering", 3rd ed., Addision-Wesley Publ., Reading, Massachusetts (1978)
317. B. R. Lawn, A. G. Evans & D. B. Marshall, "Elastic/plastic indentation damage in ceramics: the median/radial crack system", *J. Am. Ceram. Soc.*, **63** [9-10] pp.574-81 (1980)
318. H. D. Keith & F. J. Padden, "The phenomenological theory of spherulitic crystallization", *J. Appl. Phys.*, **34** [8] pp.2409-21 (1963)
319. H. D. Keith & F. J. Padden, "Spherulitic crystallization from the melt I. Fractionation and impurity segregation and their influence on crystalline morphology", *J. Appl. Phys.*, **35** [4] pp.1270-85 (1964)
320. H. D. Keith & F. J. Padden, "Spherulitic crystallization from the melt II. Influence of fractionation and impurity segregation on the kinetics of crystallization", *J. Appl. Phys.*, **35** [4] pp.1286-96 (1964)
321. S. W. Freiman, G. Y. Onoda, Jr., & A. G. Pincus, "Spherulitic crystallization in glasses", pp.141-50 in L. L. Hench & S. W. Freiman, eds., *"Advances in Nucleation and Crystallization in Glasses"*, The American Ceramic Society, Columbus, Ohio (1971)
322. M. H. Lewis, J. Metcalf-Johansen & P. S. Bell, "Crystallization mechanism in glass ceramics", *J. Am. Ceram. Soc.*, **62** [5-6] pp.278-88 (1979)
323. M. H. Lewis & G. Smith, "Spherulitic growth and recrystallization in barium silicate glasses", *J. Mater. Sci.*, **11** pp.2015-26 (1976)
324. G. Leng-Ward private communication
325. J. J. de Groot & J. A. J. M. Van Vliet, "The High Pressure Sodium Lamp", Philips Technical Library, Kluver Technische Boeken B.V., Deventer, Antwerpen (1986)
326. F. Nagel, "Factors influencing the quality of Al-Ca-Sr-Y oxide seals for HPS lamps", pp.240-50 in E. G. Zubler, ed., *"High Temperature Lamp Chemistry II."*, (1988)
327. J. J. C. Omen & J. W. Rouwendal, "High pressure sodium lamp seals based on rare-earth aluminates", pp.291-312 in E. G. Zubler, ed., *"High Temperature Lamp Chemistry"*, (1985)
328. R. K. Datta, "Emission and sealing materials chemistry of high-pressure sodium (HPS) lamp", pp.220-39 in E. G. Zubler, ed., *"High Temperature Lamp Chemistry II."*, (1988)

329. P. A. Seinen, "High intensity discharge lamps with ceramic envelopes - A key technology for the lighting future", pp. 101-9 in R. Itiani & S. Kamiya, eds., Proc. 7th Int. Symp. Sci. & Technol. Light Sources (LS:7), Kyoto, Japan, (1995)
330. H. H. K. Xu & S. Jahanmir, "Scratching and grinding of a machinable glass-ceramic with weak interfaces and rising T-curve", *J. Am. Ceram. Soc.*, **78** [2] pp.497-500 (1995)
331. M. S. Rea, "Lighting Handbook", Illuminating Engineering Society of North America, New York, 1993

Fig.II.1. A selected, representative DTA trace (MASN-10 glass composition, agate-ground powder).

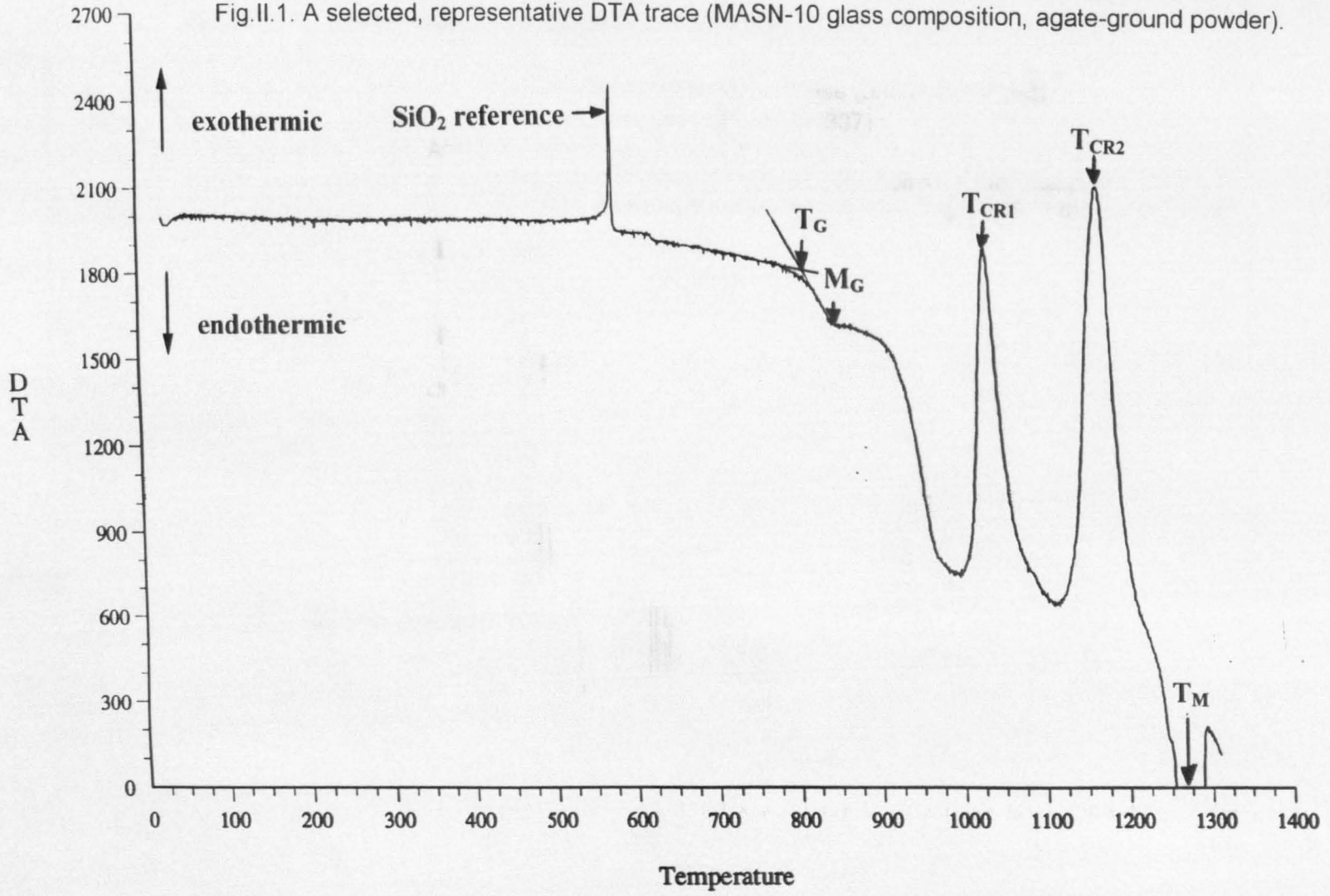

Fig.II.1. XRD trace of a Ca-La-aluminosilicate bulk glass-ceramic (CASL-2, 1150C/30min).

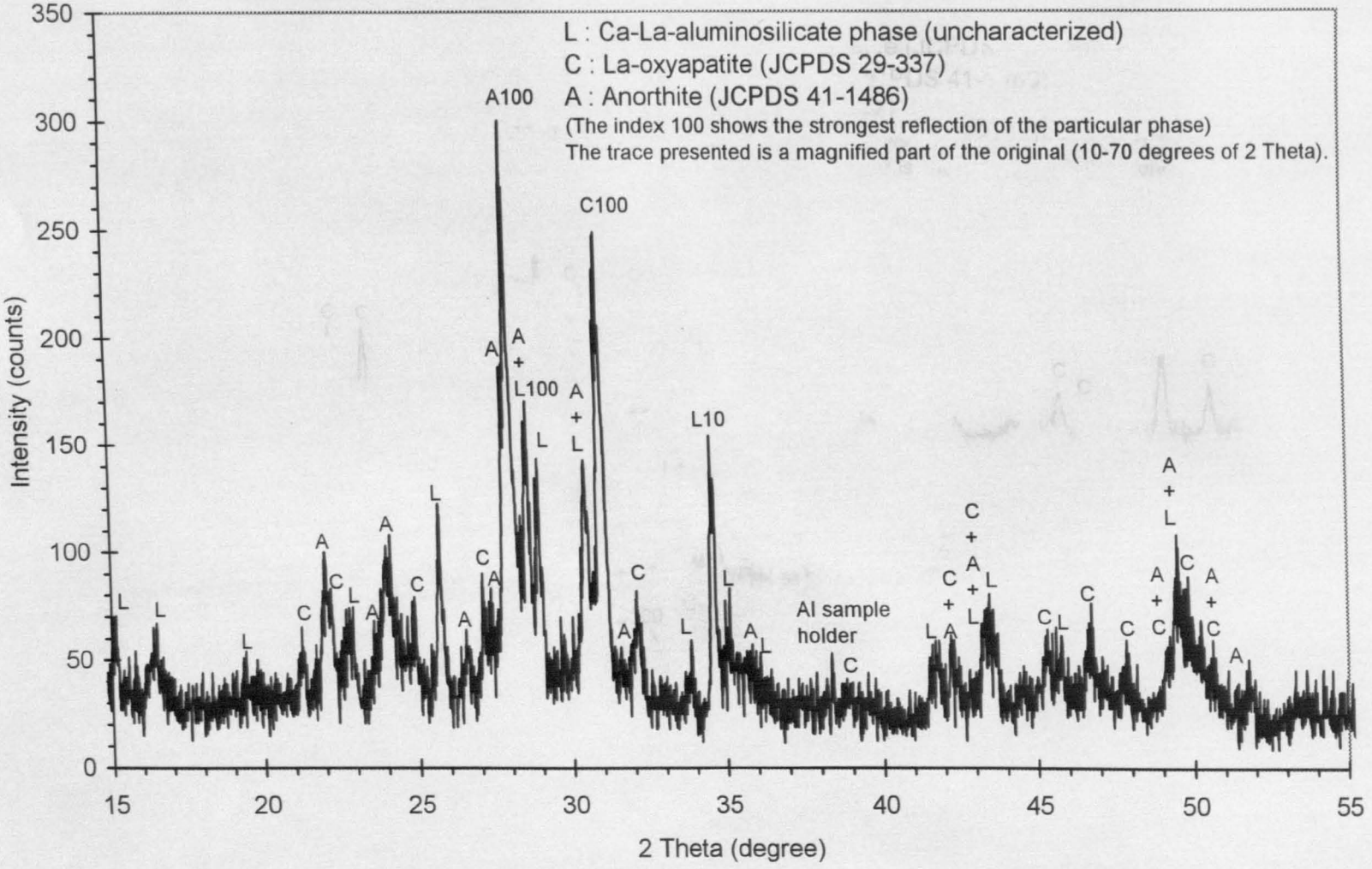

Fig.II.2. XRD traces of Ca-Nd-aluminosilicate bulk glass-ceramics.

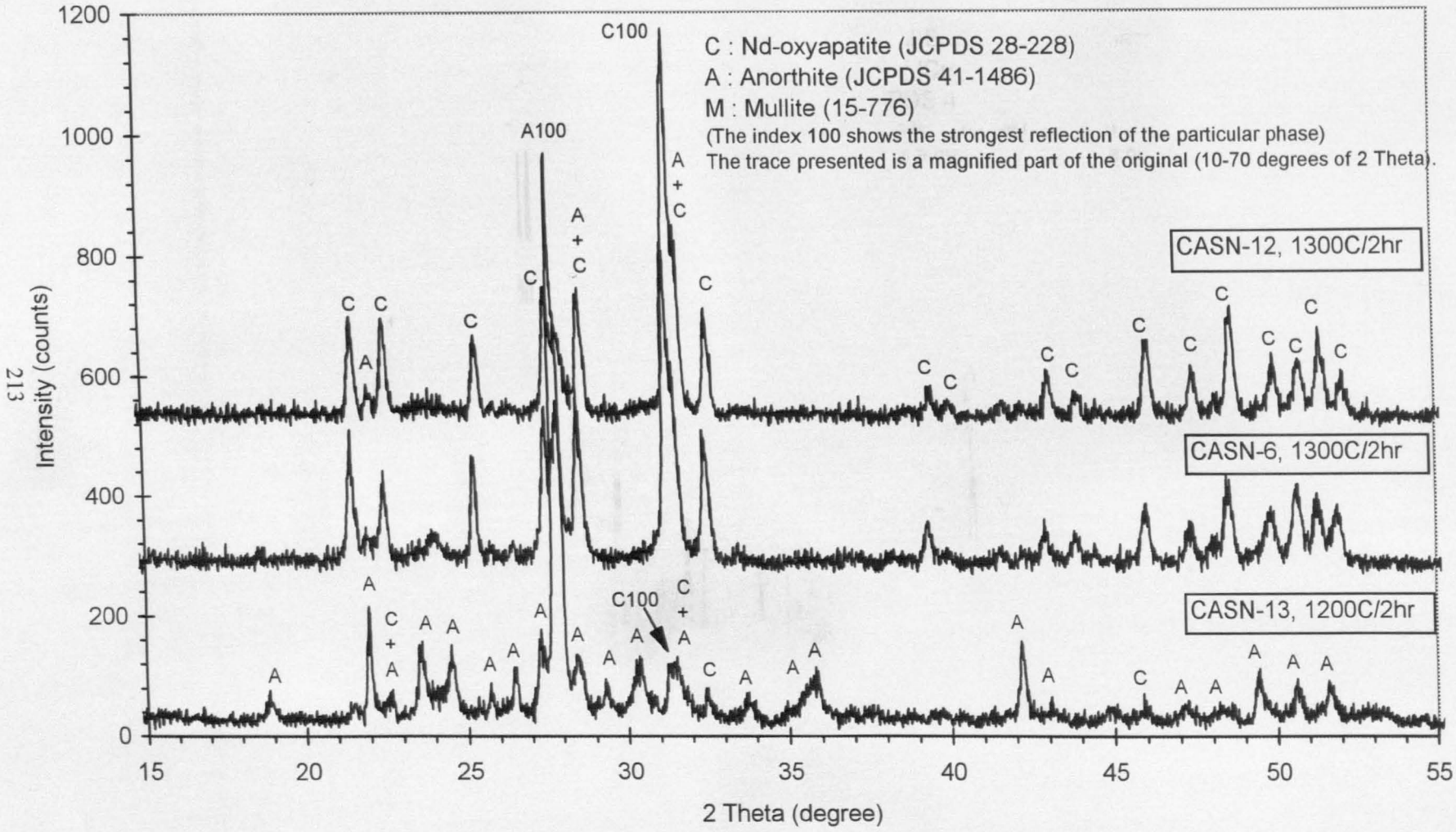

Fig.II.3. XRD trace of a Ti containing Ca-Nd-aluminosilicate glass-ceramic pellet (CASN12-T1, 1300C/2hr).

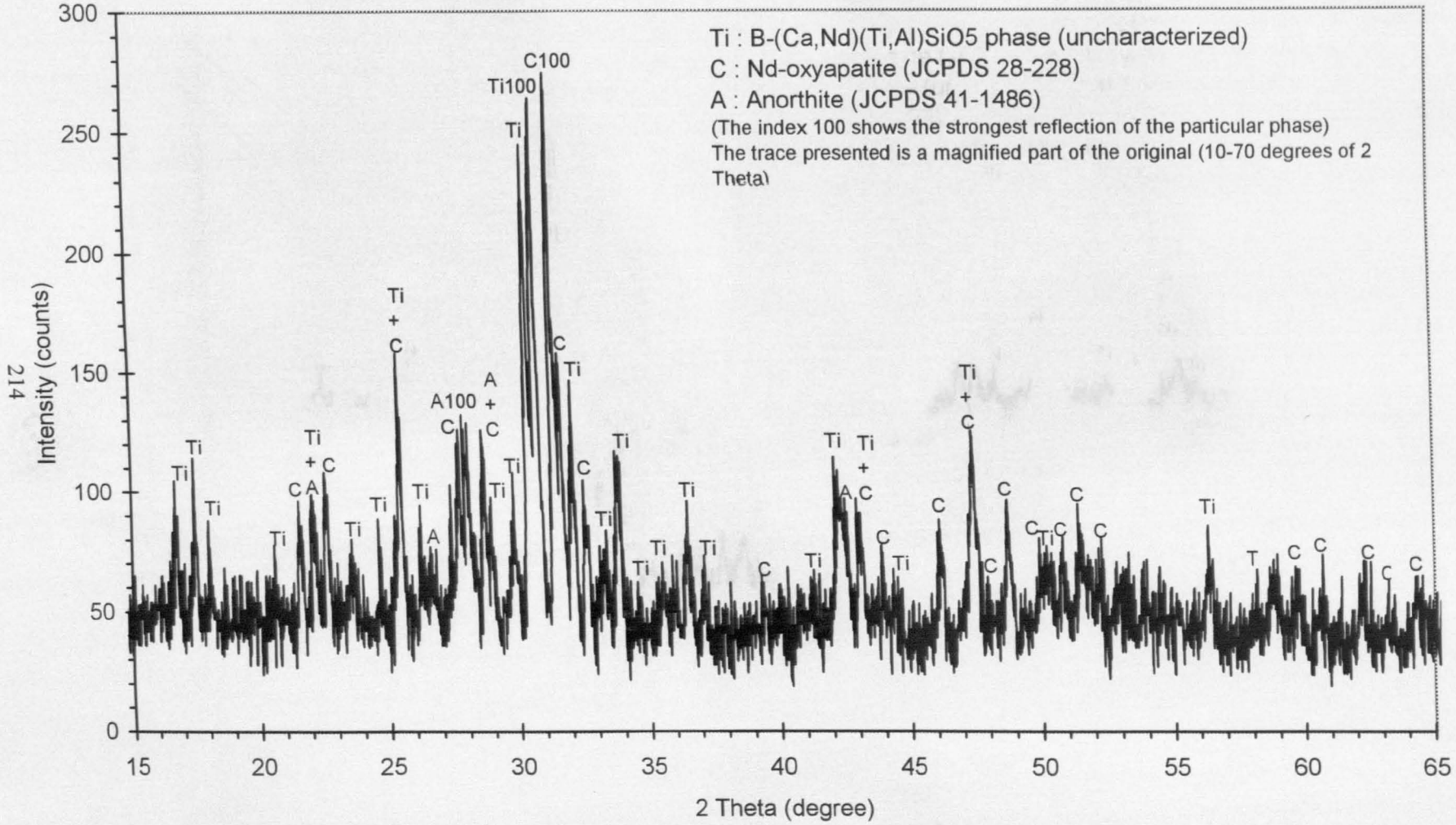

Fig.II.4. XRD traces of Mg-Nd-aluminosilicate bulk glass-ceramics.

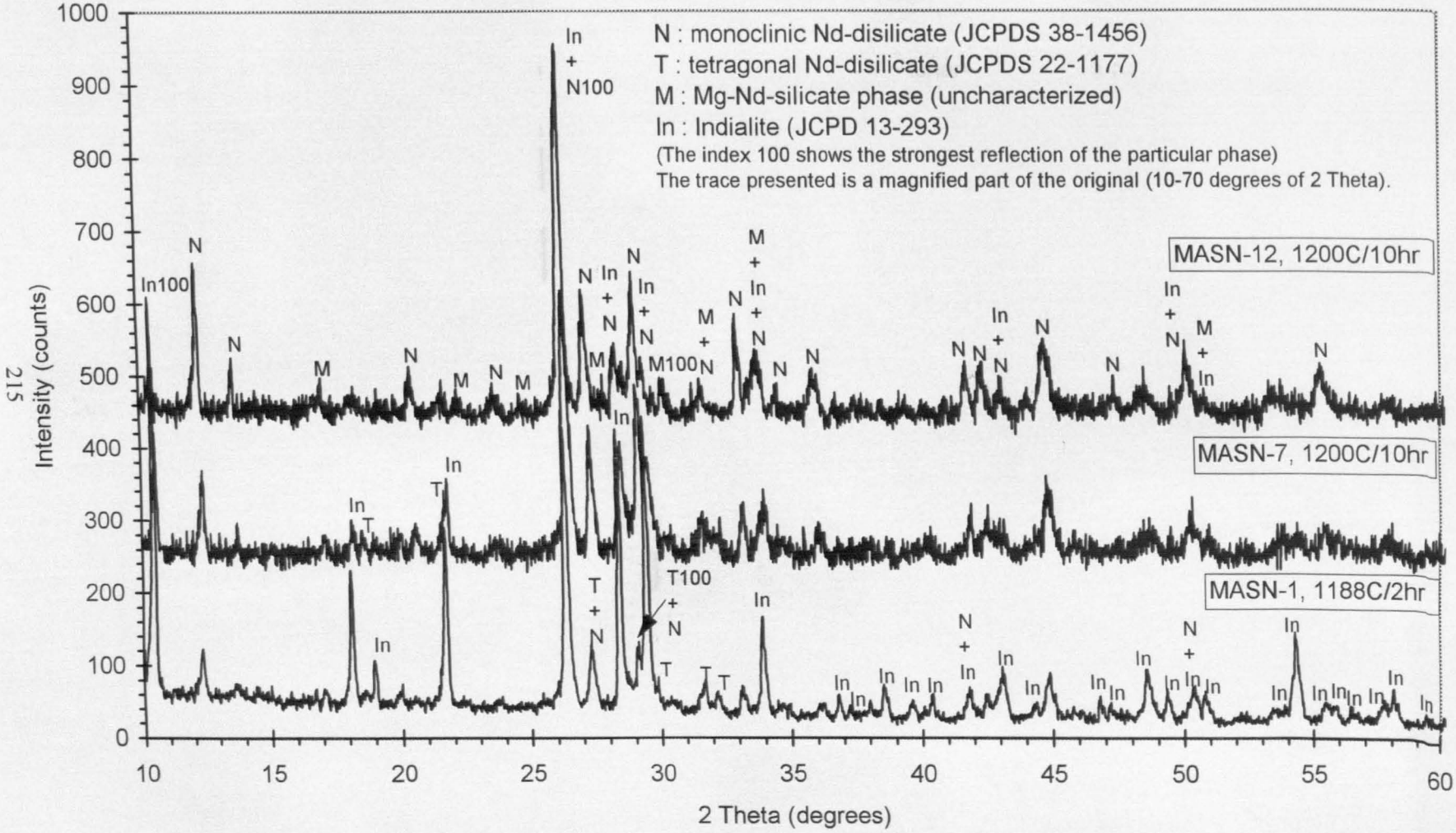

Fig.II.5. XRD trace of a Mg-Nd-aluminosilicate bulk glass-ceramic (MASN-12, 1058C/2hr)